JOURNAL OF GEOPHYSICAL RESEARCH

The continuation of

TERRESTRIAL MAGNETISM AND ATMOSPHERIC ELECTRICITY
(1896-1948)

An International Quarterly

VOLUME 61 September, 1956 NUMBER 3

CONTENTS

(Contents concluded on outside back cover)

Published at

THE WILLIAM BYRD PRESS, INC.

P. O. BOX 2-W, SHERWOOD AVE. AND DURHAM ST.

RICHMOND 5, VIRGINIA

Address all correspondence to

JOURNAL OF GEOPHYSICAL RESEARCH

5241 BROAD BRANCH ROAD, NORTHWEST

WASHINGTON 15, D.C., U.S.A.

SIX DOLLARS A YEAR SINGLE NUMBERS, TWO DOLLARS

JOURNAL OF GEOPHYSICAL RESEARCH

The continuation of

Terrestrial Magnetism and Atmospheric Electricity

(1896-1948)

An International Quarterly

Founded 1896 by L. A. BAUER *Continued 1928-1948 by* J. A. FLEMING

Fields of Interest

Terrestrial Magnetism
Atmospheric Electricity
The Ionosphere
Solar and Terrestrial Relationships
Aurora, Night Sky, and Zodiacal Light
The Ozone Layer
Meteorology of Highest Atmospheric Levels
The Constitution and Physical States of the Upper Atmosphere
Special Investigations of the Earth's Crust and Interior, including experimental seismic waves, physics of the deep ocean and ocean bottom, physics in geology
And similar topics

This Journal serves the interests of investigators concerned with terrestrial magnetism and electricity, the upper atmosphere, the earth's crust and interior by presenting papers of new analysis and interpretation or new experimental or observational approach, and contributions to international collaboration. It is not in a position to print, primarily for archive purposes, extensive tables of data from observatories or surveys, the significance of which has not been analyzed.

Forward *manuscripts* to one of the Associate Editors, or to the editorial office of the Journal at 5241 Broad Branch Road, Northwest, Washington 15, D.C., U.S.A. It is preferred that manuscripts be submitted in English, but communications in French, German, Italian, or Spanish are also acceptable. A brief abstract, preferably in English, must accompany each manuscript. A *publication charge* of $8 per page will be billed by the Editor to the institution which sponsors the work of any author; private individuals are not assessed page charges. Manuscripts from outside the United States are invited, and should not be withheld or delayed because of currency restrictions or other special difficulties relating to page charges. Costs of publication are roughly twice the total income from page charges and subscriptions, and are met by subsidies from the Carnegie Institution of Washington and international and private sources.

Back issues and *reprints* are handled by the Editorial Office, 5241 Broad Branch Road, N.W., Washington 15, D.C., U.S.A.

Subscriptions are handled by the Editorial Office, 5241 Broad Branch Road, N.W., Washington 15, D.C., U.S.A.

Second-class mail privileges authorized at Richmond, Virginia

Journal of

GEOPHYSICAL RESEARCH

The continuation of

Terrestrial Magnetism and Atmospheric Electricity

VOLUME 61 SEPTEMBER, 1956 No. 3

PULSED SEARCHLIGHTING THE ATMOSPHERE*

BY STEPHEN S. FRIEDLAND, JACK KATZENSTEIN,† AND MICHAEL R. ZATZICK‡

Department of Physics, University of Connecticut, Storrs, Connecticut

(Received March 22, 1956)

ABSTRACT

An optical pulsed searchlight system has been developed for measuring the density profile of the upper atmosphere. A light source which emits a 50-megalumen pulse, 20 μsec in duration, is placed at the focal point of a 60-inch mirror. A photomultiplier, which is part of a logarithmic recording system covering a dynamic range of four orders of magnitude, is placed at the focal point of a similar mirror. Each time the light is pulsed, an entire density profile is obtained. An altitude above 40 km has been observed. Suggestions and methods for obtaining signals from higher altitudes are discussed. The data obtained to date agree with the results of previous investigators and theoretical calculations.

SECTION 1—INTRODUCTION

1.1—HISTORY

The use of a vertically directed searchlight beam for measuring the density profile, and hence the temperature, of the upper atmosphere was first proposed by Synge [see 1 of "References" at end of paper]. The earliest attempt to carry out this experiment was that of Hulburt [2] in 1937, who photographed the inclined

*This study was supported by the Geophysics Research Directorate, Air Force Cambridge Research Center, Air Research and Development Command, under Contract No. AF19(604)-290.

†Now with the University of New Mexico.

‡Now with the Air Force Cambridge Research Center.

beam of a searchlight over an observing station 18.4 km away. The beam could be photographed to 28 km and photographic photometry was possible up to 22 km. Hulburt found that at heights above 10 km the theoretically calculated Rayleigh scatter accounted for virtually all of the scattered radiation so measured. Further experiments were made in 1939 by Johnson, Meyer, Hopkins, and Mock [3]. In these experiments, a modulated light beam and a photoelectric detector and tuned amplifier were used to reduce the effect of background light. These experiments permitted quantitative measurements of the scattered intensity to be made up to 30 km. They likewise verified Hulburt's important result that only Rayleigh scattering was important above 10 km.

The experiment of Johnson, *et al.*, was repeated by Elterman [4] in 1951 and 1952, and Bauer and Katzenstein [5] in 1951, using a more refined apparatus. Elterman used a standard 60-inch anti-aircraft searchlight, with a carbon-arc light source, modulated by a rotating shutter. The receiver consisted of an RCA 5819 photomultiplier, mounted at the focus of the 60-inch parabolic reflector of a similar searchlight. The transmitter was located at an elevation of 6,000 feet and the receiver at an elevation of 10,000 feet, near Albuquerque, New Mexico, to minimize the effect of low-level scatter due to water-vapor, dust, smoke, etc. The scatter altitude was fixed by triangulation between the transmitter beam and the receiver acceptance cone. Consistent profiles up to 60 km were obtained by Elterman in two sets of observations. The data were sufficiently accurate to permit a temperature profile to be computed that agrees very well with those obtained by other methods.

Because the Rayleigh scatter of a searchlight beam offers a simple but effective method of measuring the density and temperature of the upper atmosphere, it would be desirable if such a method could be made simpler to apply and be extended to higher altitudes. The work summarized in this paper deals with an approach to these goals by use of a pulsed searchlight, whereby the altitude of scattering is determined by the elapse of time between the transmitted and received signal.

1.2—THE ADVANTAGES AND OBJECTIVES OF THE PULSED SEARCHLIGHT SYSTEM

The system of Elterman, which we shall take as typical of all systems employing triangulation for altitude determination, is eminently successful in obtaining accurate density profiles up to 60 km. It is, however, plagued with the difficulty of operation between widely separated sites with the attendant complications of communications and supply, especially since the sites are preferably located on mountain peaks, which are accessible with difficulty. Further, since the profile is obtained "point-by-point," an entire evening is required to obtain the profile. This is undesirable for two reasons: First, there is little scientific value in comparing data taken at different times during the evening for the study of diurnal variations in the density profile; and, second, the practical consideration that weather changes may force the cessation of observations before a complete profile has been taken. The latter limitation is particularly bad when one considers that the phases of the moon eliminate half the nights of the year *ab initio* and the

thinnest overcast or haze condition will make observations impossible on the available dark nights. Exceptional air glow or auroral light (at high-latitude stations) will likewise eliminate evenings for obtaining density profiles to extreme altitudes, since the maximum altitude at which data can be taken is limited by the background light of the night sky. Lastly, the intensity of air glow and aurorae fluctuates considerably over the period of a single night and the possibility of observations during a "quiet" period is increased if the profile can be taken in a short time.

The pulse technique is capable of overcoming these difficulties. It is possible to operate from a single site, although a certain nominal separation of transmitter and receiver will be necessary for reasons which will be made clear in this report. Further, since a single observation of the entire profile requires only 500 microseconds, a great amount of data can be taken in a relatively short time.

Since the pulse technique, as now developed, does not require a light source whose flash intensity is exactly reproducible, the possibility exists of using very intense impulsive sources, such as exploding wires, with a concomitant gain in maximum altitude.

Against these advantages must be balanced the increased complexity and cost of the equipment used in the pulsed system and the considerable development cost that is involved in obtaining an optimum source of high intensity and short duration. The work of this paper concerns itself primarily with the development of the receiver and transmitter instrumentation, the source development being left to later work.

1.3—THEORY

The light that is reflected by the upper atmosphere into the receiver is proportional to the number of scattering centers present at the altitude of interest. It is assumed, in the discussion that follows, that the composition of the atmosphere remains constant. Previous results, as indicated in subsection 1.1, confirm that the method of scattering can be described by the Rayleigh law, in which it is assumed that the particles have diameters that are small compared to the wavelength of the light.

Johnson and Jones [6] have estimated the shape and magnitude of the reflected signal. The discussion that follows, which obtains their result, leans heavily on their presentation.

Data on the upper atmosphere are available from the Rocket Panel, Elterman, and others. The magnitude of the pressure and temperature, up to at least 100 km, can be deduced from their results. Hence it is possible to calculate, using the standard gas laws, the number of molecules per cubic centimeter as a function of altitude.

Hulburt [2] has given a convenient expression for the amount of light, in lumens, that is scattered back per unit solid angle, per centimeter length of path, at an angle of Φ to the incident beam.

$$i_s = \frac{i_0 2\pi^2(\mu_\lambda - 1)^2(1 + \cos^2 \Phi)}{n\lambda^4} \quad \ldots\ldots\ldots\ldots\ldots\ldots (1)$$

where λ is the wavelength of light, μ_λ the refractive index at wavelength λ, n the number of molecules per cc, and i_0 the incident beam flux in lumens.

We also have the Lorentz-Lorentz expression, which for gases may be expressed as

$$\mu_\lambda - 1 = \alpha_\lambda n \quad (2)$$

with a value of 1.08×10^{-23} for α_λ as given by Johnson, Meyer, Hopkins, and Mock [3]. Since the variation of α_λ with wavelength is small, its value for these calculations may be taken to be a constant.

The Rayleigh formula is known to be incorrect by a factor of two [4]. If all of the above relation is combined, we find that the intensity of the back-scattered light, in lumens, for $\Phi = 0$, per lumen incident, per cm length of beam, per unit solid angle, is

$$i_s = 9.05 \times 10^{-28} \times n \quad (3)$$

The intensity of light reaching any particular altitude is equal to the intensity of light source multiplied by the transmission factor up to that altitude. Similarly, the intensity of the back-scattered light, reaching the receiver, is equal to the intensity of the light scattered in the backward direction multiplied by the same transmission factor.

The transmission losses are due to two factors. The first is due to molecular scattering, and applies for all altitudes. The second is due to large particle scattering and applies only to the low altitudes.

The transmission losses that are due to molecular scattering can be computed from the Rayleigh formula

$$\sigma = \frac{32\pi^3 \alpha_\lambda^2 n}{3\lambda^4} \quad (4)$$

which is obtained from (1) by integration over a sphere. Upon so doing, Johnson and Jones conclude, taking into account losses in the lower atmosphere, that the transmission losses are not great and result in a total transmission of about 85 per cent for the first 50 km, while the losses above 50 km are negligible.

The intensity of the back-scattered light entering the receiver searchlight is given by

$$i_s = \text{const} \times n \times \frac{A}{h^2} \quad (5)$$

where A is the area of the receiving mirror and h is the altitude. Utilizing the available data for n, the size of the searchlight, etc., a plot of the expected scattered signal may be obtained. Figure 1.1, taken from the paper of Johnson and Jones [6], shows the estimated signal.

If negligible losses in the searchlight beam above 10 km are assumed, then the ratio of the signal for any two altitudes is

$$n = n_0 \left(\frac{S}{S_0}\right)\left(\frac{h}{h_0}\right)^2 \quad (6)$$

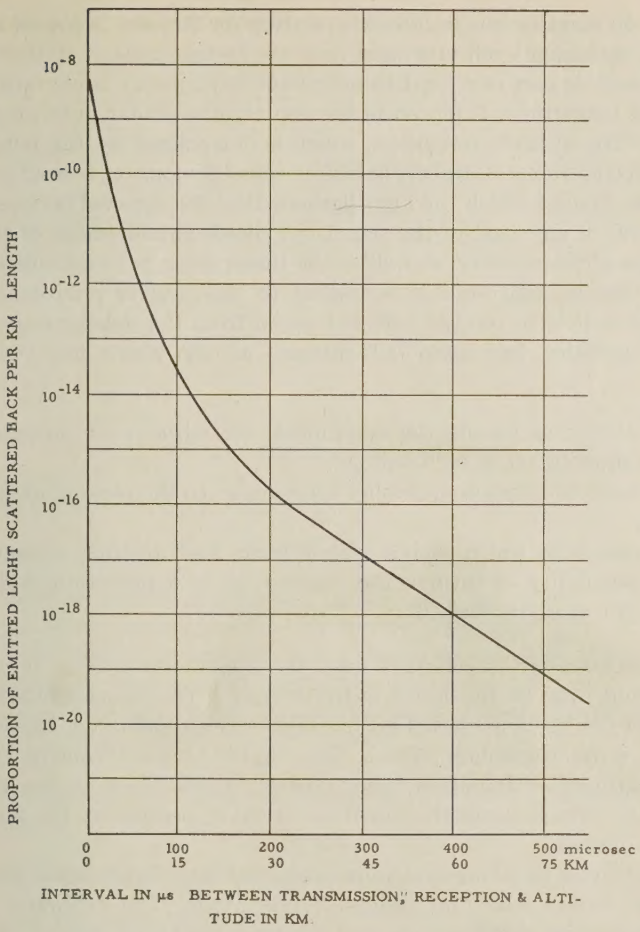

FIG. 1.1—Calculated proportion of emitted light scattered back per km length *vs* altitude

where S represents the magnitude of the signal from altitude h at the receiver. If the lower altitude is accessible to the radiosonde, it then becomes possible to compute the density profile, with the radiosonde altitude as the reference altitude.

It is important to note for further reference that between 15 and 60 km there is a change in the light signal covering four to five orders of magnitude, whereas from the ground to 60 km the change in the light signal covers 10 orders of magnitude.

SECTION II—INSTRUMENTATION

2.1—GENERAL INTRODUCTION TO THE INSTRUMENTATION

The single-site system, to be described, is basically an optical radar system. A Westinghouse FGL-1 Krypton flash-lamp, which emits a pulse of light of ap-

proximately 50 megalumens in intensity, lasting for 20 μsec, is placed at the focus of a 60-inch searchlight reflector, and acts as the transmitter. A 10-stage photomultiplier, which is part of a logarithmic circuit having a dynamic range of four to five orders of magnitude, is placed in the center of a similar reflector and acts as the receiver. The altitude resolution, which is determined by the lamp duration, is 3 km. A second photomultiplier, hereafter called a monitor, is used to determine zero time, the time at which the light flashed. Half the interval between zero time and the arrival of any part of the signal is a direct measurement of the altitude. The operation of the receiver, as well as the transmitter, is based entirely on pulse techniques; that is, high voltage is applied to the receiver photomultiplier only during the time it is to receive reflected signal from the upper atmosphere. This method of operation has many advantages, among which may be listed the following:

(1) The ability to handle the equipment, for adjustment purposes, without prior shutting off of high voltage.
(2) The removal of photomultiplier fatigue due to the passing of stray intense light.
(3) The ease with which such a system lends itself to time measurements.
(4) The possibility of turning the receiver on at a predetermined time after the light has been flashed.

As the back-scatter is collected from the upper atmosphere, it is converted into logarithmic form by the action of the circuitry. The signal profile is presented on the face of two oscilloscopes. The first one, a Tektronix 511A, called the record oscilloscope, is photographed with a Type 321A Dumont camera. The second oscilloscope utilizes a Memotron tube, a recent development of the Hughes Aircraft Company, which stores the signal for visual inspection by the operator until erased when desired.

The logarithmic receiving system is calibrated by a light source whose magnitude may be varied over four orders of magnitude. The calibrator includes a Strobotron lamp, its power-supply, and required triggering circuits. A calibrated neutral density wedge is translated across the slit by a micrometer screw. The wedge has a density range of zero to four, thus offering a light output, well calibrated over an intensity range of 10,000 to 1.

The electronic system is required to perform in proper sequence the following operations:

(1) Energize the recording equipment
(2) Activate the receiver
(3) Flash the lamp
(4) De-energize the recording equipment and prepare for the next flash

Figure 2.1 is a functional block-diagram of the entire system. The sequence is controlled by the program unit shown in the upper left of the diagram. It in turn controls the timing unit and the camera. The remaining equipment is controlled by the timing unit.

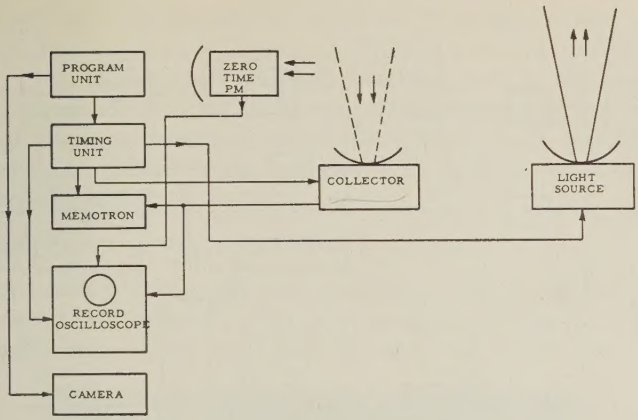

FIG. 2.1—Functional block-diagram

2.2—THE PROGRAM UNIT SEQUENCING

The sequence of operations controlled by the program unit is as follows:

(1) The camera shutter is opened.
(2) A sync pulse, to activate the timing unit, is generated.
(3) A frame counter in the camera is illuminated and then turned off, so that each signal profile is numbered on the film.
(4) The film is advanced, the camera shutter is closed, and the frame-counter is advanced one digit.

An entire sequence of the program unit takes 17 seconds. It is presently actuated once each minute.

2.3—TIMING UNIT SEQUENCING

The timing unit must assure that

(1) The oscilloscope traces are started
(2) The receiver is activated by applying high voltage to the photomultiplier
(3) The lamp is fired

The electronic sequencing that is performed by the timing unit, once it has received a trigger signal from the program unit, is explained by Figures 2.2 and 2.3. The first sharp and narrow spike (*a*) shown, is the generator of all the gates that follow and the external trigger pulse for the scope and Memotron horizontal sweeps. The first square gate (*b*) is the record gate which begins without delay after the sync pulse, but with variable width of 150 to 2500 μsec. It is used to unblank the Memotron writing gun beam.

The second square gate (*c*) can occur from 10 to 250 μsec after the sync pulse and lasts for 150 to 2500 μsec. It is used to gate on the receiver at a predetermined time. Lastly, the sharp pulse (*d*) is the transmitter trigger pulse with adjustable delay of 10 to 500 μsec after the sync pulse.

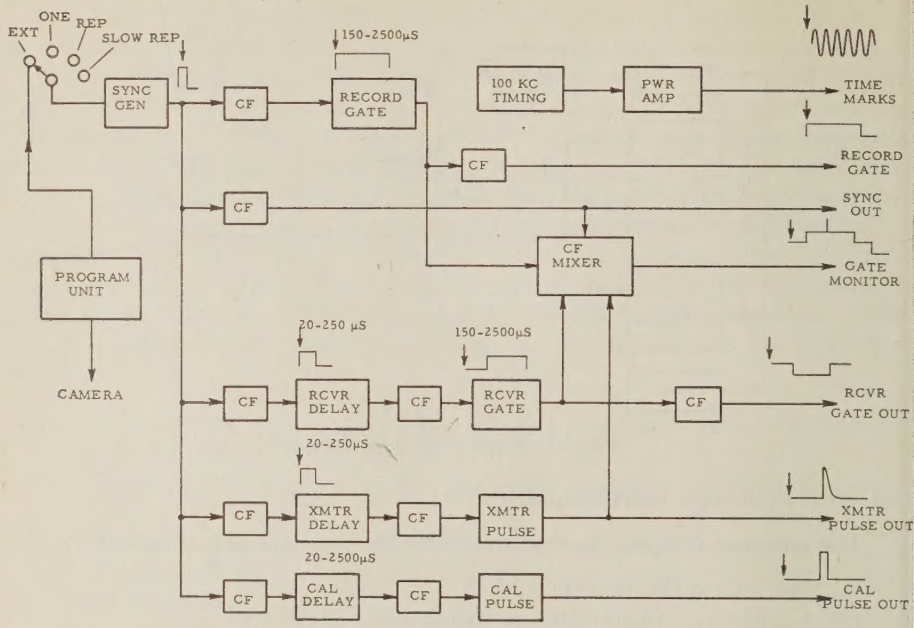

FIG. 2.2—Block-diagram timing unit

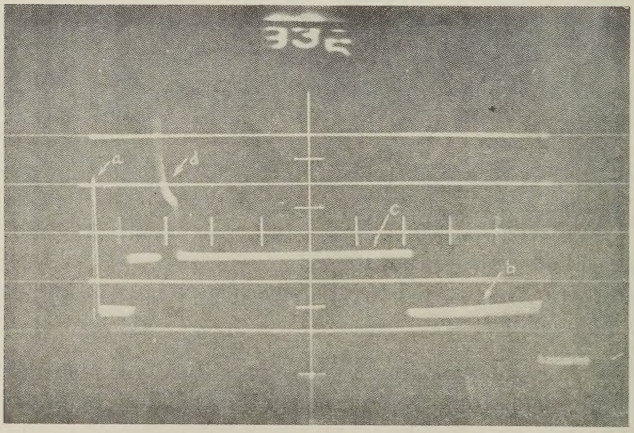

FIG. 2.3—Gate monitor output

SECTION III—THE LIGHT SOURCE

3.1—THE IDEAL LIGHT SOURCE

The ideal light source, for density profile measurements, should emit a rectangular pulse of light which is 10 μsec in duration and 10,000 megalumens in intensity. Such a source would allow, with the system described in Section II, for

an altitude resolution 1.5 km and the measurement of the density profile to 75 km and higher. At present, such a light source does not exist. However, the recent work of Hey, *et al.*, at the Radar Research Establishment, in Malvern, England, indicates that present limitations on forming a truly square pulse are due to the fluorescence of the glass containing the source, which is not a fundamental limitation [7]. Recently reported work indicates that light sources have been improved in intensity and in shortness of duration [8].

3.2—THE WESTINGHOUSE FGL-1 KRYPTON FLASH-LAMP

All measurements given in this work were made with an FGL-1 lamp as the pulsed light source. A photograph of the lamp is shown in Figure 3.1. The lamp is only 5-3/4 inches long, with a maximum diameter of 3/4 inch. The actual light

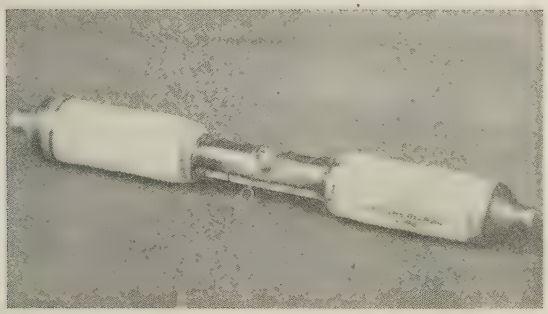

FIG. 3.1—Photograph of Westinghouse lamp FGL-1 (one-half actual size)

source is contained in a clear quartz section, about 40 mm in length and 10 mm outside diameter. The heavy quartz wall of the tubing withstands the high internal gas pressure and temperature developed at high current loading which makes possible the high brilliance of the flash.

The FGL-1 lamp is designed to be operated at approximately 40 flashes per minute at a loading of 50-60 watt sec per flash. Operation at higher voltage was found to lead to an oscillating discharge which was undesirable. Operation of the lamp under these conditions requires a 2,000 to 2,500 volt, 0.1 ampere, dc power-supply and a 2 to 12.5 microfarad discharge condenser. A spark-coil connected to the external helix initiates the discharge. No special cooling is required. On the contrary, the use of a one-per-minute repetition rate made it necessary to install a hot-air blower to keep the lamp warm and dry while exposed to cool night air. Water-vapor condensation on the glass envelope may cause unreliable flashing and possible fracture of the glass envelope.

3.3—EFFECT OF A LIGHT TAIL

If the light source has a long persistence of the order of 10^{-5} to 10^{-6} of its peak intensity, then the light scattered from all but the lowest altitudes is of lower intensity than the light of the afterglow scattered from the low altitudes. Unfortunately, the peak light, scattered from the high altitudes, enters the receiver at the same time as the light of the afterglow scattered from the low altitudes.

3.4—A MODIFIED SINGLE-SITE SYSTEM

It is possible to evade the problem of the lamp afterglow by separating the transmitter and receiver. All of the benefits of a true single-site system, as described in Section I, may be retained if the required separation is less than one kilometer. A separation of 0.5 km, with both stations routinely operated by one man, has been established with the transmitter-station slave controlled by pulses from the receiver site.

The introduction of a base-line separation between the receiver and transmitter results in a minimum altitude from which the back-scattered light may enter the receiver. For a base-line separation of 0.5 km, this minimum altitude corresponds to approximately 12 km. For this altitude, the ratio of scattered light to incident intensity, as shown in Figure 1.1, is 10^{-13}. Thus, if we consider the light intensity of the long-time afterglow to be 10^{-6} of the peak intensity, the intensity of the afterglow light scattered from the intersection altitude will be 10^{-19} of the peak flash intensity. If the reflected light of the tail is to contribute no more than one per cent of the total scattered light, it should be possible to extend measurements to an altitude where the ratio of incident light to scattered light is 10^{-17}. From the Figure 1.1, this corresponds to an altitude of approximately 50 km.

It should be possible to extend the limit imposed by the scattered light of the afterglow by increasing the separation until the limitation on the measurement is imposed by the light of the night sky, rather than the long afterglow of the lamp. Since the intersection altitude, to a first approximation, increases with increasing separation of the transmitter and receiver and the molecular scattering decreases as an exponential function of the altitude, the intensity of the light from the long-time afterglow also decreases exponentially with increasing separation. It should be possible to eliminate the effect of the long-time afterglow by a separation of transmitter and receiver that still retains the operational advantages of the single-site system.

3.5—THE DYNAMIC RANGE OF THE RECEIVER AND THE MODIFIED SINGLE-SITE SYSTEM

It was shown in Section 1.3 that the expected signal from reflection of the upper atmosphere covers a dynamic range of 10 orders of magnitude from the earth's surface up to 60 km. On the other hand, since most of the attenuation is in the lower altitudes, this dynamic range is reduced to four orders of magnitude from 15 to 60 km.

It was stated that the dynamic range of the logarithmic receiver is four or five orders of magnitude. Thus, if it is desired to obtain the density profile up to 60 km, it is necessary that the largest signal entering the receiver start from a minimum altitude of 15 km. A modified single-site system is dictated by this consideration in addition to the previously described issue of the light tail.

3.6—EXPERIMENTAL PROGRAM

To evaluate the modified single-site system, three base-line separations were used. At the first site, the receiver and transmitter were located side by side. The

second site had a base-line separation of 0.17 km. The third site had a base-line separation of 0.5 km.

At the time measurements were taken at the first site, a question of oscillations in the lamp discharge arose. Thus, all the data from this site, which contained deviations from a density profile that could be attributed to the effect of afterglow, could be partially explained by oscillations in the lamp. By the time the second site had been established, the oscillation difficulties in the lamp were clarified and removed, and the results obtained from this site are discussed later.

The present method of analyzing the data makes direct use of equation (6) in Section I. Each signal pulse, which is a deflection representing the log of the light intensity, is projected onto a linear millimeter scale. The ordinate for each of the 10-μsec markers is plotted against time, as shown in Figures 4.1 and 4.4. The ordinate scale cannot be arbitrarily chosen. It is determined by means of a calibration curve, which represents the linearity of the receiver over four decades of light intensity. Since the same deflection sensitivity (of the record oscilloscope) was maintained for both the signal and calibration pulse, the ordinate scale of the calibration curve was superimposed on the data signal curve, matching the zero or minimum light level of the calibration curve with the minimum light level of the signal as obtained by dark capping the photomultiplier.

The relative ordinate values of each 10-μsec marker were read graphically and tabulated. The molecular density is obtained by normalizing to a reference density for an altitude just above the intersection altitude of the transmitter beam and the receiver acceptance cone. Ordinarily, the density of the reference altitude is supplied by radiosonde data.

SECTION IV—RESULTS AND CONCLUSIONS

4.1—OBSERVATION PERIODS

The instrument described in Section II was installed at Sacramento Peak, Sunspot, New Mexico, during the month of August, 1955. Density profile measurements were made during the dark moon periods of August through December, 1955. Over 8,000 profiles were compiled during this period, as compared to the less than 100 profiles obtained by all previous investigators utilizing searchlight techniques.

4.2—DENSITY PROFILES

A radiosonde measurement was not available for the evening of December 15, 1955. Therefore, it was necessary to use an average value obtained from previous results shown in Figure 4.3. The calculated densities for December 15, 1955, are plotted in Figure 4.5.

The process of obtaining the molecular densities following the method described is tedious. Some selection of the signal profiles may be made, since atmospheric conditions from night to night, or even during a single night, will permit the obtaining of data from the higher altitudes. For example, the results of December 15, 1955, extend to 41 km, as compared to only 36 km on the night of September 13, 1955. Superimposed on this last curve are the data of Elterman for the same

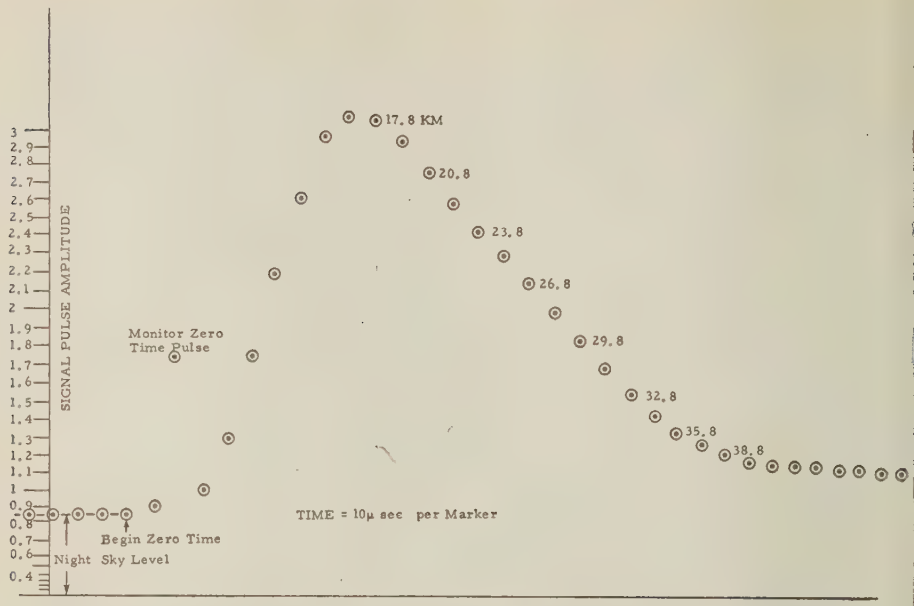

FIG. 4.1—Data curve, September 13, 1955 (elevation 2.8 km, site separation 0.17 km)

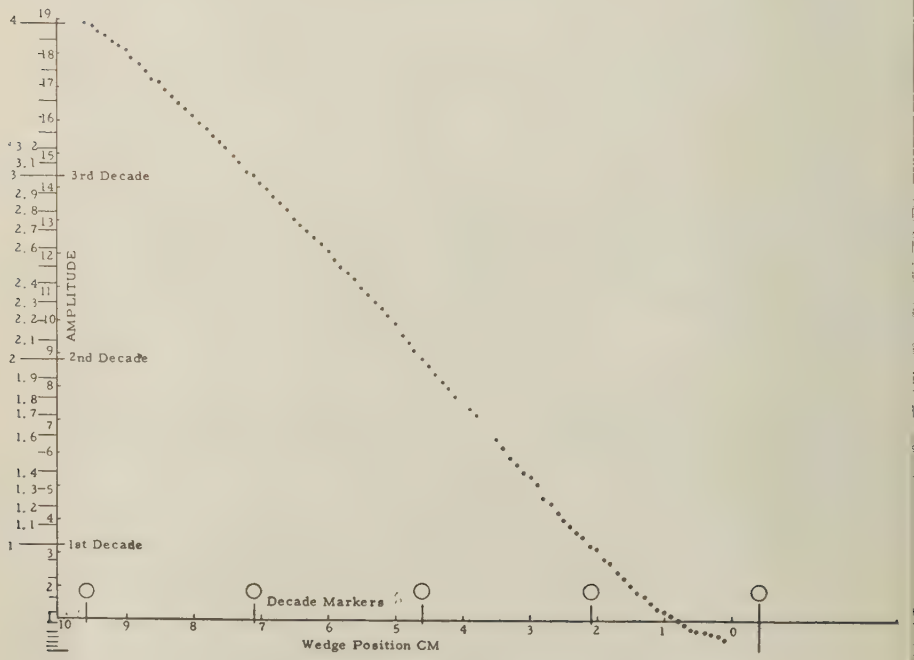

FIG. 4.2—Calibration curve, September 13, 1955

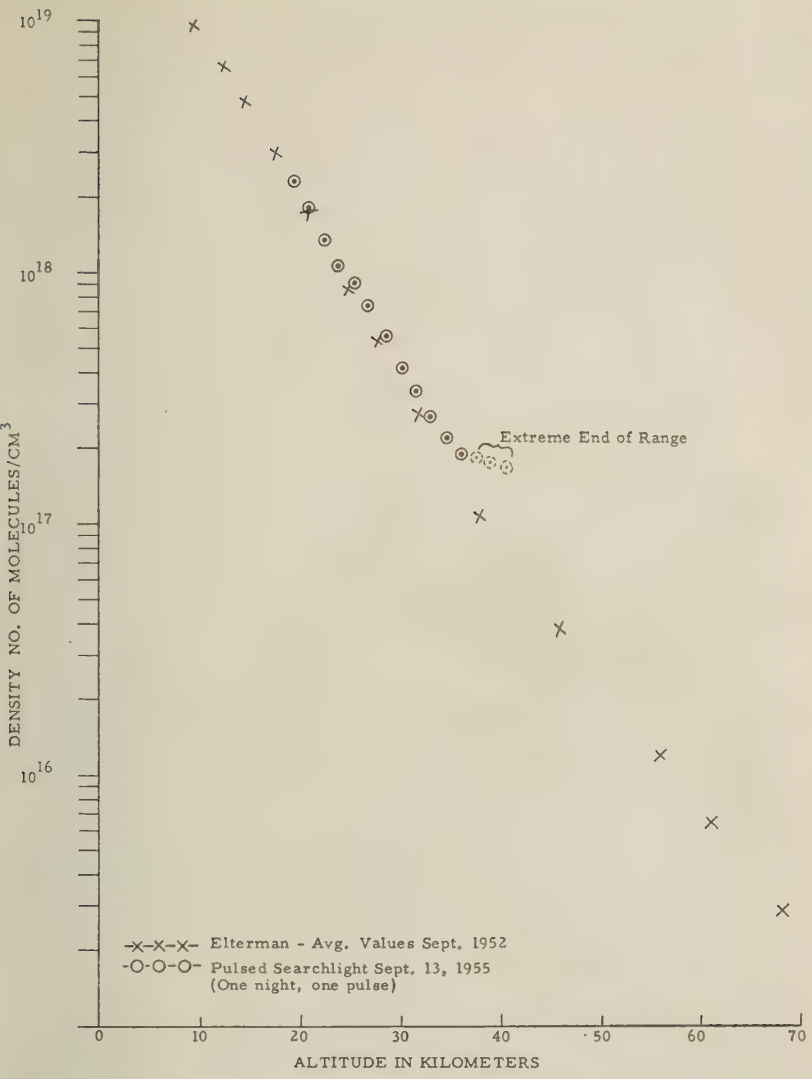

FIG. 4.3—Density profile, September 13, 1955

period in New Mexico in 1952. Note that the December data show considerably lower densities at the higher altitudes.

4.3—COMMENTS ON THE RESULTS

The results described in the previous subsection indicate that the single-pulse light system produces results which are in agreement with previous investigators and theoretical calculations. Data up to an altitude of 41 km were obtained during the observation period of December, 1955. It is felt that with a better procedure

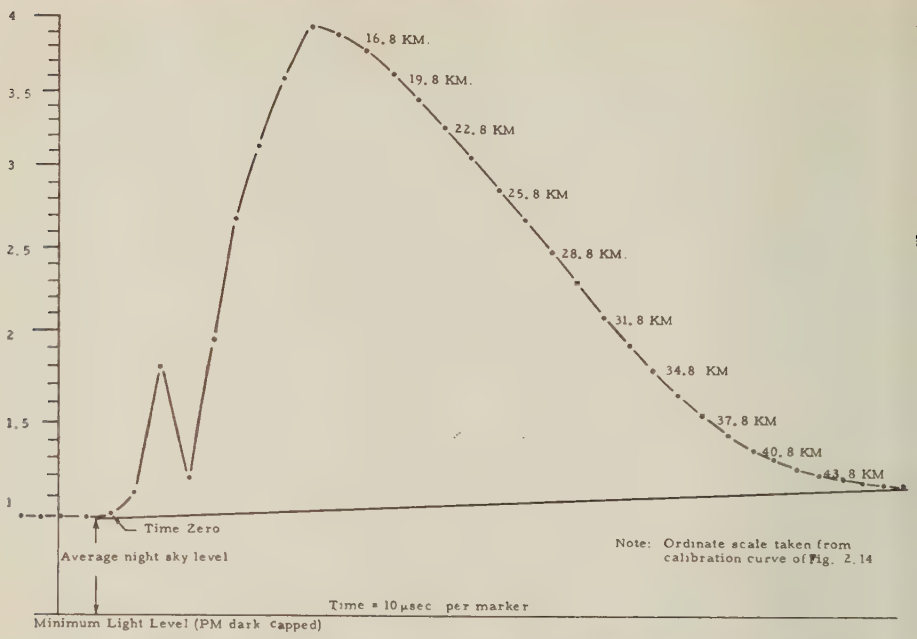

FIG. 4.4 Data curve, December 15, 1955 (elevation 2.8 km, site separation 0.5 km)

for alignment of the mirrors, including concrete mounting platforms for the searchlights, still higher altitudes could be obtained without any additional modification to the equipment. The objective of single-site operation has been accomplished and it should be noted that all the observations during the month of December were made by one technical operator.

The required separation of 0.2 to 0.5 km is necessary for two reasons; one, to put the signal within the dynamic range of the receiver, and, two, to overcome the effect of the light tail. At the present time, it is felt that any effort to obtain a true single-site system is not in order because of the ease and facility of establishing the present type of station.

4.4—EXPERIMENTAL STUDIES OF THE EFFECT OF THE LIGHT TAIL

Figures 4.2 and 4.5 show the effect on the received signal as the receiving cone is inclined toward and away from the transmitting cone. As the receiver is inclined toward the transmitter, the effect is to lower the intersection altitude and thus to enhance the effect of the lamp afterglow. The presence of a second peak on the density profile curve as the angle is increased is attributed, at the time of this writing, to the afterglow. The absence of such a peak when the two mirror axes are vertical and when the receiver is inclined away from the transmitter tends to substantiate this point of view.

4.5—MULTIPLE SCATTERING

The possibility of light undergoing multiple scattering and producing a signal in the receiver from low altitudes, at a time when the principal signal is entering

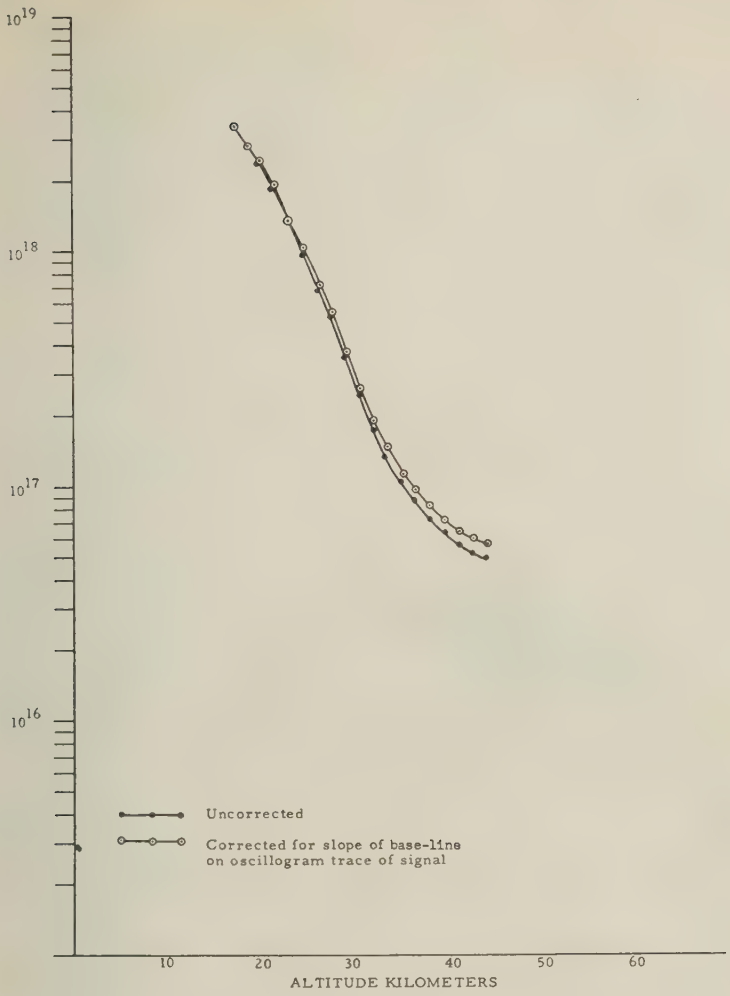

FIG. 4.5—Density profile, December 15, 1955

from higher altitudes, has been considered. The effect of secondary and tertiary scattering is to introduce a multiplying factor, since the Rayleigh formula accounts for primary scattering only. Synge [1] has shown that secondary and tertiary scattering becomes significant for altitudes above 50 km. Experimentally, as shown in Figure 4.9, where the receiver cone and transmitter cone just miss having any overlap, the signal obtained, which must be entirely due to scattering, is less than one per cent of the normal signal.

4.6—NEW LIGHT SOURCES

Much effort has been made during the past few years to develop light sources of higher intensity and shorter duration. Unfortunately, such development pro-

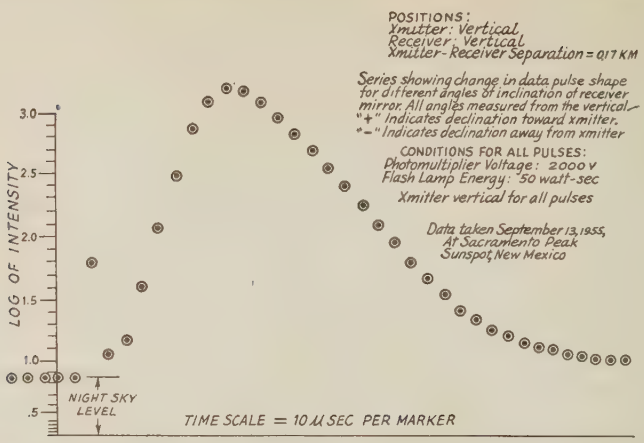

FIG. 4.6—Figures 4.6, 4.7, 4.8, and 4.9 are in sequence, showing change in data pulse shape for different angles of inclination of receiver mirror

grams have not been described in the unclassified literature, and it is only recently that we have been made aware of their existence. Quantitative information concerning the relative merit of these lamps is not available, but indications are that the improvement they may offer over the FGL-1 would introduce considerable gain in altitude. The first step in future efforts for searchlight measurements should therefore include an investigation and experimentation with the new sources.

4.7—USE OF FILTERS TO OBTAIN HIGHER ALTITUDES

Consideration has been given to the measurement of the spectral energy distribution of visible light scattered by the upper atmosphere. The purpose of such an experiment would be to determine if the light scattered for each wavelength follows the Rayleigh law. Deviations, if observed, could be used to say

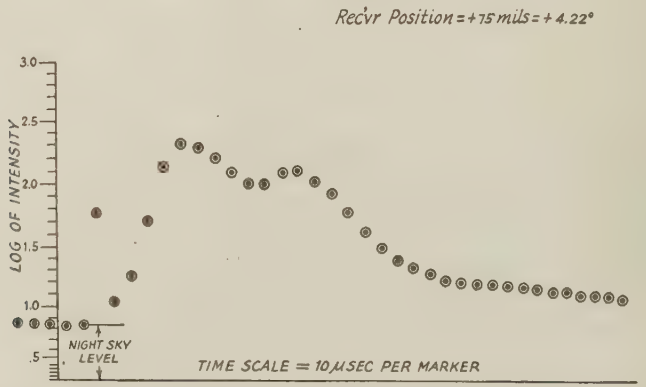

FIG. 4.7—Figures 4.6, 4.7, 4.8, and 4.9 are in sequence, showing change in data pulse shape for different angles of inclination of receiver mirror

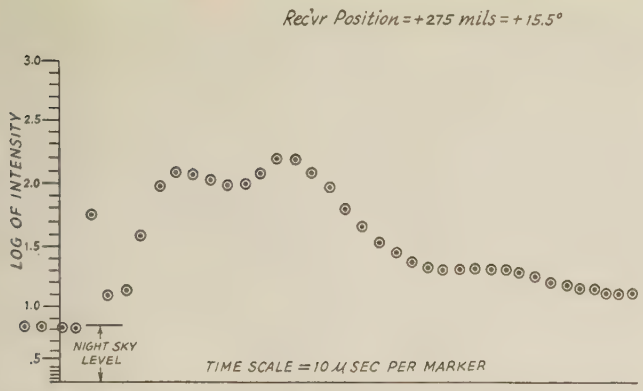

FIG. 4.8—Figures 4.6, 4.7, 4.8, and 4.9 are in sequence, showing change in data pulse shape for different angles of inclination of receiver mirror

something about the size of the molecules. Further, it may be possible to determine what wavelengths are best for measuring the density profile, and thus influence the design of the light source.

Results of some preliminary measurements using Kodak Wratten filters are shown in Figures 4.6 and 4.7. In Figures 4.6 an unfiltered signal pulse is compared with one taken a short time later on the same night with a Kodak Wratten filter No. 12. The two outstanding differences, in amplitude and night sky level, are easily explained by comparing the FGL-1 emission spectrum (Figure 3.2*b*) with the spectrophotometric absorption curve of the No. 12 filter.* The No. 12 filter has a sharp cut-off at 5000A, absorbing nearly all wavelengths in the blue and ultraviolet region. It has a transmittance of 91 per cent or better from 5080A to the infrared. Since the maximum of the FGL-1 emission spectrum occurs in the band 4300A to 4600A, the signal pulse amplitude is severely attenuated. The

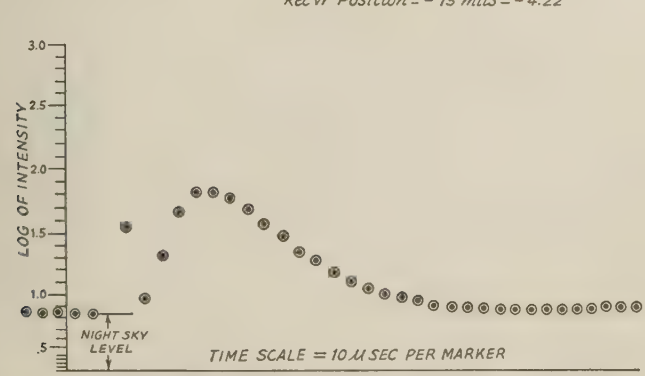

FIG. 4.9—Figures 4.6, 4.7, 4.9, and 4.9 are in sequence, showing change in data pulse shape for different angles of inclination of receiver mirror

*"Kodak Wratten Filters," 18th ed., Eastman Kodak Company, Rochester, N.Y.

major contributions to the night sky emission, which also occur in the visible blue and ultraviolet (excluding the infrared, to which the photomultiplier is not sensitive) will likewise be attenuated.

The effect of using a Kodak Wratten filter No. 47B is shown in Figure 4.11. A spectrophotometric absorption curve of the No. 47B filter shows a central maximum at 4300A with a transmittance of 50 per cent. Hence the signal pulse amplitude is not attenuated as severely as it was with the No. 12 filter, while the night sky level is reduced by nearly the same amount.

The conclusion is that a net gain in altitude can be expected with the use of an ideal filter which has a band pass wide enough to transmit the peak emission bank of the light source with nearly 100 per cent transmittance and yet narrow enough to eliminate most of the night sky emission.

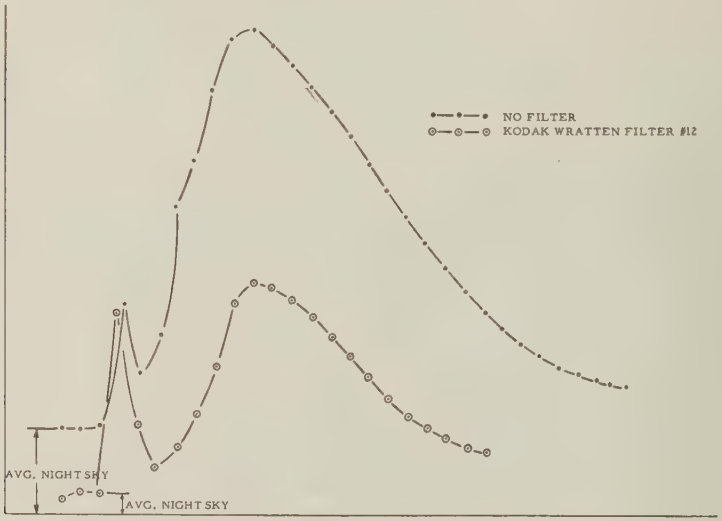

FIG. 4.10—Effect of Kodak Wratten filter No. 12 on density profile data

4.8—NIGHT SKY, NOISE, SIGNAL TO NOISE, AND INTEGRATION

By averaging over a number of observations, it is possible to measure a signal in the presence of noise of comparable amplitude to the signal being measured. This may be demonstrated as follows: Let I_0 be the intensity of the light source. Then the intensity of the beam at an altitude h will be $I_0\ T/h^2$, where T is the fractional transmission for altitude h. If σ is the attenuation coefficient, then

$$T = e^{-\tau} \quad \text{where} \quad \tau = \int_0^h \sigma\, dh$$

If ρ is the coefficient for back-scattering of the air at the altitude h, then the magnitude of the light signal reaching the receiver is

$$\frac{I_0 T \rho}{4\pi h^4}$$

If a is the size of the receiver mirror and S is the photocell sensitivity in amp/lumen, we obtain for the current in the phototube

$$I = \frac{I_0 T \rho a S}{4\pi h^4}$$

The signal in the phototube due to the light of the night sky may be obtained in a similar way. If the light of the night sky has a level of L lumens/unit area, then photocell current is

$$I_e = LaS$$

The r.m.s. fluctuation noise current may be calculated from

$$i_n = (2eI_e \delta f)^{1/2}$$

where e is the electronic charge and δf is the receiver band-width. The signal-to-noise current is, therefore,

$$\frac{I}{i_n} = \frac{I_0 T \rho a S}{4\pi h^4} \cdot \frac{1}{(2eI_e \delta f)^{1/2}}$$

We must note that storing, or integrating many signals over a period of time, reduces the band-width requirements of the system and therefore the background noise improves. This follows directly from the considerations used in radar techniques [9] to enhance the signal-to-noise ratio. It is shown that the gain in signal-to-noise ratio is proportional to $n^{1/2}$, where n is the number of pulses that are used in the integration.

The problem of integration directly involves data handling. Let us consider a bank of condensers, one for each measurable increment of altitude. Consider a light source emitting n pulses per second. As the light signal enters the receiver,

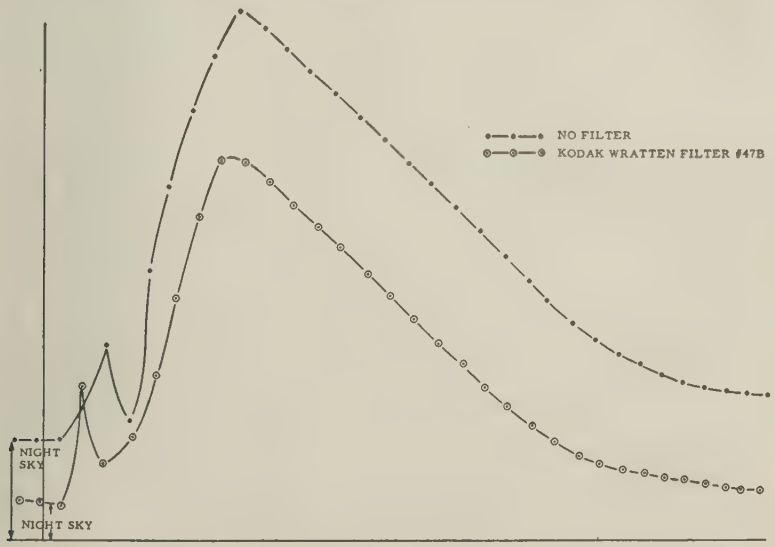

FIG. 4.11—Effect of Kodak Wratten filter No. 47B on density profile data

the condensers in the bank are gated on in succession in such a way that each condenser obtains charge, from successive flashes, from only one altitude. The potential difference across each condenser is proportional to the summed signal from the altitude to which it has been gated, but the signal-to-noise ratio has been aided by the method described above. At this point, simple read-out methods could be utilized, the proper ratios automatically computed, the calibration information supplied to a computer, together with a radiosonde reference point, and the density profile printed out.

ACKNOWLEDGMENTS

We wish to express our thanks to Dr. J. Evans and the staff of the Air Force Observatory at Sacramento Peak, Sunspot, New Mexico, for their hospitality and many kindnesses during our stay there.

We wish to acknowledge the assistance of Mr. Jack Sherman for the construction of most of the electronics and assistance in development of some of the circuitry.

We further wish to thank Dr. Henry S. Katzenstein for many suggestions and assistance in the instrumentation during the early stages of this work.

References

[1] E. H. Synge, A method of investigating the higher atmosphere, Phil. Mag., **9**, 1014 (1930).
[2] E. O. Hulburt, Observations of a searchlight beam to an altitude of 28 kilometers, J. Optical Soc. Amer., **27**, 377-382 (1937).
[3] E. A. Johnson, R. C. Meyer, R. E. Hopkins, and W. H. Mock, The measurement of light scattered by the upper atmosphere from a search-light beam, J. Optical Soc. Amer., **29**, 512-517 (1939).
[4] L. Elterman, Seasonal trends of temperature, density and pressure in the stratosphere obtained with the searchlight probing technique, Air Force Cambridge Research Center, Cambridge, Massachusetts, Geophysical Research Paper No. 29 (1954).
[5] J. R. Bauer and J. Katzenstein, State of the earth's atmosphere in the arctic, Reports 9-14.
[6] Johnson and Jones, Radar Research and Development Establishment, Malvern, England. Report No. 367.
[7] Private communication.
[8] Papers given at the Optical Pulse Ranging Conference on January 12 and 13, 1956, at the Air Force Cambridge Research Center.
[9] L. N. Ridenour, Radar system engineering, McGraw-Hill Book Co., Inc., New York (1947). [M.I.T. Radiation Laboratory, Vol. 1.]

MEAN RESULTS OF GEOMAGNETIC OBSERVATIONS IN TROMSØ, NORWAY, FOR THE YEARS 1930–50

By John Frøshaug

Roald Amundsenveien 16, Ålesund, Norway.

(Received February 17, 1956)

ABSTRACT

Graphs showing variations in the earth's magnetic field over short and long time-intervals and analyses of the field are presented for Tromsø, Norway, years 1930–50.

The following Tables and Figures give mean values of the results of the geomagnetic observations at the Auroral Observatory, Tromsø, Norway, for the years 1930–50, as they were given in the year-books, to which we refer for definitions and details. They are published in "Publikasjoner fra Det Norske Institutt for Kosmisk Fysikk." The instrumental equipment used for geomagnetic measurements are described in Nos. 1 and 33, and the definition of the storminess and the method of separation are given in Nos. 2 and 4. The terminology does not depart noteworthily from that commonly in use, except for the word "storminess," the definition of which is quite the same as for "magnetic disturbance D" in Chapman and Bartels' "Geomagnetism," page 195.

It should be noted that the determination of the solar daily variation S_q is based on a choice of quiet hours and not on international quiet days. Further, in the year-books of Tromsø, the sign + is used for westerly declination. In the following Tables and Figures, the signs have been changed in accordance with the customary use, so that + means easterly declination.

During the years 1937–46, no base-line determinations for the Z component were made, because the Observatory did not have at its disposal reliable instruments for that purpose. From 1949, regular determinations were made by means of the instruments BMZ 39 and BMZ 57. Fortunately, the base-line values of the Observatory remain quite constant, and during the above-mentioned period the base-line estimates may be regarded as good. The Z determined by BMZ 39 in 1949 showed 20γ less than previously estimated.

The D and H base-lines have been regularly determined during the years.

The geographical coordinates of the Auroral Observatory in Tromsø are $\varphi = 69° 39'.8$ north and $\lambda = 18° 56'.9$ east; the geomagnetic latitude is 67°.1.

The Observatory is indebted to Norges Almenvitenskapelige Forskningsråd for financial support in the preparation of the Table and Figures.

Resuming Tables.

Diurnal Variation.
QUIET VALUES.

TABLE I

Tromsø.

Declination. Unit Gamma.

GR. M. T.

1931-50	0	1	2	3	4	5	6	7	8	9	10	11	12	13	14	15	16	17	18	19	20	21	22	23	24
JANUARY	+3	+3	+3	+3	+3	+3	+2	+1	0	-1	-3	-5	-5	-5	-5	-4	-3	-2	-1	-0	+2	+2	+3	+3	
FEBRUARY	+3	+3	+4	+4	+4	+4	+5	+4	+2	0	-3	-5	-7	-7	-6	-4	+4	-4	-3	-1	0	+2	+2	+3	
MARCH	+3	+4	+6	+8	+9	+10	+10	+8	+5	0	-6	-10	-12	-11	-9	-7	-5	-4	-3	-2	-1	0	+1	+2	
APRIL	+5	+7	+10	+13	+16	+17	+17	+14	+9	0	-8	-14	-17	-16	-13	-9	-7	-6	-6	-5	-4	-2	0	+3	
MAY	+8	+13	+17	+21	+22	+22	+19	+14	+7	-3	-12	-19	-21	-19	-16	-14	-12	-11	-11	-10	-7	-4	0	+4	
JUNE	+11	+14	+20	+23	+26	+25	+21	+15	+8	-2	-11	-17	-21	-20	-18	-16	-14	-13	-13	-12	-9	-5	0	+6	
JULY	+11	+15	+19	+20	+25	+24	+23	+17	+10	+1	-9	-18	-22	-22	-20	-17	-14	-14	-13	-12	-9	-5	0	+6	
AUGUST	+9	+13	+16	+20	+22	+22	+20	+14	+6	-3	-12	-19	-21	-19	-16	-13	-11	-10	-10	-9	-6	-2	+2	+5	
SEPTEMBER	+8	+10	+12	+14	+16	+16	+13	+10	+5	-2	-10	-15	-17	-16	-13	-10	-8	-7	-6	-5	-3	0	+2	+5	
OCTOBER	+5	+5	+7	+8	+8	+9	+8	+6	+3	-2	-7	-10	-11	-10	-8	-6	-6	-5	-4	-2	0	+2	+3	+5	
NOVEMBER	+4	+4	+4	+5	+5	+5	+4	+3	+1	-2	-5	-6	-7	-7	-6	-5	-4	-3	-2	-1	+1	+3	+4	+5	
DECEMBER	+3	+3	+3	+3	+3	+3	+2	0	+1	-2	-4	-5	-6	-5	-4	-3	-3	-1	0	+1	+2	+3	+3	+4	
MEAN	+6	+8	+10	+12	+13	+13	+12	+9	+5	-1	-8	-12	-14	-13	-11	-9	-8	-7	-6	-5	-3	-1	+2	+4	

Horizontal Intensity. Unit Gamma.

JANUARY	-2	-1	0	1	2	2	1	0	-2	-3	-4	-3	-2	0	1	1	2	2	2	2	1	0	-2	-2	
FEBRUARY	0	1	2	3	3	3	1	-1	-3	-6	-8	-7	-5	-3	-1	1	3	3	4	3	2	1	0	-1	
MARCH	2	3	4	5	6	4	1	-4	-9	-14	-16	-14	-10	-6	-1	2	5	7	8	7	7	5	4	3	
APRIL	5	6	7	7	5	2	-3	-10	-17	-22	-23	-19	-13	-6	-1	4	9	12	13	12	10	8	6	5	
MAY	6	7	8	7	3	-1	-7	-13	-19	-23	-23	-17	-10	-3	2	6	10	12	14	13	11	8	7	5	
JUNE	6	7	8	7	4	-2	-8	-15	-20	-24	-23	-18	-10	-3	3	8	11	14	14	13	11	8	6	5	
JULY	6	8	8	6	3	-2	-8	-15	-20	-24	-23	-18	-12	-4	1	7	10	13	15	14	12	9	7	5	
AUGUST	4	6	7	7	4	0	-6	-13	-19	-23	-23	-17	-10	-3	3	7	10	12	13	13	11	8	6	4	
SEPTEMBER	5	6	7	6	5	1	-3	-9	-15	-20	-20	-16	-10	-5	0	3	7	10	11	11	10	8	6	4	
OCTOBER	3	4	5	5	5	4	0	-5	-10	-14	-16	-14	-10	-6	-2	2	5	7	8	9	7	6	4	3	
NOVEMBER	-1	0	2	3	4	3	2	-1	-4	-7	-9	-7	-4	-1	1	3	4	4	4	4	3	2	0	-1	
DECEMBER	-2	-1	0	1	2	2	1	0	-2	-3	-4	-3	-2	0	-1	2	3	3	3	2	-1	-1	-2	-2	
MEAN	3	4	5	5	4	1	-2	-8	-12	-17	-18	-13	-8	-3	0	4	7	8	9	8	7	5	3	2	

Vertical Intensity. Unit Gamma.

JANUARY	-3	-3	-2	-3	-3	-3	-4	-3	-2	-1	0	1	3	4	4	4	3	3	2	1	0	-1	-2	-3	
FEBRUARY	-4	-3	-3	-3	-3	-3	-3	-2	-1	-1	1	2	3	4	5	4	4	3	2	1	0	-1	-3	-4	
MARCH	-2	-2	-2	-2	-2	-2	-2	-2	-1	0	1	2	3	4	4	4	3	3	2	0	-1	-2	-3	-3	
APRIL	-2	-2	0	0	-1	-2	-2	-2	-1	0	0	1	3	3	4	4	3	2	1	-1	-2	-3	-3	-3	
MAY	-1	0	0	0	0	-1	-3	-3	-3	-3	-2	-1	1	2	3	4	4	4	3	2	1	0	-1	-1	
JUNE	-1	-1	0	-1	-1	-2	-3	-3	-3	-3	-2	-1	0	1	3	4	4	4	2	1	0	-1	-1	-2	
JULY	-1	-1	0	-0	-1	-1	-2	-3	-3	-2	-2	-2	-1	1	3	4	4	3	3	3	0	-1	-1	-2	
AUGUST	-1	0	0	1	0	-1	-2	-3	-4	-3	-2	-1	0	2	2	4	4	4	2	1	0	-2	-2	-3	
SEPTEMBER	-3	-2	-1	0	-1	-1	-2	-1	-1	0	0	1	2	3	4	4	3	2	1	0	-2	-3	-3	-4	
OCTOBER	-3	-2	-2	-1	-2	-2	-2	-2	-1	1	1	2	3	4	4	4	4	3	2	1	0	-1	-2	-3	
NOVEMBER	-2	-2	-2	-2	-3	-3	-3	-3	-2	-1	0	2	3	4	4	4	4	3	3	2	0	-1	-2	-3	
DECEMBER	-2	-2	-2	-2	-2	-3	-3	-3	-2	-1	0	2	3	4	4	4	3	3	2	2	1	0	-1	-2	-3
MEAN	-2	-2	-1	-1	-2	-2	-3	-2	-2	-1	0	1	2	3	4	4	4	3	2	1	0	-1	-2	-3	

Monthly Means.

DECLINATION	JAN	FEB	MAR	APR	MAY	JUN	JUL	AUG	SEP	OCT	NOV	DEC	MEAN
DIRECT VALUES, DEPARTURES FROM SECULAR VAR.	-0'.3	+0'.7	+0'.4	+0'.5	-0'.6	-1'.1	+0'.7	-0'.5	+0'.1	+0'.6	+0'.6	-0'.1	0'.0
QUIET VALUES, DEPARTURES FROM SECULAR VAR.	-0'.3	-0'.3	-0'.1	+0'.1	+0'.1	-0'.4	+0'.2	-0'.1	-0'.1	+0'.1	+0'.4	+0'.1	0'.0
RANGE (UNIT MINUTES) FROM 0 H TO 24 H GMT.	77	84	105	99	94	81	86	81	92	101	73	76	87
QUIET RANGE (UNIT γ) FROM 0 H TO 24 H GMT.	11	10	22	34	43	46	47	42	33	19	13	11	29
STORMINESS ("ALL DAYS MINUS QUIET DAYS")	+4	+4	+7	+5	+3	+2	+1	+2	+4	+6	+5	+3	+4
ABSOLUTE STORMINESS (UNIT γ) DIURNAL SUM	304	365	466	446	440	402	267	380	416	409	309	286	377
HORIZONTAL INTENSITY													
DIRECT VALUES, DEPARTURES FROM SECULAR VAR.	1	0	-12	-6	1	8	12	4	-6	-10	1	6	0
QUIET VALUES, DEPARTURES FROM SECULAR VAR.	-2	+1	-1	-2	0	4	3	0	-2	1	-1	2	0
RANGE (IN γ FROM 0 TO 24 H GMT.)	396	419	519	493	484	422	426	453	485	514	398	379	306
QUIET RANGE (IN γ FROM 0 TO 24 H GMT.)	9	14	25	37	40	40	40	39	33	24	14	8	28
STORMINESS ("ALL DAYS MINUS QUIET DAYS")	-13	-16	-26	-20	-15	-8	-7	-11	-20	-24	-14	-10	-15
ABSOLUTE STORMINESS, DIURNAL SUM	851	1027	1461	1418	1321	1258	1211	1238	1397	1361	983	815	1208
VERTICAL INTENSITY													
DIRECT VALUES, DEPARTURES FROM SECULAR VAR.	-9	-8	-1	6	5	2	2	4	5	4	-3	-8	0
QUIET VALUES, DEPARTURES FROM SECULAR VAR.	-3	-4	-2	2	1	0	0	0	1	4	1	-2	0
RANGE (IN γ FROM 0 TO 24 H GMT.)	261	290	328	321	302	253	254	271	332	348	277	260	288
QUIET RANGE (IN γ FROM 0 TO 24 H GMT.)	10	11	10	9	11	11	11	11	11	10	9	9	10
STORMINESS ("ALL DAYS MINUS QUIET DAYS")	-5	-3	2	5	5	3	3	5	5	2	-3	-5	1
ABSOLUTE STORMINESS, DIURNAL SUM	513	573	755	692	660	581	582	649	745	731	555	510	630

Resuming Tables. Diurnal Variation. Storminess. TABLE II

Tromsø. Declination. Unit Gamma. GR. M. T.

1930-50	0	1	2	3	4	5	6	7	8	9	10	11	12	13	14	15	16	17	18	19	20	21	22	23	24
JANUARY	+22	+28	+18	+11	+7	+2	-1	-2	-1	0	-1	-2	-4	-4	-4	-4	-6	-5	-4	-0	+4	+10	+18	+19	
FEBRUARY	+27	+29	+28	+20	+11	+4	-1	-2	-2	-2	-3	-6	-7	-9	-8	-7	-8	-11	-5	-3	+3	+13	+20	+26	
MARCH	+37	+40	+37	+28	+17	+7	+4	+2	+3	+2	-1	-5	-7	-10	-10	-10	-11	-11	-10	-6	+4	+17	+25	+31	
APRIL	+35	+38	+35	+24	+14	+7	+4	+3	+2	+1	-2	-5	-7	-11	-13	-16	-17	-17	-16	-12	0	+12	+22	+30	
MAY	+22	+36	+32	+25	+16	+10	+5	+2	0	-2	-3	-5	-7	-10	-13	-15	-18	-21	-20	-16	-9	+3	+16	+24	
JUNE	+27	+36	+33	+23	+13	+6	+4	+4	+3	+2	-2	-3	-6	-9	-12	-15	-18	-20	-21	-16	-12	-4	+8	+15	
JULY	+24	+33	+27	+19	+10	+3	+2	+1	0	+1	-1	-3	-5	-8	-10	-14	-17	-18	-20	-18	-12	-1	+8	+16	
AUGUST	+25	+30	+29	+18	+10	+4	+1	0	+1	+1	0	-3	-5	-8	-12	-13	-15	-15	-15	-13	-6	+2	+12	+21	
SEPTEMBER	+32	+35	+30	+19	+10	+4	+1	0	0	-2	-2	-3	-6	-9	-11	-11	-13	-14	-11	-7	+3	+15	+24	+32	
OCTOBER	+35	+36	+29	+18	+9	+4	+2	0	0	+1	-1	-4	-7	-9	-10	-8	-12	-11	-8	-1	+10	+20	+26	+33	
NOVEMBER	+27	+23	+18	+12	+4	-1	-3	-2	-1	-1	-1	-4	-4	-5	-5	-4	-4	-4	-3	+1	+8	+14	+24	+25	
DECEMBER	+22	+20	+15	+10	+3	-2	-3	-2	-1	-1	-2	-4	-4	-4	-4	-6	-7	-7	-5	-2	+5	+12	+18	+22	
MEAN	+28	+32	+28	-19	+10	+4	+1	0	0	0	-2	-4	-6	-8	-10	-10	-12	-13	-12	-8	0	+10	+18	+25	

Horizontal Intensity. Unit Gamma.

JANUARY	-67	-56	-41	-23	-15	-5	-1	1	1	2	5	9	15	22	27	30	29	22	5	-12	-36	-61	-81	-77	
FEBRUARY	-87	-78	-59	-38	-22	-11	-4	0	3	5	11	17	22	32	41	41	37	27	5	-20	-47	-73	-90	-89	
MARCH	-124	-111	-87	-66	-40	-21	-10	-3	3	10	21	31	40	51	55	52	46	25	-5	-38	-79	-112	-125	-125	
APRIL	-121	-108	-82	-56	-32	-18	-12	-5	3	11	21	33	46	59	63	62	56	36	7	-33	-68	-96	-116	-128	
MAY	-118	-109	-90	-66	-43	-25	-10	-1	5	14	25	36	52	61	68	70	64	50	23	-9	-50	-78	-107	-120	
JUNE	-103	-107	-80	-55	-32	-16	-6	0	4	14	24	35	46	57	66	64	63	51	30	2	-28	-55	-80	-93	
JULY	-100	-92	-68	-44	-27	-18	-9	-4	2	11	22	33	48	62	65	67	60	48	26	3	-29	-57	-79	-92	
AUGUST	-101	-90	-76	-46	-29	-18	-7	-2	4	13	22	32	45	58	68	64	56	42	18	-13	-45	-71	-93	-102	
SEPTEMBER	-109	-102	-76	-49	-28	-15	-6	-1	5	14	19	36	46	55	65	58	46	26	-7	-38	-76	-106	-126	-121	
OCTOBER	-103	-91	-68	-45	-27	-14	-5	2	5	12	24	35	45	51	52	46	31	6	-22	-50	-89	-109	-111	-113	
NOVEMBER	-78	-59	-43	-30	-14	-5	-1	2	6	11	15	20	27	34	38	37	28	12	1	-22	-59	-84	-94	-92	
DECEMBER	-64	-43	-32	-23	-13	-4	0	2	2	5	8	12	18	25	28	32	29	21	10	-12	-35	-59	-76	-77	
MEAN	-96	-85	-65	-44	-26	-14	-6	-1	3	10	18	27	37	46	52	51	45	29	7	-19	-51	-79	-97	-101	

Vertical Intensity. Unit Gamma.

JANUARY	-7	-9	-14	-16	-14	-11	-7	-1	3	5	5	6	6	6	4	1	-7	-13	-12	-15	-11	-7	0	-3	
FEBRUARY	3	-2	-10	-16	-17	-14	-9	-3	-2	5	7	7	6	6	4	-1	-11	-15	-12	-11	-6	4	9	5	
MARCH	20	10	3	-14	-17	-15	-6	0	7	8	6	5	5	3	5	-1	-5	-13	-11	-2	10	16	25	24	
APRIL	21	10	-2	-12	-13	-8	-2	1	4	6	6	5	4	5	3	3	0	-3	-6	1	17	28	33	28	
MAY	21	11	-8	-18	-16	-12	-5	0	4	5	6	9	11	11	10	9	3	-2	-4	-2	12	22	26	25	
JUNE	21	6	-13	-19	-17	-12	-5	0	4	6	7	9	10	10	9	3	1	-1	-3	-1	6	14	23	26	
JULY	16	2	-9	-16	-15	-11	-4	2	5	7	8	11	9	8	9	5	5	1	-3	-1	3	11	15	15	
AUGUST	15	10	-3	-10	-10	-7	-2	3	6	8	9	10	10	8	7	7	5	4	0	2	6	15	23	24	
SEPTEMBER	13	5	-12	-19	-18	-9	-1	3	6	9	9	9	7	6	2	0	-4	-5	1	8	20	31	25	22	
OCTOBER	17	4	-11	-16	-18	-12	-2	2	7	8	8	7	6	3	1	-20	-18	-15	-5	4	20	21	25	24	
NOVEMBER	-3	-10	-14	-17	-16	-10	-2	3	6	8	8	7	5	3	-2	-4	-8	-12	-12	-6	0	4	4	4	
DECEMBER	-4	-10	-14	-15	-15	-11	-5	0	3	5	5	6	7	7	6	-1	-7	-13	-12	-11	-8	-1	2	0	
MEAN	12	2	-11	-16	-18	-13	-5	1	5	7	8	8	7	6	4	0	-6	-8	-8	-4	6	15	19	18	

Yearly Means.

	Declination.		Horizontal Intensity.		Vertical Intensity.		INCLINATION	
YEAR	DIRECT VALUES	QUIET VALUES	DIRECT VALUES	QUIET VALUES	DIRECT VALUES	QUIET VALUES	QUIET VALUES	YEAR
1930	4° 07.7 W	4° 09.5 W	.11567	11595				1930
31	3 59.3	4 01.0	11548	11563	50198	50201	77° 01.7	31
32	3 49.0	3 50.6	11499	11520	50195	50198	77 04.5	32
33	3 37.3	3 38.2	11472	11488	50233	50205	77 06.7	33
34	3 25.9	3 26.3	11441	11452	50223	50226	77 09.3	34
35	3 14.3	3 15.0	11407	11420	50247	50248	77 11.7	35
36	3 04.8	3 05.6	11379	11389	50276	50274	77 14.1	36
37	2 53.7	2 53.6	11350	11368	50308	50302	77 16.5	37
38	2 44.1	2 45.2	11325	11338	50340	50333	77 18.4	38
39	2 35.0	2 36.2	11297	11319	50362	50358	77 20.0	39
40	2 26.6	2 25.2	11278	11294	50381	50383	77 22.0	40
41	2 16.6	2 19.1	11256	11279	50417	50419	77 23.4	41
42	2 10.6	2 11.5	11244	11252	50424	50423	77 24.6	42
43	2 02.5	2 03.9	11222	11245	50449	50446	77 26.1	43
44	1 54.3	1 55.8	11213	11229	50467	50469	77 27.4	44
45	1 45.7	1 47.9	11199	11211	50503	50505	77 29.1	45
46	1 34.6	1 35.2	11179	11193	50554	50551	77 30.9	46
47	1 26.5	1 27.2	11174	11179	50585	50574	77 32.2	47
48	1 18.4	1 19.1	11156	11166	50594	50590	77 32.2	48
49	1 10.5	1 11.5	11153	11164	50612	50608	77 33.6	49
50	1 03.6	1 04.9	11152	11170	50647	50645	77 33.7	50
51	0 54.1	0 56.1	11143	11166	50693	50691	77 34.7	51

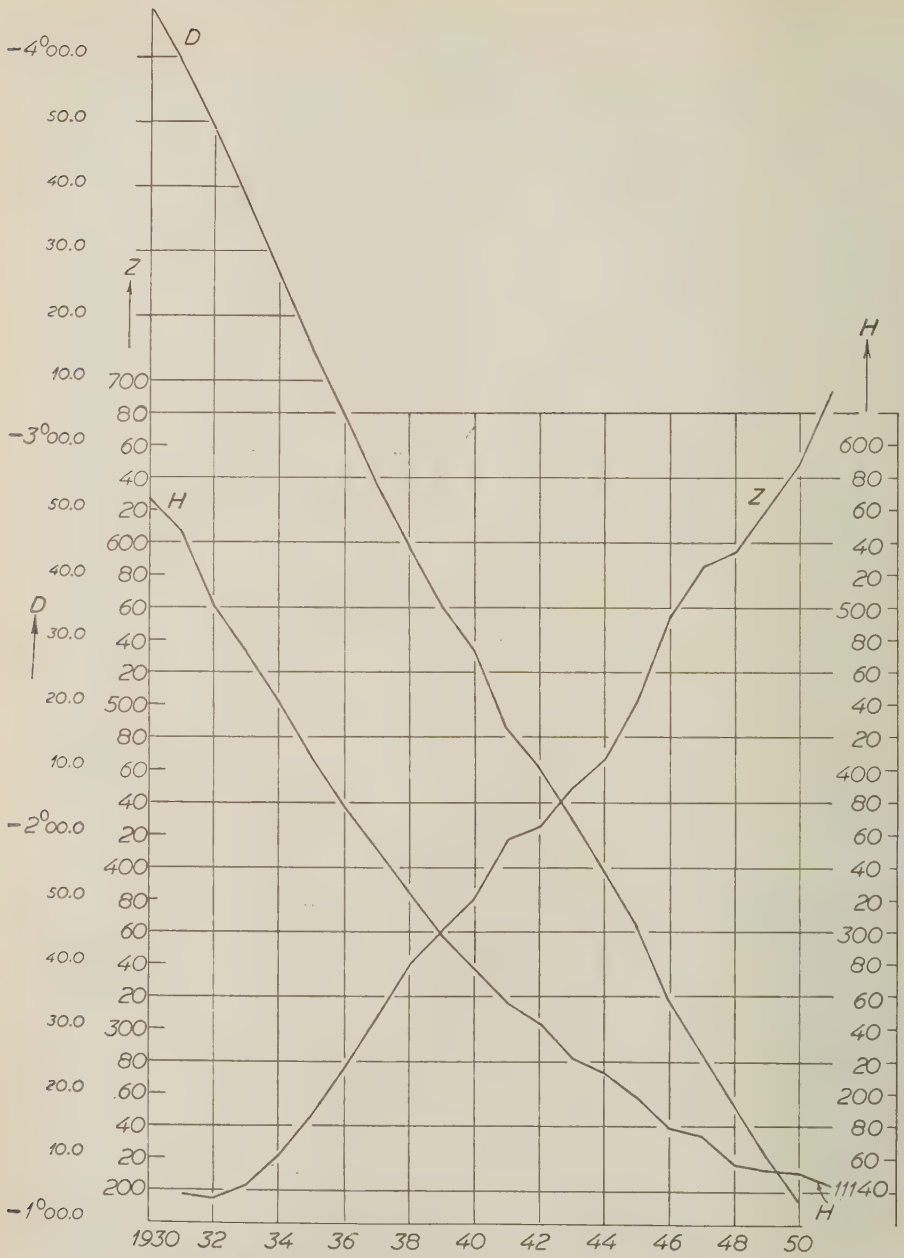

THE SECULAR VARIATION IN D, H, AND Z, 1930 – 1950

FIG. 1

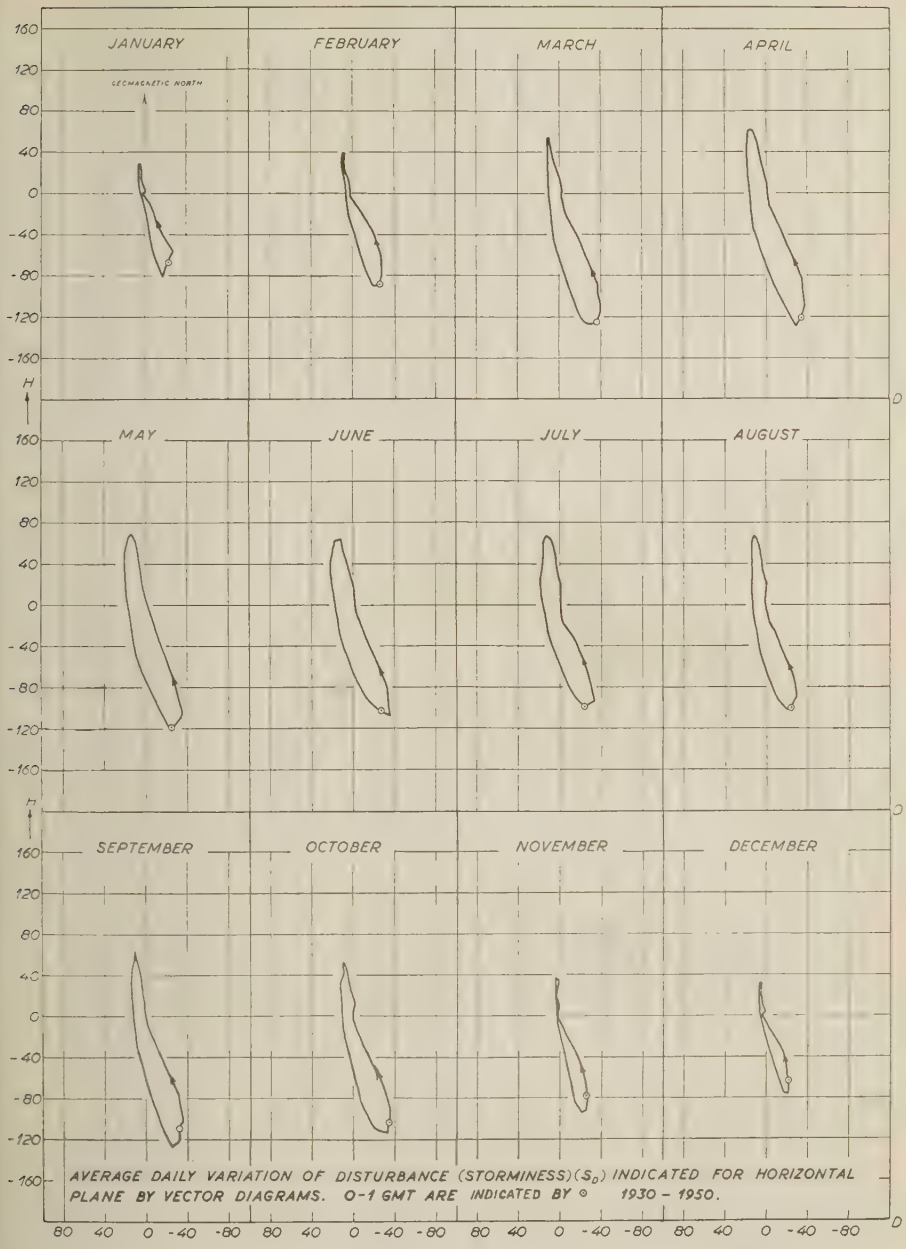

AVERAGE DAILY VARIATION OF DISTURBANCE (STORMINESS) (S_D) INDICATED FOR HORIZONTAL PLANE BY VECTOR DIAGRAMS. 0-1 GMT ARE INDICATED BY ⊙ 1930 – 1950.

FIG. 2

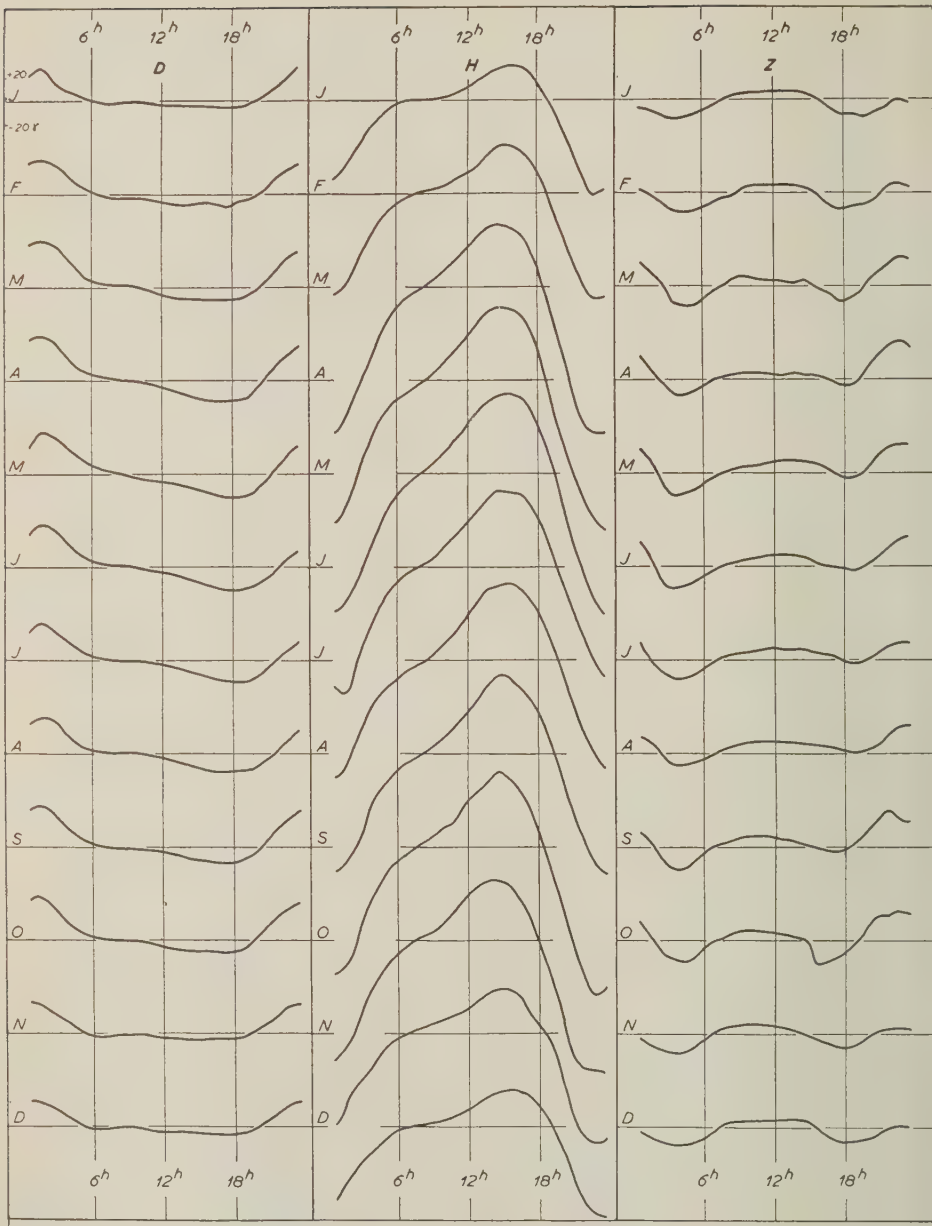

DISTURBANCE DAILY VARIATION OR STORMINESS (S_0), ALL DAYS, 1930–1950

FIG. 3

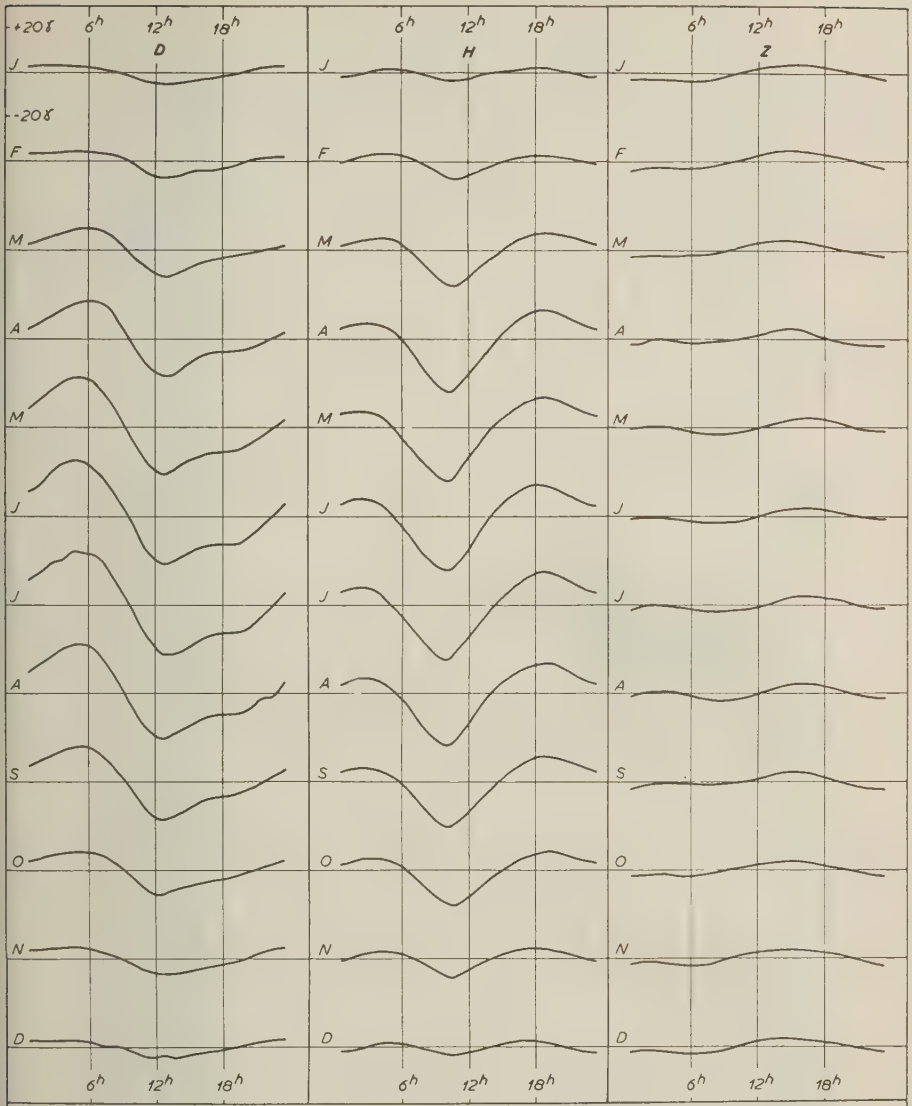

THE QUIET DIURNAL-VARIATION SMOOTHED VALUES, MEANS 1930–1950

FIG. 4

MONTHLY MEANS, STORMINESS 1930 - 1950
(ALL DAYS MINUS QUIET DAYS)

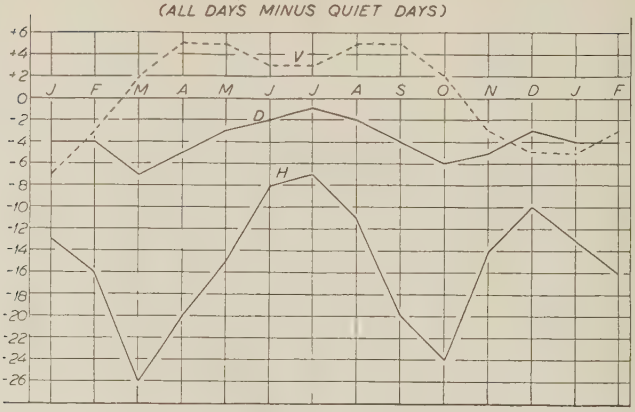

FIG. 5

DAILY RANGE, MONTHLY MEANS 1930 - 1950

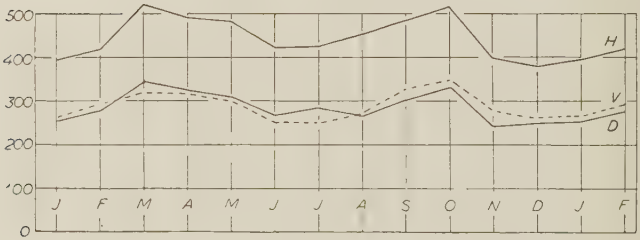

FIG. 6

MEAN DIURNAL SUMS OF ABSOLUTE STORMINESS (ΣAS)
D, H, Z AND RELATIVE SUNSPOT-NUMBERS (S)

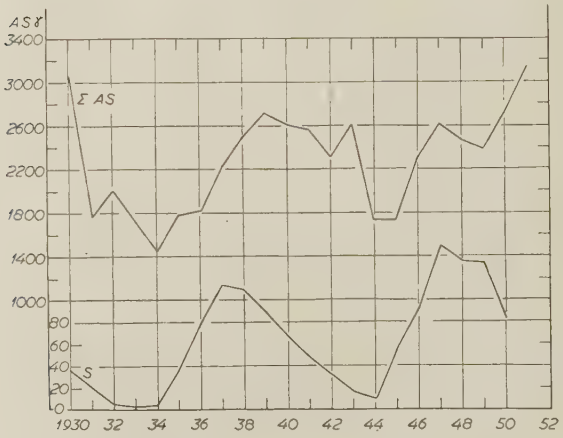

FIG. 7

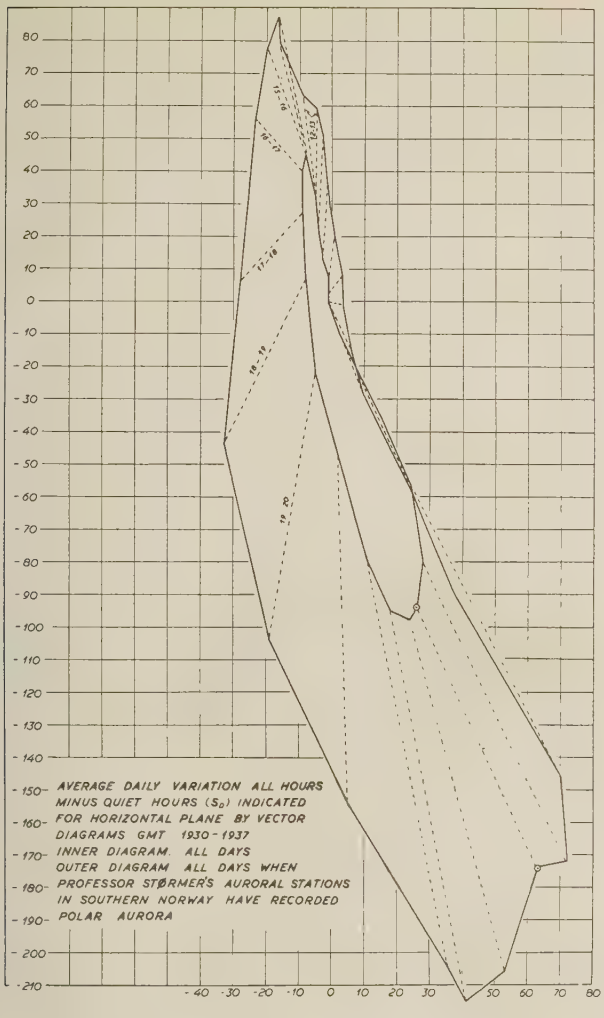
AVERAGE DAILY VARIATION ALL HOURS
MINUS QUIET HOURS (S_D) INDICATED
FOR HORIZONTAL PLANE BY VECTOR
DIAGRAMS GMT 1930-1937
INNER DIAGRAM. ALL DAYS
OUTER DIAGRAM ALL DAYS WHEN
PROFESSOR STØRMER'S AURORAL STATIONS
IN SOUTHERN NORWAY HAVE RECORDED
POLAR AURORA

FIG 8

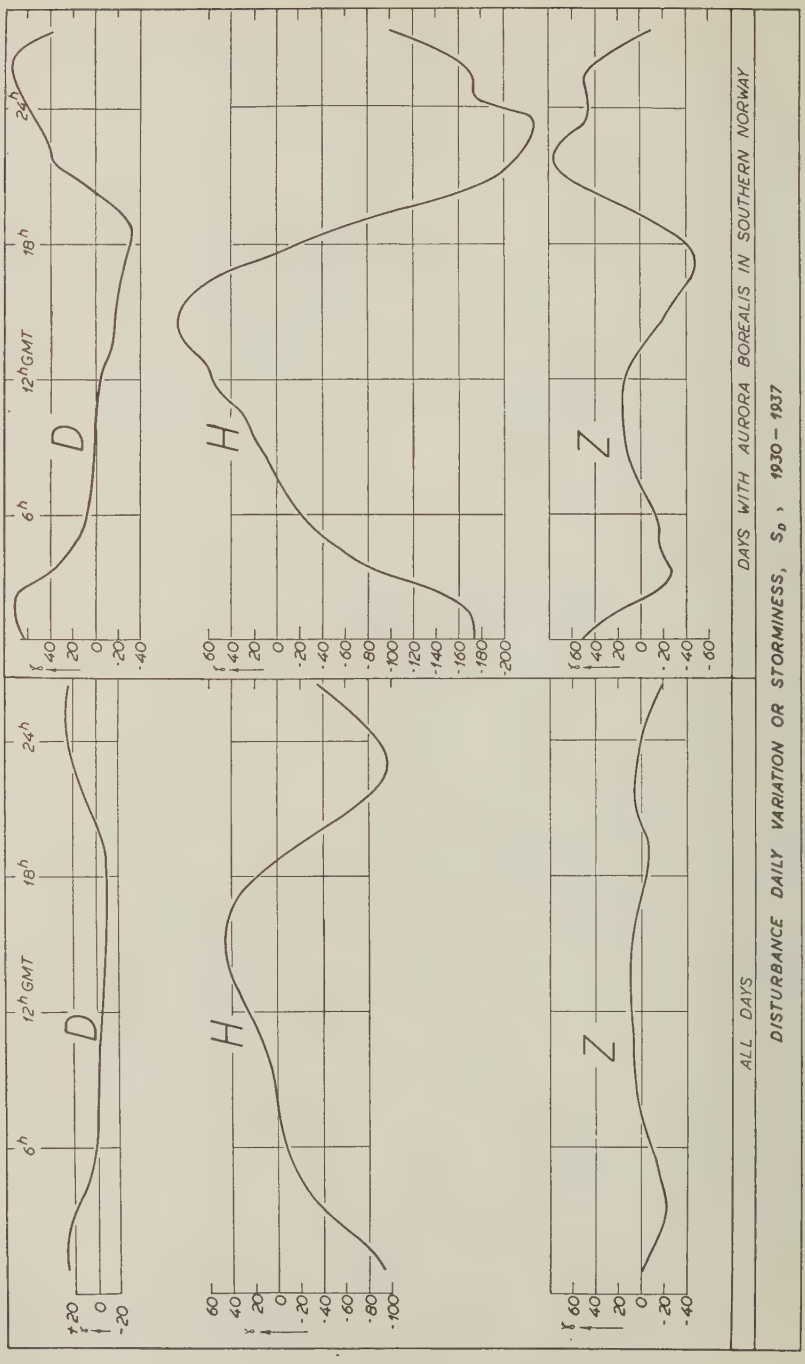
DISTURBANCE DAILY VARIATION OR STORMINESS, S_D, 1930 – 1937
ALL DAYS
DAYS WITH AURORA BOREALIS IN SOUTHERN NORWAY
D
H
Z
6h
12h GMT
18h
24h
γ

FIG. 9

A METHOD FOR DRAWING THE GREAT-CIRCLE PATH BETWEEN ANY TWO POINTS ON EARTH

BY J. H. MEEK*

University of Saskatchewan, Saskatoon, Canada

(Received April 9, 1956)

ABSTRACT

Quick and convenient ways are given of tracing around the earth the great circle joining two points or the great circle of given bearing at a point. While the methods outlined are not new or original, they have many applications in geophysics and appear to have been lost in the literature.

INTRODUCTION

Frequently it is desired to draw on a map, without the need for any calculations, the great-circle path between two distant points. If the two points are closer together than about 120° of arc around the earth, it is simple to use a gnomonic projection containing both points. The required great circle is the straight line joining them. For longer distances, the distortion of the gnomonic projection makes it inconvenient to use. Usually a family of great circles is drawn on an overlay to the same projection as the map being used. The path is then traced from one point to the other along a great-circle curve. The method outlined below is adapted from a description by Turner (1910) and may be used to draw the great circle between two points anywhere on the earth as segments of straight lines.

CONSTRUCTION OF THE MAP PROJECTION

The earth is enclosed in its tangent cube, the sides touching it at the poles and at four points around the equator. A gnomonic projection is made on to the six faces of this cube (in this projection, the "source" is at the center of the earth). The characteristics of the gnomonic projection are described in many standard texts, for example, Raisz (1938).

This results in two basic latitude-longitude grids. The *polar grid* is illustrated in Figure 1. The face tangent to the north pole is shown, but that tangent to the south pole is similar except that the longitudes are labeled in the opposite direction. The *equatorial grid*, of which there are four altogether, is shown in Figure 2. The top and bottom of this grid will match any side of the polar grid. The side of the grid will match that of its neighbour, of course. Several of these grids may be matched in order to trace the great circle around the earth. The great circle from a point in one grid to a point in another grid will be a straight line, with a discontinuity occurring at the common boundary of the two grids.

*The author is on the staff of the Defense Research Board.

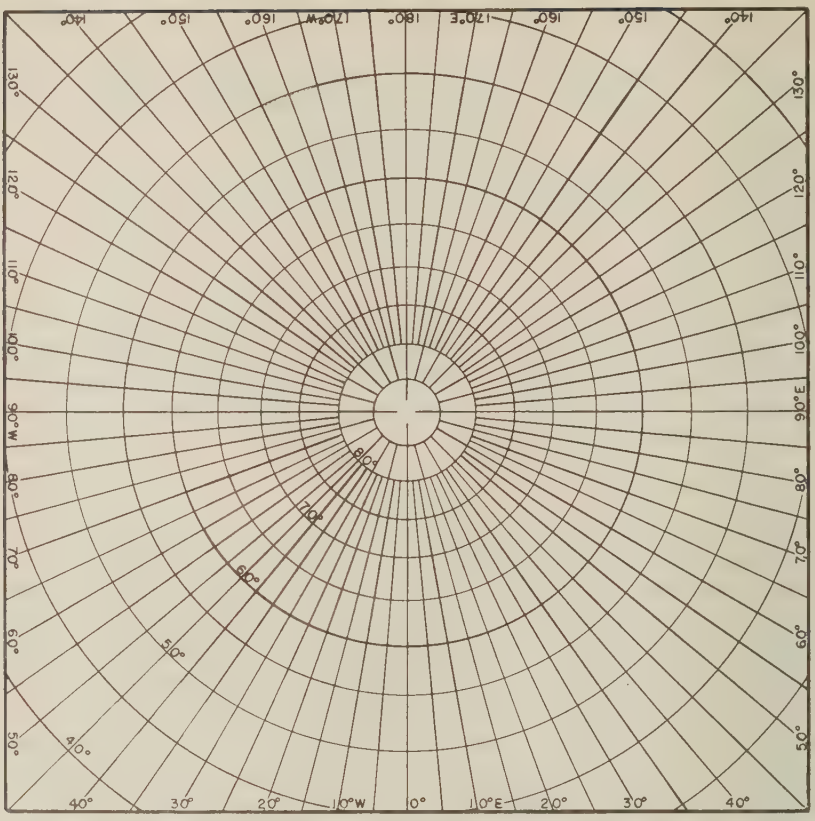

FIG. 1—Polar gnomonic grid

DRAWING THE GREAT CIRCLE

The methods and proofs of construction of the great circles have been worked out in detail, by Turner, so that here it is sufficient to state the three basic principles.

(1) A great circle through the mid-point of a boundary common to two grids is unchanged in direction.
(2) A great circle passing through the centre of one grid is parallel to the boundaries in the next grid.
(3) All great circles passing through a point in one grid are parallel to each other in a neighbouring grid, and *vice versa*.

In order to draw the great circle from A to B (or B')—see Figure 3—draw a straight line from A through O, the centre of the common boundary of the two grids and produce (extend) into the grid containing the point B (or B'). Through B (or B') draw a straight line parallel to this line and find the intersection C on the common boundary (produced if necessary to C'). Join this point to A. ACB is the required great-circle path between A and B.

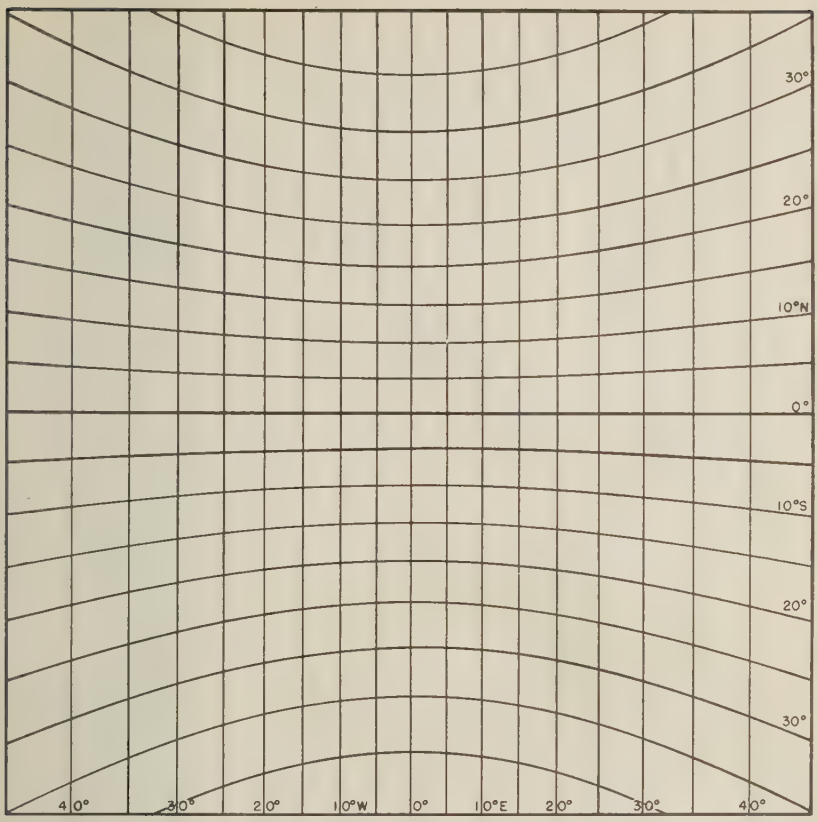

Fig. 2—Equatorial gnomonic grid

To produce the great circle of a given bearing at a point A into the next grid, draw the bearing line to the boundary intersecting it at D. Draw a straight line through D parallel to AO produced. DF is the required great-circle line. Alternatively, draw the straight line parallel to AD through O and produce it to cut the central meridian of the next grid at F. As a second alternative, draw a straight line parallel to AD through the centre T of the grid intersecting the common boundary at E. Draw a straight line through E parallel to the side of the next grid. It will

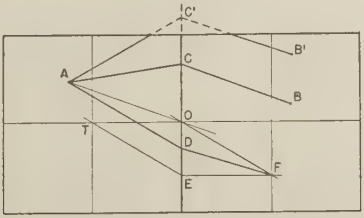

Fig. 3—Extension of a great circle across a grid boundary

also intersect the central meridian at F. Join DF, which is the given bearing line produced.

It may be necessary to draw the great circle between two points which are not in adjacent grids. In this case, the antipodal point of the first will lie in the same grid as the second point. The great circle may then be drawn immediately.

CONCLUSION

This method provides a quick and practical way of tracing around the earth the great circle joining two points or the great circle of given bearing at a point.

References

Raisz, E. (1938); General Cartography, McGraw-Hill Book Co., Inc., New York.
Turner, H. H. (1910); Mon. Not. R. Astr. Soc., **70**, 204.

MAGNETIZATION OF THE COLUMBIA RIVER BASALTS IN WASHINGTON AND NORTHERN OREGON

By C. D. Campbell

Department of Geology, The State College of Washington, Pullman, Washington

AND

S. K. Runcorn*

The Institute of Geophysics, University of California, Los Angeles, California

(Received May 7, 1956)

ABSTRACT

The remanent magnetization of late-Tertiary lavas in seven sections of Columbia River basalts has been examined. Approximately equal numbers of normally and reversely magnetized lava flows have been found. At least three field reversals during their eruption are indicated, if the reversed magnetization is interpreted as the result of a reversed geomagnetic field at the time of cooling of the lavas.

Introduction

The sampling and testing of this preliminary study were undertaken for three reasons: first, in order to throw light upon the causes of anomalous magnetization in lavas; second, to investigate the possibility of using the remanent magnetization of the flows as a basis for stratigraphic correlation; and, third, to provide suites of oriented sections for more general systematic petrologic studies of the basalts in the future.

The Collection and Preparation of the Specimens

In seven areas of nearly horizontal basalts, some 114 flows aggregating 11,350 feet in thickness were examined. Oriented fist-sized samples were collected from those flows in which the remanent magnetism seemed likely to be least disturbed by chemical alteration or by movements after hardening. The choice of sampling areas was intended to give evenness of geographical distribution in the basalt series and, in the group of three eastern areas, comparisons within single wide-ranging flows. The number of samples that were collected from each flow, however, are hardly sufficient to investigate the effects of lightning strikes on the outcrop, the effects of reheating of flow tops by the later flows, or any contrasts between rinds and centers of flows. These matters need careful study in the future.

The present collecting was done with the aid of a Brunton pocket transit and cannot be guaranteed to be more accurate than about three degrees. Preliminary tests made next to cliffs of various types of basalt indicated declination changes of perhaps two degrees at a distance of three feet. The specimens were easily-detached joint blocks of suitable size and freshness, marked with "dip and strike" lines

*Now at the Department of Physics, King's College, Newcastle-upon-Tyne, England.

penciled on adhesive strips and measured before being lifted away from the outcrop. Most of these specimens deflected the magnetic needle less than one degree when held next to it.

In the laboratory, vertical cores were drilled from the specimens. These were then sliced to make cylinders, approximately $1\frac{1}{4}$ inch in diameter and $1\frac{1}{4}$ inch long. The orientation marks were transferred to the horizontal surface.

The always debatable distinction between flows and flow-units was borne in mind during the collecting but was not an important one for this preliminary study. More probably two or more true flows were occasionally taken to be one single flow in places where crumbling vesicular tops were concealed by soil and grass on flatter slopes.

Measurement of Direction of Magnetization

The angles of declination and dip of the magnetic polarization of the cylindrical samples were measured on a simple astatic magnetometer. Such an instrument, suitable for the measurement of igneous rocks, has been described by Collinson, Creer, Irving, and Runcorn [see 1 of "References" at end of paper]. An accuracy of 1° is aimed at, but the errors in collection are probably about 2° to 3°, and the scatter of directions within a single flow is often 5° to 10°, but may be much larger occasionally, for reasons not at present understood.

TABLE 1—*Directions of magnetization of lava flows*

Series of flows	Normally magnetized				Reversely magnetized			
	D	*I*	α	κ	*D*	*I*	α	κ
		°	°			°	°	
Imnaha River (Wallowa Co., Oregon)	N. 30.2°E.	+70.9	14.1	5.0	S. 9.0°E.	−69.4	21.6	3.4
Grande Ronde River (Asotin Co., Wash.)	N. 39.0°W.	+85.4	24.1	3.1	S. 51.1°E.	−71.7	28.2	2.9
Steptoe Canyon (Whitman Co., Wash.)	.....	.....	.....	.....	.....	.....	.....	.....
Blue Lake (Grant Co., Wash.)	N. 6.0°W.	+70.4	14.8	7.0	S. 19.0°W.	−67.2	17.6	7.7
Wallula Gap (Umatilla Co., Ore.)	N. 13.0°E.	+58.1	8.7	26.2	.....	.....	.....	.....
Union Gap (Yakima Co., Wash.)	N. 0.2°E.	+67.7	30.0	3.5	S.20.5°W.	−56.9	.....	.....
Multnomah Falls (30 mi. E. of Portland)	N. 3.9°E.	+39.4	.....	.....	S.15.7°W.	−47.6	18.9	17.4
Mean of all flows	N. 11.4°E.	73.5	7.6	4.6	S. 3.1°E.	−66.0	10.7	4.2
Present direction of geomagnetic field	N. 20° to 22°E.	+70° to 72°						
Dipole direction	N. 0°	69°						

As is found for other Tertiary lava flows (see [2], for example), the directions of magnetization can be divided into two groups—one normal, scattered about the direction of the present earth's field, and one reversed, antiparallel to the other group. Table 1 shows the mean directions of magnetization of the normal and reversed flows from the seven different sites at which the lava series were sampled. The statistical treatment is that due to Fisher [3]; α is the semi-angle of the cone described about the mean direction which includes to a probability of 95 per cent the true direction, while κ is a measure of the precision. Stereograms 2 to 7 show the directions of magnetization of each sample measured. The magnetization of a single sample from a flow will usually diverge considerably from the mean direction of magnetization of a flow. This study, therefore, throws no light on the secular variation of the geomagnetic field such as would be obtained if the mean direction of magnetization of the separate flows were known. In the sections shown in Figure 1, directions are classified as normal (N) or reversed (R), or are left

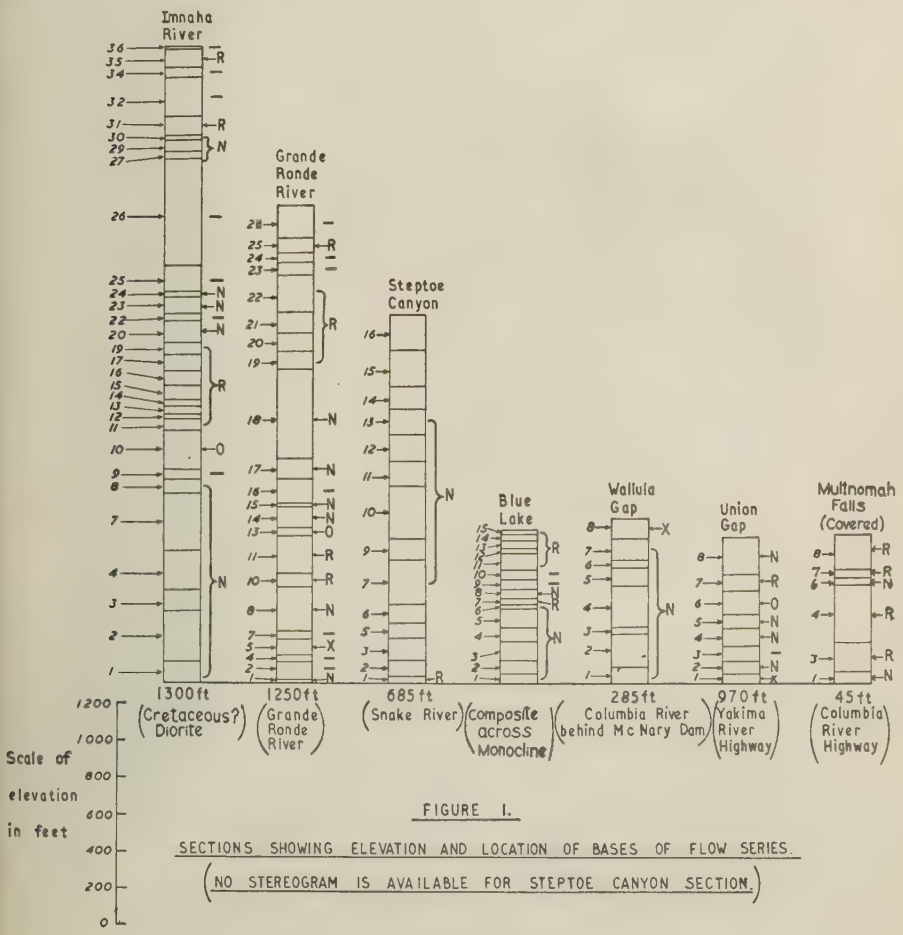

FIGURE 1.

SECTIONS SHOWING ELEVATION AND LOCATION OF BASES OF FLOW SERIES.

(NO STEREOGRAM IS AVAILABLE FOR STEPTOE CANYON SECTION.)

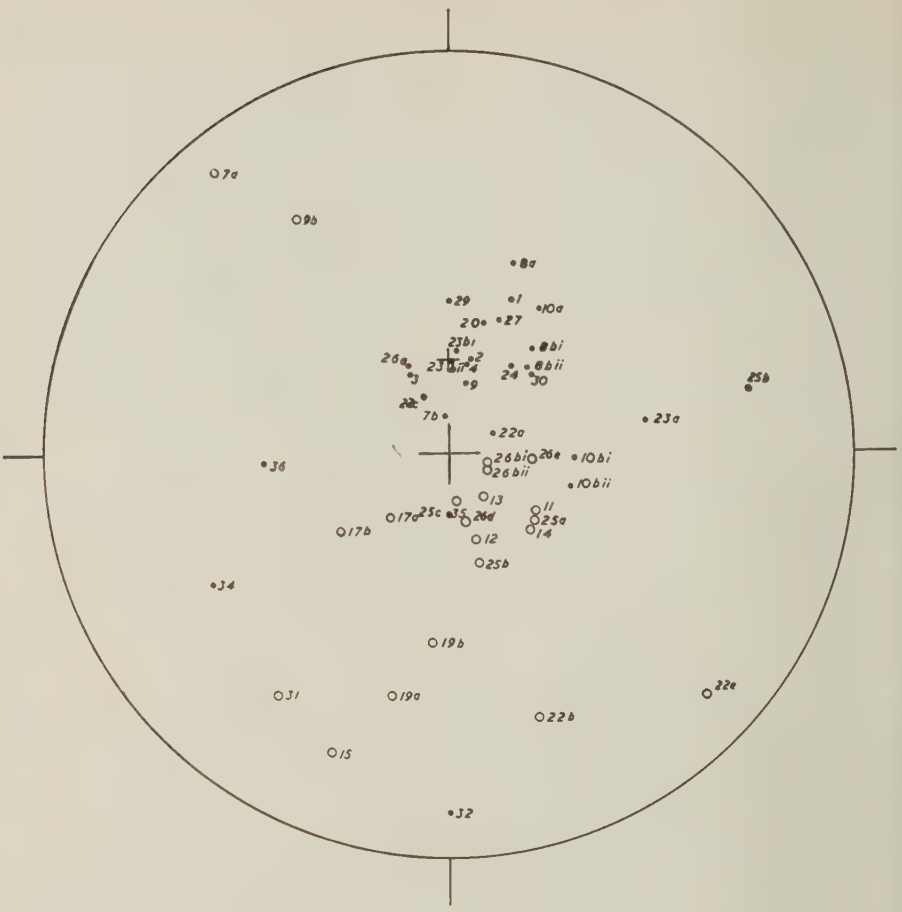

Imnaha River Basalt Series, Wallowa County, Oregon.

FIGURE 2.

○ denotes north pole on upper hemisphere of stereographic projection.
• denotes north pole on lower hemisphere of the projection.

unclassified (—) if these are not in reasonable accord with the predominant directions. *X* denotes flows not sampled. Lavas are numbered from the base upwards. Letters after the lava number denote separate samples from the same flow; numerals denote separate cores from the lava sample.

The directions of magnetization of the normal and reversed group are not significantly different from those of a geomagnetic dipole field with the polarity of the present field and its opposite, respectively.

Microscopic Examination of Specimens

The 138 samples collected for magnetic testing were also examined petrographically and in reflected light, in order to discover any correlations existing

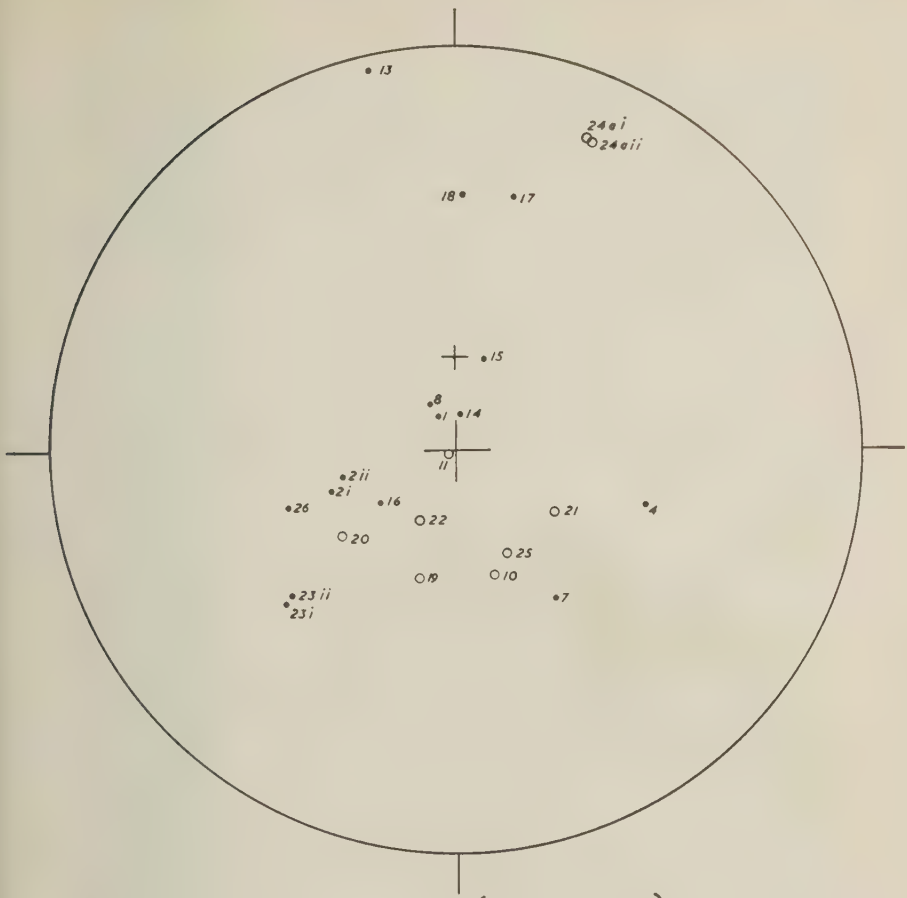

Grande Ronde River (Rattlesnake Creek) Basalt Series, Asotin County, Washington.

FIGURE 3.

between content of ilmenite and the magnetic polarity of the rocks, such as has been suggested by the work of Balsley and Buddington in the Adirondacks [4]. No chemical analyses were made which would show the total non-silicate titanium, of which much might be present dissolved in the abundant magnetite of the more rapidly cooled lavas. The results of the microscopic work are summarized by histograms shown in Figures 8 and 9.

The following general relationships were noted:

(1) The content of magnetite is usually greatest (10 to 20 per cent) in rocks with the greatest per cent (40 to 80) of glassy residuum or its devitrified equivalent; in the glass, magnetite assumes dendritic forms, and in the dense devitrified rocks it forms a peppering of unjoined minute crystals.

(2) Ilmenite is more abundant in the basalts with a low content (under 10

Blue Lake Basalt Series, Grant County, Washington.

FIGURE 4.

per cent) of glassy residuum and therefore a low content of magnetite (under 5 per cent). The maximum ilmenite seen was 5 per cent.

(3) There is no clear relationship between the percentage of glass and average diameter of crystals other than phenocrysts.

(4) Of all specimens tested magnetically, 65 per cent are normally polarized; of the ilmenite-bearing ones only, about 60 cent are normally polarized; of those containing 30 per cent or more of glass—that is, those presumed to have chilled most rapidly—about 45 per cent are normally polarized.

Conclusion

The number of normally magnetized flows found was 44, and the reversely

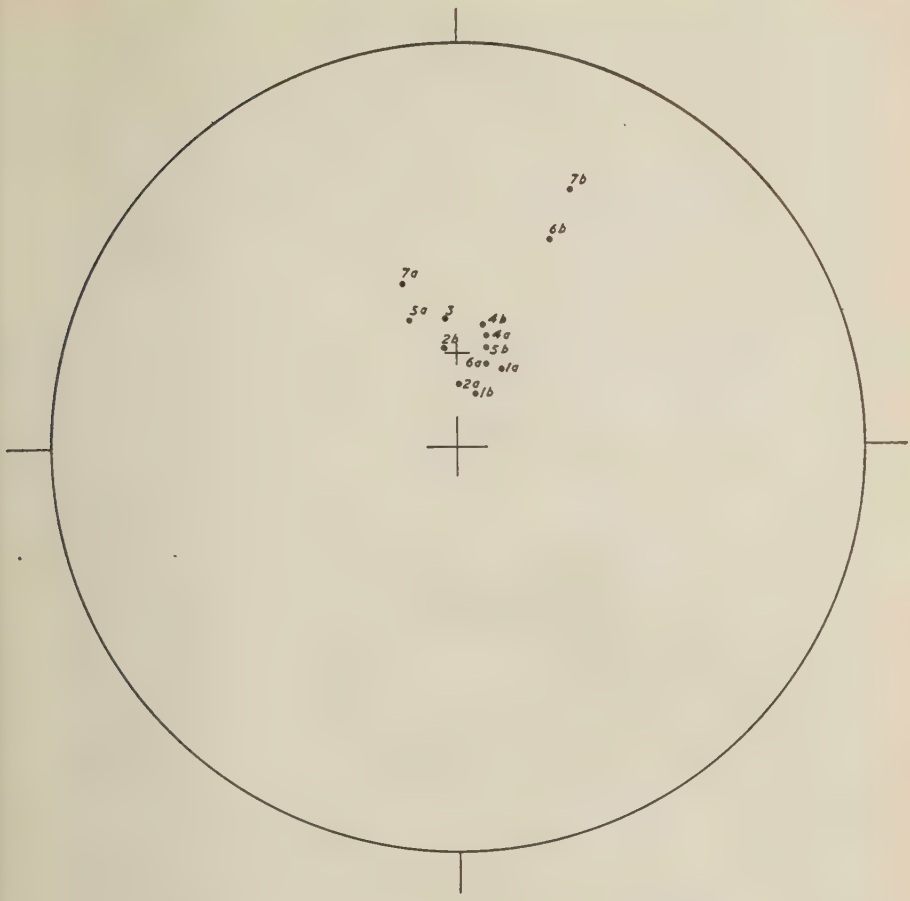

Wallula Gap Basalt Series, Umatilla County, Oregon.

FIGURE 5.

magnetized flows numbered 29—a similar ratio to that observed in Iceland. The mean number of flows between successive reversals is 3.9. This is considerably less than the figure for the Icelandic lavas and possibly indicates a much slower mean rate of extrusion of flows, offsetting a greater mean thickness of 98 feet per flow.

These basaltic flows are of Miocene and perhaps Pliocene age [5]. If the reversed magnetization is interpreted as having arisen from a field opposite to the present one, the evidence from the Grande Ronde and Multnomah Falls series indicates that at least three field reversals occurred during the time of eruption. It has been urged that reversed magnetization is due to anomalous properties of the iron-titanium oxide minerals and not to reversals of the geomagnetic field. The petrological examination reveals no obvious difference between reversed and normal flows. If this is the true explanation, anomalous properties must be present to an

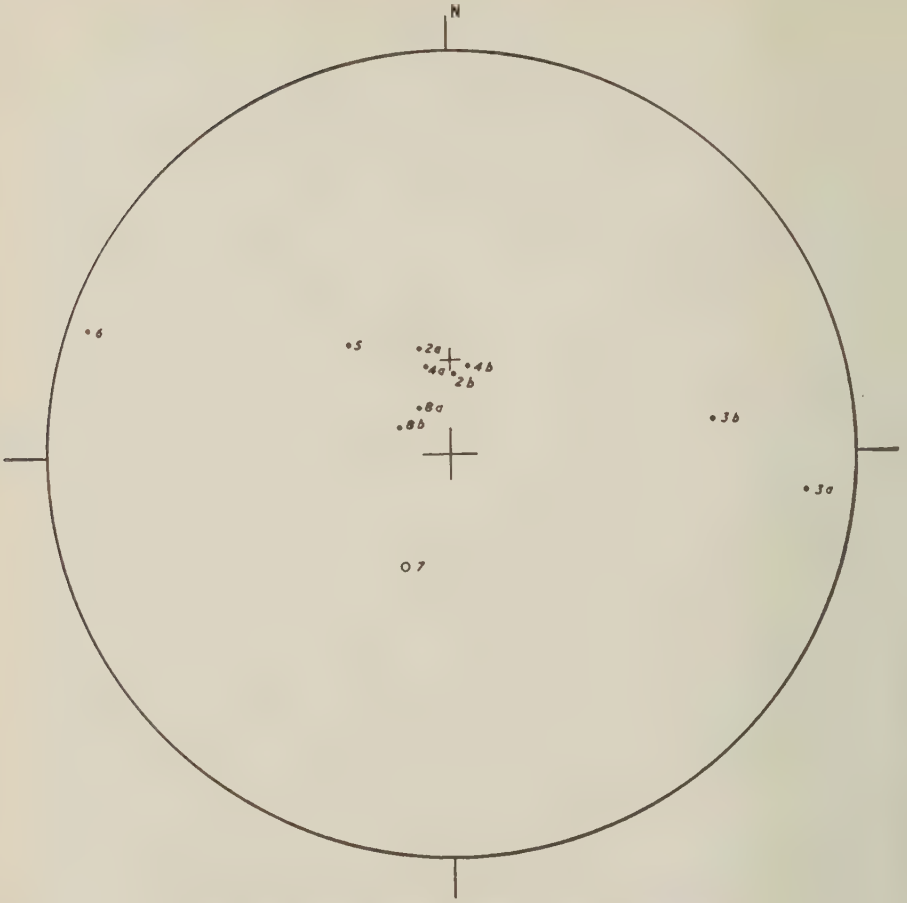

Union Gap Basalt Series, Yakima County, Washington.

FIGURE 6.

approximately equal degree in the Columbia River basalts and the Icelandic basalts.

Flow 10 of the Imnaha series appears to have a magnetization markedly different from either the well-grouped series of six normal flows below or the seven reversed flows above. Flow 6 in the Union Gap seems similarly oblique to the prevalent directions. These flows may therefore have been extruded during the time in which the field was changing between its two stable polarities. Cases of such intermediate magnetization need further study.

Acknowledgments

The initiation of this work and preliminary measurements of the specimens was done by one of us (S.K.R.) during the summer of 1953 while he was a research

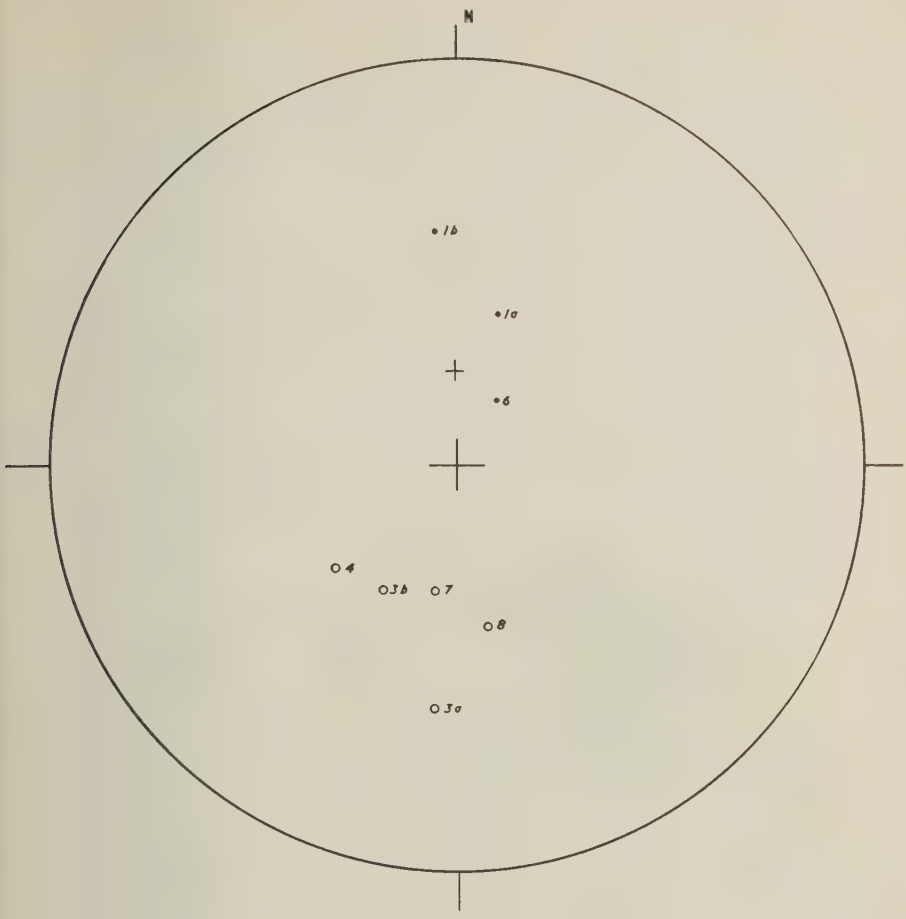

Multnomah Falls Basalt Section, 30 miles east of Portland, Oregon.

FIGURE 7.

geophysicist at the Institute of Geophysics of the University of California at Los Angeles; he is grateful to Drs. A. C. Waters and R. E. Wilcox for an initiation into the geology of the Columbia River lavas. We are much indebted to the Director of the Institute, Dr. L. B. Slichter, for his interest. Funds for the collection, shipping, and sectioning of samples were provided by the State College of Washington, as Project 85 of the College Committee on Research. We are indebted for field assistance to Mr. and Mrs. A. Keppler and Messrs. F. Howd, A. Parmer, Q. Aune, H. Praetorius, and R. Page; to Mr. Howd for work on polished sections; and to Mr. G. Turnbull for help with the measurements and computations.

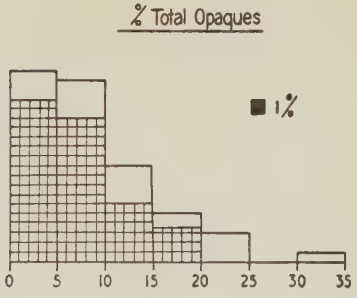

FIGURE 8.

Normally Magnetized Flows.

Reversely Magnetized Flows.

Histogram of percentage of total opaques

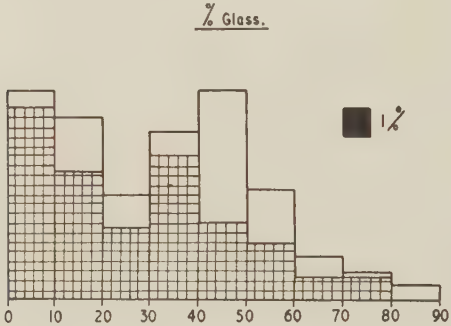

FIGURE 9.

Normally Magnetized Flows.

Reversely Magnetized Flows.

Histogram of percentage of glass.

References

[1] D. W. Collinson, K. M. Creer, E. Irving, and S. K. Runcorn, Phil. Trans., Ser. 8, **1**, in press.
[2] J. Hospers, J. Geomag. Geoelectr., **6**, 172-175 (1954).
[3] R. A. Fisher, Proc. R. Soc., A, **217**, 295-305 (1953).
[4] J. R. Balsley and A. F. Buddington, J. Geomag. Geoelectr., **6**, 176-181 (1954).
[5] A. C. Waters, Bull. Geol. Soc. Amer., **66**, 663-684 (1955).

CIRCULATION IN THE UPPER ATMOSPHERE*

BY PEMMARAJU S. PANT

Department of Meteorology and Oceanography, New York University, New York 53, N.Y.

(Received May 2, 1956)

ABSTRACT

The winds in the region of the atmosphere from 20 to 100 km elevation over the northern hemisphere are critically examined. The summer and winter temperatures are computed from the wind field with the aid of rocket mean pressure data and under the assumption that the wind field is geostrophic. The temperatures obtained are found to agree with direct observations. Thus the observed wind and temperature distributions are shown to be consistent. Possible causes of some of the observed seasonal temperature changes in different parts of the upper atmosphere are discussed.

The zonal wind cross-sections prepared in this investigation are compared with wind distributions published earlier and found to agree fairly well with them. On the basis of the wind distributions and of theoretical considerations, the circulation in the mesosphere and thermosphere is derived.

1. *Introduction*

Interest in the study of upper atmospheric circulation has increased during the past few years. New methods of obtaining upper atmospheric data have also been developed. As a result, more data are becoming available. These data can be used to enlarge and, where necessary, modify our past picture of the upper atmospheric circulation. With this end in view, the present investigation was undertaken.

In this paper, the region of the atmosphere above the tropopause will be referred to as the "upper atmosphere." Further, the nomenclature proposed by Chapman [1953] for the different regions of the upper atmosphere will be used here. According to Chapman, the 20 (or 30) to 50 km region in which the temperature increases with height is called the "mesoincline." The temperature reaches its maximum value at the "mesopeak," above which it decreases with height in the "mesodecline" and attains a minimum value at the "mesopause." The whole region starting from the mesoincline to the mesopause is referred to as the "mesosphere." This region is followed by the "thermosphere," in which temperature increases with height.

The first extensive survey of available wind data for the 20 to 120 km region of the upper atmosphere was made by Kellogg and Schilling [1951]. Since then, more wind data have become available. Many of those are included in the summaries of winds for summer and winter published by Gerson [1953, 1955],

*The research for preparation of this paper has been sponsored by the Geophysics Research Directorate, Air Force Cambridge Research Center, under Contract AF19(604)-1006.

which have proved to be of immense value for the present investigation. Recently, Haurwitz [1954] made an attempt to combine the wind data available for the 20 to 90 km region of the upper atmosphere into a coherent picture of the mean seasonal wind field. The present investigation is an extension of his preliminary study, based on more data and making a more detailed critical analysis of the wind observations.

It is proposed here to examine the wind data available for the 20 to 100 km region of the upper atmosphere over the northern hemisphere. It has been considered advisable to check the reliability of the wind data, before they can be used for the discussion of circulation in the upper atmosphere. For this purpose, the summer and winter temperature fields are obtained from the available pressure and wind data, by means of certain plausible assumptions.

2. *Computation of temperatures*

It is assumed that zonal symmetry exists in the wind field and that the winds are geostrophic in the region under consideration. Yerg [1951] concluded that viscosity causes the wind to deviate from the geostrophic wind only above 150 km. Thus it does not seem unreasonable to make the geostrophic assumption, at least up to 100 km. Then the slope of an isobaric surface is given by

$$(dz/dy)_p = \frac{2\omega U_g \sin \varphi}{g}$$

where ω = angular velocity of the earth's rotation, U_g = zonal geostrophic wind (positive from the east and negative from the west), φ = latitude, y-axis positive toward north, z-axis positive upwards starting from the earth's surface, and g = acceleration of gravity, constant with latitude and height.

The heights of different isobaric surfaces in summer and winter at different latitudes are obtained using the rocket mean pressure data (Havens, *et al.*, 1952) and the wind data. It has also been assumed for reasons of continuity that the isobaric surfaces are horizontal at the equator where the geostrophic wind relation does not hold, and at the pole. At 33° north, the same set of isobaric heights is adopted both for summer and winter, because the seasonal change in the pressures at different heights has so far not been definitely established at this latitude. From the hydrostatic relation, the mean temperature between two isobaric surfaces is given by

$$T = \frac{g \cdot \Delta z}{R ln_e(p_0/p)}$$

where Δz is the difference in height between the two isobaric surfaces, R is the gas constant for dry air (assumed constant for the layers under consideration), p_0 is the pressure at the lower surface, and p is the pressure at the higher surface.

The computed temperatures are presented in the form of temperature-height curves for summer and winter at different latitudes in Figure 1.

3. *Comparison of computed and directly observed temperature fields*

Some observed temperatures and the corresponding computed values are presented in Tables 1, 2, and 3. It is encouraging to notice that the differences

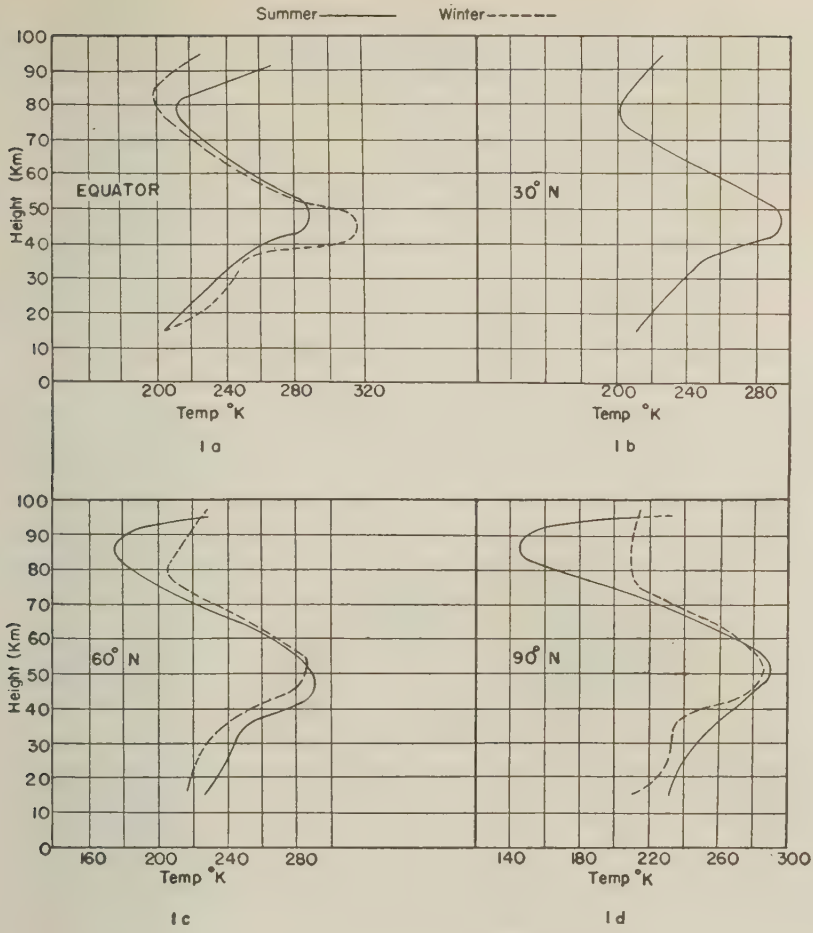

FIG. 1—Summer and winter temperatures (°K)

are not more than 15°K and in many cases much less. Equally good agreement is noticed between the temperatures presented in Tables 1 to 3 and the corresponding observed temperatures published more recently (Kochanski [1955] and Conover and Wentzien [1955]).

It is also interesting to examine whether the seasonal temperature changes associated with the computed temperature field agree with the observed and theoretically expected changes. The seasonal temperature changes obtained in this investigation will have to be corrected for the fact that their values at 33° north could not be taken into consideration because they have not been definitely established, as mentioned before. From the thermal wind relation, it follows that for a given wind shear and mean temperature between two levels the mean meridional temperature gradient of that layer will be a constant. Then, if the temperature at any particular level and latitude is changed by ΔT, the temperatures

Table 1—*Computed temperatures at 30°N compared with observed temperatures as presented by Gutenberg (1949)*

Height	Summer temperatures		Winter temperatures	
	Computed 30°N	Observed 32°N	Computed 30°N	Observed 32°N
km	°*K*	°*K*	°*K*	°*K*
15	211	208	211	212
25	229	225	230	221
35	248	245	249	235

at this same level but at other latitudes will have to be changed by an equal amount in order to keep the meridional temperature gradient constant. If the observed values of the winter to summer temperature change are available at any single latitude for each level, then all the computed values of this temperature change can be corrected for other latitudes. The corrected seasonal temperature changes in the 15 to 45 km region shown in Table 4 are obtained from the temperature data published by Gutenberg [1949] and Crary [1950], and the values of $(T_{\text{summer}} - T_{\text{winter}})$ are obtained from the computed temperatures.

In the mesoincline, the seasonal change increases with height at any latitude, and, at any level, it generally increases toward higher latitudes (at some levels up to 50° to 60° north and in others up to the pole). These features largely agree with Wexler's [1950] conclusions about the seasonal temperature changes in the layer from 20 to 50 km. The July minus January differences of mean temperatures obtained by Kochanski [1955] for the region between 20 and 30 km are in qualitative agreement with the above-mentioned features of seasonal temperature change. Pressman [1955] computed for different seasons the 24-hour temperature changes in the ozonosphere (mesoincline) caused by the absorption of solar radiation by ozone alone. He found that the height of maximum 24-hour temperature increase is located at approximately 45 km, and that the region of maximum 24-hour temperature increase is over the poles during the respective summer seasons

Table 2—*Computed temperatures at 40°N compared with temperatures observed at 40°N presented by Brasefield (1950)*

Height	Summer temperatures		Winter temperatures	
	Computed 40°N	Observed 40°N	Computed 40°N	Observed 40°N
km	°*K*	°*K*	°*K*	°*K*
15	214	216	215	221
25	231	226	228	221
35	250	243	245	241

TABLE 3—*Computed summer temperatures at 30°N compared with observed temperatures over New Mexico as presented by Elterman (1954)*

Height	Computed temperatures at 30°N	Elterman's values (June 1952)
km	°*K*	°*K*
15	211	205
25	229	219
35	248	248
45	293	285
55	270	280
65	250	235

and lasts about three months. These results indicate that the effect of ozone absorption alone is to cause seasonal temperature change in the mesoincline, which increases with height and latitude. But the total seasonal temperature change in this region also depends on the water vapor and CO_2 absorption. The effect of water vapor and CO_2 on the seasonal temperature change in the mesoincline can be expected to be much smaller than that of ozone.

From Table 4, it is also apparent that at all latitudes north of 10° north and above 20 km the summer temperatures are higher than the corresponding winter temperatures. This can be explained, as has been done by Kellogg and Schilling (1951), in terms of the seasonal variation of solar zenith angle, of the amounts of ozone, and of the long wave radiation from the earth.

Another interesting feature shown by the seasonal temperature changes obtained here is the summer to winter warming at 15 km from 0 to 50° north and at 25 km from 0 to 10° north. Similar summer to winter warming at 15 km and between 0 to 50° north is also indicated by the mean values of the observed temperatures presented by Kochanski [1955]. Observed temperatures presented in Tables 1 and 2, as well as those published by Conover and Wentzien [1955], show such warming. The explanation for this warming may be the occurrence of subsidence from higher levels in winter, at least in the equatorial regions. Another possible cause may be found in radiative processes. According to Dobson, *et al.* [1946], an increase in the proportion of water vapor and carbon dioxide relative to ozone in the region above the tropopause will cause a decrease of radiative equilibrium temperature. Hence, the cause of lower temperatures in the region

TABLE 4—*Corrected* ($T_{summer} - T_{winter}$)

Height	Equator	10°N	20°N	30°N	40°N	50°N	60°N	70°N	80°N	N. pole
km										
15	− 3.4	− 2.8	− 2.6	− 3.6	− 3.3	− 1.7	+ 4.1	+ 9.6	+16.7	+18.8
25	− 4.5	− 3.5	+ 0.2	+ 4.5	+ 8.9	+14.9	+22.2	+20.9	+14.9	+14.2
35	+ 7.7	+ 8.2	+ 8.6	+ 8.3	+14.9	+19.8	+21.1	+25.4	+28.0	+30.6
45	+17.0	+25.6	+36.3	+45.2	+57.5	+60.4	+57.4	+54.0	+51.4	+49.0

just above the tropopause may be the occurrence of larger amounts of water vapor and/or carbon dioxide at the respective heights and latitudes. But it remains to be seen if this can be justified from observational or other evidence.

With regard to the seasonal temperature changes in the mesodecline, it has been found in this investigation that north of 30° north the temperatures are lower in summer than in winter (Figs. 1*c* and 1*d*). The same result has been obtained by Kellogg and Schilling [1951]. Brasefield [1954] from a study of winds came to a similar conclusion, namely, that there is warming from summer to winter in the region from 53 to 73 km at 30° north to 40° north. Further confirmation of this is found in the temperatures published by Elterman [1954], which clearly indicate a warming from June to October at 45 to 68 km over New Mexico. Thus it appears that this temperature rise from summer to winter in the mesodecline at middle and high latitudes, also found in this investigation, is real.

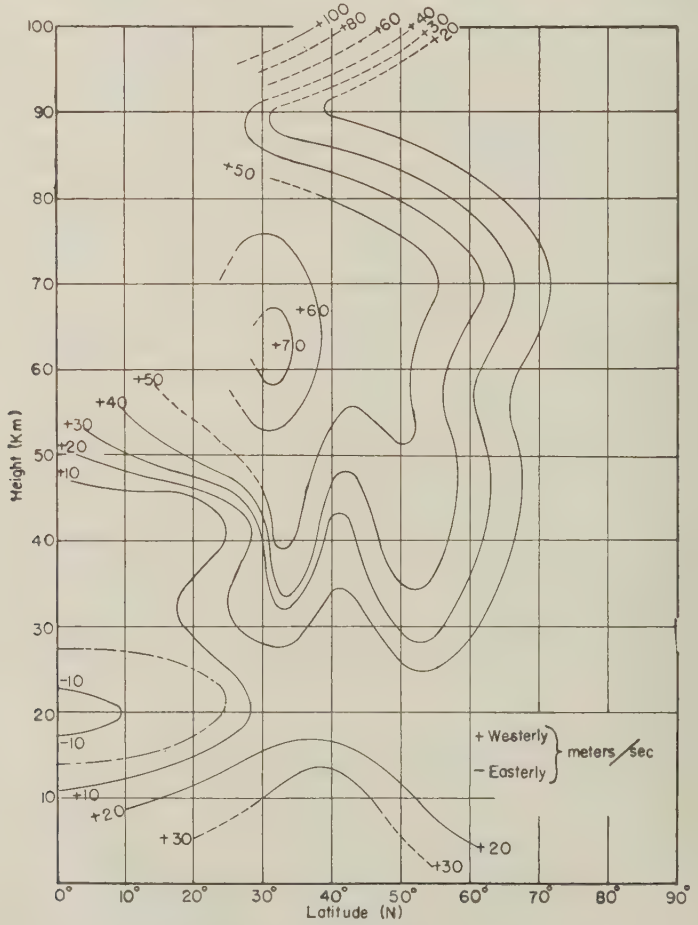

FIG. 2—Northern-hemisphere summer zonal wind distribution

A qualitative explanation of this warming in the mesodecline will be attempted here on the basis of the discussion of Dobson, *et al.* [1946]. It may be hypothesized that the temperature changes in the mesodecline are largely due to variations in the amounts of ozone, water vapor, and carbon dioxide. It will also be assumed that in the mesodecline the radiative equilibrium temperature of ozone is higher than that of water vapor or carbon dioxide, similar to the conditions which Dobson, *et al.*, have found for the stratosphere. Then the lower temperature in summer in this region may be due either to the increase of the relative proportions of water vapor and carbon dioxide, or to the decrease in the relative proportion of ozone, or to both the above-mentioned factors. Moreover, Mitra [1952] points out that water vapor acts as a catalyst in the destruction of ozone. Hence the occurrence of larger quantities of water vapor in this region in summer would further decrease the amount of ozone usually present in this region and thus contribute to an

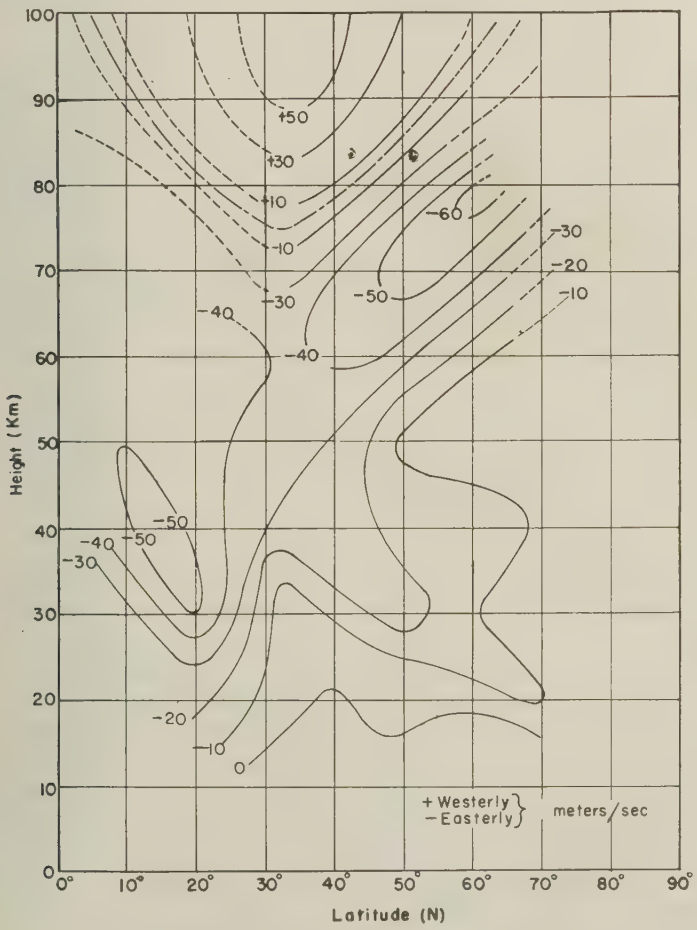

FIG. 3—Northern-hemisphere winter zonal wind distribution

additional lowering of summer temperatures. The cause of an increased mixing ratio of water vapor and carbon dioxide during summer at these levels may be stronger vertical mixing with the lower layers, where the sources of water vapor and carbon dioxide are. At the mesopeak, there is considerable warming from winter to summer, whereas in the mesodecline there is a slight cooling. Hence it can be surmised that larger lapse rates and greater mixing are likely to be found in summer in the mesodecline. Not much is known about the amounts of ozone, water vapor, and carbon dioxide, and even less about their seasonal variations in the mesodecline. According to one theory, the noctilucent clouds, so far observed only in summer around 80 km at high latitudes, are composed of ice crystals. If this theory is correct, it may indicate the presence of considerable amounts of water vapor in summer at these high levels, strengthening further the case for the suggested explanation of the lower summer temperatures in the mesodecline.

The magnitudes of the seasonal temperature changes above the mesopeak are not included in Table 4, since they are considered to be correct only as to their sign.

At latitudes below 30° north in the mesodecline, a cooling from summer to winter is indicated. There is no observational evidence either for or against this. It is possible that this feature appears in our Figures because the seasonal temperature change at 33° north in the mesodecline is not taken into consideration.

The temperature rises from winter to summer in the thermosphere over middle and high latitudes, as shown by the temperatures obtained from the wind field. Figures 1*c* and 1*d* show that above 90 km summer temperatures are higher than winter temperatures. The temperature in this region is largely dependent on the absorption of solar radiation. Hence, at least qualitatively, it seems reasonable to expect that in summer, when the solar radiation available for absorption in the thermosphere is greater than in winter, the temperature will be higher.

The comparison of the observed and computed temperature fields presented above shows that the winds are consistent with the observed and theoretically expected temperature field. These winds will now be used for the discussion of the circulation in the upper atmosphere.

4. *Circulation below the mesopeak*

The winds which will be used here for the discussion of atmospheric circulation are presented in the form of zonal wind distributions in Figures 2 and 3. The sources of the wind data are given in Tables 5 and 6. The geostrophic winds computed by Goldie [1950] for the region below 45 km, the curves of variation of wind with height presented by Sheppard [1949] for middle latitudes, the summary of winds prepared by Gerson [1953, 1955], and the preliminary wind cross-sections derived by Haurwitz [1954] are all in fairly good agreement with the winds presented here. The zonal components of geostrophic flow between the levels 20 and 30 km obtained by Kochanski [1955] show largely the same features as the corresponding wind distributions presented in Figures 2 and 3. However, Kochanski shows the presence of westerlies around 15° north and above 20 km in January, whereas these are not to be found in the wind cross-section presented here. This difference might have

arisen out of the fact that winds presented by Kochanski refer to one longitude, whereas zonal symmetry has been assumed in this investigation.

Figures 4 and 5 show the meridional circulation of the atmosphere in summer and winter, based on our investigation and the work of other authors. The broken lines with arrows in the above-mentioned Figures merely indicate the directions

TABLE 5—*Summer wind data*

Latitude	Level	Author	Reference
	km		
80°, 70°, 60°, 50°, 40°, 30°, and 20°N	At 12, 16.5, 21, and 25	Air Weather Service	[1]
32°N	30 to 60	Brasefield, C. J	[3], [4]
40°N	10 to 40		
42°N	100	Briggs, B. H.	[5]
40°N	10 to 30	Conover and Wentzien	[8]
9°N	30 to 55	Crary, A. P.	[10], [11], [12], [13]
32°N	20 to 50		
64°N	20 to 50		
45° and 35°N	At 16 and 20	Darling, E. M.	[14]
60°N	70	Elvey, C. T.	[17]
10°, 20°, 30°, . . ., up to 60°N	0 to 30	Flohn, H.	[18]
37°N	95	Gerson, N. C.	[19], [20]
39°N	100		
41°N	92		
60°N	30 and 82		
65°N	30 to 45		
53°30′N	85, 92 and 96	Greenhow, J. S.	[22]
40°N	10 to 50	Jenkins, C. F.	[27]
9°N	30 and 50	Kennedy, W. B.	[32]
21°N	20 and 50		
32°N	30 and 50		
65°N	50 to 60		
40°N	5 to 50	Richardson and Kennedy; Kennedy, *et al.*	[38] [33]
52°36′N 60°08′N	5 to 30	Scrase, F. J.	[40]

of meridional and vertical motions. The letters "*E*" and "*W*" stand for easterly and westerly zonal winds, respectively. The scheme of the circulation in the troposphere as developed by Rossby [1948] is roughly indicated in the lowest parts of the above Figures. The region immediately above the tropopause and below the mesosphere is important as the region of interaction between the troposphere and

TABLE 6—*Winter wind data*

Latitude	Level	Author	Reference
	km		
80°, 70°, ..., up to 20°N	At 12, 16.5, 21	Air Weather Service	[1]
32°N	30 to 80	Brasefield, C. J.	[3], [4]
40°N	10 to 40		
42°N	100	Briggs, B. H.	[5]
40°N	10 to 30	Conover and Wentzien	[8]
9°, 28°, 32°, and 64°N	20 to 60	Crary, A. P.	[10], [11], [12], [13]
35°, 40° and 45°N	At 20 and 16	Darling, E. M.	[14]
60°N	70	Elvey, C. T.	[17]
10°, 20°, ..., up to 60°N	0 to 30	Flohn, H.	[18]
33°N	50 and 60	Gerson, N. C.	[19], [20]
39°N	100		
41°N	75 and 92		
52°N	25 to 50		
60°N	25 and 28		
65°N	25 to 60		
40°N	10 to 45	Jenkins, C. F.	[27]
21°N	20 and 50	Kennedy, W. B.	[32]
32°N	30 and 60		
40°N	5 to 60		
65°N	50 to 60		
40°N	5 to 60	Richardson and Kennedy; Kennedy, *et al.*	[38] [33]
52°36′N	5 to 30	Scrase, F. J.	[40]
60°08′N			
32°N	88	Whipple, F. L.	[45]

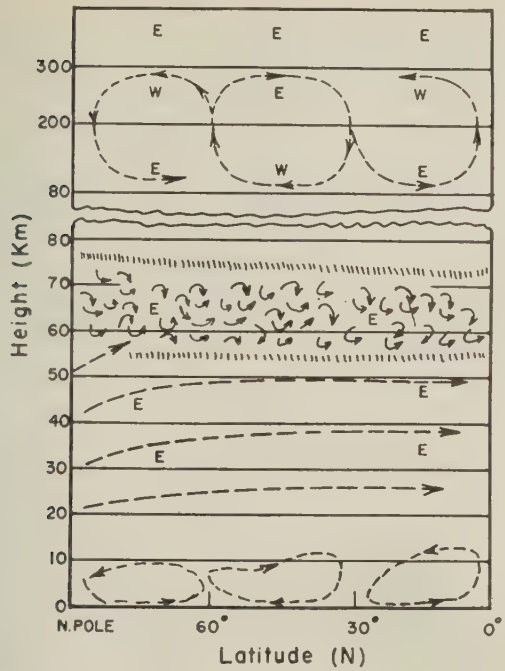

FIG. 4—General meridional circulation in summer in the northern hemisphere

the upper atmosphere. It is not intended here to go into a detailed consideration of circulation in this lower region, because the winds investigated are those in the regions above 20 km. The meridional circulation suggested by Goldie [1950] for the region below 25 km appears to be satisfactory. But it remains to be confirmed by a more extensive investigation of circulation in this region using all the more recently obtained wind observations for this region.

One very important feature of the zonal winds presented in Figures 2 and 3 is the seasonal reversal from easterlies in summer to westerlies in winter in the region from 20 to 70 km. Such a reversal has been found by many other investigators—Johnson [1946], Sheppard [1949], and Kellogg and Schilling [1951], just to mention a few. This feature is also shown in the wind distributions published by Gerson [1953, 1955] and Haurwitz [1954]. This reversal of winds, which appears to be well established, is known to take place during spring and fall, soon after the equinoxes.

In order to obtain the temperatures from the wind field, the simplifying assumption was made that the winds are geostrophic in the 20 to 100 km region. In the mesoincline, friction, though quite small, will cause cross-isobaric wind toward low pressure. Any such cross-isobaric motions cannot be strong enough to invalidate completely the geostrophic assumption, especially in view of the good results for the temperature computations which were obtained here. During summer, in the mesoincline, easterlies associated with a pressure decreasing from

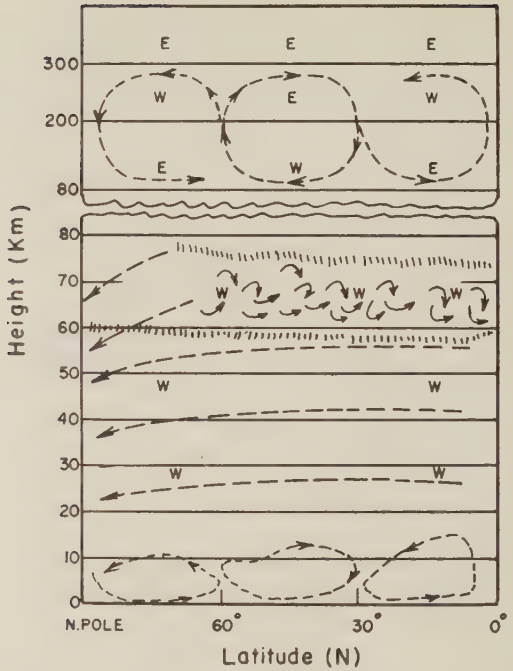

Fig. 5—General meridional circulation in winter in the northern hemisphere

pole to equator are present. This pressure gradient increases with elevation. As has just been pointed out, the effect of friction and of any unbalanced pressure gradient will be to cause meridional motion from higher to lower pressure, that is, from the pole toward the equator. In winter in the mesoincline, westerlies associated with pressure decreasing from equator to pole are present. Hence the meridional motion due to the same effects as mentioned above will be from the equator toward the pole. Such a type of meridional motion in this region in winter has been suggested by Wulf [1942] and Craig [1948] to explain the increase of ozone from fall to spring at the higher latitudes. But they also suggest the occurrence of subsidence at the higher latitudes. The latter feature has also been incorporated in the model of winter circulation suggested here for the mesoincline (Fig. 5).

Even in the mesodecline, easterlies in summer and westerlies in winter are present, at least up to 70 km. But superposed over these winds, turbulence is known to occur in this region, especially during summer and during the day. Evidence for such turbulent activity is provided by observations of meteor trails [Kahlke, 1921; Whipple, 1943; and Olivier, 1947] and noctilucent clouds [Vestine, 1934]. Examining all the available evidence, Kellogg [1950] came to the conclusion that the existence of turbulence between 50 and 80 km seems certain. Chiu [1951] pointed out that this turbulence in the mesodecline will be stronger during the day than during the night. As has been shown in section 2, larger lapse rates may be expected in the mesodecline in summer than in winter at all latitudes. Hence

turbulent activity is likely to be strongest in summer. It has also been considered necessary to assume the occurrence of subsidence over the winter pole in order to explain the high temperatures around 45 to 50 km.

5. *Circulation in the thermosphere*

In connection with the movements of air in the thermosphere, certain additional influences are to be considered, which are not important at the lower levels. Some of these are the effect of kinematic viscosity, the effect of tidal forces, and the storage of energy provided by the dissociation processes in the thermosphere.

Examining now the winds in the region above 80 km, we find in summer (Fig. 2) westerlies over middle latitudes. There is also a strong indication of easterlies at the low and high latitudes. In winter, westerlies are present above 80 km in middle latitudes, decreasing in strength toward higher latitudes. The winter wind data for this region are much fewer than for summer, and from Figure 3 the presence of easterlies above 80 km at the low and high latitudes is not apparent. In keeping with the criterion adopted in this investigation, it will be worth while to see if the assumption of some arbitrary values of easterlies at the very low and very high latitudes in the 80 to 100 km region in winter will improve the temperature distribution which was obtained for this region without making any such assumption. The computations show that the temperatures obtained after assuming the easterlies are more in accord with our theoretical expectations than those obtained without such assumption. Thus there seems to be fairly good indirect evidence for the presence of easterlies at low and high latitudes in winter in the 80 to 100 km region.

Yerg's investigations [1951, 1952] have shown that kinematic viscosity becomes important around 80 km, reaches its maximum value somewhere between 80 and 300 km, and becomes negligible above 300 km. The effect of viscosity in this region will be to cause meridional motions from the north in the region of easterly zonal winds and from the south in the region of westerly zonal winds. From the distribution of zonal winds in the 80 to 100 km region discussed above, the meridional motions due to the effect of viscosity are inferred. These meridional motions reach their maximum value at about 200 km, where the kinematic viscosity reaches its maximum [Yerg, 1951]. From considerations of continuity, it is reasonable to expect that the return meridional flow will occur above 200 km and below 300 km. Above 300 km, the kinematic viscosity becomes negligible. Hence slipping will take place and easterlies will appear at all latitudes in the region above 300 km. From these considerations, the thermospheric circulation shown in the upper parts of Figures 4 and 5 is arrived at. Sheppard's [1949] curves of variation of wind with height over middle latitudes and Hoffmeister's [1946] observations of winds at 50° north and around 120 km are in accord with the circulation suggested here. Moreover, Yerg [1951] suggested a similar circulation for the 100 to 300 km region from theoretical considerations and used this circulation to explain successfully the longitudinal differences observed in electron concentrations for the $F2$ layer.

It has to be borne in mind that the above is a very simplified picture of the circulation, over which will be superposed such effects as that of the periodic tidal

winds and of aperiodic variations. Many more direct observations are required to confirm the thermospheric circulation model shown here in Figures 4 and 5.

6. *Summary and conclusions*

The winds adopted here for the discussion of the circulation have been shown to be consistent with the observed temperature field. The proposed mesopheric circulation is in agreement with that suggested by Kellogg and Schilling [1951]. But the circulation adopted for the thermosphere differs considerably from the model indicated by the above authors for the region from 80 to 120 km. The main difference between the two models lies in the fact that the circulation suggested by Kellogg and Schilling requires the presence of westerlies between 100 and 120 km and easterlies around 80 km at all latitudes, whereas according to our model easterly zonal winds exist at very low and very high latitudes and westerlies over middle latitudes in the region from 80 to 200 km. The thermospheric circulation proposed here is similar to the circulation suggested by Yerg [1951] for the 100 to 300 km region. The winds above 100 km and over middle latitudes presented by Sheppard [1949] and Hoffmeister [1946] are also in agreement with our model of circulation. Certain parts of our model, especially in the regions above 100 km and over the very low and very high latitudes, are still very much in need of confirmation by direct wind observations.

From a consideration of the gradients of zonal winds, it seems more likely that hydrodynamic instability will occur in the thermosphere than at lower levels. The result of any such instability will be the breakdown of zonal motion and zonal symmetry assumed here.

7. *Acknowledgments*

The writer wishes to thank Prof. Bernhard Haurwitz for his guidance, suggestions, and encouragement in all phases of the reported research. The writer also wishes to thank the following: Prof. James E. Miller for his advice and help during the author's stay at New York University, and Prof. Julius London for his suggestions and encouragement.

References

[1] Air Weather Service (1953); Analysis and wind flow at the 50- and 25-mb levels, Tech. Rep. 105-96.

[2] Brasefield, C. J. (1950); Winds and temperatures in the lower stratosphere, J. Met., 7, 66-69.

[3] —— (1953); Wind data, especially between 30 and 80 kilometers, Proceedings of the Conference on Motions in the Upper Atmosphere, held at Albuquerque, New Mexico, Sept. 7-9, 1953, pp. 36-37.

[4] —— (1954); Winds at altitudes up to 80 kilometers, J. Geophys. Res., 59, 233-237.

[5] Briggs, B. H. (1953); Detection of ionospheric movements by a radio method, Proceedings of the Conference on Motions in the Upper Atmosphere, held at Albuquerque, New Mexico, Sept. 7-9, 1953, pp. 19-20.

[6] Chapman, S. (1953); Some causes of winds in the ionosphere, Proceedings of the Conference on Motions in the Upper Atmosphere, held at Albuquerque, New Mexico, Sept. 7-9, 1953, pp. 5-14.

[7] Chiu, Wan-Cheng (1951); The general circulation of the upper atmosphere, Upper Atmospheric Research, California Institute of Technology, Appendix 4, pp. 107-139.

[8] Conover, W. C., and C. J. Wentzien (1955); Winds and temperatures to forty kilometers, J. Met., **12**, 160-164.
[9] Craig, R. A. (1948); The observations and photochemistry of atmospheric ozone and their meteorological significance, Massachusetts Institute of Technology, Sc.D. thesis.
[10] Crary, A. P. (1950); Stratospheric winds and temperatures from acoustical propagation studies, J. Met., **7**, 233-242.
[11] —— (1952); Stratospheric winds and temperatures in low latitudes from acoustical studies, J. Met., **9**, 93-109.
[12] —— (1953); Annual variations of upper winds and temperatures in Alaska from acoustical measurements, J. Met., **10**, 380-389.
[13] —— (1954); Revision of high-level wind and temperature measurements in Bermuda, J. Met., **11**, 257.
[14] Darling, E. M., Jr. (1953); Winds at 100 mb and 50 mb over the United States in 1952, Bull. Amer. Met. Soc., **34**, 458-461.
[15] Dobson, G. M. B., *et al.* (1946); Meteorology of the lower stratosphere, Proc. R. Soc., A, **185**, 144-175.
[16] Elterman, L. (1954); Seasonal trends of temperature, density, and pressure up to 67.6 km obtained with the searchlight probing technique, J. Geophys. Res., **59**, 351-358.
[17] Elvey, C. T. (1953); OH bands and their possible relationship to motions in the upper atmosphere, Proceedings of the Conference on Motions in the Upper Atmosphere, held at Albuquerque, New Mexico, Sept. 7-9, 1953, p. 15.
[18] Flohn, H. (1950); Die Planetarische Zirkulation der Atmosphäre bis 30 km Höhe, Ber. D. Wetterdienst US-Zone, No. 12, p. 156.
[19] Gerson, N. C. (1953); Seasonal variations in wind velocity, Proceedings of the Conference on Motions in the Upper Atmosphere, held at Albuquerque, New Mexico, Sept. 7-9, 1953, pp. 32-33.
[20] —— (1955); Sporadic *E* movements, J. Met., **12**, 78-79.
[21] Goldie, A. H. R. (1950); The average planetary circulation in vertical meridian planes, Centenary Proceedings of the Royal Meteorological Society, pp. 175-180.
[22] Greenhow, J. S. (1954); Systematic wind measurements at altitudes of 80-100 km using radio echoes from meteor trails, Phil. Mag., Ser. 7, **45**, 471-490.
[23] Gutenberg, B. (1949); New data on the lower stratophere, Bull. Amer. Met. Soc., **30**, 62-64.
[24] Haurwitz, B. (1954); The zonal wind field in the upper atmosphere, Dept. of Met. and Ocean., New York University, Sci. Rep. No. 7.
[25] Havens, R. J., *et al.* (1952); The pressure, density, and temperature of the earth's atmosphere to 160 kilometers, J. Geophys. Res., **57**, 59-71.
[26] Hoffmeister, C. (1946); Die Strömungen der Atmosphäre in 120 km Höhe, Zs. Meteorol., No. 1, p. 33.
[27] Jenkins, C. F. (1952); A survey of available information on winds above 30,000 feet, Air Force Surveys in Geophysics, No. 24.
[28] Johnson, N. K. (1946); Wind measurements at 30 km, Nature, **157**, 24.
[29] Kahlke, S. (1921); Meteorschweife und hochatmosphärische Windströmungen, Ann. Hydrogr., **49**, 294.
[30] Kellogg, W. W. (1950); Turbulence in the upper stratosphere, U.C.L.A. Institute of Geophysics, U.S. Weather Bureau Contract, Cwb 7904 (part II).
[31] —— and G. F. Schilling (1951); A proposed model of circulation in the upper stratosphere, J. Met., **8**, 222-230.
[32] Kennedy, W. B. (1953); High altitude wind measurements by acoustic propagation studies, Proceedings of the Conference on Motions in the Upper Atmosphere, held at Albuquerque, New Mexico, Sept. 7-9, 1953, p. 45.
[33] —— *et al.* (1954); Atmospheric winds and temperatures in the 30 to 60 km region over eastern Colorado, Denver Research Institute, University of Denver, Sci. Rep. No. 3.
[34] Kochanski, A. (1955); Cross-sections of the mean zonal flow and temperature along 80°W, J. Met., **12**, 95.
[35] Mitra, S. K. (1952); The Upper Atmosphere, Asiatic Society of Bengal, Calcutta, 2nd ed. pp. 136-137.

[36] Olivier, C. P. (1947); Long enduring meteor trains, Proc. Amer. Phil. Soc., **91**, 315-327.
[37] Pressman, J. (1955); Seasonal and latitudinal temperature changes in the ozonosphere, J. Met., **12**, 87-89.
[38] Richardson, J. M., and W. B. Kennedy (1952); Atmospheric winds and temperatures to 50 kilometers altitude as determined by acoustical propagation studies, J. Acoust. Soc. Amer., **24**, 731-741.
[39] Rossby, C. G. (1948); On the nature of the general circulation of the lower atmosphere, in "Atmospheres of the Earth and Planets," edited by G. P. Kuiper, University of Chicago Press, Chicago, Chap. **2**.
[40] Scrase, F. J. (1951); Radiosonde and radar wind measurements in the stratosphere over the British Isles, Q. J. R. Met. Soc., **77**, 483-488.
[41] Sheppard, P. A. (1949); The exploration of the upper atmosphere, Sci. Prog., **37**, 488-503.
[42] Vestine, E. H. (1934); Noctilucent clouds, J. R. Astr. Soc. Can., **28**, 249-272 and 303-317.
[43] Wexler, H. (1950); Annual and diurnal temperature variations in the upper atmosphere, Tellus, **2**, 262-274.
[44] Whipple, F. L. (1943); Meteors and the earth's upper atmosphere, Rev. Mod. Phys., **15**, 246-264.
[45] —— (1953); Winds in the upper atmosphere by meteor-train photography, J. Met., **10**, 390-392.
[46] Wulf, O. R. (1942); The distribution of atmospheric ozone, Proceedings of the Eighth American Science Congress, Washington, D.C., p. 439.
[47] Yerg, D. G. (1951); Ionospheric wind systems and electron concentrations in the *F*-layer, J. Met., **8**, 244-250.
[48] —— (1952); A tentative evaluation of kinematic viscosity for ionospheric regions, J. Geophys. Res., **57**, 217-220.

VLF PHASE SHIFTS ASSOCIATED WITH THE DISTURBANCE OF FEBRUARY 23, 1956*

BY J. A. PIERCE

Cruft Laboratory, Harvard University, Cambridge 38, Massachusetts

(Received May 10, 1956)

ABSTRACT

During the magneto-ionic disturbance following a solar flare at about $03^h\ 34^m$ U.T. on February 23, 1956, the phase of a signal received at Cambridge, Massachusetts, at 16 kc/s from a transmitter, at Rugby, England, was advanced by about 44 microseconds or 250°. The peak Doppler effect on the received frequency occurred at $03^h\ 47^m$, and corresponded approximately to a falling of the effective height of reflection at 1 km/min, assuming that the phase change was produced solely by a change in height.

The record of this phenomenon is contrasted with those made during daytime sudden ionospheric disturbances. It is shown that in the latter case an increase in signal amplitude is observed at 60 kc/s but not at 16 kc/s, and that there must be changes in the phase shift at reflection from the ionosphere, as well as changes in the height of reflection.

Some comparisons are given between the time of occurrence of this phenomenon and the times of various other effects of this disturbance that have already been reported.

Introduction

An interesting, and apparently rare, magneto-ionic disturbance occurred on the (local) night of February 22–23, 1956. It was characterized by an unusually large and sudden increase in cosmic-ray activity, quoted in newspaper reports as beginning at $03^h\ 45^m$ Universal Time on February 23, and persisting for many hours.

Dr. Kurt Toman, of the U.S. Air Force Cambridge Research Center, has kindly investigated the data available to that organization. He reports privately that a solar flare, accompanied by a sudden ionospheric disturbance, was observed at Tokyo at $03^h\ 34^m$ U.T. It is apparently not yet clear whether this S.I.D. was of unusual intensity, but its duration was exceptionally long.

With equal kindness, Dr. Alan Shapley, Chief of the Sun-Earth Relationships Section of the National Bureau of Standards, has written me that this was an unusual event, in that increased absorption of radio waves was observed at ionospheric observatories in the auroral zone on the dark side of the earth. This ab-

*The research reported in this paper was made possible through support extended Cruft Laboratory, Harvard University, jointly by the Navy Department (Office of Naval Research), the Signal Corps of the U.S. Army, and the U.S. Air Force, under ONR Contract Nonr-1866(07).

sorption apparently began within an hour after the event and persisted for a day or two. Dr. Shapley reports the beginning of the increase in cosmic-ray intensity at $03^h\ 50^m\ 30^s$ U.T.

The purpose of this note is to report the nearly simultaneous effects observed on a very low frequency transatlantic signal. Although this technique is relatively new, the effects in this instance are rare, in the sense that nothing similar has been noted in substantially continuous observations over some 20 months.

Background of the Experimental Method

The experimental technique involved records of the received phase of the 16 kc/s carrier from Rugby, England, with respect to the phase of a standard oscillator at Cambridge, Massachusetts. A summary of the technique and a description of the normal diurnal variations have been published [see 1 of "References" at end of paper].

Although the first-order phase variations observed by this method are those caused by differences between the two sources of frequency, the use of very stable oscillators, plus care and good luck, has made it possible to measure the diurnal variations in transmission time with fair accuracy. The ordinary change from night to day is about 35 microseconds in the transmission time, and individual normal days' records seldom show a deviation from the average of more than ± 5 microseconds. There is, however, a tendency to exceed this deviation during nights of unusually high magnetic activity.

An alternative way of expressing the high stability of VLF propagation is in terms of Doppler effects on the received frequency. These are caused by changes in height of the reflecting layer or by changes in the phase shift at reflection. In the average, there is no measurable Doppler shift during the hours of daylight or darkness over the whole path. During the sunrise period (from the first incidence of solar rays on the first reflection point until about the time the sun is on the horizon of the last reflection point), the layer is falling and the received frequency is increased by about 2 parts in 10^9. Similarly, a Doppler shift of $-2/10^9$ is observed during the sunset period. Deviations from these values are usually less than 1 in 10^9, even over short intervals but, again, high magnetic activity at night may induce quasi-cyclic variations of 2 or 3 parts in 10^9.

Observations on February 23, 1956

The event of February 22–23 is unique in having produced a Doppler shift of no less than $+65/10^9$, something like 20 times the magnitude of the normal maxima. The phase diagram for this event is the original record shown in the upper part of Figure 1. This record has a vertical breadth of approximately one period (62.5 μsec) of the carrier frequency. The dark and light bands shown are simply the positive and negative amplitude excursions of the carrier cycle. At the bottom is a normal record for a magnetically quiet night, showing a little of the sunset slope at the left and the beginning of the sunrise slope at the right-hand end. Beginning at about $03^h\ 45^m$ U.T. in the upper record is the phase anomaly presumably associated with the solar flare of $03^h\ 34^m$ U.T., February 23, and the subsequent increase in cosmic-ray intensity. The deviation in phase has the sense

of decreasing transmission time, or reduction in the equivalent height of reflection. If we, for the moment, regard these phase changes as simply caused by variations in height of reflection, it appears that the drop of some 44 microseconds corresponds to a reduction from the normal night-time height to somewhat below the normal

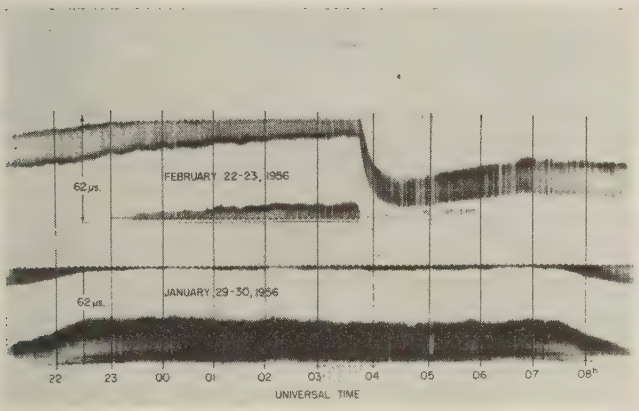

FIG. 1—Night-time variation of 16 kc/s phase at 5,200 km:
Above—During anomaly of February 23, 1956
Below—On a sample magnetically quiet night

daytime height. As can be seen from Figure 1, or perhaps better from Figure 2 where these phase changes are replotted on a more convenient scale, the "height" failed to return to the night-time value and became normal only when daylight had returned to the whole path. There is some indication, in either Figure 1 or Figure 2, that some kind of primary effect persisted for about three hours. Presumably this is the period over which the height of reflection was below the normal

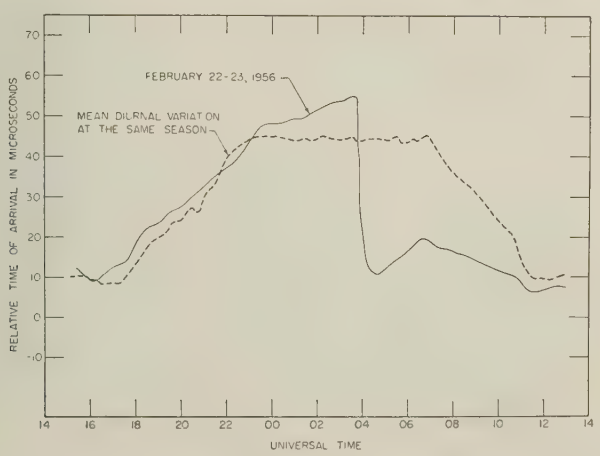

FIG. 2—Diurnal variation of 16 kc/s time of arrival, February 23, 1956

daytime level, although there is certainly no conclusive evidence to this effect. It should be realized that changes of a few microseconds over several hours, such as the increase between 23^h Feb. 22 and 03^h Feb. 23, may be caused by oscillator vagaries.

Figure 3 shows the detail of the phase variation near 04^h U.T., so far as it can

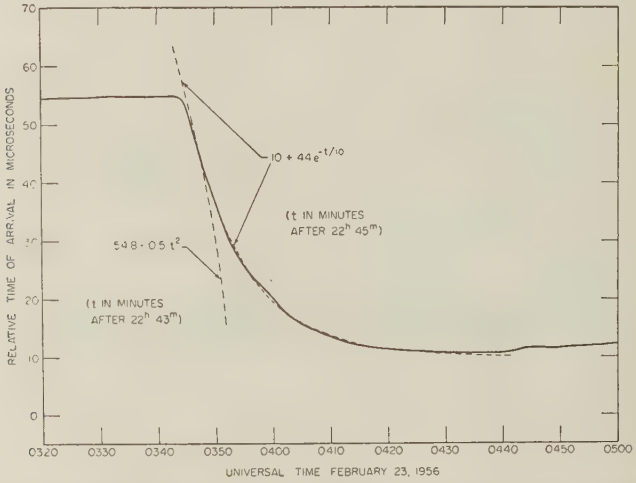

FIG. 3—Detail of the sudden reduction in transmission time near 04^h U.T., February 23, 1956

be scaled from the record, and Figure 4 gives the Doppler effect on the received frequency, which is, of course, proportional to the negative of the slope of Figure 3. In Figure 3, dotted lines with appended approximate equations serve to define the rates of change. Perhaps the most curious feature of this phenomenon is the parabolic way the phase departed from normal for no less than the four minutes

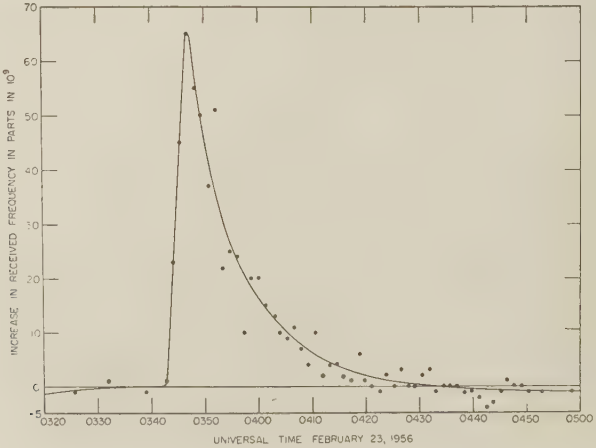

FIG. 4 —Doppler effect on the received frequency of GBR (Rugby, England), February 23, 1956

rom $03^h\ 43^m$ to $03^h\ 47^m$ U.T. This is best seen in the linearity of the curve of Figure for this interval. In this respect, this event differs from the normal daytime .I.D., whose onset is often almost instantaneous, as will be shown in an example elow.

The chronology of this event, as observed at 16 kc at least, may be divided nto five periods, as follows:

(*a*) $03^h\ 43^m$ to $03^h\ 47^m$—A smooth increase in the rate of change of phase, perhaps corresponding to the building up of the force applied to the reflecting layer. At $03^h\ 47^m$, the layer height was apparently falling at a rate of at least one kilometer per minute.

(*b*) $03^h\ 47^m$ to $04^h\ 35^m$—Continuing change in phase but at a decreasing rate that is approximately a negative exponential. This may correspond to a sustained applied force acting upon an atmospheric density exponentially increasing as the height of reflection decreases.

(*c*) $04^h\ 35^m$ to $06^h\ 40^m$—A slow return of the phase, but not extending appreciably above the normal daytime level. The end of this period may indicate the time at which the applied force fell below that necessary to push the height of reflection below the normal daytime value.

(*d*) $06^h\ 40^m$ to $11^h\ 30^m$—Phase maintained at more or less the daytime value. This presumably indicates continuing incoming energy, at a lower level but still exceeding the ionizing energy normally available at night.

(*e*) After $11^h\ 30^m$—The effects of the phenomenon may have continued, but at a level so low as to be obscured by normal daytime ionization.

Sudden Ionospheric Disturbances

For purposes of comparison, examples of normal (daytime) sudden ionospheric disturbances are given in Figures 5 and 6. The S.I.D. of March 15, 1956, shown n Figure 5, was of longer than average duration—an hour or more—but of relatively ow intensity. On this occasion, the 5 Mc/s signal from WWV (over a path of 650

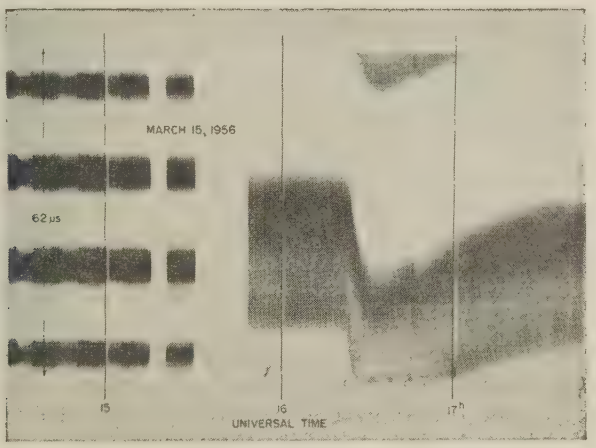

Fig. 5—Phase shift, at 16 kc/s, associated with S.I.D. at $16^h\ 23^m$, March 15, 1956

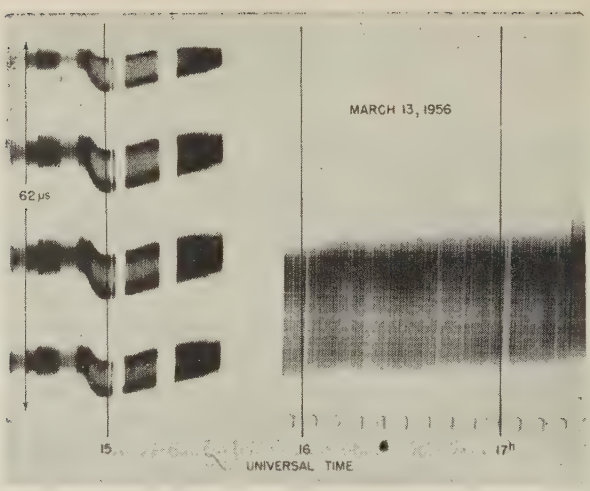

Fig. 6—Phase shift, at 60 kc/s, associated with S.I.D. at $14^h\ 53^m$, March 13, 1956

km) was totally absorbed from $16^h\ 23^m$ to $17^h\ 30^m$ U.T., almost exactly the interva in which the phase diagram of Figure 5 shows appreciable curvature. Signals a higher frequencies, however, were less affected. For example, pulses recorded her from North Carolina (1300 km) at 9.1 Mc/s were barely perceptibly attenuated and similar pulse signals at 12.9 Mc/s showed no effect whatever. The phase o the 16 kc/s signal from Rugby, Figure 5, was advanced by about 18 μsec, but show no significant change in amplitude. It should be noted that, in contrast to th night-time phenomenon of Figure 1, the onset of the phase shift is very rapid.

The pattern with approximately four bars, at the left in Figures 5 and 6, is recording of the phase of the 60 kc/s standard-frequency signal, MSF, also fron Rugby, England. Because this transmission is made only from $14^h\ 30^m$ to $15^h\ 30$ U.T., and because GBR is shut down for maintenance between 13^h and 15^h, w use the same recording equipment for both signals with a loss of only a small par of the GBR record.

Figure 6 shows the phase shift produced by an S.I.D. that occurred while th 60 kc/s record was being made, at $14^h\ 53^m$ U.T. on March 13, 1956. In this case the S.I.D. was of shorter duration but greater intensity than that of Figure 5 The signals at 5 Mc/s, 9.1 Mc/s, and 12.9 Mc/s, mentioned above, were all com pletely absorbed from $14^h\ 53^m$ to $15^h\ 33^m$ U.T.

There are two interesting features in Figure 6. One is the indication of a con siderable increase in amplitude of the signal, shown here by the broadening an blackening of the trace. This increase in field strength during an S.I.D. has ofte been reported at low frequencies. The effect, however, does not seem to obtain a VLF, as the amplitude of the signal at 16 kc/s, in Figure 5, is sensibly unaffected

The second interesting point concerns the small variation in phase during th S.I.D. observed at 60 kc/s. It will be recalled that this S.I.D. appeared to b more intense than that shown in Figure 5. The phase shift, however, in Figure 6 was only about 3.2 microseconds or 70° of phase, whereas the effect in Figure

was about 18 microseconds or 100° of phase. This indicates that we must be careful about attributing these phase effects to simple changes in height of the reflecting layer. It is possible that, without much change in height, the primary physical phenomenon is a steepening of the ionization gradient, with an accompanying reduction in the phase lag at reflection. In all probability, the effects we observe in Figures 1, 5, and 6 are a resultant of changes in both height and phase shift.

Other Concurrent Observations

During the preparation of this note, interesting reports have been received from other sources. Through the courtesy of Dr. Toman, we have received a pre-publication copy of a paper [2] by Meyer and Simpson, of the University of Chicago, reporting the details of a twentyfold increase in cosmic-ray intensity beginning at $03^h\ 50^m\ 30^s$ U.T. on the day in question. A relatively constant high level was maintained for some 25 minutes beginning at about $04^h\ 10^m$; the subsequent quasi-exponential decrease persisted for at least 18 hours. Meyer and Simpson reported several associated phenomena: a radio-noise outburst (Sydney) beginning at $03^h\ 35^m$, and the onset of the sudden ionospheric disturbance at $03^h\ 40^m$. They differ from Dr. Toman in quoting the observed flare as beginning at $03^h\ 31^m$ and having maximum intensity at $03^h\ 42^m$.

Allan, Crombie, and Penton have reported [3] their technique for and preliminary results of frequency measurements on the GBR signal. They have very kindly sent me a copy of a record obtained during this disturbance. I have taken the liberty of transcribing their data into a form comparable with Figure 3. The resultant curve drops some 70 or 80 microseconds between $03^h\ 33^m$ and $03^h\ 39^m$, and then declines slowly another 40 microseconds to a low plateau, maintained from at least $04^h\ 05^m$ to $04^h\ 35^m$, followed by a gradual increase. The total phase shift was more than twice that observed at Cambridge; the path length is 18,700 km instead of 5,200 km. About two-thirds of the transmission path was in daylight and one-third in darkness.

It will have been noted that the phase shift in New Zealand started a full 10 minutes before the similar effect in Massachusetts. The approximate coincidence between the New Zealand effect and the solar flare presumably indicates that the controlling transmission to New Zealand was primarily through the sunlit hemisphere and that the initial phase shift, at least, was due to direct ionization by photons.

A further letter from Dr. Shapley states that high frequency absorption began, in the auroral zone on the dark side of the earth, between $04^h\ 00^m$ and $04^h\ 05^m$ U.T. This was about 30 minutes after the flare and the onset of high frequency absorption in the sunlit hemisphere. Dr. Shapley also transmitted a copy of an extremely interesting paper [4] by Ellison and Reid, of the Royal Observatory at Edinburgh, who observed an unprecedented reduction in atmospherics at 24 kc/s at $03^h\ 45^m$ U.T. The record of Ellison and Reid, although of the amplitude of atmospherics from random directions rather than the phase of a signal, is closely similar to Figure 1 or Figure 2 above. This must be taken as clear evidence of a *D*-layer transition similar to that between night and day over much, if not all, of the dark hemisphere.

Ellison and Reid also quote reports of several other phenomena, notably a magnetic crochet observed at Kodaikanal between $03^h\ 35^m$ and $04^h\ 54^m$, and high frequency absorption at Singapore from $03^h\ 35^m$ to 06^h.

All these various observations mentioned above are brought into more or less chronological order in Table I. Except for items 5 and 7, which have scaling errors

TABLE I—*Chronology of various phenomena on February 23, 1956*

Item	Phenomenon	Point of Observation	Side of earth	Greenwich mean time			Authority
				Beginning	Maximum	End	
				h m	*h m*	*h m*	
1	Solar flare	Tokyo	Sunlit	03 34			Toman
				or 03 31	03 42	04 15	Meyer and Simpson
		Kodaikanal	Sunlit	03 35	<03 40	05 10	Ellison and Reid
2	Very high frequency solar radio noise	Sydney	Sunlit	03 35	.....	.....	Meyer and Simpson
3	Magnetic crochet	Kodaikanal	Sunlit	03 35	.....	04 54	Ellison and Reid
4	High frequency radio fadeout	Kodaikanal	Sunlit	03 32	.....	07 00	Ellison and Reid
		Singapore	Sunlit	03 35	.....	06 00	Ellison and Reid
		Australia	Sunlit	03 40	.....	.....	Meyer and Simpson
5*a*	Very low frequency radio phase	Wellington	Sunlit/Dark	03 33	04 20±10	.....	Allan, Crombie, and Penton
5*b*		Massachusetts	Dark	03 43	04 35	>11 30	Pierce
6	Very low frequency radio noise	Edinburgh	Dark	03 45	.....	>07 30	Ellison and Reid
7	Cosmic radiation	Chicago	Dark	03 50½	04 10	>22 00	Meyer and Simpson
8	High frequency radio absorption	Auroral zone	Dark	>04 00 <04 05	.....	.....	Shapley

of ±0.5 minute, and item 8, which has a total uncertainty of <5 minutes, the precision of the various time determinations is unknown. It seems, however, that scaling errors may account for all of the variations in time of beginning for items 1 through 5*a*. Except for item 2, these immediate effects may all be presumed to stem from ultraviolet irradiation of the atmosphere. In comparison with these various instantaneous effects, the VLF radio effects on the dark side of the earth were delayed about 10 minutes, and the observed cosmic radiation was delayed fully 15 minutes. The auroral-zone high-frequency absorption, as mentioned above, made its appearance about 30 minutes after the flare.

From the rarity of both such a cosmic-ray burst and the VLF radio effects it must be presumed that they are directly associated. We have here, apparently, a simple case of ionization (weak, but detectable at low radio frequencies) produced at *D*-layer height through direct bombardment by charged particles traveling at the unusual velocity of four-tenths that of light, yet affecting the dark side of the earth.

Conclusions

We have shown the effect of an apparently unusual magneto-ionic phenomenon upon the transmission time of a VLF radio signal, and have given examples of the corresponding effects associated with more ordinary solar flares.

This new method of observation casts no light, at present, on the question of the height in the atmosphere at which these effects are produced. It is probable, however, that when this technique can be applied simultaneously to several radio frequencies, it may yield new and valuable data.

References

[1] J. A. Pierce, The diurnal carrier-phase variation of a 16-kilocycle transatlantic signal, Proc. Inst. Radio Eng., **43**, 584-588 (1955).

[2] Peter Meyer and J. A. Simpson, Temporary increase of cosmic ray intensity following the solar flare of February 23, 1956, submitted to Phys. Rev.

[3] A. H. Allan, D. D. Crombie, and W. A. Penton, Frequency variations in New Zealand of 16 kc./s. transmissions from GBR Rugby, Nature, **177**, 178-179 (1956).

[4] M. A. Ellison and J. H. Reid, A long-wave anomaly associated with the arrival of cosmic-ray particles of solar origin on 23 February, 1956, J. Atmos. Terr. Phys., 8, 291-293 (1956).

ARC-LENGTHS ALONG THE LINES OF FORCE OF A MAGNETIC DIPOLE*

By Sydney Chapman

Geophysical Institute, University of Alaska, College, Alaska, and High Altitude Observatory, University of Colorado, Boulder, Colorado,

AND

Masahisa Sugiura

Geophysical Institute, University of Alaska, College, Alaska

(Received May 8, 1956)

ABSTRACT

Formulae and tables for the arc-length along the lines of force of a magnetic dipole are given with reference to the earth treated as a sphere. These tables may prove useful in connection with the study of radio whistlers and of the motion of charged particles along the lines of geomagnetic force.

Auroral observations and theory alike suggest that protons travel for some distance along the lines of force of the earth's magnetic field to enter the auroral zone. The radio signals known as whistlers also appear to travel along the lines of force, sometimes traversing their whole length from one hemisphere to the other, one or more times. Hence it seems useful to give formulae and tables for the arc-length along the lines of force. This is done here, for the idealized case of a magnetic dipole field.

In Figure 1, O represents the earth's center, and B the boreal geomagnetic

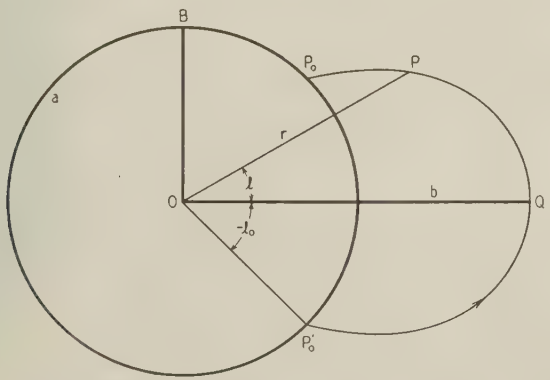

FIG. 1

*Assisted in part by the Air Force Cambridge Research Center, Air Research and Development Command, through Contract No. AF 19(604)1048, and by the National Bureau of Standards.

pole. The earth is regarded as a sphere of radius a. Consider a line of force starting from the surface at P_o' in latitude $-l_o$, crossing the geomagnetic equator at Q, and ending at P_o in latitude l_o. Let P be any point on the line, at latitude l and at distance r from O. Then it is known that

$$r = b \cos^2 l$$

where

$$b = OQ,$$

and

$$b = a \sec^2 l_o$$

Hence an element of arc along the line is given by

$$ds = b(1 + 3 \sin^2 l)^{1/2} \cos l \, dl$$

It is convenient to make the transformation

$$\sinh x = \sqrt{3} \sin l$$

A simple integration then gives

$$s = QP = (\tfrac{1}{2}b/\sqrt{3})(x + \sinh x \cosh x)$$
$$= bf(l)$$

For small values of l, in circular measure, s/b is given approximately by

$$s/b = f(l) = l + \frac{1}{3} l^3 - \frac{7}{15} l^5$$

For small values of l_o, in circular measure, the arc-length s_o from Q to P_o is given approximately by

$$s_o/a = l_o + \frac{4}{3} l_o^3 + \frac{8}{15} l_o^5$$

For each degree of latitude, Table 1 gives the value of b for the line of force ending in that latitude; in calculating b, the earth's radius a has been taken as 6371.229 meters.† The values of $f(l)$ are also given for each degree of latitude, with their first differences Δf; if $f(l)$ is multiplied by b for any value of l_o, it gives QP for the corresponding line of force; similarly $b\Delta f$ gives the arc-length for 1° interval of latitude along that line of force.

Table 2 gives s/a for latitude l at 5° intervals along the lines of force ending in latitude l_o at 5° intervals. The values of b and of s/a are given to four significant figures only.

It is of interest to note that for the outlying lines of force (l_o large) the ratio s_o/b of the total arc-length s_o to the equatorial radius b of the line approaches a finite limiting value (for $l_o = 90°$)

$$1 + (\sinh^{-1} \sqrt{3})/(2\sqrt{3})$$

equal to 1.380; s_o and b themselves tend to infinity as l_o tends to 90°.

In connection with the lines of force of the geomagnetic field, N. Herlofson

†This value for the earth's mean radius was taken from "Landolt-Börnstein, Zahlenwerte und Funktionen aus Physik, Chemie, Astronomie, Geophysik und Technik, Band III, Astronomie und Geophysik," p. 259, Springer-Verlag, Berlin (1952).

TABLE 1—*Values of b (in km) and of f(l) for each degree of latitude. For b, the symbol x, s means x. 10^s; for example, b for $l_0 = 85°$ is 838,700 km.*

l_0 or l	b	$f(l)$	$10^4\Delta f$	l_0 or l	b	$f(l)$	$10^4\Delta f$
°	*km*			°	*km*		
0	6371,0	0.0000					
1	6373,0	0.0175	175	46	1320,1	0.8763	195
2	6379,0	0.0349	174	47	1370,1	0.8956	193
3	6389,0	0.0524	175	48	1423,1	0.9147	191
4	6402,0	0.0699	175	49	1480,1	0.9337	190
5	6420,0	0.0875	176	50	1542,1	0.9524	187
6	6442,0	0.1051	176	51	1609,1	0.9709	185
7	6467,0	0.1228	177	52	1681,1	0.9892	183
8	6497,0	0.1405	177	53	1759,1	1.0073	181
9	6531,0	0.1583	178	54	1844,1	1.0251	178
10	6569,0	0.1762	179	55	1937,1	1.0426	175
11	6612,0	0.1942	180	56	2038,1	1.0598	172
12	6659,0	0.2123	181	57	2148,1	1.0767	169
13	6711,0	0.2305	182	58	2269,1	1.0933	166
14	6767,0	0.2488	183	59	2402,1	1.1096	163
15	6829,0	0.2673	185	60	2549,1	1.1255	159
16	6895,0	0.2858	185	61	2711,1	1.1411	156
17	6967,0	0.3044	186	62	2891,1	1.1563	152
18	7044,0	0.3232	188	63	3091,1	1.1710	147
19	7127,0	0.3421	189	64	3315,1	1.1854	144
20	7215,0	0.3611	190	65	3567,1	1.1993	139
21	7310,0	0.3802	191	66	3851,1	1.2128	135
22	7411,0	0.3994	192	67	4173,1	1.2259	131
23	7519,0	0.4188	194	68	4540,1	1.2385	126
24	7634,0	0.4382	194	69	4961,1	1.2506	121
25	7757,0	0.4578	196	70	5447,1	1.2623	117
26	7887,0	0.4774	196	71	6011,1	1.2734	111
27	8025,0	0.4972	198	72	6672,1	1.2841	107
28	8172,0	0.5170	198	73	7453,1	1.2942	101
29	8329,0	0.5369	199	74	8386,1	1.3038	96
30	8495,0	0.5569	200	75	9511,1	1.3129	91
31	8671,0	0.5769	200	76	1089,2	1.3214	85
32	8859,0	0.5970	201	77	1259,2	1.3294	80
33	9058,0	0.6171	201	78	1474,2	1.3368	74
34	9270,0	0.6372	201	79	1750,2	1.3437	69
35	9495,0	0.6573	201	80	2113,2	1.3500	63
36	9734,0	0.6775	202	81	2604,2	1.3557	57
37	9989,0	0.6977	202	82	3289,2	1.3608	51
38	1026,1	0.7178	201	83	4290,2	1.3653	45
39	1055,1	0.7379	201	84	5831,2	1.3692	39
40	1086,1	0.7579	200	85	8387,2	1.3726	34
41	1119,1	0.7779	200	86	1309,3	1.3753	27
42	1154,1	0.7978	199	87	2326,3	1.3774	21
43	1191,1	0.8176	198	88	5231,3	1.3789	15
44	1231,1	0.8373	197	89	2092,4	1.3799	10
45	1274,1	0.8568	195	90	Infinite	1.3802	3

Table 2—*Values of s/a for latitudes l at 5° intervals along the lines of force ending in latitude l_0 at 5° intervals. The symbol x, s means x. 10^{-s}; for example, s/a at l = 40° for the line of force ending in latitude l_0 = 65° is 4.243.*

l_0 \ l	5°	10°	15°	20°	25°	30°	35°	40°	45°
°									
5	8816,5								
10	9021,5	1817,4							
15	9377,5	1889,4	2864,4						
20	9908,5	1996,4	3027,4	4089,4					
25	1065,4	2146,4	3254,4	4396,4	5573,4				
30	1167,4	2350,4	3563,4	4814,4	6104,4	7425,4			
35	1304,4	2626,4	3983,4	5381,4	6822,4	8299,4	9796,4		
40	1491,4	3003,4	4554,4	6153,4	7801,4	9489,4	1120,3	1292,3	
45	1750,4	3525,4	5345,4	7221,4	9156,4	1114,3	1315,3	1516,3	1714,3
50	2118,4	4265,4	6468,4	8739,4	1108,3	1348,3	1591,3	1834,3	2074,3
55	2660,4	5357,4	8124,4	1098,3	1392,3	1693,3	1998,3	2304,3	2604,3
60	3500,4	7049,4	1069,3	1444,3	1831,3	2227,3	2629,3	3032,3	3427,3
65	4899,4	9867,4	1496,3	2022,3	2563,3	3118,3	3680,3	4243,3	4797,3
70	7480,4	1507,3	2285,3	3087,3	3913,3	4760,3	5619,3	6479,3	7325,3
75	1306,3	2631,3	3990,3	5390,3	6834,3	8313,3	9813,3	1131,2	1279,2
80	2902,3	5845,3	8863,3	1197,2	1518,2	1847,2	2180,2	2513,2	2842,2
85	1152,2	2320,2	3518,2	4753,2	6027,2	7331,2	8654,2	9977,2	1128,1
90	Infinite								

l_0 \ l	50°	55°	60°	65°	70°	75°	80°	85°	
°									
50	2305,3								
55	2895,3	3169,3							
60	3810,3	4170,3	4502,3						
65	5332,3	5838,3	6302,3	6715,3					
70	8142,3	8913,3	9622,3	1025,2	1079,2				
75	1422,2	1556,2	1680,2	1790,2	1884,2	1960,2			
80	3158,2	3458,2	3733,2	3977,2	4186,2	4354,2	4477,2		
85	1254,1	1373,1	1482,1	1579,1	1662,1	1728,1	1777,1	1807,1	
90	Infinite								

and L. Block† have calculated the positions of the northern and southern ends of 123 lines of force, taking into account also the quadrupole terms in the magnetic potential. According to their results, the maximum difference between the "dipole" end P_0' of a line of force beginning at a point P_0, and the calculated (other) end point P_0'' increases from about 0°.4 of arc on the globe at geomagnetic latitude 90° to about 6°.7 at 50°, owing to the equatorial anomalies.

†Tellus, **8**, 210-214 (1956).

GRAVITATIONAL AND THERMAL OSCILLATIONS IN THE EARTH'S UPPER ATMOSPHERE

By Marvin L. White

National Bureau of Standards, Boulder, Colorado

(Received April 26, 1956)

ABSTRACT

The recent work of Sen and White [1] on the excitation of large-scale oscillations in an atmosphere on a rotating globe by gravitational and thermally induced forces is extended to include heating in any portion of the atmosphere. The region where the heating occurs is unrestricted regarding temperature profile. The solution $\chi(z)$ of the radial differential equation of motion consists of (1) a complementary function $ye^{z/2}$, and (2) a particular solution $q(z)/\gamma H(z) + e^{z/2} I(x)$ where I is obtained by integrating the heat source function (with appropriate weight factor) from the top of the atmosphere to the level in question, γ is the ratio of specific heats, $H(z)$ is the scale height, $x = \int dz/H$ where z is the altitude, q is the heat source function, and $\chi(z)$ is the divergence of the velocities. With this representation of the wave function, one recovers the expressions for the velocity components and pressure variations of Pekeris [2] and of Weekes and Wilkes [3] for the purely gravitational case, provided the wave function y is replaced by $[y + I]$. General expressions are also obtained for the vertical and horizontal displacements and for the amplification over equilibrium tide at any level. The latter expression is useful for establishing the so-called solar control of the dynamics of a given layer by radiation absorbed in any other layer. The boundary conditions of Weekes and Wilkes [3] are shown valid for a "top" with constant positive temperature gradient, believed to be the case above 100 km. Finally, the solar and lunar semi-diurnal winds as collected by Briggs and Spencer [4] for the E region when tested by present theory are found to have the same azimuthal dependence as exists at the ground. This is consistent with the original assumption of "variables separable."

1. INTRODUCTION

In a recent paper by Sen and White [see 1 of "References" at end of paper], a unified treatment was given for the excitation of atmospheric oscillations by both

gravitational and thermal action.* They showed that within the framework of a linearized theory, the total wave function χ (divergence of velocities) could be considered as the sum of the gravitational wave function plus the thermal wave function and that, quite generally, the radial wave equation is

$$\left.\begin{aligned}\gamma H\frac{d^2\chi}{dz^2}+\gamma\left(\frac{dH}{dz}-1\right)\frac{d\chi}{dz}+\left(\gamma\frac{dH}{dz}+\gamma-1\right)\frac{\chi}{h}\\ =\frac{1}{Hh}\left(\frac{dH}{dz}+1\right)q-\frac{d}{dz}\left[\frac{1}{H}\left(\frac{dH}{dz}+1\right)q\right]+\frac{d^2q}{dz^2}\end{aligned}\right\}\quad\ldots.(1)$$

where the symbols are those of Sen and White [1] and Wilkes [5]; γ is the ratio of specific heats, $H(z)$ is the scale height, z is the altitude, q is the heat source function, $\chi(z)$ is the divergence of velocities, and h is a constant depending upon the mode of oscillations and the period of the perturbing force ($=7.9$ for S_2). Equation (1) was first obtained by Wilkes for the case of excitation by thermal sources only. Sen and White, using the method of variation of parameters, solve equation (1) for the case where heat is applied only at the base of the atmosphere by eddy conductivity upward, an assumption made by Chapman [6] many years earlier; it is also assumed that over the particular region in which the heating occurs the atmosphere has a constant negative temperature gradient, which is the case for the actual troposphere. The conclusions reached by Sen and White were that current atmospheric models are insufficiently resonant to produce the observed pressure variations S_2, even when both solar grativational tidal forces and thermal excitation at the ground are included.

The above paradox could be resolved by the inclusion of thermal excitation elsewhere in the atmosphere. In the present paper, the radial wave equation (1) is solved for the most general case, that is, one where heating can occur within any atmospheric layer with any temperature profile. The solution consists of a complementary function and a particular solution, $q/\gamma H(z) + Ie^{\frac{1}{2}z}$, where I is an integral easily evaluated by numerical methods and $x = \int dz/H$. Two other representations of the integral I are given, namely, (1) for a special model of the source function $q = q_0 z^\kappa$, where $\kappa = 0, 1, 2, \cdots$, in a region having a constant positive temperature gradient, and (2) for any source function and again a region with constant positive temperature gradient. The solution of the first is given by Lommel's function.

For the general case, expressions are obtained for the velocity components and pressure variation for any height which are identical with the corresponding equations for the purely gravitational case except for a new interpretation of the wave function. This is important for the evaluation of solar winds. An expression is also found for the vertical and horizontal displacements at a given altitude.

The amplification at any point over equilibrium tide is given by

*Note added in proof: It has recently come to the author's attention that this problem is also considered by Manfred Siebert, Bericht des Deutschen Wetterdienstes Nr. 22, 1955.

$$\text{Ampl.} = \frac{p}{p_{\text{equil}}}$$

$$= 1 + \mathbf{N} - \frac{i\gamma g h}{\sigma\Omega} e^{x/2} \left\{ \left[\frac{\left(\frac{H}{h} - \frac{1}{2} + \frac{\mathrm{d}}{\mathrm{d}x}\right) I(x)}{\left(\frac{H}{h} - \frac{1}{2} + \frac{\mathrm{d}}{\mathrm{d}x}\right)(y_1 + iy_2)} \right]_g \left(\frac{\mathrm{d}}{\mathrm{d}x} - \frac{1}{2}\right)(y_1 + iy_2) \right.$$

$$\left. - \left(\frac{\mathrm{d}}{\mathrm{d}x} - \frac{1}{2}\right) I(x) \right\} \quad \ldots\ldots (2)$$

where

$$\mathbf{N} = -e^{x/2} \left\{ \frac{\left(\frac{\mathrm{d}}{\mathrm{d}x} - \frac{1}{2}\right)(y_1 + iy_2)}{\left[\left(\frac{H}{h} - \frac{1}{2} + \frac{\mathrm{d}}{\mathrm{d}x}\right)(y_1 + iy_2)\right]_g} \right\}$$

represents the ratio of the dynamical tide to the equilibrium tide, while the final term represents the contribution to the amplification by thermal sources alone. Here y_1 and y_2 are independent solutions of the homogeneous counterpart of the wave equation (5), the integral $I(x)$ depends upon integrations over the heating action, $x = \int dz/H$ is a pure number, a function of the height, g is the acceleration of gravity, excepting as a subscript where it refers to the ground, σ is the apparent angular velocity of the perturbing body, and Ω is the gravitational potential of the perturbing body. From equation (2), one can obtain, for example, that portion of the amplification at a given level due to solar heating in any layer or combination of layers in the atmosphere by appropriately adjusting the limits of integration of $I(x)$ over which the heating function q is integrated. This is important in determining the so-called solar control, by absorption of radiant energy in an upper layer, over the dynamics of a lower layer.

In Section 3, a simplified boundary condition for the "top" of the atmosphere is introduced, namely, that after a sufficient height above the ground, only an outgoing wave should be present. It is shown that one is justified in eliminating one of the complex constants of integration, not only for an isothermal "top" but for one with a constant temperature gradient as well.

Finally, the solar and lunar semi-diurnal wind data for the E region as summarized by Briggs and Spencer [4] are examined for internal consistency by equations from present theory; good agreement is found regarding both phase and magnitude, from which it can be concluded that the assumption of "variable separable" is justified.

2. GENERAL SOLUTION OF THE RADIAL WAVE EQUATION

The key to the solution of the radial wave equation (1) is to express χ by

$$\chi = \frac{q(z)}{\gamma H(z)} + \chi_1(z) \quad \ldots\ldots (3)$$

where both q and H are any arbitrary functions of z; substituting equation (3) into equation (1), we obtain

$$\frac{d^2\chi_1}{dz^2} + \frac{1}{H}\left(\frac{dH}{dz} - 1\right)\frac{d\chi_1}{dz} + \left(\gamma\frac{dH}{dz} + \gamma - 1\right)\frac{\chi_1}{\gamma hH} = \frac{q}{(\gamma H)^2 h} \quad \ldots\ldots(4)$$

Introducing the Weekes and Wilkes [3] variables into equation (4), namely,

$$x = \int \frac{dz}{H} \quad \text{and} \quad \chi_1 = e^{z/2}y(x)$$

we obtain

$$\left.\begin{aligned} \frac{d^2y}{dx^2} + \mu^2 y &= \frac{qe^{-z/2}}{\gamma^2 h} \\ &= T(x), \quad \text{say} \end{aligned}\right\} \quad \ldots\ldots(5)$$

where

$$\mu^2 = \left[-\frac{1}{4} + \frac{1}{h}\left(\frac{dH}{dx} + \frac{\gamma - 1}{\gamma}H\right)\right]$$

μ corresponding to the index of refraction [3]. The complementary function for the differential equation (5) can be expressed as

$$y = (P + iQ)(y_1 + iy_2) + (R + iS)(y_1 - iy_2) \quad \ldots\ldots(6)$$

where $(P + iQ)$ and $(R + iS)$ are complex constants of integration [7]. Some justification for putting $(R + iS)$ equal to zero will be given in Section 4. A particular solution of equation (5) can be found by the method of variation of parameters, so that the general solution for the radial wave equation becomes

$$\chi = \frac{q(z)}{\gamma H(z)} + e^{z/2}[(P + iQ)(y_1 + iy_2) + (R + iS)(y_1 - iy_2) + I(x)] \quad \ldots\ldots(7)$$

where the particular integral $I(x)$ is given by

$$I(x) = y_1(x)\int_\infty^x \frac{y_2 T(x)}{y_1' y_2 - y_1 y_2'}\,dx - y_2(x)\int_\infty^x \frac{y_1 T(x)}{y_1' y_2 - y_1 y_2'}\,dx \quad \ldots\ldots(8)$$

where $y_\kappa' = dy_\kappa/dx$. Equation (8) shows that $I(x)$ is found by integrating the heat source function (with appropriate weight factor) over that region of the atmosphere at and above the level in question. When no heating sources are present, the particular integral vanishes. Substitution of equation (7) into the general equations (2) and (3) of Sen and White [1] for the pressure variation $p(z)$ and the vertical velocity $w(z)$ leads to the following equations

$$p = \frac{p_0}{H}\left[-\frac{\Omega e^{-z}}{g} + \frac{\gamma h e^{-z/2}}{i\sigma}\left(\frac{d}{dx} - \frac{1}{2}\right)(y + I)\right]\Theta_\gamma^s(\theta)e^{i(\sigma t + s\Phi)} \quad \ldots\ldots(9)$$

and

$$w = \left\{-\frac{i\sigma}{g}\Omega + \gamma h e^{z/2}\left[\left(\frac{H}{h} - \frac{1}{2} + \frac{d}{dx}\right)(y + I)\right]\right\}\Theta_\gamma^s(\theta)e^{i(\sigma t + s\Phi)} \quad \ldots\ldots(10)$$

which are just the equations given by Weekes and Wilkes [3] for the purely gravitational case, provided y is replaced by $(y + I)$. By substitution of equation (9) for $[(p/\rho_0) + \Omega]$ into the general expressions for u and v, the southward and eastward components of air velocity, given by Perkeris [2], and by Weekes and Wilkes [3], one obtains

$$u = \frac{\gamma g h e^{z/2}}{4a\omega^2(f^2 - \cos^2\theta)}\left(\frac{\mathrm{d}}{\mathrm{d}x} - \frac{1}{2}\right)(y + I)\left(\frac{\mathrm{d}}{\mathrm{d}\theta} + \frac{s\cot\theta}{f}\right)\Theta_\gamma^s(\theta)e^{i(\sigma t + s\Phi)} \quad \ldots\ldots(11)$$

$$v = \frac{i\gamma g h e^{z/2}}{4a\omega^2(f^2 - \cos^2\theta)}\left(\frac{\mathrm{d}}{\mathrm{d}x} - \frac{1}{2}\right)(y + I)\left(\frac{\cos\theta}{f}\frac{\mathrm{d}}{\mathrm{d}\theta} + \frac{s}{\sin\theta}\right)\Theta_\gamma^s(\theta)e^{(\sigma t + s\Phi)} \quad \ldots\ldots(12)$$

which agrees with the expressions obtained by Pekeris [2] and by Weekes and Wilkes [3] for the purely gravitational case, provided y is replaced by $(y + I)$.

Of considerable interest in studies of the behavior of the ionized regions of the earth's upper atmosphere are the diurnal and semi-diurnal height variations due to so-called "tidal" effects. For lunar height variations, we do have a simple tidal phenomenon. However, solar oscillations in height are more complicated and are due in part to (1) gravitational causes, (2) thermal heating effects, and (3) diurnal changes in the height which take place independently of atmospheric oscillations. It is the first two effects which are covered by present theory. With this understanding, the vertical (and horizontal) displacements of the neutral particles from their equilibrium position can be found by integrating equations (10), (11), and (12) with respect to time. Thus,

$$\delta x = \frac{u}{i\sigma}, \qquad \delta y = \frac{v}{i\sigma}, \quad \text{and} \quad \delta z = \frac{w}{i\sigma} \quad \ldots\ldots(13)$$

where, as for simple harmonic motion, the phase of the displacements lags by 90° that of the velocities. The path of a unit mass is thus represented by a three-dimensional closed Lissajous figure. Comparing the expression for δz with equation (9), it is immediately seen that the vertical displacements are not, in general, proportional to the pressure variations.*

Let us finally consider the derivation of the amplification over equilibrium tide for any level in the atmosphere. Combining the expressions for the pressure variation and the vertical velocity, and since $p_{\text{equil}} = -\Omega\rho_0$, we have

$$\text{Ampl.} = \frac{p(z)}{p_{\text{equil}}} = -\frac{ig}{\sigma\Omega}[\gamma H\chi - q - w(z)] \quad \ldots\ldots(14)$$

$$= \frac{ig}{\sigma\Omega}\{\gamma H[(P + iQ)(y_1 + iy_2) + I(x)]e^{z/2} - w(z)\} \quad \ldots\ldots(15)$$

*E. V. Appleton, and K. Weekes, Proc. R. Soc., A, **171**, 171 (1939), obtain an expression for the displacement $\delta z = H_0 p/p_0$, using the perfect gas law and the hydrostatic equation of equilibrium and assuming the temperature to be constant; as another example, Martyn obtains the same expression for the tidal displacement in a Chapman layer at the level of maximum ionization, URSI Report No. 2, "Tidal Phenomena in the Ionosphere." These approximations may not be too bad, but one should be cautious in applying quasi-static conditions to dynamical situations. We obtain

$$\frac{\delta z}{H} = \left[\frac{p}{p_0} - \frac{p(0)}{p_g}\frac{(y + I)}{(y + I)_g}\right]e^{z/2}$$

which, as might be expected, vanishes at ground level.

where according to Section 4, $(R + iS)$ has been set equal to zero. $(P + iQ)$ is found by setting $w = 0$ at the ground; thus

$$(P + iQ) = \frac{i\sigma\Omega(0)/\gamma gh - \left[\left(\frac{H_0}{h} - \frac{1}{2} + \frac{\mathrm{d}}{\mathrm{d}x}\right)I\right]_g}{\left[\left(\frac{H_0}{h} - \frac{1}{2} + \frac{\mathrm{d}}{\mathrm{d}x}\right)(y_1 + iy_2)\right]_g} \quad \ldots\ldots\ldots\ldots (16)$$

Substituting $w(z)$ from equation (10) into equation (14) and with the further substitution of $(P + iQ)$ from equation (16), one obtains equation (2) given in the introduction. From equation (2), we see, for example, that when no heating sources are present, the amplification is given by

$$\left.\begin{aligned} \mathbf{M}(z) &= \frac{\text{Equilibrium gravitational + dynamical gravitational}}{\text{Equilibrium gravitational}} \\ &= 1 - e^{z/2}\left[\frac{\left(\frac{\mathrm{d}}{\mathrm{d}x} - \frac{1}{2}\right)(y_1 + iy_2)}{\left[\left(\frac{H_0}{h} - \frac{1}{2} + \frac{\mathrm{d}}{\mathrm{d}x}\right)(y_1 + iy_2)\right]_g}\right] \end{aligned}\right\} \quad \ldots\ldots (17)$$

which, at the ground, reduces to the value $\mathbf{M}(0)$ obtained by Sen and White [1] and Jacchia and Kopal [7]. The last term in equation (2), therefore, represents thermal effects only. It depends, of course, as does the second term, upon the atmospheric profile through the functions y_1 and y_2 . By limiting the range of integration in the expression (8) for I over which q, the heat source function, is integrated, one obtains that contribution to the amplification at some level z, due to the particular heat source under consideration.

3. HEATING IN AN ATMOSPHERE WITH A UNIFORM VERTICAL GRADIENT OF TEMPERATURE

Equation (8) gives the value of the integral I for heating in a layer with any arbitrary temperature distribution. It can be evaluated exactly by numerical integration once y_1 and y_2 are known, and can easily be applied to the Rocket Panel [8] or Rand [9] profiles. However, for an atmospheric model in which the vertical gradient of temperature has a succession of constant values, or for one in which the heating occurs in a region where the temperature gradient is nearly constant, it may perhaps be advantageous to have an analytical expression for the wave function χ for a linear temperature profile. Let us consider, for example, the special case where the atmosphere has a positive temperature gradient and the heat source function has the form $q = q_0 z^\kappa$ in some interval where $\kappa = 0, 1, 2, 3, \cdots$. For $\kappa = 0$, q is a step function. We now make the following transformations:

where

$$\left.\begin{aligned} x' &= 4mz, \quad \text{and} \quad \chi_1 = x'^{1/b} f(x') \\ m &= (\gamma b + \gamma - 1)/\gamma bh \end{aligned}\right\} \quad \ldots\ldots\ldots\ldots (18)$$

assume that $H = bz$, so that the origin of z as used here is the intersection of the temperature profile and the z-axis. The differential equation in $f(x')$ now becomes

$$x'^2 \frac{d^2f}{dx'^2} + x' \frac{df}{dx'} + \left(x'^2 - \frac{1}{b^2}\right)f = 4qx'^{-(1/b)}h(\gamma b)^2 = T_1(x'), \quad \text{say} \qquad \text{.....(19)}$$

a non-homogeneous equation for which the corresponding homogeneous equation is Bessel's equation of order $1/b$.

The solution of equation (19) is given by Lommel's function [10], and the corresponding particular solution of equation (1) is

$$\chi = \frac{q(z)}{\gamma H(z)} + kx'^{1/b} S_{\mu',\nu}(x') \qquad \text{.....(20)}$$

where

$$k = \frac{q_0}{(4m)^\kappa h}\left(\frac{2}{\gamma b}\right)^2, \qquad \mu' = 2\kappa - \frac{b+1}{b}, \qquad \nu = \frac{1}{b}$$

The case of greatest physical interest is probably $\kappa = 0$ and $b = 0.2$. Another solution of the radial wave equation for a straight-line profile with positive slope, valid for any source function, is found from equation (5), using the transformation of Jacchia and Kopal† (our reference [7]), namely,

$$r = r_1 e^{b(x-x_1)/2}$$

where

$$r_1 = \frac{2}{b}\left[\frac{H_1}{h}\left(b + \frac{\gamma - 1}{\gamma}\right)\right]^{1/2} \qquad \text{.....(21)}$$

where $dH/dz = b$, and where x_1 may be interpreted as the level of maximum heating. Then $H = H_1 e^{-b(x-x_1)}$ and

$$\frac{d^2y}{dr^2} + \frac{1}{r}\frac{dy}{dr} + \left[1 - \frac{1}{b^2r^2}\right]y = \left(\frac{2}{br}\right)^2 \frac{qe^{-x/2}}{\gamma^2 h} = T(r), \quad \text{say} \qquad \text{.....(22)}$$

Applying the method of variation of parameters, and recognizing the homogeneous part of equation (22) as Bessel's equation, we obtain

$$\chi = \frac{q}{\gamma H} + e^{x/2}\{(P + iQ)J_{1/b}(r) + iY_{1/b}(r) + (R + iS)[J_{1/b}(r) - iY_{1/b}(r)] + I(r)\} \qquad \text{.....(23)}$$

where

$$I(r) = -\frac{\pi}{2}\left[J_{1/b}(r)\int^r rY_{1/b}(r)T(r)\,dr - Y_{1/b}(r)\int^r rJ_{1/b}(r)T(r)\,dr\right] \qquad \text{.....(24)}$$

for $1/b$ an integer; $J_{1/b}(r)$ and $Y_{1/b}(r)$ are Bessel functions of the first and second kinds, respectively, of order $(1/b)$ and $(P + iQ)$ and $(R + iS)$ are complex con-

†The present author has corrected the Jacchia and Kopal value for α (corresponds to r_1 here) and their equations pertaining to a "top" with a constant positive temperature gradient.

stants of integration.† For an atmosphere whose temperature profile consists o straight segments only, the complex constants of integration are found by equatin the wave function χ and its first derivative at any point where the analytica representation of χ changes. Equations (23) and (24) can be used in place o equations (7) and (8) if y_1 and y_2 are not known at frequent enough intervals t accurately evaluate the integral I, and provided, of course, that the heatin occurs in a region whose temperature profile closely approximates that of a straigh line.

The preceding equations for an atmosphere with constant temperature gradien will be used in the following section to determine boundary conditions for a straight line "top."

4. BOUNDARY CONDITIONS

The two complex constants of integration are determined from the boundar conditions that the vertical component of velocity must vanish at the surface o the earth and some boundary condition at the top of the atmosphere, for whic it is necessary to suppose an isothermal top. If no heat sources are present at th so-called "top" of the atmosphere and if further the temperature is constant then the solution of equation (5) is

$$y = A_1 e^{+i\mu z} + A_2 e^{-i\mu z} \quad \ldots\ldots\ldots\ldots\ldots\ldots\ldots\ldots (25$$

Weekes and Wilkes [3] employ the condition that the rate of energy flow in vertical direction ($\sim \mathcal{I}[y^*(\mathrm{d}y/\mathrm{d}x)]$, where $\mathcal{I}$ denotes imaginary part) be upwar at a sufficiently high level. Now, if one tests the quantity $A_1 e^{i\mu z} + A_2 e^{-i\mu z}$ in th boundary condition of Weekes and Wilkes, one obtains

$$| A_1 | > | A_2 |$$

that is, the outward flow > the inward flow. To eliminate A_2 altogether, we mus suppose only an outgoing wave present, namely, $y(x, t) = A_1 e^{i(\mu x + \sigma t)}$. (The con ventional outgoing wave has the form $e^{i(\sigma t - \mu x)}$, but the resolution of the apparen paradox, by Weekes and Wilkes [3], is that y corresponds to the complex conjugat E^* of electromagnetic theory.)

The condition that only an outgoing wave be present at sufficient heights als makes possible the application of the upper boundary condition to a straight-lin top with positive slope, believed to be the case above the 80-km level. At th "top," the argument $r \to \infty$, so that the complementary part of solution (23) ca be written

$$y(r, t) \underset{r\to\infty}{\to} \sqrt{\frac{2}{\pi r}} \left[(P + iQ) \exp\left\{ i\left(r + \sigma t - \frac{\pi}{4} - \frac{\pi}{2b} \right) \right\} \right.$$

$$\left. + (R + iS) \exp\left\{ -i\left(r - \sigma t - \frac{\pi}{4} - \frac{\pi}{2b} \right) \right\} \right]$$

†M. L. White, "Extension of the Sen-White paper on atmospheric oscillations," J. Geophy Res., 60, 531 (1955), eq. (3). In this equation, a symmetrical model for the source function employed, namely, $q = q_0 \exp\{-\beta(z - z_1)^2\}$ in the expression for $T(r)$. A possible asymmetric model is $q = q_1 (z/H_1)^\kappa e^{-\alpha z/H_1}$, or its equivalent $q = q_0 z^\kappa e^{-\alpha_0 z}$, where H_1 is the scale heig at some reference level and κ, α, and α_0 are constants. Wilkes [5] suggests a model of the ty $q = q_0 z^\kappa e^{-\alpha z/H(z)}$.

indicating that $J_{1/b}(r) + iY_{1/b}(r)$ may be considered as an outgoing wave, so that for a straight-line "top" with positive slope we have

$$\underset{r\to\infty}{y} = (P + iQ)[J_{1/b}(r) + iY_{1/b}(r)] = (P + iQ)H^{(1)}_{1/b}(r) \quad \ldots\ldots (26)$$

where $H^{(1)}_{1/b}(r)$ is a Hankel function of the first type.

The initial conditions for the integration of equation (5) downward for an isothermal top whose base is at $x = x_1$ are from equation (25)

$$y_1 = \cos \mu x_1 , \qquad y_2 = \sin \mu x_1$$

$$\left(\frac{dy_1}{dx}\right)_1 = -\mu \sin \mu x_1 , \qquad \left(\frac{dy_2}{dx}\right)_1 = \mu \cos \mu x_1 , \qquad \mu = \mu(x_1)$$

rather than $y_1 = 1$, $y_2 = 0$, as sometimes employed in the literature [7].

The initial condition for a "top" with positive temperature gradient can be obtained from equations (26) and (21), where it is now convenient to interpret x_1 as the x-value at the base of the straight-line top. Then, we obtain

$$y_1 = J_{1/b}(r_1) \quad \text{and} \quad y_2 = Y_{1/b}(r_1) \quad \ldots\ldots (27)$$

where from the definitions of μ and r_1

$$r_1 = \frac{2}{b}\left(\mu^2 + \frac{1}{4}\right)^{1/2} \quad \ldots\ldots (28)$$

5. A BRIEF APPLICATION: LUNAR AND SOLAR SEMI-DIURNAL WINDS IN THE *E* LAYER

The wave functions y_1 and y_2 have been obtained on the National Bureau of Standards electronic automatic computer (SEAC) by Dr. H. Herbert Howe, based on Rocket Panel [8] and Rand [9] profiles for both isothermal and straight-line "tops." From these values, the lunar winds and vertical displacements can be easily obtained. For the solar winds and vertical displacements, some knowledge of atmospheric heating is required, particularly an ozonospheric model. Presentation of these results is left for a future paper. However, at this point, it might be interesting to test the internal consistency of the lunar and solar semi-diurnal winds as collected by Briggs and Spencer [4] for the E region, assuming that the neutral particles and ions partake of the same motion. Equations (11) and (12) for u and v, respectively, have been used for this purpose. For this test, it is assumed that all measurements were made at the same height, that is, that variations of u and v from station to station are due to azimuthal factors only, the radial dependence remaining unchanged. For this reason, the degree of consistency is thought best illustrated by allowing B in Schmidt's formula [11]

$$\Theta_2^2(\theta) \sim (P_2^2 - BP_4^2) \quad \ldots\ldots (29)$$

to be adjustable. The P's are associated Legendre functions. The B-values are recorded in Table 1, where the elements in the upper left corner of each square are found from solar semi-diurnal winds, and in the lower left from the lunar semi-diurnal winds. The elements in the upper and lower right corners of the squares indicate the phase disagreement $|\ \Delta\phi\ |$ between observation and theory

TABLE I—*For the E region:* (1) *Semi-empirical B-values as defined by equation* (29) *appear in columns headed by B, and* (2) *phase discrepancy* $|\Delta\phi|$ *between observed and theoretically determined wind component ratios (given by* $\frac{u \text{ (station 1)}}{v \text{ (station 1)}}$ *or* $\frac{u \text{ (station 1)}}{u \text{ (station 2)}}$ *appear in columns headed by* $|\Delta\phi|$*; in each square of the Table, upper values are for solar and lower for lunar semi-diurnal wind. For comparison,* $B \cong +0.14$ *on the ground.*

Locality and observer	Ottawa (45°N) (J. H. Chapman)		Cambridge (52°N) results combined		Lower Hutt (41°S) (Burtt)	
	B	$\lvert\Delta\phi\rvert$	B	$\lvert\Delta\phi\rvert$	B	$\lvert\Delta\phi\rvert$
Ottawa (45°N) (J. H. Chapman)	+0.12 +0.10	13° 19°				
Cambridge (52°N) results combined	+0.14 +0.11	2° 1°	+0.30 §	9° [5°]		
Lower Hutt (41°S) (Burtt)	+0.17	{77°}	+0.12	21° ...	+0.07	24° ...

§Value not accurate because of loss of significant figures in calculations.
[ ]Observations due to G. J. Phillips.
{ }Comparison for corresponding seasons not available, causing large discrepany.
... No lunar wind data available for Lower Hutt.

for the solar and lunar winds, respectively. These values should be zero. Returning to the B-values, if the azimuthal dependence is the same in the E region as at the ground, then B, according to ground observations of barometric pressure variations by Schmidt [11], should be about +0.14. In computing B-values, ratios of east-west wind components have been used when comparing different stations. For a given station, B-values are obtained by forming the ratio of the east-west and north-south wind components. Phase discrepancies have been neglected in computing B, not only because they are small, but because they should probably be

absorbed in the normalization. In computing phases for Lower Hutt (41° south), it should be noted that u reverses sign (for the southern hemisphere) while v does not, and, further, the September to March date of Lower Hutt should be compared with the spring, summer, and autumn data of Cambridge (52° north). From Table 1, it is seen that the sign of B is always positive, as found by Schmidt. The mean value of $B \simeq +0.14$ agrees with Schmidt's value [11] and the spread is small. The mean phase discrepancy $|\overline{\Delta\phi}|$ is about 10°. Any marked inconsistencies shown in Table 1 seem to be explainable as follows: (1) Comparing data that cover different seasons of the year (because of the strong seasonal dependence), and (2) a 180° change in phase at latitudes 2° to 4° north of Cambridge, so that the azimuthal factor becomes very sensitive to changes in latitude and higher-order terms in equation (29) become important. Taking these points into consideration, the observations do seem favorable to the conclusion that Schmidt's formula holds reasonably well for the E region as well as the ground, and that the assumption in the theory of variable separable seems vindicated.*

In conclusion, the author would like to express his appreciation to Mr. Vaughn Agy and Dr. Edwin L. Crow for their encouragement and interest in this work.

References

[1] H. K. Sen and M. L. White, J. Geophys. Res., **60**, 483 (1955).
[2] C. L. Pekeris, Proc. R. Soc., A, **158**, 650 (1937).
[3] K. Weekes and M. V. Wilkes, Proc. R. Soc., A, **192**, 80 (1947).
[4] B. H. Briggs and M. Spencer, The Physical Society, Reports on Progress in Physics, **17**, 245 (1945); Tables 3 and 4.
[5] M. V. Wilkes, Proc. R. Soc., A, **207**, 358 (1951).
[6] S. Chapman, Q. J. R. Met. Soc., **50**, 165 (1924).
[7] L. G. Jacchia and F. Kopal, J. Met., **9**, 13 (1952).
[8] The Rocket Panel, Phys. Rev., **88**, 1027 (1952).
[9] G. Grimminger, Rand Report R-105, The Rand Corporation, Santa Monica, Calif. (Nov. 1948).
[10] G. N. Watson, "Theory of Bessel functions," Cambridge, University Press, 2nd ed. (1952); p. 345.
[11] A. Schmidt, Handbuch der Experimentalphysik, Band 25, Teil 1, Geophysik (1928); footnote p. 176.

*Table 1 should not be construed as supporting all reductions and interpretations of the semi-diurnal wind observations. Briggs and Spencer [4, p. 258] have, for example, pointed out that "results for the lunar semi-diurnal variations are not conclusive."

APPLICATION OF THE BALDWIN CRATER RELATION TO THE SCALING OF EXPLOSION CRATERS

BY J. E. HILL AND J. J. GILVARRY

The RAND Corporation, Santa Monica, California

(Received May 7, 1956)

ABSTRACT

Baldwin has demonstrated that the curve of diameter *vs* depth for craters due to surface explosions on the earth shows a continuous variation through the analogous curve for the terrestrial meteoritic craters into the corresponding curve for lunar craters; the latter two classes are presumed due to explosions associated with meteoritic impact. This relation is shown to be inconsistent with the conventional (cube-root) method of scaling dimensions of an explosion crater from a prototype crater for different energy releases, by which diameter and depth are each taken proportional to the 1/3 power of the energy. Two methods of scaling are developed which are consistent with the Baldwin relation and preserve different features of cube-root scaling; in one the crater volume is taken proportional to energy release, and in the second the scaling exponent for the diameter is set equal to 1/3. A comparison of the two scaling methods with experimental data is carried out. The results permit one to assign an energy scale to the terrestrial meteoritic and the lunar craters.

I. INTRODUCTION

This paper is concerned with the problem of predicting the dimensions (diameter and depth) of a crater produced in the earth by detonation of a charge of high explosive. Since the problem is intractable when approached from first principles, such predictions are usually made by scaling, in accordance with the energy release of the explosive, dimensions obtained from a test or model crater (due to a charge of known energy release under controlled conditions) to the case in question.

As a result of considerable experimentation, it has been shown [see 1 of "References" at end of paper] that, for a given type of soil and explosive, the crater diameter D and depth d for a surface explosion can be represented well by

$$D \propto E^{1/3}, \qquad d \propto E^{1/3} \ldots\ldots\ldots\ldots\ldots\ldots\ldots\ldots (1)$$

respectively, if E is the total energy release. The modeling implied by these laws is usually referred to as "cube-root scaling," or, in the United States, as Lampson scaling [1]. The relations have been found very useful in correlating the results of cratering experiments, within the rather wide scatter usual in such data. It is clear that the relations (1) imply a constant ratio of diameter to depth for the scaled and the prototype crater. If the shape of the crater is taken as a cone or a para-

boloid of revolution, it follows that $V \propto D^2d$ if V is the volume, and hence the volume of the crater is proportional to the energy release. The question of this proportionality has been the subject of numerous investigations [2 to 6]. Within the errors due to the difficulty of controlling experimental conditions accurately, the assumption seems to be fulfilled approximately, at least for low energy.

In an extensive monograph, Baldwin [7] has discussed the origin of lunar craters on the basis of the theory that these features are due to explosions associated with the impact of large meteorites on the lunar surface. Computation by the authors [8], on an idealized model, of the pressure and temperature generated behind a shock wave in such high-velocity impacts confirms the fact of their explosive magnitude, sufficient to blast out craters far larger than the volume of the impinging mass. A salient argument for the theory is Baldwin's demonstration that the curve of diameter *vs* depth for surface explosions on the earth (due to small artillery shells and bombs at low energy and accidental chemical explosions at high energy) shows a continuous variation through the analogous curve for the terrestrial meteoritic craters into the corresponding curve for lunar craters. The range of crater size covered runs from diameters of a few feet to diameters of hundreds of miles, over which Baldwin's empirical curve fits the data within reasonable error.

Analytically, the Baldwin relation can be written as

$$\log D = \alpha + \beta \log d + \gamma(\log d)^2 \ldots\ldots\ldots\ldots\ldots\ldots (2)$$

where D and d are the crater diameter and depth, respectively, and α, β, and γ are the constants

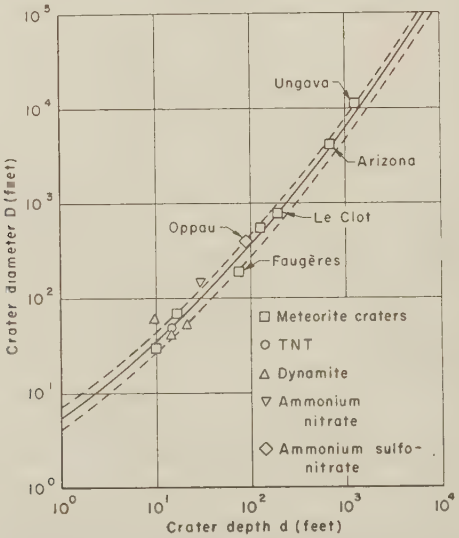

FIG. 1—The Baldwin curve (full) with data points corresponding to explosion and meteoritic craters for comparison. The dashed curves represent a band of plus or minus 25 per cent of the diameter corresponding to the Baldwin curve.

$$\alpha = 0.75, \qquad \beta = 0.6917, \qquad \gamma = 0.1083 \ldots\ldots\ldots\ldots\ldots (3)$$

if D and d are expressed in feet. Equation (2) is represented by the full curve in Figure 1. The constant ratio of diameter to depth in cube-root scaling implies the analog of the Baldwin relation given by

$$\log D = \alpha' + \log d \ldots\ldots\ldots\ldots\ldots\ldots\ldots\ldots (4)$$

with α' a constant. Hence, cube-root scaling corresponds to the degenerate form of the Baldwin relation* for $\beta = 1$ and $\gamma = 0$; in such a case, the full curve of Figure 1 should be a straight line of inclination 45° on the plot shown, which it definitely is not.

II. SCALING RELATIONS

In the following, two generalizations of the cube-root scaling law will be considered, which are consistent with the Baldwin relation. The explosion craters used by Baldwin to determine the constants of equation (2) were all of surface or near-surface type. From results of the authors [8], it can be assumed that the impact explosion of a meteorite is a surface explosion, to a first approximation. Hence, the results obtained apply in the first instance only to surface explosions, and generalization will be deferred to Section II-*B*, where the question of variation of soil and explosive type will be considered. The geometric shape of a crater can be approximated by a paraboloid of revolution, which is correct for the majority of the lunar craters [9], and is reasonable for an explosion crater [7].

A. Surface Explosions

Since the Baldwin relation (2) requires a continuously varying value of the ratio D/d as the dimensions of the crater increase, scaling relations of the type

$$D = \lambda_D (E/E_0)^n, \qquad d = \lambda_d (E/E_0)^m \ldots\ldots\ldots\ldots\ldots\ldots (5)$$

suggest themselves as generalizations of the Lampson form; in these equations, λ_D and λ_d are *constant* characteristic lengths for the diameter and depth, respectively, E_0 is a characteristic energy which depends on the type of explosive and on the nature of the soil, and n and m are exponents as yet unspecified. Clearly, λ_D and λ_d are the diameter and depth, respectively, for a crater produced by the energy release $E = E_0$, and thus must satisfy equation (2) themselves; the parameter E_0 must be determined by experiment.

Elimination of the energy ratio E/E_0 between the two scaling equations (5) and substitution of the result in the Baldwin equation yields

$$D = 10^{\alpha} d^{\beta + \gamma \log d} = \lambda_D \lambda_d^{-n/m} d^{n/m} \ldots\ldots\ldots\ldots\ldots\ldots (6)$$

as the condition which must be met for consistency of the postulated scaling laws with the Baldwin relation. These equalities reduce to $D = 10^{\alpha} d = \lambda_D \lambda_d^{-1} d$ in the Lampson limit corresponding to $\beta = 1$, $\gamma = 0$, and $n = m = 1/3$, in which case they merely express the proportionality of diameter to depth on cube-root scaling; it will be demanded that equalities (6) show the property characteristic of the

*Lately, Dr. Baldwin has revised the values of the coefficients so that $\beta = 1$, to agree to first order with cube-root scaling (private communication).

Lampson limit, of representing identities in the powers of d which explicitly appear as factors. On this assumption, one must have

$$n/m = \beta + \gamma \log d \quad (7)$$

implying from equation (6) that $10^{\alpha} = \lambda_D \lambda_d^{-(\beta+\gamma \log d)}$, which can be satisfied for constant values of λ_D and λ_d for all values of d only by

$$\lambda_D = 10^{\alpha}, \qquad \lambda_d = 1 \quad (8)$$

in which case all assumptions become consistent. Note that λ_D and λ_d are independent of the Baldwin constants β and γ, and that proportionality of diameter to depth is replaced by $D = \lambda_D d^{n/m}$.

From equation (7), the Baldwin relation fixes only the ratio of n to m, and is insufficient to determine n and m separately without an auxiliary condition. Since the volume of the crater varies as $D^2 d$, it is proportional by equations (5) to $(E/E_0)^l$, where

$$l = 2n + m \quad (9)$$

Inasmuch as n/m is fixed, a determinate problem can be obtained only in two ways, by choosing l (as a function or a constant), which fixes n and m, or by choosing either n or m, which fixes the other exponent and l. Note that at most only one exponent n or m can be a constant.

In Method I of scaling, the auxiliary condition to determine the scaling exponents will be taken as $l = 1$, which represents the proportionality of crater volume to energy release implied by Lampson scaling. Solution of equations (7) and (9) yields

$$n = (\beta + \gamma \log d)/(1 + 2\beta + 2\gamma \log d) \quad (10a)$$

$$m = 1/(1 + 2\beta + 2\gamma \log d) \quad (10b)$$

for the scaling exponents. In terms of the energy ratio E/E_0, one obtains

$$m = \{[(1 + 2\beta)^2 + 8\gamma \log (E/E_0)]^{1/2} - (1 + 2\beta)\}[4\gamma \log (E/E_0)]^{-1} \quad (11a)$$

$$n = [\beta + \gamma m \log (E/E_0)][1 + 2\beta + 2\gamma m \log (E/E_0)]^{-1} \quad (11b)$$

which yield

$$n = \beta(1 + 2\beta)^{-1}[1 + 2\gamma\beta^{-1}(1 + 2\beta)^{-2} \log (E/E_0)] \quad (12a)$$

$$m = (1 + 2\beta)^{-1}[1 - 2\gamma(1 + 2\beta)^{-2} \log (E/E_0)] \quad (12b)$$

for $\log (E/E_0)$ small. The values of n and m are shown in Figure 2 as a function of crater depth d. One notes that while m shows fair variation, n changes very slowly for a wide variation in crater size, and is approximately constant at the Lampson value.

The fact that n for Method I is close to the Lampson value suggests use of $n = 1/3$ as the auxiliary condition in a second method, Method II, of scaling. With this assumption, equation (7) yields

$$m = 1/[3(\beta + \gamma \log d)] \quad (13)$$

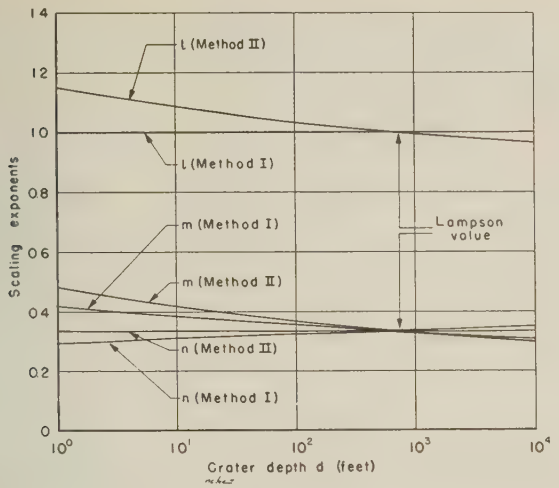

FIG. 2—Scaling exponents on Methods I and II of scaling, for comparison with Lampson values

and the scaling exponent for the volume becomes

$$l = (1/3)[2 + 1/(\beta + \gamma \log d)] \quad \ldots\ldots (14)$$

In terms of the energy ratio E/E_0, one obtains

$$m = \{[9\beta^2 + 12\gamma \log (E/E_0)]^{1/2} - 3\beta\}[6\gamma \log (E/E_0)]^{-1} \quad \ldots\ldots (15)$$

which yields

$$m = (1/3\beta)[1 - (\gamma/3\beta^2) \log (E/E_0)] \quad \ldots\ldots (16)$$

for log (E/E_0) small. The value of m is shown as a function of depth in Figure 2. It shows stronger variation from the Lampson value than does either n or m on Method I. The value of l is shown likewise; it is only approximately equal to the Lampson value.

On both Methods I and II, the two scaling exponents n and m become equal to the Lampson value for the crater whose depth and diameter are, respectively,

$$d = 10^{(1-\beta)/\gamma} \qquad D = 10^{\alpha+(1-\beta)/\gamma} \quad \ldots\ldots (17)$$

in which case l on Method II has the Lampson value. This crater corresponds to the energy ratio

$$E/E_0 = 10^{3(1-\beta)/\gamma} \quad \ldots\ldots (18)$$

at which both Methods I and II yield the same crater dimensions. Another energy ratio $E/E_0 = 1$ obviously exists at which both scaling methods agree; no other such ratio appears. For the case $\beta = 1$ and $\gamma = 0$, corresponding to the degenerate form (4) of the Baldwin relation for cube-root scaling, all results given here reduce to the corresponding Lampson forms.

B. Effect of Soil Type, Explosive Type, and Depth of Burst

Lampson [1] has given the scaling relation for the diameter on cube-root scaling explicitly as

$$D = Kk^{1/12}eCE^{1/3} \quad (19)$$

for D in feet and E in pounds of explosive, where $K = 2.6$, the soil constant k (for which Lampson provides a table) takes account of variation of soil type, e is an explosive factor which is unity for TNT, and the effect of depth of burst is taken into account by the depth-factor C, which Lampson gives graphically as a function of "scaled depth of burst" (depth in feet divided by cube root of E in pounds of TNT equivalent). Equation (19) becomes identical with the scaling law for the diameter on Method II if one takes

$$E_0 = 10^{3\alpha}K^{-3}k^{-1/4}e^{-3}C^{-3} \quad (20)$$

Furthermore, the scaling exponents n and m on either scaling method are in no case grossly different from 1/3. These facts suggest that in zero-order approximation, at least, the results of this paper can be generalized to cover effects of variation of soil and explosive type, and of depth of burst, by evaluating E_0 from equation (20) in both Methods I and II of scaling.

One can note that equations (5) are simply parametric representations of the Baldwin curve in terms of a running parameter E/E_0. Since the generalization represented by equation (20) demands that any effect of the factors in question be contained in the parameter E_0, it follows that variation in these factors at fixed energy release E merely displaces the representative point for the crater up or down the Baldwin curve on the plot of Figure 1. Some scanty experimental data available to the authors support this conclusion, in general, and Baldwin has noted it empirically as regards depth of burst. A similar behavior is implied by cube-root scaling if it is assumed that the corresponding factors in the scaling relation for the depth are the same as those of equation (19) for the diameter; Lampson does not give an explicit relation for the depth analogous to equation (19).

III. COMPARISON WITH EXPERIMENTAL DATA

The portion of the Baldwin curve (solid line) shown in Figure 1 corresponds to craters varying from some 50 feet in diameter for chemical explosions up to the terrestrial meteoritic craters of the order of miles in diameter. The points for chemical explosions were plotted from data given by Baldwin (his Table 6). The craters correspond to varied explosives and soil types. Most were produced by accidental detonation of explosives stored on or near the ground (the largest is from the explosion of September 21, 1921, at Oppau, Germany). The craters in Baldwin's table corresponding to military mines or otherwise ambiguous cases were omitted.

The seven points shown by squares on the plot of Figure 1 correspond to terrestrial meteoritic craters. The dimensions of four of the larger of these craters, which appear at the upper end of the Baldwin curve, are shown in Table 1.

Three of the smaller craters shown in Figure 1 were plotted from Table 5 of

TABLE 1—*Dimensions of terrestrial meteoritic craters*

Crater	Diameter	Depth	Reference
	feet	*feet*	
Ungava (Quebec, Canada)	11,500	1,330	[10]
Coon Butte (Arizona, U.S.)	4,150	700	[7]
Le Clot (Hérault, France)	800[a]	200	[11], [12]
Faugères (Hérault, France)	180[b]	75	[11], [12]

[a]Average of range 200 to 300 meters given.
[b]Average of range 55 to 60 meters given.

Baldwin, which contains in common with Table 1 the well-known Arizona crater. The remaining three craters, Ungava or Chubb [10], Le Clot [11, 12], and Faugères [11, 12] of Table 1 were discovered subsequent to the publication of Baldwin's results. Discovery of Ungava yielded a terrestrial meteorite crater† with dimensions larger than many of the craters that can be measured on the moon. The dashed curves of Figure 1 indicate a band of plus or minus 25 per cent of the diameter specified by the Baldwin curve, outside of which only four or about 1/3 of the 13 points fall. Furthermore, three of these points have been added by the authors, and were not available to Baldwin. The closeness of fit to the empirical Baldwin relation is remarkably good, when it is considered that cratering data may show a scatter of some 25 per cent, or larger, even when taken under controlled experimental conditions [1].

A value of E_0 for surface explosions can be obtained from equation (20) if a representative soil and average explosive type are assumed. The representative soil will be taken as a dry clay, for which Lampson [1] gives $k = 15{,}000$ as an average, and TNT will be selected as the average explosive, for which $e = 1$. Use of these values for k and e yields $E_0 = 21$ lb of TNT, for $C = 0.35$ corresponding to the surface value of the depth-factor C.

Figure 3 shows graphs of equations (5) corresponding to Method I and Method II, based on this value of E_0 ; the Figure gives the energy release in kilotons (KT) of TNT against the corresponding diameter or depth in feet. The energies of the chemical explosions for which crater data appear in Figure 1 have been plotted in Figure 3 as a function of both diameter and depth, from the data given in Baldwin's table. One notes that the points straddle the scaling curves fairly well. Both sets of scaling relations predict the same crater dimensions at two values of energy release; one of these is the energy E_0 , and the other is the energy determined by equation (18). For intermediate energies, agreement of the two methods is so close that the data shown do not make a choice possible.

†The meteoritic origin of this crater is in some doubt, since Meen [10] failed to find positive evidence of such origin at the site. A later expedition from the Dominion Observatory of Canada [see Sky and Telescope, **14**, 374 (1955)] likewise failed to obtain conclusive evidence. In this paper, the crater will be assumed meteoritic, on the basis of the fact that its dimensions fit the Baldwin curve so well in a region where lunar craters of comparable size can be measured. The lack of meteoritic iron can be explained on the supposition that the meteorite which produced the crater was entirely stone. La Paz [13] takes a contrary view.

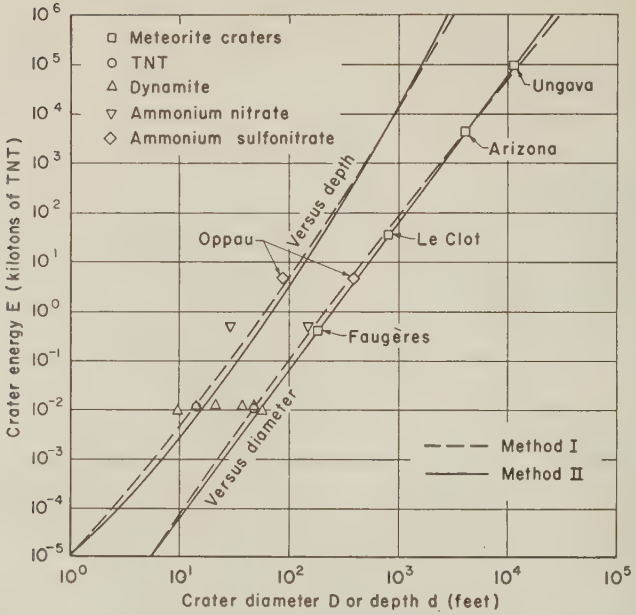

FIG. 3—Scaling of energy against diameter or depth of crater on Methods I and II, with data points from explosion craters for comparison. Points corresponding to meteoritic craters have been located on the scaling curve for energy *vs* diameter on Method II.

The energies predicted by the scaling curves can be taken as estimates of the kinetic energy prior to impact of the meteorite producing a terrestrial meteoritic or lunar crater, if one assumes that at least for the larger of such craters the explosion is essentially of surface type, and that such explosions have the same cratering efficiencies per unit of energy release as TNT. The corresponding energies implied by Methods I and II are shown in Table 2 for the Ungava and Arizona craters. The scaling curve for energy against diameter has been used, since the depth is the dimension subject to the greater uncertainty (because of the effect of erosion in filling the bottom of the crater with silt). One notes that the energies shown are of the order of megatons (MT) or higher, and thus are far above the energy (20 KT) of a nominal atomic bomb [1]. For the Arizona crater, Rinehart

TABLE 2—*Energies of terrestrial meteoritic craters*

Crater	Energy on Method I		Energy on Method II	
	(MT)[a]	(ergs)	(MT)[a]	(ergs)
Ungava	70	30×10^{23}	90	40×10^{23}
Arizona	4	2×10^{23}	4	2×10^{23}

[a]One MT (megaton TNT equivalent) = 4.2×10^{22} ergs.

5] has estimated an energy of about 1×10^{22} ergs, lower by an order of magnitude han the corresponding value of Table 2, and Baldwin has estimated the still ower value 3×10^{21} ergs; on the other hand, Öpik [14] gives figures implying an energy higher by an order of magnitude than corresponds to Table 2.

The Ungava and Arizona craters lie in granite and sandstone, respectively, and thus validity of the energy estimates of Table 2 depends on showing that he soil constant k for these rock types is reasonably close to the value for the representative soil (dry clay) selected to determine E_0 from equation (20). Lampson provides no values of k for rock, but gives an empirical expression for the parameter; from available data [15], this equation yields $k = 37 \times 10^4$ and $k = 11 \times 10^4$ for granite and sandstone, respectively. The corresponding values of $k^{1/4}$ are 25 and 18, respectively, which are concordant only within a factor of about two with the value $k^{1/4} = 11$ used to determine E_0 for detonation of TNT over dry clay. These values for $k^{1/4}$ imply that the figures of Table 2 should be divided by a factor of approximately two to take account of the difference between the rocks in question and dry clay; the correction has not been applied because of the inherent uncertainties associated with other factors in extrapolating over so large a range of crater diameters.

If estimates of the impact velocities of the meteorites responsible for the terrestrial meteoritic craters are combined with the energies of Table 2, corresponding estimates of the mass of the meteorite prior to impact can be made. If the bodies that produced these craters were members of the solar system, it follows that their maximum geocentric velocity is the sum of the parabolic limit (42.2 km/sec) corresponding to the mean distance of the earth from the sun in the latter's gravitational field, and the orbital velocity (29.7 km/sec) of the earth about the sun, or about 72 km/sec. This limit is in agreement with the general results of measurements of meteor velocities in the earth's upper atmosphere by photographic and radio techniques [16]; the limit may be reduced substantially if it is established (as suspected) that meteorites come from orbits similar to those of the observed asteroids [17]. The minimum velocity of a meteorite at the top of the atmosphere is the earth's velocity (11.3 km/sec) of escape, but the velocity for impact will be reduced by retardation in the atmosphere. As a reasonable figure, a lower limit of 10 km/sec will be adopted in this paper for the velocity of a crater-producing meteorite; the kinetic energy per unit mass of a body moving with this velocity exceeds by a factor of ten the energy release (about 5×10^{10} ergs/gm) of TNT on explosion [1].

For the Ungava and Arizona craters, the energy estimates of Table 2 yield masses for the meteorites which produced the craters, as tabulated in Table 3 for impact velocities of 10 and 70 km/sec. Rinehart [5] and Wylie [18] have estimated masses of 12,500 and 8,500 tons, respectively, for an impact velocity of about 15 km/sec in the case of the Arizona crater; these figures are below the corresponding ones of Table 3 by an order of magnitude. The meteorite which produced the Arizona crater presumably was an iron, in view of the large amount of meteoritic iron found in the neighborhood and below the surface of the crater. The range of diameters for a spherical meteorite of iron to produce the crater, corresponding to the range of masses in Table 3, is 150 to 40 feet, for impact velocities of 10 and

Table 3—*Masses of meteorites producing craters, for two impact velocities*

Crater	Mass on Method I		Mass on Method II	
	(10 km/sec)	(70 km/sec)	(10 km/sec)	(70 km/sec)
Ungava	7×10^6 ton	1×10^5 ton	8×10^6 ton	2×10^5 ton
Arizona	4×10^5	8×10^3	4×10^5	8×10^3

70 km/sec, respectively. For this crater, Öpik [14] has estimated a meteorite diameter of 300 feet for an impact velocity of about 10 to 20 km/sec, while the estimate given by Baldwin is about 50 feet for 10 km/sec.

In a meteorite explosion on impact, the velocity of the shock wave in the meteorite relative to the meteorite itself is of the order of the impact velocity, so that the explosive pressures and temperatures are created in a time of the order of that required for the impinging mass to traverse a distance equal to its diameter [8]. It follows that the effective center of such an explosion must lie within a depth below the surface of the order of a linear dimension of the impinging mass. For the average of the diameters above and the energy figures of Table 2, the uncertainty in "scaled depth of burst" for the Arizona crater is about 0.025 ft/lb$^{1/3}$, which, according to Lampson's curve for the depth-factor C, corresponds to negligible variation of this parameter from its surface value. These considerations tend to justify the assumption that the larger terrestrial meteoritic and lunar craters represent surface explosions, essentially.

It should be stated that collision of a meteorite with the surface of the earth does not necessarily result in an explosion, since geocentric velocities down to low values are possible, because of atmospheric deceleration. A continuous gradation must exist, from energy transfer by shock formation at the higher velocities, to transfer by plastic yield or elastic strain at the lower velocities.

IV. CONCLUSION

In conclusion, it is seen that both Methods I and II of scaling, yielding consistency with the Baldwin crater relation but preserving different features of cube-root scaling, lead to scaling relations for the depth of an explosion crater of high energy which are not simple power laws. While conventional scaling probably gives a good estimate of the diameter of a crater, it is likely that the Baldwin relation gives a better estimate of the depth, particularly for scaling over a wide energy range to large craters. The sense of the error made by cube-root scaling is to predict depths which are too large. In general, energies and derived quantities predicted by the methods of this paper for the terrestrial meteoritic craters lie in the range between the larger (such as those of Öpik) and the smaller (as those of Baldwin) given by others.

The authors wish to thank Dr. Baldwin for discussions. Thanks are likewise due Dr. F. R. Gilmore of the RAND Corporation for a critical discussion of the manuscript.

References

[1] C. W. Lampson, in "Effects of Atomic Weapons," edited by S. Glasstone, Combat Forces Press, Washington, D.C. (1950); p. 410.
[2] F. Helié, Traité de Balistique Experimentale, Dumaine, Paris (1840).
[3] J. Ôkubo and M. Hara, Sci. Rep. Tôhoku Imp. Univ., **47**, 1011 (1928).
[4] E. E. Burlot, Mémorial de L'Artillerie Français, **13**, 115 (1933).
[5] J. S. Rinehart, Pop. Astr., **58**, 458 (1950).
[6] J. S. Rinehart and W. C. White, Amer. J. Phys., **20**, 14 (1952).
[7] R. B. Baldwin, The Face of the Moon, University of Chicago Press, Chicago (1949); chaps. 3 to 8; in particular, pp. 124, 131, 138, 141, 155, 224.
[8] J. J. Gilvarry and J. E. Hill, Pub. Astr. Soc. Pacific (in press).
[9] C. A. Cross, J. Brit. Astr. Assoc., **65**, 72 (1955).
[10] V. B. Meen, J. R. Astr. Soc. Can., **44**, 169 (1950).
[11] B. Gèze and A. Cailleux, Paris, C.-R. Acad. sci., **230**, 1534 (1950).
[12] C. L. Janssen, J. R. Astr. Soc. Can., **45**, 190 (1951).
[13] L. La Paz, Meteoritics, **1**, 228 (1954).
[14] E. Öpik, Irish Astr. J., **1**, 22 (1950).
[15] F. Birch, J. F. Schairer, and H. C. Spicer (editors), "Handbook of Physical Constants," Geological Society of America, New York (1942); pp. 14, 20, 95.
[16] A. C. Lovell, Meteor Astronomy, Clarendon Press, Oxford (1954); chaps. 11, 12.
[17] F. L. Whipple, in "Meteors," edited by T. R. Kaiser, Pergamon Press, London (1955).
[18] C. C. Wylie, Pop. Astr., **51**, 97 (1943).

PHYSICAL PROPERTIES OF THE ATMOSPHERE FROM 90 TO 300 KILOMETERS

(Proposed "Speculative Atmosphere" submitted to the Working Group on Extension to the U. S. Standard Atmosphere Tables)

BY H. K. KALLMANN,* W. B. WHITE,† AND H. E. NEWELL, JR.§

*The RAND Corporation, Consultant;**

†The RAND Corporation, Santa Monica, California

§Naval Research Laboratory, Washington, D.C.

(Received May 21, 1956)

ABSTRACT

Based on recent experimental and theoretical studies of the physical properties of the atmosphere at high altitudes, an average model atmosphere is presented for the region between 90 and 300 km. This model is consistent with the following assumptions: Molecular oxygen begins to dissociate appreciably only above 90 km; at around 130 km, about 30 per cent of O_2 is still in the undissociated state; molecular nitrogen begins to dissociate above 220 km; the concentrations of molecular oxygen and nitrogen decrease with altitude exponentially; the temperature becomes isothermal in the region of the exosphere, approximately above 360 km.

All physical quantities have been calculated from self-consistent equations as continuous functions of altitude, without assuming any particular form of the temperature gradient. The results show lower temperatures and densities throughout the region of the ionosphere than have been deduced previously.

I. INTRODUCTION

A model atmosphere is presented which has been determined on the basis of recent experimental and theoretical studies. This work has been carried out at the request of the working group on the extension of the U. S. Standard Atmosphere and was submitted to the group at the beginning of this year. Since these writers were asked to estimate physical properties of the atmosphere in the high-altitude region, the results given here cover primarily the region between 90 and 300 km. The final version of the revised "U. S. Atmosphere Tables" is presently being prepared by the Geophysics Research Directorate of the Air Force Cambridge Research Center. Their model will be in close agreement with the model presented here, except that the temperature variation with altitude will be linearly segmented instead of continuous, as is proposed in this model.***

**Member of the Institute of Geophysics, University of California, at Los Angeles.

***In fact, this model atmosphere presents a scientific study made in preparation for the final version of the tables to be issued by GRD in the near future for engineering purposes; that is, it is not intended to be used as an engineering standard.

II. TECHNICAL DISCUSSION

Observations of atmospheric properties by means of high-altitude research rockets and advanced theories of the physical state of the atmosphere have made desirable a quantitative estimate of pressure, density, and temperature distribution to great heights. Because of the uncertainties still involved in such a study, the best that can be hoped for at present is to arrive at an average model atmosphere whose properties are consistent with quantitative, semi-quantitative, and qualitative information obtained from observations and derived from theory.

The problem, therefore, has been approached by:

(*A*) Stating the physical properties of the atmosphere to which the model must conform
(*B*) Outlining the mathematical procedure by which the model is derived
(*C*) Presenting the numerical results and comparing them with the requirements stated under (*A*) and with other investigations

A. *Physical Properties of the Atmosphere to Which the Model Must Conform*

The proposed model should conform to the following quantitative and semi-quantitative information which is available from observation and theory:

(1) The variation of density and pressure with altitude must be in agreement with the experimental data obtained by means of rockets [see 1 of "References" at end of paper]. Below 100 km, pressure and density measurements are probably accurate to within 10 per cent. Between 100 and 156 km, densities have been deduced from measurements described by Newell [1]. A single measure of density at 219 km is available, the accuracy of which may be within about 20 per cent.

(2) Molecular oxygen begins to dissociate appreciably around 90 km [2]. The region of dissociation of O_2 is larger than had previously been assumed. Above 130 km, about (25 $\pm$ 5) per cent of O_2 is still present [3].

(3) Molecular nitrogen dissociates at higher altitudes than molecular oxygen, and the decrease of concentration of N_2 is more gradual than that of O_2. Since no atomic ions of nitrogen have been observed below 219 km [4], it was assumed that N_2 begins to dissociate appreciably only above 220 km.

Consistent with the macroscopic concepts of the thermodynamic properties of the atmosphere, an exponential decrease of concentration of O_2 and N_2 , and consequently of molecular weight, has been assumed. Only an exponential, rather than a linear, decrease of molecular weight can account for the presence of molecular species at great altitudes where, from the macroscopic point of view, the dissociation is complete. It should be noted that molecular oxygen and nitrogen emission from great heights has been observed.

(4) The true kinetic temperature of the model atmosphere becomes isothermal in the exosphere, the exosphere being defined as the outermost region of the earth's atmosphere where collisions are negligible and particles may escape [5]. Moreover, the temperature approaches asymptotically the temperature at the base of the exosphere. At the base of the exosphere, also called the "critical region" or "level of escape" of particles, the temperature must be higher than 500°K and less than 2000°K [6], and the scale height must be greater than 30 km.

(5) The temperature gradient throughout the ionosphere (100 km to 300 km) cannot exceed 5° per km, and for most of this region should be less. This is according to studies made by Bates [7] and others [8] on the basis of the heat conduction theory. No temperature gradient, linear or otherwise, has been assumed, temperature being a derived property in this model.

(6) The neutral particle density, derived from pressure and temperature, must be such as to account for the presence of the ionosphere. More precisely, the neutral particle density at the critical level cannot be less than 10^7 particles per cm^3 [6].

(7) Diffusive separation due to gravity and difference in molecular weight of the air particles has been neglected, since it can be shown [9, 10] that the effect on pressure and density even up to altitudes of 300 km is relatively small.

Vertical transport phenomena [9] which may become important in the F region have not been considered, since the general dynamics of the upper atmosphere are not yet well understood.

B. *Mathematical Procedure by Which the Model Is Derived*

1. *General Method*

If hydrostatic equilibrium is attained in the atmosphere, then pressure P and density ρ are related by the equation

$$dP = -g\rho\, dh \qquad (1)$$

At high altitudes, the variation of gravity, g, with altitude must be taken into account. This is expressed by the relation

$$g = g_0\left(\frac{a}{a+h}\right)^2 \qquad (2)$$

where a is the mean radius of the earth and h is the height above the earth's surface. For a latitude of 45° 32′ 40″ [12]

$$g_0 = 980.665 \text{ cm sec}^{-2}$$

$$a = 6.356\,766 \times 10^8 \text{ cm}$$

If the perfect gas law is assumed, then a relationship between temperature T, molecular weight M, pressure P, density ρ, etc., may be expressed in either of the following forms:

$$\rho = \frac{PM}{RT} \quad \text{or} \quad C_i = \frac{PX_i}{RT} = \frac{\rho X_i}{M} \qquad (3)$$

Here C_i is the concentration in mols or particles per unit volume of constituent i, X_i is the mol fraction of constituent i, and R is the gas constant (8.31436 ergs per degree per mol).

For altitudes below 90 km, a constant, known molecular weight can be assumed, and all atmospheric properties can be computed when one of them, for example, the pressure, is determined experimentally as a function of altitude. In accordance with the working group on the extension of the U. S. Standard Atmosphere, the

basic composition of air at 90 km was assumed to be the same as for the ICAO-atmosphere, except for the removal of CO_2 . Thus, the gas is composed of 78.114 per cent nitrogen, 20.956 per cent oxygen, and 0.930 per cent argon, resulting in a molecular weight of 28.962.

For the altitudes of interest here, constant composition cannot be assumed and a further relationship is needed. An exponential decrease of diatomic constituents with altitude has been assumed [13], such that

$$dC_i = -K_i C_i \, dh \quad \ldots\ldots(4)$$

Here, C_i is the concentration of molecular oxygen (or nitrogen) at any height, and K_i is the concentration coefficient.

Linear relations exist between the molecular weight of the mixture and the mol fractions of the constituent species. If the dissociation of diatomic oxygen and diatomic nitrogen takes place in separate altitude layers, with the dissociation of oxygen essentially completed at an altitude lower than that where the dissociation of nitrogen begins, the relations are particularly simple:

$$\left.\begin{aligned} X_{O_2} &= \frac{M_h}{M_I} - 1 \\ \text{and} \qquad X_{N_2} &= \frac{M_h}{M_{II}} - 1 \end{aligned}\right\} \quad \ldots\ldots(5)$$

Here M_I^* indicates the molecular weight when all oxygen (but no nitrogen) is dissociated, and M_{II}^{**} is the molecular weight when all nitrogen (and oxygen) is dissociated. M_h is the molecular weight at an altitude where the mol fraction of the dissociating constituent is X_i .

Combining (3) and (5),

$$C_i = \frac{\rho}{M} X_i = \frac{\rho}{M_h}\left(\frac{M_h}{M_i} - 1\right) = \frac{\rho}{M_i} - \frac{\rho}{M_h} = \frac{\rho}{M_i} - \frac{P}{RT} \quad \ldots\ldots(6)$$

where M_i is the molecular weight when diatomic constituent i is completely dissociated. Differentiating with respect to altitude,

$$\frac{dC_i}{dh} = \frac{1}{M_i}\frac{d\rho}{dh} - \frac{1}{RT}\frac{dP}{dh} + \frac{P}{RT^2}\frac{dT}{dh} \quad \ldots\ldots(7)$$

Using equation (4),

$$\frac{1}{C_i}\frac{dC_i}{dh} = -K_i = \frac{\dfrac{1}{M_i}\dfrac{d\rho}{dh} - \dfrac{1}{RT}\dfrac{dP}{dh} + \dfrac{P}{RT^2}\dfrac{dT}{dh}}{\dfrac{\rho}{M_i} - \dfrac{P}{RT}} \quad \ldots\ldots(8)$$

Solving for dT/dh,

$$\frac{dT}{dh} = T\left(K_i + \frac{1}{P}\frac{dP}{dh}\right) - T^2\left(\frac{K_i R\rho}{PM_i} + \frac{R}{PM_i}\frac{d\rho}{dh}\right) \quad \ldots\ldots(9)$$

*M_I = 23.944.
**M_{II} = 14.549.

This has the form of a Bernoulli equation,

$$\frac{dT}{dh} = TF(h) - T^2G(h) \quad \text{.....(10)}$$

and has the solution (reference [14])

$$\frac{1}{T} = \frac{1}{T_0}\exp\left[-\int_{h_0}^{h} F(s)\,ds\right] + \int_{h_0}^{h}\exp\left[-\int_{t}^{h} F(s)\,ds\right]G(t)\,dt \quad \text{.....(11)}$$

which can be greatly simplified, since

$$\exp\left[-\int_{h_0}^{h} F(s)\,ds\right] = \exp\left[-\int_{h_0}^{h}(K_i + d\ln P)\,dh\right] = \frac{P_0}{P_h}\exp\left[-K_i(h - h_0)\right] \quad (12)$$

and

$$\int_{h_0}^{h}\exp\left[-\int_{t}^{h} F(s)\,ds\right]G(t)\,dt = \int_{h_0}^{h}\frac{P_t}{P_h}\frac{e^{K_i t}}{e^{K_i h}}\left(\frac{R}{M_i}\right)\left(\frac{K_i\rho_t}{P_t} - \frac{1}{P_t}\frac{d\rho}{dt}\right)dt$$

$$= \frac{R}{M_i P_h e^{K_i h}}\int_{h_0}^{h}\left(K_i e^{K_i t}\rho_t + e^{K_i t}\frac{d\rho}{dt}\right)dt$$

Integrating by parts, two terms cancel, and the equality becomes

$$\left.\begin{aligned}\int_{h_0}^{h}\exp\left[-\int_{t}^{h} F(s)\,ds\right]G(t)\,dt &= \frac{R}{M_i P_h e^{K_i h}}\left(\rho_h e^{K_i h} - \rho_0 e^{K_i h_0}\right)\\ &= \frac{R}{M_i P_h}\left(\rho_h - \rho_0 e^{-K_i(h-h_0)}\right)\end{aligned}\right\} \quad \text{.....(13)}$$

so that

$$\frac{1}{T_h} = \frac{1}{T_0}\frac{P_0}{P_h}e^{-K_i(h-h_0)} + \frac{R}{M_i P_h}\left(\rho_h - \rho_0 e^{-K_i(h-h_0)}\right) \quad \text{.....(14)}$$

This can be reduced to

$$\frac{T_0}{T_h} = \frac{P_0}{P_h}\left[\frac{\rho_h}{\rho_0}\frac{M_0}{M_i} - \left(\frac{M_0}{M_i} - 1\right)e^{K_i(h-h_0)}\right] \quad \text{.....(15)}$$

or

$$\frac{T_0}{T_h} = \frac{P_0}{P_h}\left[\frac{\rho_h}{\rho_0}\frac{M_0}{M_i} - X_0 e^{-K_i(h-h_0)}\right] \quad \text{.....(16)}$$

where subscript zero refers to an arbitrary reference altitude.

2. *Graphical Relationships*

These results may be put into a form convenient for graphical interpretation. Defining a quantity f_d which denotes the fractional dissociation ($f_d = 0$ when $M = M_0$; $f_d = 1$ when $M = M_i$), and making use of the perfect gas law in conjunction with equation (16),

$$\frac{M_0}{M_h} = \frac{\rho_0 P_h}{\rho_h P_0}\frac{T_0}{T_h} = \frac{M_0}{M_i} - X_0\frac{\rho_0 e^{-K_i(h-h_0)}}{\rho_h} \quad \text{.....(17)}$$

But:

$$\frac{M_0}{M_h} = 1 + X_0 f_d \quad \text{.....(18)}$$

and

$$\frac{M_0}{M_i} = 1 + X_0 \quad \text{.....(19)}$$

so that

$$f_d = 1 - \frac{\rho_0 e^{-K_i(h-h_0)}}{\rho_h} \quad \text{.....(20)}$$

Looking at a logarithmic density *versus* altitude graph such as Figure 1, it is seen that if a tangent line is constructed at the altitude at which dissociation is

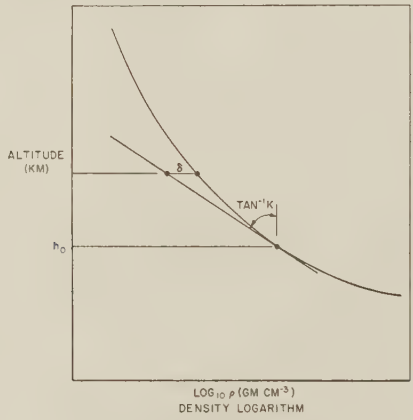

FIG. 1
DETERMINATION OF CONCENTRATION COEFFICIENT, K, FROM CURVE OF LOG DENSITY VERSUS ALTITUDE

considered to begin, the slope of this line is the value of the concentration constant K_i . The deviation δ of the density curve from the straight line gives the degree of dissociation by equation (20), which may be written in the form

$$f_d = 1 - \exp \delta \quad \text{.....(21)}$$

Furthermore, with f_d obtained from the density curve, the temperature relations may be expressed, rewriting (16), as

$$T_h = \frac{T_h^*}{1 + X_0 f_d} \quad \text{.....(22)}$$

where T_h^* indicates the temperature if no dissociation had occurred; that is, T_h^* is the molecular scale temperature.

3. *Computational Procedure*

Calculations have been made for the determination of high-altitude atmospheric properties according to the theory outlined above.

All existing data regarding atmospheric density were used and extrapolated with the help of estimates concerning the magnitude of dissociation effects and with the aid of theory regarding probable conditions at the critical level of escape for helium.

The quantitative considerations and assumptions necessary in this computation are the following:

(1) At the critical altitude, the mean free path of the particles equals the scale height. The mean effective collision radius for the particles involved is 1.7×10^{-8} cm.
(2) Nitrogen is approximately 75 per cent dissociated at the critical altitude.
(3) The lapse rate is essentially zero at the critical altitude; that is, the temperature asymptotically approaches a constant value at the critical height.
(4) Oxygen dissociation begins at 90 km, nitrogen dissociation at 220 km.
(5) The altitude of escape is indeterminate by these considerations. By extrapolating the density curve above the experimental data, remembering that the slope of this curve at the point where dissociation starts determines the dissociation gradient and also eventually the temperature gradient, a critical temperature in the region of escape is obtained which fulfills the requirements imposed upon the model. A temperature of about 910°K is obtained for the critical region; that is, the region where the temperature gradient is approximately zero. This region is at an altitude of about 360 km, where the scale height is equal to the mean free path.

On the basis of these assumptions and the accepted theories, the uncertainty of extrapolation up to 300 km decreases considerably.

For example, the curvature of the upper end of the log density curve is limited by the assumption of 75 per cent dissociation of nitrogen, so that the entire upper end of this curve is only slightly bent.

Furthermore, assumption 1 results in the following relation between density and temperature at the critical altitude:

$$\rho = \frac{M^2 g}{\pi \sqrt{2}\, A \sigma^2 R T}$$

where ρ = density, M = molecular weight, g = acceleration due to gravity, A = Avogadro's number, σ = effective particle diameter, R = gas constant, and T = temperature.

Finally, assumption 3 results, through the use of the perfect gas law and the hydrostatic equation, in a relation between the slope of the density curve and the temperature, at the critical altitude:

$$\frac{\mathrm{d} \ln \rho}{\mathrm{d}h} = -\frac{Mg}{RT} + \frac{\mathrm{d} \ln M}{\mathrm{d}h} \approx -\frac{Mg}{RT}$$

Thus, for a critical altitude of 360 km, the upper end of the log density curve is restricted, depending on the critical temperature, to combinations of values and derivatives of density as indicated in Figure 2. Because of this, the range of critical temperatures which fits the experimental data is seen to be quite limited. The temperature which fits the experimental data best for the average density curve is in the neighborhood of 910°K.

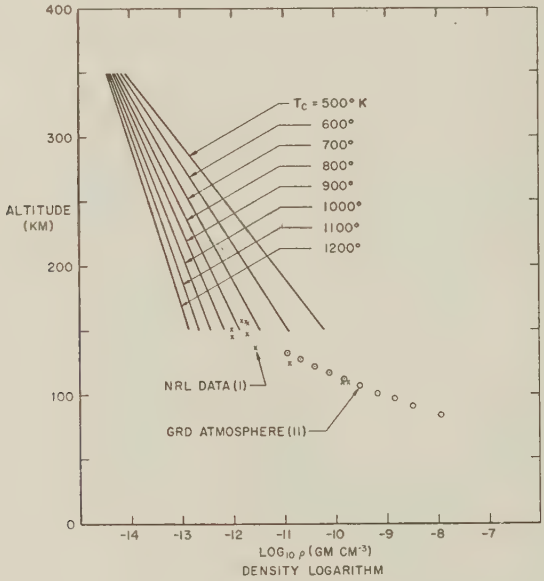

FIG. 2
ALLOWABLE VALUES AND SLOPES FOR
DENSITY CURVE AT CRITICAL ALTITUDE

With density curves so obtained, all remaining calculations follow without further assumptions. In the digital computation, pressure was obtained from density by numerical integration,† after the density logarithm had been approximated by a smooth analytic function. The atmospheric properties thus calculated are inherently and without exception continuously variable with altitude.

C. *Numerical Results*

Table 1 shows temperature, pressure, and density values calculated according to the theory outlined above. The pressure and density values up to 220 km are

†Advantage was taken of the fact that, for functions whose behavior is approximately exponential, an accurate integration formula is

$$\int_{h_1}^{h_2} F\,dh = \frac{F_2 - F_1}{\ln F_2 - \ln F_1}(h_2 - h_1)$$

where in this case $F(h) = g(h)\rho(h)$ and $(h_2 - h_1)$ is taken to be a sufficiently small altitude increment. It is believed that this type of integration gives the greatest possible accuracy in the pressure values.

TABLE 1—*Temperature, pressure, and density as functions of altitude*

Altitude h	Temperature T	Pressure P	Density ρ
km	°*Kelvin*	*dynes cm*$^{-2}$	*gm cm*$^{-3}$
90	211	2.50×10^{0}	4.12×10^{-9}
100	237	5.69×10^{-1}	8.29×10^{-10}
110	267	1.58	1.97
120	301	5.32×10^{-2}	5.61×10^{-11}
130	340	2.13	1.90
140	380	9.72×10^{-3}	7.57×10^{-12}
150	418	4.88	3.40
160	461	2.63	1.65
170	505	1.51	8.61×10^{-13}
180	553	9.08×10^{-4}	4.73
190	601	5.72	2.74
200	647	3.73	1.66
220	732	1.73	6.82×10^{-14}
240	798	8.74×10^{-5}	3.11
250	827	6.38	2.15
260	853	4.74	1.52
280	887	2.74	7.93×10^{-15}
300	901	1.66×10^{-5}	4.42×10^{-15}

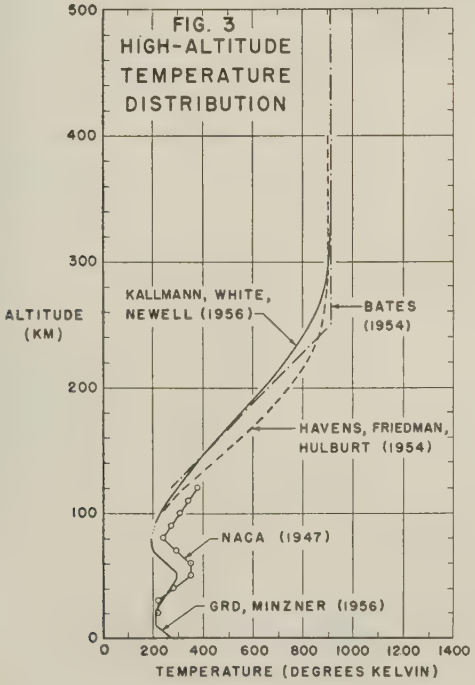

very similar to the results presented by Newell [1] and by the Rocket Panel [15]. The variation of temperature with altitude is shown in Figure 3. The lower portion of the temperature curve is taken from Minzner's evaluation of pressure and density data below 80 km [11]. On the basis of his studies, the temperature remains constant from 75 to 91 km. The dots in Figure 3 indicate a smooth continuation of the temperature profile between 80 and 90 km. Also shown in Figure 3 are evaluations by Bates [16], and Havens, Friedman, and Hulburt [2] of the temperature distribution through these altitudes. Bates's analysis is based on the Rocket Panel atmosphere [15] below 160 km, and above 160 km on the Nicolet and Mange [17] study of diffusive equilibrium between molecular nitrogen and atomic oxygen. Havens and his colleagues have estimated the temperature above 219 km on the basis of the heat conduction theory. The results of both investigations are very similar to the results obtained here.

TABLE 2—*Individual particle concentration as function of altitude*

Altitude h	Total particle concentration	$N(N_2)$	$N(O)$	$N(N)$
km	cm^{-3}	cm^{-3}	cm^{-3}	cm^{-3}
90	8.57×10^{13}	6.70×10^{13}	0	.....
100	1.74	1.35×10^{13}	4.58×10^{11}	.....
110	4.28×10^{12}	3.17×10^{12}	4.37×10^{11}	.....
120	1.28	9.02×10^{11}	2.46×10^{11}	.....
		(9.2×10^{11})*	(4.9×10^{11})*	.....
130	4.53×10^{11}	3.07×10^{11}	1.20×10^{11}	.....
		(3.1×10^{11})	(1.7×10^{11})	.....
140	1.85	1.22×10^{11}	5.72×10^{10}	.....
		(1.2×10^{11})	(6.7×10^{10})	.....
150	8.45×10^{10}	5.51×10^{10}	2.80×10^{10}	.....
		(5.6×10^{10})	(3.0×10^{10})	.....
160	4.13	2.68×10^{10}	1.41×10^{10}	.....
		(2.7×10^{10})	(1.5×10^{10})	.....
170	2.16	1.40×10^{10}	7.44×10^{9}	.....
		(1.3×10^{10})	(9.0×10^{9})	.....
180	1.19	7.68×10^{9}	4.11×10^{9}	.....
		(6.5×10^{9})	(5.9×10^{9})	.....
190	6.89×10^{9}	4.45×10^{9}	2.39×10^{9}	.....
		(3.5×10^{9})	(4.0×10^{9})	.....
200	4.18	$2.70 \times 10^{9})$	1.45×10^{9}	.....
		(2.0×10^{9})	(2.8×10^{9})	.....
220	1.72	1.11×10^{9}	5.95×10^{8}	.....
		(7.0×10^{8})	(1.5×10^{9})	.....
240	7.94×10^{8}	4.81×10^{8}	2.69×10^{8}	3.82×10^{7}
250	5.59	3.16×10^{8}	1.84×10^{8}	5.48×10^{7}
		(1.9×10^{8})	(6.5×10^{8})	.....
260	4.03	2.07×10^{8}	1.28×10^{8}	6.44×10^{7}
280	2.23	8.90×10^{7}	6.58×10^{7}	6.73×10^{7}
300	1.34×10^{8}	3.86×10^{7}	3.63×10^{7}	5.81×10^{7}
		(3.7×10^{7})	(2.5×10^{8})	.....

*The numbers in parentheses are taken from Bates, reference [16].

Table 2 shows the individual particle concentration as a function of altitude for molecular and atomic nitrogen and atomic oxygen. The concentration of molecular oxygen is not tabulated but may be calculated from the equation

$$N(O_2) = \frac{20.956}{78.114}[N(N_2)] - \frac{1}{2}N(O)$$

The fraction of oxygen molecules dissociated at any one altitude, as defined by equations (20) and (21), can also be obtained from the tabulated data by using the following relation:

$$f_d = \left(\frac{1}{2}\right)\left(\frac{78.114}{20.956}\right)[N(O)/N(N_2)]$$

Above 130 km, about 27 per cent of O_2 is still in the undissociated state. The values in brackets give the calculations obtained by Bates for molecular nitrogen and oxygen. Bates's model actually extends to 1,000 km. Above 250 km, he presents an alternative model, not noted here, where the temperature becomes isothermal at 400 km (T = 1660°K). It is only above these altitudes that the individual particle concentration for his two models begins to differ appreciably. Up to 300 km, there is rather close agreement between the particle concentration calculated on the basis of the theory outlined in Section *B* above and Bates's calculation. Nicolet [18] has studied extensively the problem of oxygen dissociation in the high atmosphere. He concludes that the process of molecular diffusion contributes increasingly to the molecular oxygen concentration at greater heights. On the basis of this consideration, Nicolet finds that at 140 km and 160 km 89.5 per cent and 92 per cent, respectively, of oxygen is dissociated. This may be compared with 87 per cent and 98 per cent dissociation calculated for these altitudes by the method outlined above.

A comparison with the NACA temperature curve published in 1947 [19] shows that these temperatures are higher in the region between 40 and 120 km (see Fig. 3). This indicates that the pressure-to-density ratio is, on the average, lower than previously assumed, a fact which is in accordance with observations.

References

[1] H. E. Newell, Jr., Ann. Géophys., **11**, 115 (1955).
[2] R. J. Havens, H. Friedman, and E. O. Hulburt, The Physical Society, London, Report of 1954 Cambridge Conference, p. 237.
[3] E. T. Byram, T. A. Chubb, and H. Friedman, Phys. Rev., **98**, 1594 (1955).
[4] C. Y. Johnson and E. B. Meadows, J. Geophys. Res., **60**, 193 (1955).
[5] E. O. Hulburt, Rev. Modern Phys., **9**, 44 (1937).
[6] L. Spitzer, The Atmospheres of the Earth and Planets (edited by G. P. Kuiper), University of Chicago Press, Chicago, 2nd ed. (1951); pp. 211-247.
[7] D. R. Bates, Proc. R. Soc. (London), B, **64**, 805 (1951).
[8] H. E. LaGow, Naval Research Laboratory, Washington, D.C. (unpublished).
[9] M. Nicolet and P. Mange, J. Geophys. Res., **59**, 15 (1954).
[10] H. K. Kallmann, The Rand Corporation, Santa Monica, Calif., Pub. No. RM-1047 (1953).
[11] R. A. Minzner, Proposed extension to the ICAO standard atmosphere (draft), Geophysics Research Directorate, Air Force Cambridge Res. Center (Feb. 1956).
[12] Smithsonian Meteorological Tables, 6th ed., Vol. 114, Pub. 4014 (1951).

[13] H. K. Kallmann, J. Geophys. Res., 58, 209 (1953).
[14] Kindly supplied to the authors by M. L. Juncosa, Mathematics Division, The Rand Corporation, Santa Monica, Calif.
[15] The Rocket Panel, Phys. Rev., 88, 1027 (1952).
[16] D. R. Bates, Rocket Exploration of the Upper Atmosphere (edited by R. L. F. Boyd and M. J. Seaton), Pergamon Press, Ltd., London (1954); pp. 347-355.
[17] M. Nicolet and P. Mange, Ionosphere Res. Lab., Pennsylvania State University, Sci. Rep. No. 35 (1952).
[18] M. Nicolet, J. Atmos. Terr. Phys., 5, 132 (1954).
[19] Nation. Advisory Comm. Aeronaut., Washington, D.C., Tech. Note No. 1200 (Jan. 1947).

ON THE ATMOSPHERIC CIRCULATION AT 500 MB IN THE AURORAL BELT*

BY HERBERT RIEHL

The University of Chicago, Chicago 37, Illinois

(Received May 25, 1956)

ABSTRACT

The 500-mb circulation along the auroral belt is calculated for the period December 1954 to June 1955 with a view toward determining whether circulation changes in the belt are related to preceding solar disturbances, especially corpuscular streams. Such a relation is not found; however, circulation increases and decreases take place with a period which can be related to the mean solar rotation in the equatorial zone. Changes in wind are produced by mechanical momentum convergence as in the temperate zone westerlies.

Introduction

In the past, possible relations between irregular outbursts of solar energy and tropospheric circulation changes on the scale of days to weeks have been studied mostly by statistical correlation. A preliminary attempt is made in this paper to explore *methods* of establishing physical relations. For this purpose, the auroral zone offers the most striking opportunity, since solar corpuscular streams are channeled into a narrow belt in this zone which leads to the creation of large *horizontal* temperature gradients at very high levels. Such differential heating in short distances has appeal for the meteorologist because it must lead to the development of motion in the high atmosphere; some effects of this motion may be transmitted to the troposphere.

There are two parts to the problem of studying the behavior of the troposphere in relation to a solar outburst: (1) transmission of energy absorbed at very low atmospheric pressures to the troposphere, and (2) the mechanism by which the troposphere reacts to such transmission. Only the second problem is taken up here. This is considered permissible, since irrespective of the vertical transfer mechanism sizable reactions at low levels should set in rapidly after a solar outburst if there is to be any tropospheric reaction. The energy involved in an outburst is very small compared to that in tropospheric circulation changes; it would at best act as a starter. Thus, if its influence is not felt, say in a time interval on the order of one to three days, one would presume that it will have no influence at all, since lateral mixing will scatter the energy over wide regions of the globe.

*This work was initiated and partly carried out under the sponsorship of the Munitalp Foundation, while the author held a summer appointment on the staff of the High Altitude Observatory of the University of Colorado, in Boulder, Colorado. It was completed under contracts between the Office of Naval Research and the University of Chicago.

Data and Computations

In winter, the cold source of the Arctic has its greatest influence on tropospheric flow changes. Further, an intense westerly jet-stream exists at that time of year near the rim of the Arctic which reaches to much higher levels than the mid-tropospheric and tropical jet-streams. Indeed, the altitude of strongest winds is as yet unclear; one merely knows that at 25 mb it is not yet attained [see 1 of "References" at end of paper]. For both of these reasons, one would expect that possible solar influences should be most easily recognized in winter, and the study was therefore begun with the period December 1954 to February 1955. Later, the computations were extended through June 1955 to compare winter and transition seasons.

Choice of the latest available winter data was prompted in part by the fact that the frequency of meteorological observations in the Arctic has been rising steadily in recent years, partly by the suggestion of Dr. Walter O. Roberts† that the years near the 1954 sunspot minimum provide the simplest solar picture, with long periods of recurrent corpuscular streams. The dates of arrival of these streams were obtained from the linearized geomagnetic index A_p . Dr. Roberts, in particular, pointed out a recurrent series beginning in February 1955 and lasting through June 1955, with periods ranging from 27 to 30 days. The index A_p was the principal source of solar data. Later, the provisional Zürich sunspot numbers were also analyzed. They showed two sets of recurrent peaks with a 24-day period, interrupted by a lack of sunspot activity during most of March 1955.

For the troposphere, the only available charts were the 500-mb hemisphere charts prepared by the United States Weather Bureau in Washington, D. C. Choice of the 500-mb surface is satisfactory, since it is known to be representative of the circulation in the bulk of the troposphere. The main drawbacks arise from scarcity of observations in part of the Arctic and the fact that the charts must be prepared rapidly for facsimile distribution. Maps drawn by detailed post-analysis were not available. The author attempted to overcome this difficulty, at least partly, by averaging all calculations over two-day and four-day (non-overlapping) intervals.

The initial hypothesis was that any solar influence would most likely be reflected by initiating changes in the velocity component along the auroral belt, and this was the primary quantity computed. Since wind measurements were insufficient, this component was calculated from the topography of the 500-mb surface using the geostrophic approximation. Considering the high latitude and and the fact that circulation changes over days and weeks are to be computed, this approximation is surely valid. For the computation, a grid for tabulating the 500-mb surface was laid out, as shown in Figure 1. The central elliptical-shaped curve follows the center of the auroral zone as given by Vestine [2]. The other points lie normal to this curve at a distance of 7.5° latitude.‡ Geostrophic winds were computed from this grid for two belts of 7.5° width poleward and equatorward from the central curve and for the whole belt of 15° latitude in width. The grid

†High Altitude Observatory, University of Colorado, Boulder, Colorado.

‡Measured from the center of the auroral belt (approximately 84° north, 70° west).

ayout is experimental, of course. It is uncertain how wide a belt one should take nto consideration meteorologically. Further, the location of the auroral belt luctuates, and since this fluctuation is not charted on a daily basis one can only ssume the mean position and allow for some migration. On rare occasions, the elt is known to expand equatorward, far beyond the grid. When this happens, alculations as performed here will become meaningless.

IG. 1—Grid for tabulation of 500-mb heights. Heavy curve shows mean position of auroral belt [2].

In addition to the flow component along the belt, the cross-components were lso calculated. When summed around the belt without respect to sign, this omponent gives a measure of the perturbation of the flow. The variability of the 00-mb heights over two-day periods, the vorticity of the flow between the inner nd outer limits of the belt, and the 500-mb height iteself were also tabulated and nalyzed in time section form, as was the strength of the 500-mb westerlies between atitudes 40° and 50° north.

hanges in Momentum

We shall consider a spherical coordinate system with pole at the center of the uroral belt. If the mass is constant in the belt, the first equation of motion, asuming no friction, may be written after integration around the belt between two losely adjacent constant-pressure surfaces

$$\frac{\partial \overline{u}}{\partial t} + \frac{1}{r^2}\frac{\partial}{a\,\partial\varphi}\overline{uv}r^2 + \frac{\partial \overline{uw}}{\partial z} - \overline{fv} = 0 \quad \ldots\ldots\ldots\ldots\ldots\ldots (1)$$

Here u and v are the horizontal velocity components, parallel and normal to the auroral belt, which is considered a latitude circle; w is the vertical component of velocity, r is the distance from the polar axis, φ the latitude, a the earth's radius, z the vertical coordinate, t the time, and f the Coriolis parameter, still measured for convenience in the geographic system. The bar denotes mean values around the belt.

Equation (1) is identical with the corresponding equation in a coordinate system centered on the geographic pole, except that, because of variations of geographic latitude along the latitude circles of the eccentric coordinate system, we have the Coriolis term $\overline{fv}$ instead of $f\bar{v}$. The equations governing the motion in eccentric spherical-coordinate systems have been discussed more fully by E. Barrett.§

Since the geostrophic approximation is assumed valid, the second equation of motion is

$$f u_g = -\frac{\partial \Phi}{a\,\partial \varphi} \qquad (2)$$

where Φ is the geopotential measured along a constant-pressure surface. Equation (1) may now be rewritten to read

$$\frac{\partial U}{\partial t} + \frac{1}{r^2}\frac{\partial}{a\,\partial \varphi}\overline{u_g v_g} r^2 + \frac{\partial \overline{u_g w}}{\partial z} - \overline{fv} - \overline{f' v_g} = 0 \qquad (3)$$

where the geostrophic assumption has been introduced everywhere except in the meridional circulation term $\overline{fv}$. U denotes the mean geostrophic zonal flow of the belt and f' the departure of the Coriolis parameter at any longitude from the mean for an eccentric latitude circle.

At the outset, one would expect any solar outburst to have a uniform effect around the auroral belt and to manifest itself through development of a meridional circulation. Due to lack of wind observations, the meridional circulation cannot be measured. However, if it is a primary factor in producing changes in U, we can try the relation $\partial U/\partial t = \overline{fv}$. Following rises in the geomagnetic index A_p, U should consistently increase according to this equation, if the solar energy input is transmitted so that it acts in a circulation-accelerating sense even at 500 mb.

Figure 2 is a time section of the period studied. At the bottom, U is shown computed for the whole belt of 15° width. Little difference was discernible between the behavior of U measured separately in the southern and northern halves of the belt, except that increases in U on most occasions started at first in the northern zone. The heavy arrows denote the main geophysical events. It is seen that marked increases in U followed rises of A_p only a few times. During most of the period, no correlation is discernible; comparison with the sunspot curve produces no improvement. We must, therefore, discard the hypothesis that initiation of a strong meridional circulation governs the behavior of U.

Further inspection of Figure 1 shows that U went through a semi-cyclical oscillation. There are, roughly, two peaks in every month, some larger and some smaller. Most of the major peaks subsequently propagated to the middle latitudes

§To be published.

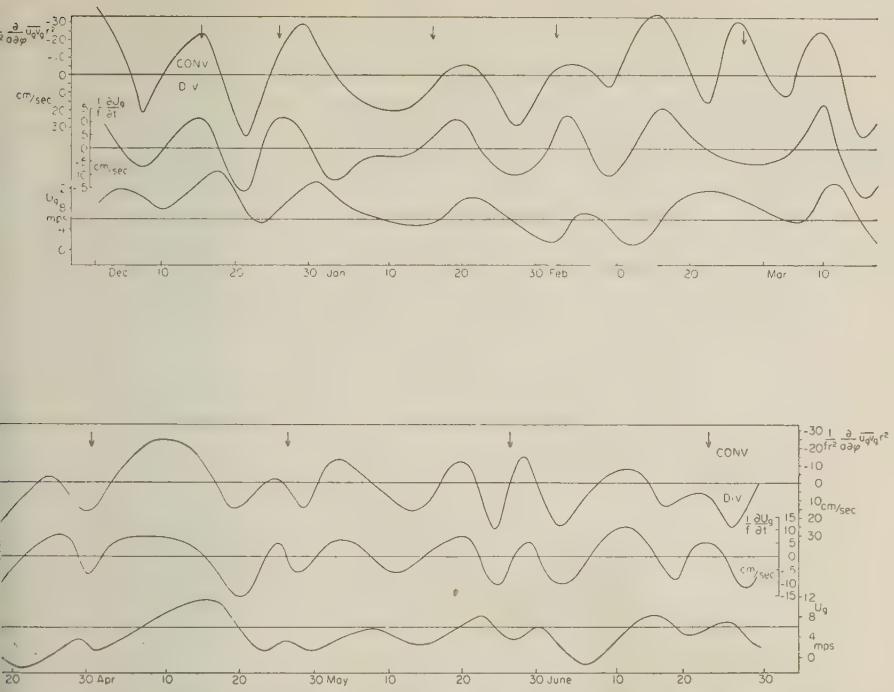

IG. 2 —Time sections of mechanical momentum convergence (top), time rate of change of U (middle) and of U (bottom), December 1954 to June 1955

s southward trends of the westerlies [3], especially in winter. The oscillation is lso brought out clearly by the curve of $(1/f)(\partial U/\partial t)$, shown in the center of igure 2. Division by the mean Coriolis parameter of the belt has been performed r convenience, to determine the strength of the meridional circulation that ould be necessary to bring about the observed changes in U. We can see whether ie oscillations of this curve are sufficiently regular to be considered cyclical. ithin the scope of this preliminary investigation, only qualitative fitting has been rried out, with a method frequently employed in geophysical problems. A rtain basic time interval is selected and the whole time series is broken up and ranged according to this interval. While several irregular peaks may occur ithin any given interval, the arrangement may show that one or more of these aks fall in the same position relative to the basic interval over longer periods. hree intervals have been tried out to subdivide the central curve of Figure 2: 7 days, corresponding to A_r ; 24 days, corresponding to the rotation rate of unspots for the period studied; and 25.5 days, corresponding to the mean solar tation in the equatorial zone. Only the last of these showed features of possible terest and has been reproduced (Fig. 3).

In successive cycles, maxima are never more than two days distant from the rtical line in Figure 3, which marks the center of the period. In contrast, the condary maximum does not occur in each cycle and is more variable in timing.

No inferences, however, can be drawn, as the subdivision may be artificial or we may be encountering mere coincidence; the observed periodicity may indicate merely a natural "relaxation" period of the atmosphere, successive accumulation and depletion of cold air in the Arctic. Hyde [4] and Fultz [5] have noted cycles with a frequency similar to that of Figure 3 in rotating dishpan experiments. Nevertheless, the matter is of sufficient interest to inquire further into the mechanism which produces the variations of U.

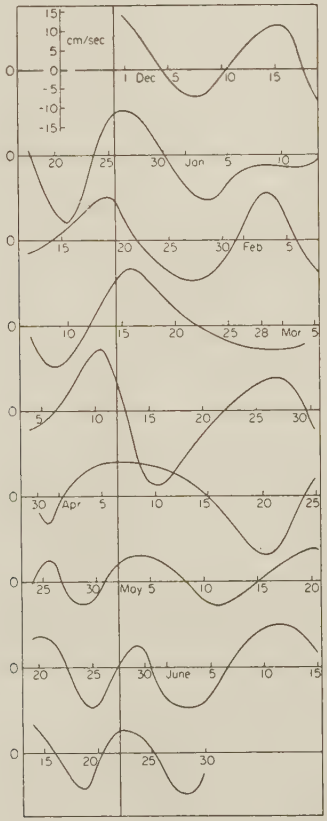

FIG. 3—Central curve of Figure 2 arranged according to 25.5-day intervals

Equation (3) cannot be solved completely, since in addition to the meridional circulation the vertical velocity is also unknown. We can, however, compute the two remaining terms which measure convergence or divergence of absolute angular momentum as brought about by the horizontal eddies around the belt. The first of these terms depends on the correlation between u_φ and v_φ on the boundaries of the belt. Such correlations are never large; therefore, the scarcity of data was especially felt in calculating this term. After forming averages over two-day intervals, however, a smooth curve could be drawn with very little approximation

This curve is shown at the top of Figure 2, with scale inverted, and again expressed as equivalent meridional circulation. Correlation by sign is excellent between the momentum convergence and momentum change curves. A notable difference occurs only in the last days of February. The amount of mechanical momentum convergence exceeds the observed momentum changes considerably. Figure 4

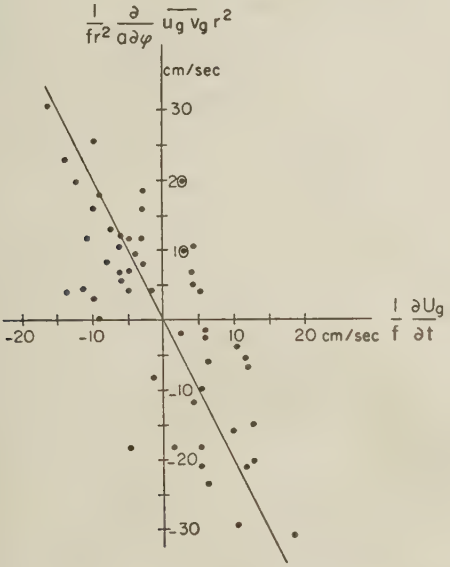

FIG. 4—Scatter diagram, showing correlation between upper and middle curves of Figure 2

shows the correlation between these two quantities, obtained by plotting every second value calculated. The regression line

$$\frac{1}{f}\frac{\partial U}{\partial t} = 0{,}5\,\frac{1}{fr^2}\,\frac{\partial}{a\,\partial\varphi}\,\overline{u_\varphi v_\varphi} r^2$$

gives a good fit.

The term $\overline{f' v_\varphi}$ arises from the special choice of coordinate system. Therefore, it cannot be given a separate physical interpretation, but must be reckoned as part of the mechanical momentum divergence. The meaning of this term is readily seen. When winds blow predominantly across the pole from Siberia towards the Atlantic Canadian sector, the inflow through the auroral belt occurs at higher Coriolis parameter than the outflow, and hence the motion along the belt is accelerated. During flow from the Atlantic to Siberia, the reverse holds. Thus, the sign of $\overline{f' v_\varphi}$ depends on the distribution of long and short waves around the belt.

The computations show that the magnitude of the term is the same as that of the $\overline{u_\varphi v_\varphi}$ term, but the sign is generally opposite and values are lower. When the two terms are added, the resulting curve (not reproduced) resembles the top curve

of Figure 2 in detail, but the amplitude is less. The regression between total momentum convergence and momentum change becomes approximately

$$\frac{1}{f}\frac{\partial U}{\partial t} = \frac{0.66}{f}\left[\frac{1}{r^2}\frac{\partial}{a\,\partial\varphi}\overline{u_\varphi v_\varphi} r^2 - \overline{f' v_\varphi}\right]$$

The foregoing demonstrates that increases in the zonal momentum along the auroral belt take place in the same manner as described for the middle latitude westerlies by Mintz and Kao [6] and other writers. If a solar index can be found which agrees in period with the momentum change and momentum convergence curves, physical linkage between the solar effect and the terrestrial change must be provided by establishing an influence of the solar outburst on the configuration of the atmospheric disturbances. Of course, a meridional circulation may still be produced by solar events; until values of $(\partial/\partial z)\ (\overline{u_\varphi w})$ can be determined, this possibility cannot be excluded.

Long Wave Pattern

An initial attempt to investigate the disturbances was made through calculation of their strength around the belt with the method described earlier, and through analysis of very long waves with wavelength of 360° longitude. The perturbation strength was negatively correlated with U, as generally noted in the westerlies by Willett [7]. Disturbances with a wavelength of 360° longitude were present, as brought out in Figure 5.

This Figure shows time sections of 500-mb height around the belt. In order to eliminate all but the largest disturbances, 500-mb heights were averaged over 40° longitude and four-day overlapping periods. The 500-mb height scale applicable to each horizontal base-line of Figure 5 is indicated in the upper left corner. We observe that 500-mb heights generally are higher in the Atlantic area than over Siberia, due to the asymmetric location of the belt of aurora with respect to the mean westerlies; further, that the heights generally rise from winter to summer. These features are of little interest for the present discussion; important is the quasi-periodic oscillation observed on all longitudes. In Figure 5, points of maximum height at the different longitudes, that is, ridge passages, have been connected by solid lines. It is seen that most ridges are covered by this analysis; there are only a few places where a ridge appears at only one or two longitudes and then dies out again. For the most part, slow propagation of the ridges takes place. The slope of the connecting lines shows that this propagation is clockwise around the belt.

If one scans the diagram from top to bottom, it becomes apparent that over most of the period only one ridge and one trough is present at any given time; hence we are dealing with a wave of 360° longitude wavelength. There are interruptions of continuity, especially at the end of January and early in May. Generally, however, the wave is a stable feature of the circulation pattern and moves regularly. Its rate of revolution averages about 27 days. Thus, it is well correlated with A_p and poorly correlated with U. Crosses mark the major rises of A_p in Figure 5; we observe that these occur mostly when the ridge overlies Siberia. Whether or not this relation is accidental cannot be judged from the short period studied. If real, it would follow that the solar effect tends to set up very large-scale oscillations

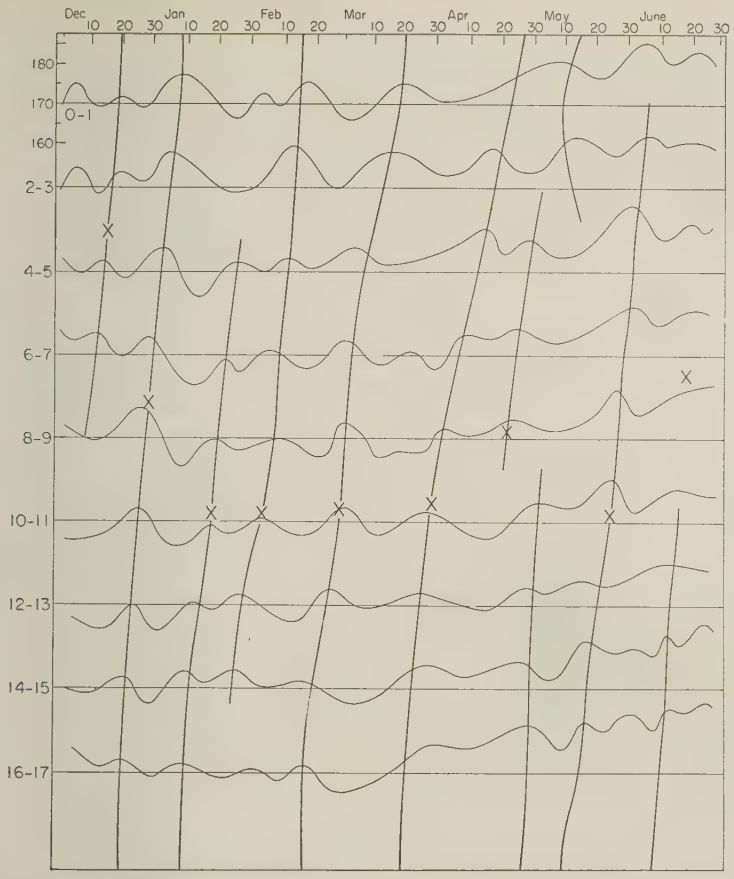

IG. 5—Cross-section of time *vs* longitude (in grid defined in Fig. 1) of 500-mb heights averaged ver four days. Solid lines connect principal ridges. Crosses mark principal rises of A_p ; they have een entered at appropriate places of the solid lines. Scale for all longitudes (100's feet) in upper left corner.

hich must be quasi-barotropic. At least, the rate of revolution of the wave noted ere can be explained satisfactorily by Petterssen's formula for barotropic wave ropagation in a belt of limited width [8].

onclusion

This study has shown some facts about the circulation and perturbations in he belt of aurora. Variations take place on a time scale with magnitude approxiating the solar rotation period. Although definite relations between solar and tmospheric events could not be established, the study also does not deny such elations, and it points to some of the mechanisms through which any solar event resumably must operate to produce an atmospheric reaction. Therefore, it appears orth while to carry out this type of approach over a period of several years and

to expand the scope of the study to permit full evaluation of equation (3). Thi will require analysis from the ground to at least 100 mb. Given enough wind data the meridional circulation can be calculated directly. Failing this, the vertica velocity can be computed from the vorticity theorem with electronic compute methods, such as are now in use at the Joint Numerical Weather Prediction Cente in Washington. Finally, any new study should introduce a parameter based on th tropospheric cooling in the Arctic and, if possible, analysis should be extende to the altitude of the wintertime Arctic jet-stream. This may become feasibl with observations collected during the International Geophysical Year.

Acknowledgment

The writer is indebted in the first place to Dr. Walter Orr Roberts, at whos initiative this study was begun and who took part in numerous discussions especially of the solar indices. Thanks are due also to Mr. Vernon M. Crudge an Dr. Vincent J. Schaefer, Munitalp Foundation, for support of the initial phase of the study, to Dr. Sydney Chapman for advice in selecting the mean position o the auroral belt, and to Dr. George Platzman and Mr. Earl Barrett, of the Uni versity of Chicago, and to Dr. H. Arakawa, Tokyo, for much aid in setting up th momentum convergence equation in a spherical coordinate system with eccentri pole.

References

[1] A. Kochanski, J. Met., **12**, 95 (1955).
[2] E. H. Vestine, Terr. Mag., **49**, 77 (1944).
[3] H. Riehl, *et al.*, J. Met., **7**, 181 (1950).
[4] R. Hyde, Q. J. R. Met. Soc., **79**, 161 (1953).
[5] D. Fultz, J. Geophys. Res., **61**, 328 (1956).
[6] Y. Mintz and S. Kao, J. Met., **9**, 87 (1952).
[7] H. C. Willett, *et al.*, Final report of the Weather Bureau—Massachusetts Institute of Tech nology extended forecasting project 1946-47.
[8] S. Petterssen, Q. J. R. Met. Soc., 78, 337 (1952).

LOW-ANGLE FLUCTUATIONS OF THE RADIO-STAR CASSIOPEIA AS OBSERVED AT ITHACA, N. Y., AND ITS RELATION TO THE INCIDENCE OF SPORADIC-*E**

BY BRAULIO DUEÑO

University of Puerto Rico, College of Agriculture and Mechanic Arts, Mayaguez, Puerto Rico

(Received June 6, 1956)

ABSTRACT

Low-angle fluctuation data of the radio-star Cassiopeia for the period comprised between September 1954 to August 1955 have been compared with ionospheric sounder data from Ottawa, Canada. A remarkable relation between the incidence of fluctuations and sporadic-*E* has been observed for the month of December 1954. The coincidence of *Es* and fluctuations was found, in general, to be very good during the midwinter period and poor afterwards. The pierce-through region for ionospheric layers at a height of 400 km comes out approximately 1500 km north of Ithaca. In this region, the normal sun-controlled forms of ionization should be a minimum during the midwinter period. It is reasonable to expect that layers at the 120-km level should be most influential in causing fluctuations during this period. Several fluctuationless days were recorded during this midwinter period and practically none at other times.

Observations and results

Low-angle fluctuation data for the winter period comprised between the months of November 1954 to March 1955 have been compared with ionospheric sounder data from Ottawa, Canada. A somewhat remarkable relation between the incidence of fluctuations and sporadic-*E* has been observed for the month of December 1954.

Since Ottawa is only 300 km almost due north of Ithaca, the ionospheric data from Ottawa is interpreted only as being representative of conditions in a region much farther north. Although comparison with an ionospheric station 600 km north of Ithaca would have been more desirable, this set-up is unfortunately non-existent. However, it seems reasonable to expect that ionospheric conditions producing fluctuations be of somewhat widespread nature.

A plot of fluctuation index and maximum penetration frequency *versus* time appears in Figure 1. The broken lines represent *fEs*, and the neighboring solid line in each case represents the fluctuation index. Figure 1(*a*) shows good agreement for all the days plotted, exception being made of the day 12-7-54, which shows strong disagreement, that is, fluctuations and no *Es*. The next Figure shows two days, 12-14-54 and 12-16-54, when there exists a complete absence of both

*The work reported in this paper was performed at Cornell University under the direction of Dr. W. E. Gordon.

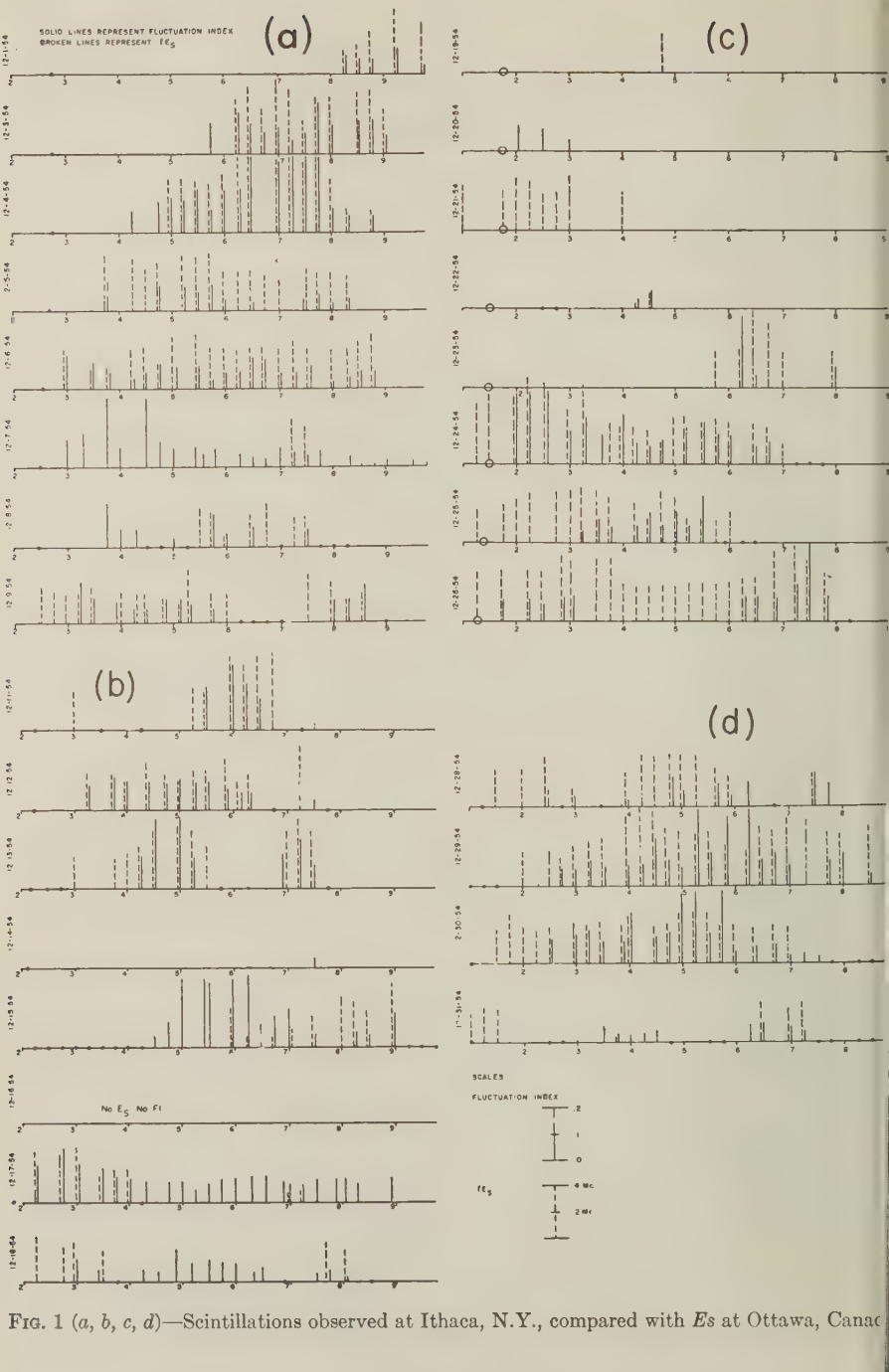

FIG. 1 (*a, b, c, d*)—Scintillations observed at Ithaca, N.Y., compared with *Es* at Ottawa, Canad

Es and fluctuations. Figure 1(*c*) shows on the days 12-22-54 and 12-23-54 very nice agreement, in the sense that it shows fluctuations and *Es* starting and stopping almost simultaneously. Figure 1(*d*) also shows rather good agreement for the four days represented.

Out of the 28 days shown in these Figures (three missing on account of equipment failure), 19 were strongly correlated, seven had medium correlation, and two had poor correlation.

Figure 2 is a plot of coincidence percentages between *Es* and fluctuations for

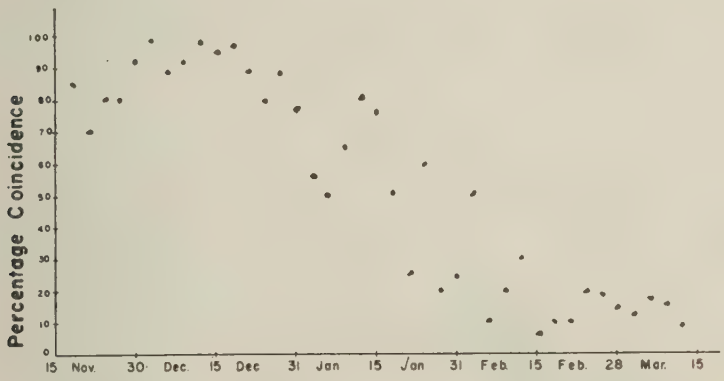

FIG. 2—Percentage coincidence between fluctuations and sporadic-*E*

the months of November 1954 and January and February 1955. A simultaneous total absence of fluctuations and *Es* is counted as a 100 per cent coincidence. The simultaneous presence of both for the totality of the time of the radio-star transit is also counted as a 100 per cent coincidence. It will be observed that the coincidence of *Es* and fluctuations appears to be very good during the midwinter period and poor afterwards.

A histogram of the occurrence of days with very small fluctuation index (less than 0.2) during the period from October 1 to June 30 was made, which shows that during the month of December there were eight days without fluctuations, while October (1954) and April, May, and June 1955 were months when appreciable fluctuations occurred every day.

The pierce-through region for ionospheric layers of a height of 400 km, using a value of 10° for the elevation angle of Cassiopeia at lower transit, comes out to be approximately 1500 km north of Ithaca. This corresponds to a region in Canada at a latitude of approximately 57°. While this region is not exactly within the polar region, it is near enough to it to expect that the average seasonal variation of ionization follows, on magnetically quiet days, the Chapman relation. This means that the normal, sun-controlled forms of ionization should be a minimum at a period comprising the endings of November, December, and the beginnings of January.

On this argument, we can conclude that the ionospheric layers at the 400-km level and 1500 km away will have its minimum influence on the fluctuation obser-

vations of Cassiopeia during this minimum daylight period. Consequently, it is to be expected that the ionospheric layers at the 120-km level should be the most influential factor in causing the radio-star fluctuations. The pierce-through region for this layer is approximately 560 km north of Ithaca. This simple picture can then be used to explain why there is good agreement between the Ottawa sounder data for *Es* and the low-angle fluctuations as recorded at Ithaca for the period comprising all of December and the first week of January 1955, and why this agreement is poor at other times. The fact that fluctuation rates during the winter period were found to be from three to four times slower than the corresponding fluctuation rates at other times appears to add substance to the suggestion that the nature of the mechanism causing fluctuations is different during the winter period.

Comparison of the average fluctuation rates recorded during the lower transit of Cassiopeia and the corresponding Cheltenham *K*-indices revealed a close correspondence between them.

An increase in the fluctuation-rate number can be due either to an increase of the drift velocity of the diffraction pattern across the point of observation or to a change of the diffraction pattern brought about by an ionization mechanism causing semiperiodic changes in the size of the irregularities. Of these two, the former is the most likely explanation for the changes in fluctuation rate, so that high drift velocities correspond to the higher fluctuation rates. This conclusion is well borne out by the results of spaced-receiver experiments.

In Figure 3(*a*, *b*, and *c*) are shown scatter diagrams of average fluctuation rates against *K*-sums for a period of several months. The reason for using *K*-sums is that a considerable span of hours is represented by the data on these diagrams. During the months of November, December, and January, the scatter diagrams

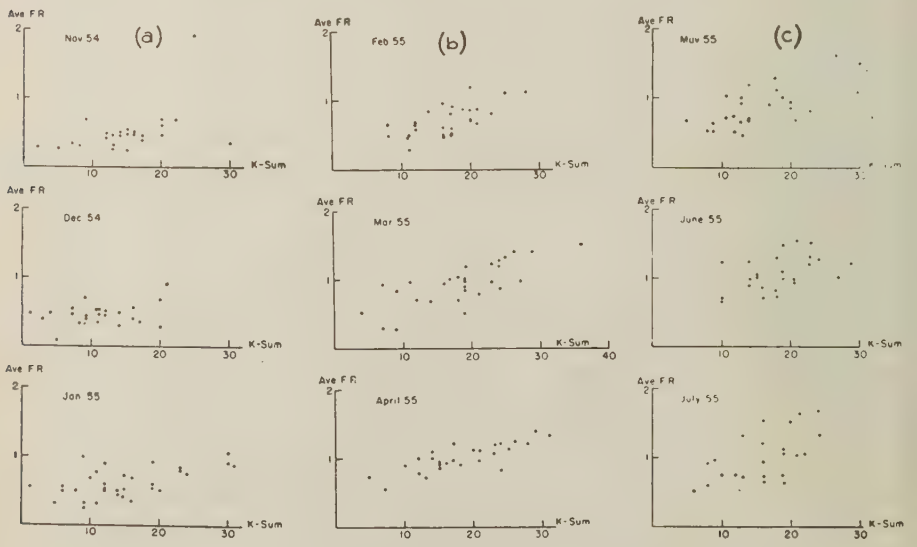

FIG. 3 (*a*, *b*, *c*)—Scatter diagrams of average fluctuation rate *vs* *K*-sum

are not particularly suggestive of any relation between the K-indices and the fluctuation rates. This is especially noticeable in the December diagram. A line through the average value of all the points would clearly lie almost parallel to the abscissa. On the other hand, for the other months, the plots clearly show an approximate linear relation between the K-sums and the fluctuation rates.

The lack of relationship between fluctuation rates and K-sums during the winter period seems to be related with the prevalent minimum ionization conditions in the near-polar regions during the post-midnight hours. Further, the lower transit of Cassiopeia takes place mostly during the post-midnight hours. For example, on December 17, the lower trace started at 1:40 and ended at 8:00. Furthermore, during this period, the lower culmination fluctuations were found to be closely related to the incidence of sporadic-E. This is especially true for the months of December and, since all other forms of sun-controlled ionizations are at a minimum at this time, the effect of sporadic-E on fluctuations is most easily discernible. Now, it has been found by Chapman [see 1 of "Reference" at end of paper] that the drift velocity of the E-layer irregularities is perceptibly independent of the K-index for values of K-index up to 4. An inspection of the Cheltenham three-hour-range indices K for December 1954 has shown that in only one instance, on December 27, was the K-index up to 5. In all other instances—with three exceptions—the K-index was lower than 4. This lack of dependence of total velocity and K-figures for values of K less than 5 in the case of the E-region has also been observed at Cambridge by Briggs and Spencer [2].

The results obtained by Chapman are concerned with the reflections of a radio wave from sporadic-E layers. Unfortunately, our spaced-receiver set-up was not yet in operation in December 1954, so that no drift-velocity measurements during this period are available.

However, the average value of fluctuation rates during the month of December is of the order of 0.45 fluctuation per minute, or 2.2 minutes per fluctuation. Now assuming that the sporadic-E irregularities causing fluctuations are also of the order of 4 km, the value of the drift velocity obtained by dividing 4 km by 130

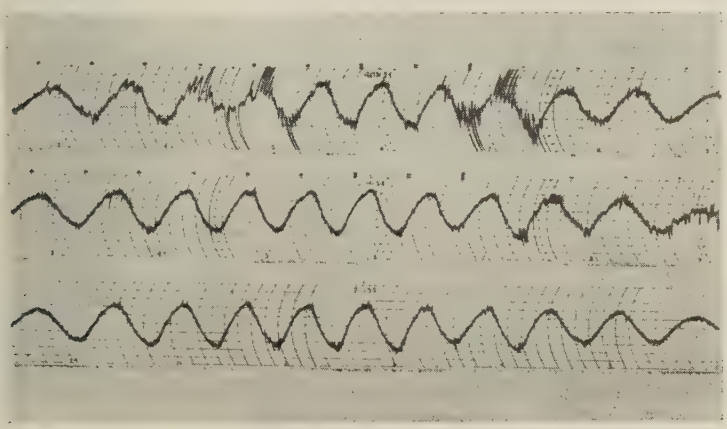

FIG. 4—Sample traces

seconds is of the order of 30 meters per second, a value which is even smaller than the values of the velocities associated with K-indices less than 5.

One notable feature of fluctuations at lower culmination which has not been observed at the upper transit of the radio star is a tendency for fluctuations to reach peaks of amplitude that on certain occasions will take values several times the value of the undisturbed signal from the radio star. This is not a very common occurrence. For example, during January, February, and March, there were only eight days out of each month in which fluctuation indices greater than 2 were observed. The months in which this conduct was most prevalescent were April, May, and June. One further feature of low-angle fluctuations of the radio star observed only on occasions when large peaks of amplitude exist is a marked decrease in the mean signal of the source for a considerable time interval. This was also a rare occurrence.

These two features of fluctuations (not readily explainable in terms of diffraction theory) are illustrated by the traces shown in Figure 4.

Since for the lower transit of Cassiopeia at the Ithaca latitude the angle of incidence of the radio-star rays to the ionospheric layers is of the order of 80°, the mean signal diminution for a considerable time interval could be explained in terms of an upward refraction of the rays due to intense forms of ionization. This is also suggestive of sporadic-E forms of ionization.

References

[1] J. H. Chapman, Can. J. Phys., **31**, 120 (1953).
[2] B. H. Briggs and M. Spencer, Rep. Prog. Phys., **17**, 262 (1954).

FLUX MEASUREMENTS OF DISCRETE RADIO SOURCES AT FREQUENCIES BELOW 30 MEGACYCLES

BY H. W. WELLS

Department of Terrestrial Magnetism, Carnegie Institution of Washington, Washington 15, D.C.

(Received June 20, 1956)

ABSTRACT

The report presents results of flux measurements at frequencies below 30 Mc and describes steps taken to minimize errors. At 26.75 Mc, Taurus A and Virgo A appear to be approximately equal at 85×10^{-24} w.m^{-2}(c/s)$^{-1}$, and at 18.5 Mc the intensity of Virgo A has climbed to 150×10^{-24} w.m^{-2}(c/s)$^{-1}$.

The ratio of relative amplitudes of Cygnus A to Cassiopeia A is 0.6 at 26.75 Mc, and drops to 0.5 at 18.5 Mc, suggestive of enhanced absorption of Cygnus A. Plans and probable limitations of further low-frequency observations are discussed.

Interest has continued in the observation and measurement of discrete radio sources at the lower range of frequencies which are available for radio astronomy. It has been pointed out by Hey and Hughes [see 1 of "References" at end of paper] that knowledge of properties of discrete radio sources at the lower frequencies is important to an understanding of the mechanism of signal production and to the determination of interstellar radio absorption.

Since oblique incidence of ionospheric transmission determines the lower limit of useful frequencies, a preliminary survey using total power radiometers was conducted in the spring of 1955 to aid in the selection of operating frequencies. Principal effects of the ionosphere may be to absorb signals from extraterrestrial sources and to propagate earth-bound interfering signals. It was established at an earlier date that it was unrealistic to attempt the selection of a clear observing channel—even with band-widths of a few kilocycles—in this area. The alternate condition of operation when the maximum usable frequency for oblique-incidence ionospheric transmission has fallen below the operating frequency (during the interval immediately preceding sunrise) established, at the same time, a minimum of ionospheric absorption. Under these conditions, the observing frequency is three or four times greater than the ionospheric critical frequency at vertical incidence. It has already been demonstrated by Mitra and Shain [2] that ionospheric absorption is negligible under these circumstances. However, the presunrise interval, although free from direct interference, often includes other unstable conditions which confuse the observations. These were principally scintillations or other bursts of short duration which could mask or obscure the radio source.

Some preliminary results were reported in September 1955 at the meeting of Commission 40 of the International Astronomical Union in Dublin [3]. At that time, it was stated that the ratio of amplitudes of Cygnus A to Cassiopeia A at

12.5 Mc appeared to be roughly 0.5. It was also estimated that the flux of Cassiopeia A at 12.5 Mc was about 220×10^{-24} w.m^{-2}(c/s)$^{-1}$ and that at 15.5 Mc the flux measured only slightly higher, being 240×10^{-24} w.m^{-2}(c/s)$^{-1}$. Subsequently, errors introduced by saturation effects in the receiver have been identified and eliminated. It is probable that the measurements reported above should be doubled, although the statement concerning relative amplitudes is still sound.

Requirements of absolute flux measurements of discrete sources include (1) knowledge of effective antenna aperture, (2) measurement of all losses in transmission lines or associated components, and (3) a dependable method for calibration. The determination of effective antenna aperture requires knowledge of the polar diagram and efficiency of the reflecting surface below the antenna. Our interferometers are composed of dipoles—the simplest of antennas—mounted over a large grid of reflecting wires. Antenna efficiency has been measured by intercomparisons, using radiometer techniques, of the relative powers in a standard reference antenna and the antenna in use. The reference dipole antenna has been mounted over a large flat continuous plate of sheet metal, which is perfectly conducting at these frequencies. It has been determined that the antennas used above the wire grids are between 90 and 95 per cent efficient at 26.75 Mc.

A standardized calibration procedure requires a dependable noise source which is equivalent to a thermal generator, and a method of applying the calibration signals under actual operating conditions; that is, with antennas connected to the receiver inputs. Comprehensive tests have been conducted to compare the noise power of conventional noise diodes with that of actual thermal sources at frequencies below 30 Mc. Independent tests were conducted over an equivalent temperature range of 0 to 200 degrees centigrade, and the agreement in each case

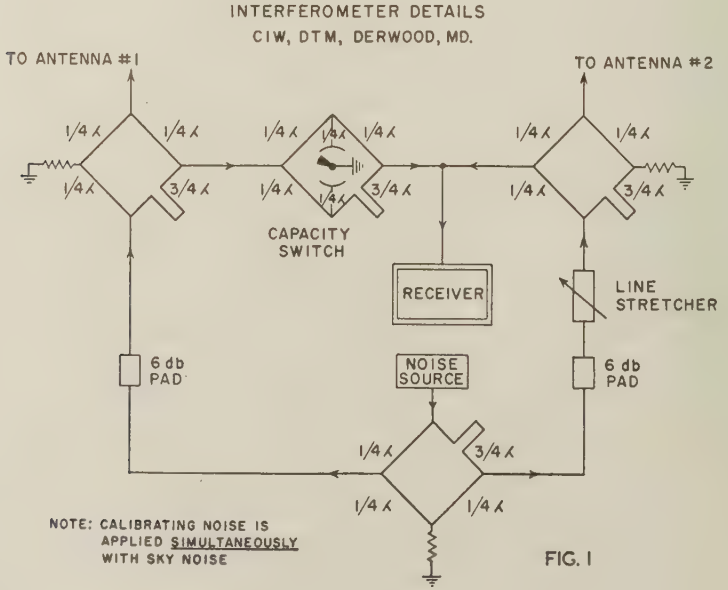

FIG. 1

was considered to be excellent—probably better than 95 per cent. The addition of precision attenuators in the noise diode output made it possible to explore its performance over a more extended range, but practical considerations made it necessary to keep the temperature of the thermal source within the above-indicated limits.

The method of applying calibration signals to the instrument without interruption of normal operation is shown in Figure 1. It is seen that output from the noise source is divided into two branches by a signal splitter and is then combined with the signals from antennas 1 or 2 through magic "*T*" devices. Lobe-switching of our Ryle-type interferometer is accomplished by the use of a capacity switch, which is also indicated in the diagram. No preamplifiers are used in either leg of the antenna. All radio frequency and related amplification are contained in the receiver after signals from the two antennas have been combined.

Measurements have been obtained on Virgo A at 26.75 and 18.5 Mc, and on Taurus A at 26.75 Mc. The results, which are shown in Figure 2, are plotted with

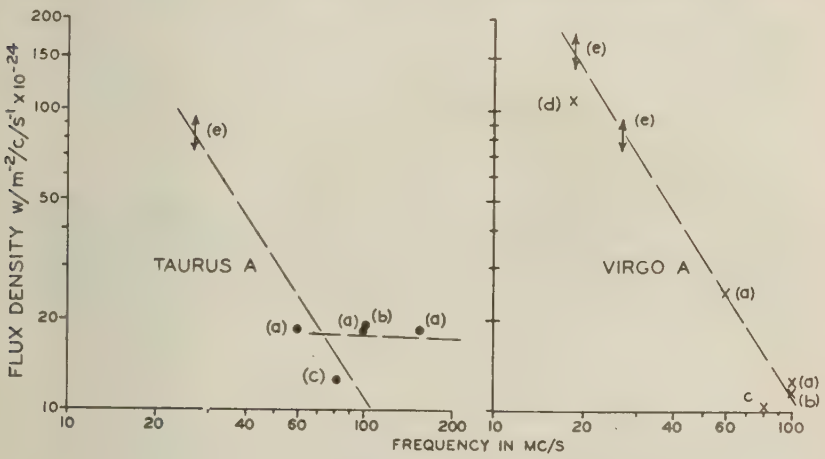

FIG. 2—FLUX DENSITY OF TAURUS A AND VIRGO A

KEY: (a) STANLEY, SLEE
(b) MILLS
(c) RYLE, SMITH
(d) SHAIN, HIGGINS
(e) WELLS

reference to measurements of other investigators. Values indicated in the Figure are approximately equal for Virgo A and Taurus A at 26.75 Mc, being 85×10^{-24} $w.m^{-2}(c/s)^{-1}$, while the flux of Virgo A at 18.5 Mc is shown to be 150×10^{-24} $w.m^{-2}(c/s)^{-1}$. Examination of Figure 3 also reveals the approximate equal intensities of these two sources at 26.75 Mc. Of special interest are the indications that the spectrum of Taurus A appears to have departed substantially from the "flat" character attributed to it at higher frequencies, and that the intensity of Virgo A is increasing uniformly without evidence of a low-frequency break.

The use of more elaborate antenna systems such as 3- or 4-element co-linear arrays has permitted measurement of the relative ratio of Cygnus A to Cassiopeia A at both 26.75 and 18.5 Mc. The ratio at 26.75 Mc is very close to 0.6, while the

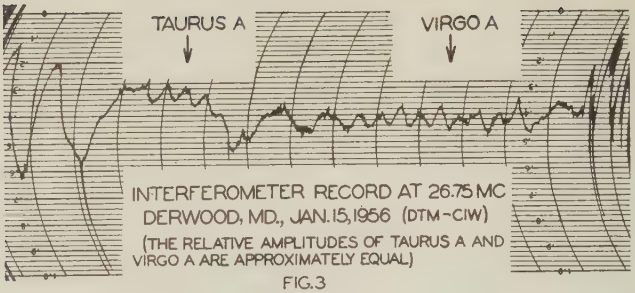

FIG. 3

ratio at 18.5 Mc is approximately 0.5. Of the two measurements, more confidence is attached to the one at 26.75 Mc, since it represents the average of many more observations than at 18.5 Mc. However, the difference is large enough to justify a conjecture that the apparent reduction in intensity of Cygnus A at the lower frequency may be related to greater interstellar absorption, in view of its extreme range (35 megaparsecs) compared to the distance of Cassiopeia A (500 parsecs). It is interesting to note that a similar trend was reported by Hey and Hughes [1]. Figure 4 is a photograph of a recent recording at 18.5 Mc, illustrating the ratio of amplitudes from these principal sources.

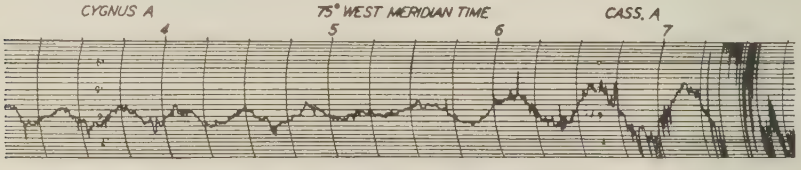

FIG. 4—INTERFEROMETER RECORD OF CYGNUS A AND CASSIOPEIA A AT 18.5 MC MAY 27, 1956 DERWOOD MD, CIW, DTM
(THE RATIO OF CASS. A TO CYGNUS A IS APPROXIMATELY 2 TO 1)

During the summer of 1956, measurements will be made of the intensity of Cassiopeia A at 26.75, 18.5, and lower frequencies if possible. These observations will be continued with dipole antennas and will provide a base for the estimate of Cygnus A intensities using the above-established ratios for conversion.

The absence of a drop in intensity of Virgo A at the lower frequencies may be particularly significant, since it is near the galactic pole. For Cassiopeia A, the drop below 20 to 25 Mc, reported independently by Lovell and Wells [3], has been examined by Roman and Haddock [4] in their model for non-thermal source spectra. Although our expectation is that a substantial increase, as stated earlier in this report, will be necessary in the low-frequency flux of Cassiopeia A, the "break" or drop below 20 to 25 Mc should continue to be pronounced. The absence of a low-frequency decrease for Virgo A (near the galactic pole) and the presence of the drop for Cassiopeia A (and probably other sources) warrant speculation that absorption in interstellar space is a controlling factor.

In view of the pronounced ionospheric effect already evident as a result of the new solar activity, there may be no opportunity to repeat the 12.5-Mc observations for many years. We still have hopes of obtaining some results at 15.5 Mc, but our

present experience indicates that the useful observing time at any frequency below 20 Mc is extremely limited.

References

[1] J. S. Hey and V. A. Hughes, Nature, **173**, 819-820 (1954).
[2] A. P. Mitra and C. A. Shain, J. Atmos. Terr. Phys., **4**, 204-218 (1953).
[3] Unpublished data, Commission 40, International Astronomical Union, Dublin, September 1955.
[4] N. G. Roman and F. T. Haddock, Naval Research Laboratory, Washington, D.C., NRL Rep. No. 4712 (March 1, 1956).

HIGH ALTITUDE MEASUREMENTS OF THE EARTH'S MAGNETIC FIELD WITH A PROTON PRECESSION MAGNETOMETER*

BY LAURENCE J. CAHILL, JR., AND JAMES A. VAN ALLEN

Department of Physics, State University of Iowa, Iowa City, Iowa

(Received June 28, 1956)

ABSTRACT

A nuclear free-precession magnetometer of the Packard-Varian type has been built and used for the precise measurement of the earth's magnetic field (scalar magnitude of total field vector) at high altitudes. The instrumentation, including the magnetometer head, amplifier, and radio telemetering transmitter, was carried to 100,000 feet altitude by a plastic Skyhook balloon. Signals were transmitted to a fixed ground station at one-minute intervals and the nuclear precession frequency was determined by standard frequency measuring techniques. Satisfactory signals were received until 2.5 hours after launching, at which time the balloon was near the radio horizon, approximately 200 miles from the ground station. The data showed a decrease in magnetic field intensity with altitude, as well as large variations in intensity with geographical position. The work described is the first phase in this laboratory's program of adapting the free precession magnetometer to the systematic study of electrical currents in the ionosphere, using rockets as experimental vehicles.

I—Introduction

The direct study of electrical current systems in the ionosphere by means of rocket-borne magnetometers was first proposed by Vestine, *et al.* [see 1 of "References" at end of paper]. A cooperative assessment of the feasibility of such investigations was conducted by interested persons from the Applied Physics Laboratory of Johns Hopkins University, the Naval Ordnance Laboratory, and the Department of Terrestrial Magnetism, on September 23, 1947. It was judged feasible to adapt the Naval Ordnance Laboratory (NOL) three-element flux-gate magnetometer to use in Aerobee rockets for high-altitude total-field measurements of sufficient accuracy [2, 3].

The results of three consequent Aerobee flights of modified NOL magnetometers to over 100 km altitude have been reported [4, 5].

In the third of these flights (made at local noon, near the geomagnetic equator, off the coast of Peru), the first direct determination of the altitude and magnitude of electrical currents in the ionosphere was made by the observation of a discontinuity in the earth's field at about 100 km altitude.

A thoroughgoing analysis of the potentialities of rocket-borne magnetometers

*Assisted by National Science Foundation Project Grant IGY-1.

for the magnetic exploration of the ionosphere has been given recently by Chapman [6].

The three-element flux-gate magnetometer which was used in our earlier work has excellent sensitivity, but possesses several practical disadvantages for rocket use, as follows:

(*a*) The scalar magnitude of the total magnetic field appears as a dc signal. Hence, the accuracy of a measurement depends upon knowledge of the amplitude calibration of the complete system, including the telemetering transmitter and receiver. The magnetometer element itself must be calibrated by a large, precisely-wound solenoid, which is magnetically shielded from the earth's field and from other fields. A trustworthy pre-flight calibration is difficult on board a ship, for example.

(*b*) The instrument is a differential one—that is, it is balanced to zero output at a pre-chosen value of the calibrating field. For a given sensitivity, its range is limited by the characteristics of the telemetering system. Moreover, it is difficult to maintain the zero balance under changes of battery voltage and changes of temperature. A small drift may be enough to take the output signal "out of the telemetering band."

(*c*) It is very difficult to align the three orthogonal flux-gate elements and to match their characteristics with the precision necessary to avoid a substantial orientational error (for example, in the order of one milligauss difference in reading for different orientations in the same magnetic field).

In contrast, the nuclear induction principle makes possible the absolute measurement of magnetic fields without any specific calibration. The intensity of the field is given by the simple quotient of the *frequency* of a (slowly decaying) sinusoidal signal and a single, fundamental nuclear constant. Hence, the measurement is not dependent upon the amplitude characteristics of the electronic system. This principle had been used in precision measurements of strong magnetic fields since the initial nuclear induction experiments of Bloch, *et al.* [7], and of Purcell, *et al.* [8]. Recently, Packard and Varian [9] have extended the nuclear induction technique to the measurement of weak, homogeneous magnetic fields ($\sim$1 gauss) and have applied it to the precision measurement of the earth's magnetic field [10].

A scheme for adapting the Packard-Varian magnetometer to high-altitude rocket measurements has been described by Van Allen [11]. The present paper describes the development of a proton precession magnetometer, using radio telemetering for remote transmission of data, and its successful use in a balloon flight to an altitude of 100,000 feet.

II—Principle of the Proton Precession Magnetometer

All nuclear induction effects depend upon the intrinsic spin angular momentum $\mathbf{a}$ and the magnetic moment $\boldsymbol{\mu}$ of the individual nucleus, these quantities being basic characteristics. They are related by the vector equation

$$\boldsymbol{\mu} = \gamma \mathbf{a} \qquad (1)$$

where γ is a scalar constant, known as the gyromagnetic ratio. The interaction of the magnetic moment with an external magnetic field $\mathbf{H}$ causes a precession of the

spin axis of the nucleus about the magnetic field in analogy with the precession of a gyroscope about a gravitational field. The precessional frequency f is very simply related to the magnitude of the total field H as follows:

$$2\pi f = \gamma H \quad \ldots\ldots (2)$$

The precession of a nucleus induces a cyclically varying voltage in a coil in its vicinity; but under ordinary circumstances, the contributions from the various nuclei in a sample of material cancel to a very high degree of accuracy. In order that an observable signal be induced in a pick-up coil by the precessing nuclei, the vector sum of the individual magnetic moments must give a measurable resultant macroscopic moment with a component perpendicular to the external field to be measured.

In the free precession magnetometer of Packard and Varian, and of Waters and Phillips, there are three separate, discontinuous steps in each measurement of a magnetic field:

(*a*) A sample of material (for example, 300 cm^3 of water) is subjected to a polarizing magnetic field of the order of 400 gauss, whose direction is at an angle θ to a fixed external field $\mathbf{H}$ whose scalar magnitude is to be measured. If the polarizing field $\mathbf{H}_0$ is maintained for an indefinitely long time, the sample acquires an equilibrium value of its nuclear magnetic moment per cm^3 of

$$\mathbf{M}_0 = \chi \mathbf{H}_0 \quad \ldots\ldots (3)$$

where the nuclear paramagnetic susceptibility is given by

$$\chi = \frac{j+1}{3j} \frac{N\mu^2}{kT} \quad \ldots\ldots (4)$$

where j is the angular momentum quantum number, N is the number of nuclei of specified type per cm^3, k is Boltzman's constant, and T is the absolute temperature. Under these circumstances, the ensemble of nuclear moments is in thermodynamic equilibrium with the molecular system in the presence of the applied magnetic field H_0 . The numerical value of χ for the protons in a water sample at room temperature is about 3.2×10^{-10} cgs; and in a 400-gauss field, the ratio of populations of protons in the parallel and antiparallel states is

$$\exp(2\mu H_0/kT) = 1 + (2.8 \times 10^{-7})$$

The temporal approach to thermal equilibrium is according to

$$M = M_0[1 - \exp(-t/T_1)] \quad \ldots\ldots (5)$$

T_1 in equation (5) is called the thermal (or longitudinal) relaxation time, after Bloch [7]. T_1 for protons in a sample of distilled water has been determined by Bloembergen, Purcell, and Pound [12] as 2.3 ± 0.5 seconds, and by Waters and Phillips [10] as about 3.0 seconds. Hence the polarizing magnetic field must be maintained for only about five seconds in order to produce substantially full saturation.

(*b*) The polarizing field is removed. The necessary rapidity of this process may

be judged by three criteria. First, H_0 must be reduced to a small value in a time much less than T_2' , the effective transverse relaxation time [see paragraph (*c*) immediately below], in order that the sample be left in a polarized state. Second, the polarizing field must be reduced from a value comparable to the fixed field H to a value considerably less than H in a time $\ll(2\pi/\gamma H)$ (that is, in a time $\ll$400 microseconds in the case of the earth's field) in order that $\mathbf{M}_0$ maintain its original orientation with respect to **H**. Third, the polarizing field must be reduced to a suitably small fraction (for example, 10^{-5}) of H before the frequency measuring period begins. In the present application, the second criterion is the most stringent of the three.

(*c*) The pick-up coil, which may conveniently be the same as the polarizing coil, is connected to a narrow band-pass, high-gain amplifier. The macroscopic polarization vector $\mathbf{M}_0$ freely precesses about the field **H**, maintaining the established angle θ. The voltage induced in the pick-up coil is the following function of time, t.

$$V = C\chi H_0 \gamma H \sin^2\theta e^{-t/T_2'} \sin(\gamma H t) \quad (6)$$

The induced signal is a damped sinusoid of cyclic frequency $f = \gamma H/2\pi$, of damping constant $1/T_2'$, and of amplitude proportional to $\sin^2\theta$ and to the other factors as given, C being a constant of the specific apparatus.

In a typical case, the initial amplitude is of the order of one microvolt.

The effective transverse relaxation time T_2' is never greater than T_1 . In a sample of distilled water, T_2' is very nearly equal to T_1 . In other substances, it may be much less than T_1 . In practice, T_2' is, of course, reduced by inhomogeneities in H which are of sufficient magnitude to cause significant phase incoherence among different parts of the polarized sample and by absorption of energy by the pick-up circuit [13].

Water† is a suitable substance for weak field magnetometry, since it has a convenient proton relaxation time and since the gyromagnetic ratio of protons in water has been determined with high precision [14]. The apparent value of γ_p in a sample of pure water (uncorrected for the diamagnetic effect in the water molecule) is $(2.67523 \pm 0.00006) \times 10^4$ sec^{-1} gauss^{-1}. Hence, by equation (2), the precessional frequency f in cycles/sec is given in terms of the field H in gauss by

$$f = 4257.8\, H \quad (7)$$

with an absolute accuracy of one part in 45,000.

The special virtue of the proton precession magnetometer may be read from equation (6), namely, the *frequency* of the induced signal depends only upon the scalar magnitude of **H** and the gyromagnetic ratio γ; it is independent of all other parameters of the situation, including specifically the angle θ between the polarizing field $\mathbf{H}_0$ and the field **H** which is to be measured. Only the *amplitude* of the induced signal is dependent on θ, being a maximum when $\theta = 90°$.

†Various hydrogen-rich oils can be used if the equipment must operate below the freezing temperature of water; see reference [12].

III—The Practical Magnetometer

1. *General description*

The present balloon-borne magnetometer was arranged to give one measurement of the magnetic field per minute. The same coil was used to establish the polarizing magnetic field and to pick up the induced precession signal. The coil consisted of approximately 500 turns of No. 16 magnet wire; over-all length of the coil was 6 cm; inside diameter, 6.7 cm; outside diameter, 10 cm. The wire was wound on a Lucite bottle, containing about 300 cm^3 of distilled and electrolytically purified water. A Brailsford sequence timer was used to operate a DPDT relay, connecting the coil to a battery power-supply for about five seconds of each minute. This allowed the protons in the water sample to reach an equilibrium distribution in the polarizing field of some 400 gauss. At the end of the polarizing period, the relay connected the coil to the amplifying circuit. The coil then became part of the primary circuit of a tuned transformer—tuned and coupled to obtain a pass-band adequate to accommodate the range of precession frequencies expected. The secondary of this transformer was connected to the grid of the first stage of a vacuum-tube amplifier. The third stage of the four-stage amplifier provided additional tuning through the use of selective negative feedback. The amplifier output was used to modulate a small FM radio transmitter. The coil and sample were suspended below the amplifier and power supply on the balloon load-line with the axis of the coil horizontal. Since the dip angle is approximately 70° at this location, the angle between the coil axis and the magnetic field was at least as great as 70° during the flight.

The total weight of all flight apparatus, including batteries for eight hours of operation, was 22 pounds.* A block diagram of the complete system is given in Figure 1.

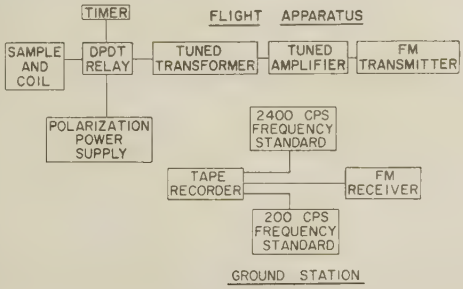

Fig. 1—Block diagram of apparatus

At the ground station, a Clarke Instrument Company telemetering receiver was used to receive the radio signal from the balloon-borne apparatus. The precessional signal, which lies in a very convenient audio-frequency range, was beat

*It is expected that the weight of a rocket magnetometer which will provide one measurement per second with a precision of 10 gammas will be about eight pounds.

with a 2400 cycles/sec precision-frequency sine wave‡ and recorded on magnetic tape. Sharp voltage spikes of 1/200-sec spacing were derived from another precision time standard,‡ were mixed with the two other signals, and were recorded simultaneously on the magnetic tape.

After the flight, the tape signal was displayed on a cathode-ray oscilloscope and photographed for visual reading. A typical portion of such a record is shown in Figure 2. The purpose of the 2400-cycles/sec beating signal is simply to reduce

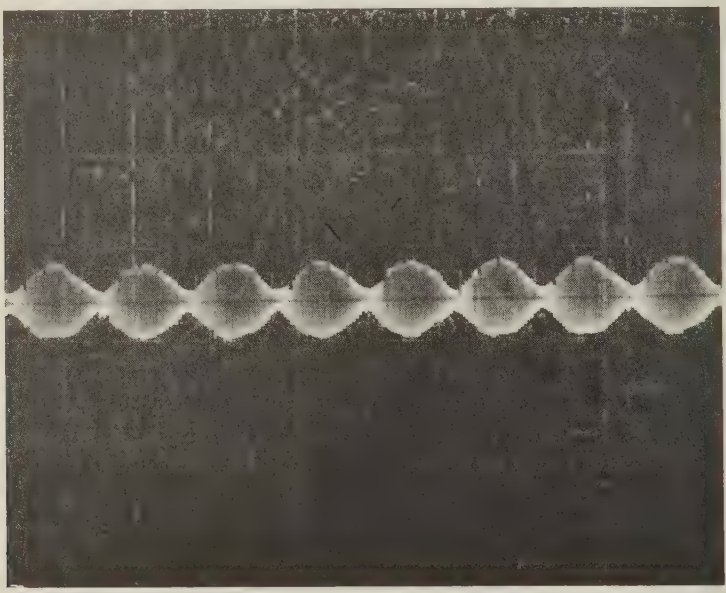

FIG. 2—Photograph of signal as displayed on oscilloscope

the amount of film that is required for accurate reading of the precessional frequency [10].

2. *Accuracy*

The two standard frequencies were checked against WWV to one part in 200,000. The number of beats within an accurately measured time interval of about two seconds length was readily measured with an uncertainty of ± 0.1. The uncertainty of frequency measurement was thus ± 0.05 cycle/sec, a value comparable to the fundamental indeterminancy of the frequency of a portion of a sine wave of this duration. Combining this uncertainty with that of the latest determination of the gyromagnetic ratio of the proton, the probable error of the absolute measurement of the earth's magnetic field was ± 2 gammas for each measurement.

This estimate applies to a fixed magnetometer. If the pick-up coil is rotating at a uniform angular rate $\pm\dot{\varphi}$ about an axis perpendicular to the coil axis, then the apparent precessional frequency differs from its true value by $\pm\dot{\varphi}/2\pi$ and the

‡American Time Products, Inc.

magnetic field which is calculated without knowledge of the rotation is in error by an amount $\pm 3.7\ \dot{\varphi}$ gammas, where $\dot{\varphi}$ is measured in radians/sec. In the presently reported balloon flight, the angular rotation of the coil was not measured; but it is believed quite unlikely that an angular rate as large as one radian/sec occurred after the initial launching transients. In the rocket application, the sense and rate of rotation will be measured by auxiliary means and appropriate corrections will be made.

Table 1 gives a set of ground measurements made in the early morning of

TABLE 1—*Ground measurements at Iowa City, March 13, 1956*
(measurement period one second)

Time	Beat frequency*	*H*
CST	*cycles/sec*	*gammas*
1:15 A.M.	82.3 ± 0.1	58301 ± 3
1:16 A.M.	82.1 ± 0.1	58296 ± 3
1:17 A.M.	82.2 ± 0.1	58299 ± 3
1:18 A.M.	82.1 ± 0.1	58296 ± 3
1:19 A.M.	82.4 ± 0.1	58303 ± 3
1:20 A.M.	82.4 ± 0.1	58303 ± 3
1:21 A.M.	82.2 ± 0.1	58299 ± 3

*Add 2400.02 cycles/sec to the beat frequency to obtain the proton precessional frequency.

March 13, 1956, with the magnetometer on the lawn west of the Physics Building in Iowa City.

3. *Coupling transformer and amplifier*

The principal technical difficulty in construction of a practical magnetometer was in providing adequate shielding and in noise-free amplification of the small signal which was originally obtained from the low-impedance pick-up coil. Therefore, it seems worth while to give a brief description of several details.

The entire flight apparatus was battery operated, of course, and only internally-generated spurious signals were of concern. Local magnetic fields were minimized by avoiding ferromagnetic material and by using twisted or coaxial conductors for current-carrying leads.

It was of greater difficulty to avoid 60 cycles/sec pick-up and other laboratory signals during development of the apparatus and during pre-flight tests. The magnetometer was usually placed several feet above the ground, at about 50 yards from the laboratory building, during developmental tests. The coil itself was enclosed in an electrostatic shield. The signal was fed by coaxial cable to the shielded transformer-amplifier box. Initial impedance transformation and amplification of the signal were accomplished by a specially-constructed, tuned transformer of a design suggested by Packard [15].

A schematic of the transformer and associated circuits is presented in Figure 3. The secondary of this transformer was a 120-mh coil, wound on a small toroidal

permalloy dust core (obtained from Lenkurt Electrical Company). The primary circuit consisted of a few turns of wire wound over the secondary, the inductance and resistance of the receiving coil, and a tuning condenser. Electrostatic shielding between the primary and secondary of the transformer was provided by winding the primary inside a short length of 1/4 inch copper tube. This tube was split

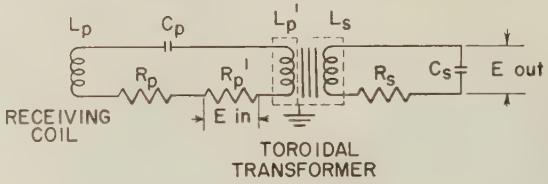

FIG. 3—Schematic of pick-up coil and transformer circuit

longitudinally, then bent around the toroid parallel to the secondary windings. The primary, including the receiving coil, was tuned for series resonance at the center of the expected range of precession frequencies. A testing signal (labeled "*E*-in" in Fig. 3) could be applied to a one-ohm resistor which was placed in the circuit for this purpose. The secondary was tuned for series resonance at the same frequency. The coupling between the primary and secondary was then varied by changing the number of primary turns on the toroid. The coupling was adjusted until the system was slightly over-coupled, giving a nearly flat pass-band approximately 100 cycles/sec wide, centered at the series resonant frequency. Additional shielding was provided by placing the transformer and the tuning condensers inside a copper can. This can and the DPDT relay were mounted in an aluminum utility-box.

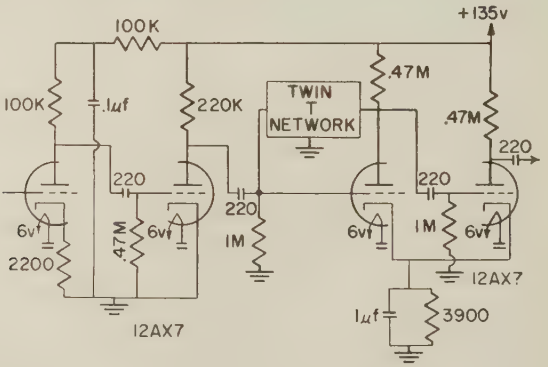

FIG. 4—Tuned amplifier

The tuned secondary of the transformer acted as the grid impedance for the first stage of the vacuum-tube amplifier (Fig. 4). The first two stages and the last stage of the amplifier were ordinary RC coupled stages; the third stage was connected to give negative feedback through a twin T network [16]. This network was designed to reject frequencies near the precession frequency; thus only frequen-

cies outside the desired pass-band were fed back to the third tube. Since the feedback was negative, these frequencies were rejected by the third stage.

The output from the amplifier frequency-modulated a simple one-tube radio transmitter, which radiated about 0.2 watt at 91 Mc/sec (Fig. 5).

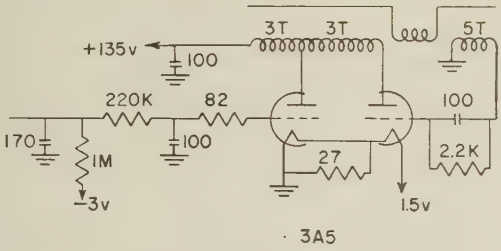

FIG. 5—FM radio transmitter (after Winckler)

Under favorable circumstances, the precession signal was adequately above the noise level for several seconds. The measurement period was usually of two seconds duration.

IV—Balloon Flight of Magnetometer

The magnetometer as described above was thermally insulated with rock wool, and was flown as a "hitch-hike" load on a large Skyhook balloon which was carrying several large pieces of cosmic-ray equipment. The balloon operation was conducted by Winzen Research, Inc., under contract with the Office of Naval Research. The launching occurred at the Iowa City Municipal Airport at 0745 CST on March 13, 1956. Satisfactory magnetic field measurements were obtained at the rate of one per minute until 1020 CST. During this period, the balloon encountered high velocity winds and was carried rapidly eastward as its altitude increased. The RF signal strength dropped as the distance between the balloon and ground station increased, and when the balloon was at a distance of approximately 200 miles the signal-to-noise ratio became so low that the signal was no longer workable. The altitude at this time was 100,000 feet.

The pressure-altitude *vs* time data were continuously telemetered and recorded by the Winzen Research party. The balloon was optically tracked by a theodolite from 0828 to 0927 CST by R. M. Missert and W. R. Webber of this laboratory. In addition, the balloon was followed by an aircraft observer, who plotted its track over the ground. The instantaneous altitude was measured to an accuracy corresponding to about ± 2 millibars and the position over the ground to an average accuracy of ± 3 miles, being more accurate in the early part of flight and less accurate during the latter part.

The trace of the balloon over the ground (vertical projection on the surface) is shown in Figure 6.

V—Flight Results and Ground Survey

The measured total magnetic field intensities are represented as a function of time in flight by the solid curve in Figure 7. The curve is comprised of 137 indi-

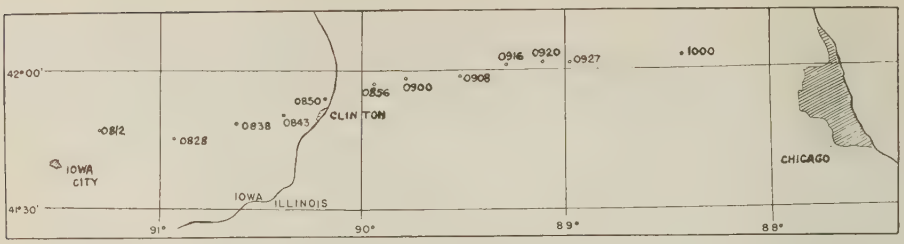

FIG. 6—Projection of balloon position on the ground

vidual measurements, each to an accuracy of ±3 gammas. The altitude is indicated by the auxiliary scale of abscissa [17].

It is seen that the total magnetic field intensity does not decrease monotonically with increasing altitude, as might be expected naively. In order to better understand the balloon-flight results, a sparse ground survey was made at 24 stations along the balloon trace between Iowa City and Chicago on April 14 and 15, 1956. A similar proton precession magnetometer was used for this survey. The stations were located as remotely as reasonably possible from obvious man-made magnetic disturbances and from obvious geological discontinuities. The set-up and measurements at each station required only about 10 minutes. A far more extensive survey

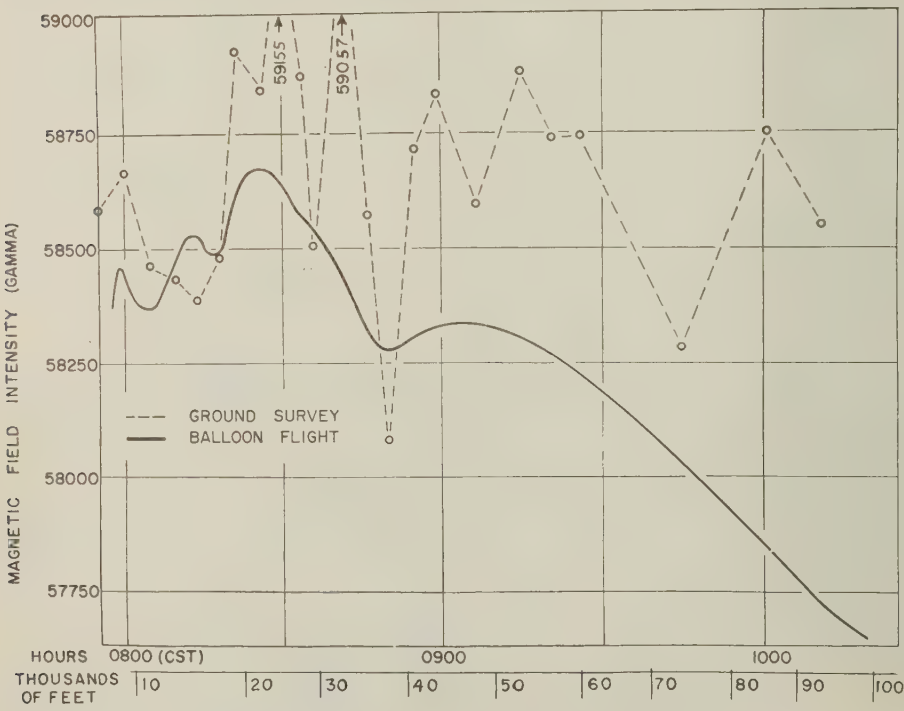

FIG. 7—Magnetic field intensity as a function of time and of altitude

would be necessary, of course, to provide an adequate basis for interpretation of the high altitude data. The ground survey measurements are plotted in Figure 7 so as to correspond to the high altitude measures and are connected by straight, dotted lines, though it is not implied that these dotted lines represent the true magnetic profile.

Nonetheless, it is seen that the ground survey data do supply a partial understanding of the major anomalies of the flight results. Of some interest is the great dip in the field intensity at the "0850" point, which was taken near the Mississippi River. A corresponding dip in the flight curve is clearly evident.

There was a steady decrease of the field intensity during the flight period 0920 to 1020; this decrease, as well as the absolute values, agree with altitude-extrapolated values from the smoothed data of current magnetic charts of the U. S. Coast and Geodetic Survey to within the significance of the latter.

In Figure 8 are plotted the differences between flight intensities and corresponding ground intensities as a function of balloon altitude. The straight, solid line represents an inverse-cube law decrease.

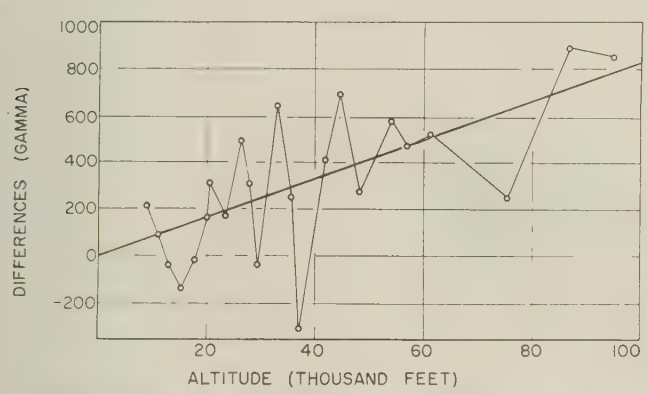

FIG. 8—Differences between flight and ground survey intensities as a function of altitude

VI—Conclusions and Comments

A proton precession magnetometer of very simple and inexpensive nature has been shown to be a splendid instrument for the conduct of high-altitude total magnetic field measurements (as well as for ground measurements). The absolute accuracy is ± 2 gammas for a measurement period of two seconds. Constructional details have been given. The operation of the instrument has been demonstrated in a balloon flight to 100,000 feet altitude and to a range from the ground station of over 200 miles. The data from this flight may be of some independent scientific interest.

Based on the foregoing experience, a prototype magnetometer which can be carried to 150 km altitude by a small rocket has now been constructed. It is expected that the total field intensity can be measured at one-second intervals with an accuracy of about ± 10 gammas. An hydrogeneous liquid having a T_1 of about

0.5 second will be used, in order that frequent measurements (approximately one measurement per kilometer of altitude) can be made. It is planned to make an extensive survey of electrical currents in the ionosphere during the International Geophysical Year. We are indebted to the National Science Foundation for a recent grant for this purpose.

References

[1] E. H. Vestine, I. Lange, L. Laporte, and W. E. Scott, The geomagnetic field, its description and analysis, Washington, D.C., Carnegie Inst. Pub. No. 580 (1947); p. 363.

[2] J. A. Van Allen, Brief notes on meeting to discuss high altitude measurements of earth's magnetic field, APL/JHU/TG-37 (Oct. 8, 1947).

[3] E. H. Vestine, The rocket technique applied to exploration of the geomagnetic field to great heights within the atmosphere, APL/JHU/CM-480 (June 16, 1948).

[4] E. Maple, W. A. Bowen, Jr., and S. F. Singer, J. Geophys. Res., **55**, 115 (1950).

[5] S. F. Singer, E. Maple, and W. A. Bowen, Jr., J. Geophys. Res., **56**, 265 (1951).

[6] S. Chapman, in "Rocket exploration of the upper atmosphere," edited by R. L. F. Boyd and M. J. Seaton, Pergamon Press, Ltd., London (1954); pp. 292-305.

[7] F. Bloch, W. W. Hansen, and M. Packard, Phys. Rev., **69**, 127 (1946); F. Bloch, Phys. Rev., **70**, 460 (1946); F. Bloch, W. W. Hansen, and M. Packard, Phys. Rev., **70**, 474 (1946).

[8] E. M. Purcell, H. C. Torrey, and R. V. Pound, Phys. Rev., **69**, 37 (1946).

[9] M. Packard and R. Varian, Bull. Amer. Phys. Soc., 28, No. 7 (Dec. 28, 1953); and Phys. Rev., **93**, 941 (1954).

[10] See also G. S. Waters, Nature, **176**, 691 (1955), and G. S. Waters and G. Phillips, Geophysical Prospecting IV, 1-9 (1956), for a more detailed description of a practical magnetometer which was developed independently, using the same principle.

[11] J. A. Van Allen, Upper Atmosphere Rocket Research Panel, Panel Report No. 37 (Feb. 4, 1954).

[12] N. Bloembergen, E. M. Purcell, and R. V. Pound, Phys. Rev., **73**, 679 (1948).

[13] N. Bloembergen and R. V. Pound, Phys. Rev., **95**, 8 (1954).

[14] H. A. Thomas, R. L. Driscoll, and J. A. Hipple, Phys. Rev., **78**, 787 (1950).

[15] Dr. M. Packard, private communication to J. A. Van Allen.

[16] G. E. Valley and H. Wallman, Vacuum tube amplifiers, McGraw-Hill Book Co., Inc., New York (1948); p. 384.

[17] Detailed tabular data are contained in the M.S. thesis of Laurence J. Cahill, Jr., on file in the State University of Iowa Library and in SUI-56-9, a research report of the Department of Physics of the State University of Iowa (June 1956), which is available on request.

GEOMAGNETIC AND SOLAR DATA

INTERNATIONAL DATA ON MAGNETIC DISTURBANCES, FIRST QUARTER, 1956

This report continues the series which has appeared regularly in this JOURNAL since Vol. 54, No. 3, 295 (1949). Please refer to that first report for an explanation of the data given, and to Vol. 59, No. 3, 423 (1954) for the definition of *Ap*.

Preliminary Report on Sudden Commencements

S.c.'s given by five or more stations are in italics. Times given are mean values, with special weight on data from quick-run records.

Sudden commencements followed by a magnetic storm or a period of storminess (s.s.c.)

1956 January 10d 04h 39m: Me Ag.—*17d 23h 43*: seventeen.—*21d 16h 44*: thirty-four.—*27d 09h 00*: twenty-seven.

1956 February *11d 00h 53m*: eight.—*19d 02h 21*: thirty-nine.—21d 00h 15: Fu Va (s.i.?).—*21d 20h 02:* thirty-five.—*22d 00h 15*: twenty-nine (s.i.?).—*25d 03h 07:* forty-two.

1956 March *02d 23h 42m:* twenty-eight.—*03d 06h 50:* eight.—14d 08h 08: Me Ag (p.s.c.?).—*20d 11h 46:* twelve.—*21d 16h 15:* seventeen (s.i.?).

Sudden commencements of polar or pulsational disturbances (p.s.c.)

1956 January Old 15h 34m: Ci SM Ka.—02d 16h 21: Ci Qu.—02d 22h 41: Cm IK Ta.—03d 21h 15: IK Eb.—03d 21h 58: Ci SM.—*04d 18h 48:* eight.—*04d 19h 06:* seven.— *05d 18h 20:* five.— 05d 18h 32: Tr Cm SM.—06d 00h 49: Ci SM MB.—06d 09h 02: Ta MB.—06d 16h 09: Tr Do El.—06d 20h 01: Wn Fu.—*07d 16h 01:* six.—07d 16h 20: Cm Gi Ta El.—07d 20h 54: Do Fu.—08d 09h 12: Me Am.—11d 18h 07: Fu Tl SF.—*11d 18h 23:* five.— 12d 19h 24: Fu Ci Tl SF.—*12d 19h 37:* nine.—*16d 00h 45:* ten.—*16d 02h 18:* eight.— *16d 19h 16:* six.— 18d 00h 07: IK Eb.—19d 19h 22: Cm Gi.—*21d 00h 10:* eleven.—*23d 21h 59:* ten.— 24d 04h 50: Cm Gi.—24d 18h 42: Gi Ta.—*24d 19h 31:* five.—24d 23h 15: Ta MB.— 25d 01h 56: Cm Gi Ta MB.—25d 18h 27: So Qu.—25d 18h 49: Tr Wn.—26d 22h 37: So Cm Fu.—26d 23h 09: Fu IK Tl Gi.—26d 23h 30: Fu Eb Gi.—28d 14h 54: So Fu Gi.—28d 19h 33: Tr Cm Gi.—29d 23h 32: Do IK MB.—*30d 17h 10:* ten.— 30d 21h 30: Cm Ta.

1956 February Old 19h 14m: Tr Fu Qu.—*02d 17h 26:* six.—*03d 18h 51:* ten.— *03d 22h 28:* twelve.—04d 21h 15: Ta MB.—05d 18h 39: Do Fu.—05d 19h 39: Fu Qu.—05d 20h 08: SF MB.—*05d 20h 19:* five.—*09d 00h 11:* nine.—10d 01h 45: CF IK.—11d 00h 20: Fu IK.—*11d 01h 46:* ten.—13d 00h 14: So Fu MB Bi.— 15d 20h 52: Fu Bi.—15d 21h 02: IK Gi.—15d 22h 51: IK Eb Tl Bi.—15d 23h 58: Ma IK Gi.—16d 02h 02: Fu Bi.—*16d 03h 15:* seven.—20d 13h 20: Ka Ap Am.—24d 11h 15: Ap Am.—*24d 21h 01:* seven.—*28d 02h 35:* five.—28d 18h 37: Ta Bi El.—29d 00h 00: Ta MB El Hr.—*29d 22h 43:* five.

TABLE 1—*Geomagnetic planetary three-hour-range indices Kp, preliminary magnetic character-figures C, average amplitudes Ap (unit 2γ), and final selected days, January to March, 1956*

January 1956

E	1	2	3	4	5	6	7	8	Sum
1	4 −	3 −	2 −	3o	2 +	4 +	4o	5 −	26 +
2	3 +	3 +	2o	2o	2 +	3 +	4 −	4 −	24 −
3	3o	3 +	3 −	3 +	2 −	3 −	2 +	4 −	23 −
4	3 −	3 +	3 −	2 +	2 +	2 +	5o	4 −	24 +
5	3 +	3 +	3 −	2o	2o	2o	4 −	2 −	21 −
6	4o	1 +	1 +	2o	4o	4o	3 +	3 −	23 −
7	1 +	1 +	0o	2 −	2 +	4o	3 −	3o	16 +
8	2 +	1 +	1o	2o	1o	1o	2o	1 −	11 +
9	2 +	4 −	2o	4 −	4 −	3 +	2o	2 −	22 +
10	0o	3 +	4 −	4 −	4 −	5 +	5 −	4o	28 +
11	6o	4 +	5 −	6o	4o	3 +	5 +	2o	36 −
12	1o	2 +	2 +	4 −	3 −	4 −	6 −	4 −	25o
13	4o	3o	2o	1 −	2o	1o	1 +	0 +	14 +
14	2 −	3 −	2o	4 −	2o	2o	2 −	2 −	17 +
15	0o	0 +	1o	2 −	2 −	1o	0 +	1 +	7 +
16	3o	1 +	1 +	2o	2 −	1 −	2 −	1o	13 −
17	1 −	2 −	2o	2 −	2 +	1 −	1 +	3o	13 +
18	5o	5 +	4 +	4o	4o	4o	5 −	6 −	37o
19	6 −	4o	4 +	4 −	5o	4 −	4 −	3 −	33 −
20	2o	2 −	2o	2 −	1o	1 −	1 −	1o	11 −
21	2o	0o	0o	1 −	1 −	3 +	3 −	4 +	14 −
22	6 −	6 −	4 +	4 −	2 −	1o	4o	1 +	27 +
23	1o	3 −	3 −	1 +	2o	3o	4o	5o	22 −
24	3o	5o	4 −	5 −	5 −	4o	6 −	5o	36 −
25	6 −	4 −	4 −	2 −	2 −	1o	3 −	2 −	22 −
26	0o	1 −	1o	1 −	1 −	1 −	1 −	1 +	6 −
27	2 −	1 +	2 +	4o	4 +	5 −	6o	3 +	28 −
28	5o	6 +	5 −	4o	4 −	3 +	4o	3 +	34 +
29	3 −	3 −	3 −	3o	4 +	4 −	4 −	2 +	25o
30	4 −	3 +	2 +	2o	3 −	4o	2 +	4 −	24o
31	3o	3 +	3 −	4 −	3 +	3 +	3 −	4 −	26 −

February 1956

1	2	3	4	5	6	7	8	Sum
4 −	3 +	4 −	2o	3 −	2 +	3 +	3 +	24 +
3 +	3o	4 −	3 +	2 +	4 −	4 −	3 +	26 +
3o	4 −	2 +	2 +	2o	2 −	3o	4o	22o
2 +	3o	2 +	2 +	3 −	1 +	3 −	2 +	19o
1o	1 +	1o	1 +	2 −	1 +	3 −	2 +	13 −
4 −	1 +	1 +	3 −	2 −	2 −	1o	0 +	14 −
1o	2 −	1o	1 −	1 −	0o	0 +	2o	7 +
1 +	0o	0 +	1o	1o	0 +	0 +	0 +	5 −
2 −	1 −	0 +	1o	0 +	0o	0 +	0 +	5 −
0o	1o	10	1 +	1 −	1 −	1 +	1 +	7 +
4o	3o	2 −	2o	3 +	3 −	5 −	5 −	26o
5o	5 −	5 +	5 −	3o	2o	2o	3o	30 −
2o	2 −	3 +	3 +	3 −	2 −	1 +	2 −	18 −
1o	2 −	1 +	2 −	1 −	1o	0o	0 +	8 −
0 +	0o	2 −	2o	1o	1 −	2 −	2 +	10 −
2 +	4 +	3o	3 −	3 +	4 −	3 −	2 +	24 +
2o	2o	2 +	2 +	1 −	2 −	1 −	0o	12 −
0o	2o	1 +	2 +	1 −	1 +	1 +	0 +	9 +
4 +	2 +	3o	4 +	4 −	2 +	2 +	2 +	25 −
1 −	1 −	1o	1o	3 +	2o	1 −	1 +	11 −
1 −	1 +	1o	1 +	2o	2o	3 +	2 −	13 +
4o	4o	3o	4 +	3 +	3o	1 +	1o	24o
1 +	0 +	1o	2 −	2o	3 +	2o	1o	13 −
1o	1 −	1 −	3 −	2 +	2 +	1 +	2 +	13 +
1 −	6o	8 +	7 +	7 −	7 −	7 −	3 +	46 −
3 +	2 +	3o	5 −	4o	1o	3 +	3 −	24 +
4o	3 +	4o	2 −	1 +	2 −	5o	4o	25o
5 −	5 +	2 +	3o	2o	3o	4o	4o	28 +
5 +	5o	5o	4 +	4o	5o	4o	5 −	37 +

March 1956

E	1	2	3	4	5	6	7	8	Sum
1	3 −	3 +	4o	4o	3 −	2 −	4 −	4 +	26 +
2	3 +	5o	5 −	4 +	3 +	3 +	3 +	3o	30 +
3	5 −	6 −	6 +	7 +	6 +	6o	7 +	7o	51 −
4	5 +	4 +	4 +	3 +	4o	3o	2 −	1 +	27 +
5	2 −	2 +	3 −	1o	2 −	3 −	3 −	2 −	16 +
6	3 −	3o	3 −	2 −	4 −	2o	4 −	2 −	21o
7	0o	0o	0 +	2 +	1 +	1o	1 −	1 −	6 +
8	1 −	1o	1 −	1 −	0 +	0 +	0o	0o	4 −
9	0o	0o	0 +	0 +	0 +	0 +	0o	1 +	3 −
10	2 −	3o	3 −	3 −	1 +	1 +	4o	6o	23 −
11	6o	4 −	4 +	3 −	2o	2o	2o	4o	27 −
12	3 −	1 +	2o	2o	2 +	2 +	2 +	2o	17o
13	2 +	3 +	3o	2o	2 −	2 −	1o	3o	18o
14	3 −	2 +	3 −	4o	4 −	3 +	1 +	2 +	22 +
15	3o	2o	2 +	2 +	2 −	2 +	2 −	1 −	16o
16	1o	0 +	2o	2o	1 +	1o	1o	3 −	11 +
17	1 −	1o	1o	1o	1 −	0 +	0 +	1 +	6 +
18	0 +	0 +	2 −	2 −	2o	2 +	1 −	2 −	11 −
19	3o	3 −	2 −	2 −	2o	2o	2 +	4o	19 +
20	4o	3o	1 −	1 +	2o	2o	2o	3o	18o
21	4 +	3 +	5 +	4 +	3 +	5 −	5o	6 −	36o
22	7o	6 +	5o	4 −	4o	4 +	4 +	6 +	41o
23	6 +	6o	5o	2o	2 −	1 +	1o	0 +	24 −
24	2o	2o	3o	4 +	4o	6o	4o	4 +	30 −
25	5 −	3 +	3 −	3 +	2o	3 −	4 −	5 −	27o
26	3o	3 −	3o	4o	4 +	3o	3o	4o	27o
27	3o	3 −	1 +	2o	2o	3 +	3 −	3 +	20 +
28	5 −	4 +	2 +	3 −	3 +	3 +	5 −	5o	30 +
29	6 +	5 −	5o	4o	3 −	4o	4o	4 +	35o
30	1 −	3 +	3 −	1 +	2o	2 +	3 +	4 +	20o
31	5 −	4o	3o	2 +	3 +	2 +	2 +	2 −	24 −

Preliminary *C*, 1956			Average amplitude *Ap*		
Jan.	Feb.	Mar.	Jan.	Feb.	Mar.
1.1	0.8	1.2	20	16	20
0.9	0.9	1.1	15	18	26
0.8	0.8	1.9	14	14	102
1.2	0.6	1.2	17	10	24
0.9	0.4	0.6	12	6	8
1.0	0.4	0.8	16	8	13
1.0	0.2	0.1	10	4	3
0.2	0.0	0.1	5	3	2
0.9	0.0	0.0	14	3	2
1.4	0.2	1.2	26	4	20
1.6	1.2	1.3	42	20	24
1.4	1.4	0.6	21	28	8
0.6	0.4	0.7	9	10	10
0.7	0.0	0.8	9	4	14
0.0	0.3	0.4	4	5	8
0.2	1.0	0.3	6	16	6
0.3	0.2	0.0	7	6	3
1.7	0.0	0.3	40	4	5
1.3	1.1	0.9	32	17	11
0.1	0.4	0.7	5	6	11
0.8	0.4	1.5	9	7	39
1.4	1.1	1.8	29	18	60
1.2	0.5	1.3	16	7	31
1.5	0.5	1.2	38	7	28
0.9	2.0	1.1	18	103	21
0.0	1.2	1.2	3	18	20
1.6	1.1	0.8	27	20	12
1.6	1.1	1.2	37	24	27
1.0	1.5	1.5	17	41	38
1.0		0.9	16		13
0.9		0.9	17		16

TABLE 1—(Concluded)—*Final magnetically selected days, January to March, 1956*

Month	Five quiet days	Ten quiet days	Five disturbed days
1956			
January	8 15 16 20 26	7 8 13 14 15 16 17 20 21 26	11 18 19 24 28
February	7 8 9 10 14	5 7 8 9 10 14 15 17 18 20	11 12 25 28 29
March	7 8 9 17 18	5 7 8 9 12 13 15 16 17 18	3 21 22 24 29

1956 March *01d 20h 37m:* seven.—*06d 19h 14:* five.—07d 17h 13: Cm Qu.—*10d 22h 17:* eight.—10d 22h 43: SM Hr.—10d 23h 10: Tr Ta.—11d 01h 25: Gi Ta Hr.—*11d 22h 18:* twenty.—*13d 22h 45:* twenty.—14d 09h 20: SM Am.—14d 12h 32: Ka Wa To.—17d 22h 57: Tr So IK.—*19d 21h 07:* six.—23d 00h 13: Bi Hr.—24d 10h 19: SM Ap To Am.—24d 15h 11: Tr Gi Qu Bi.—24d 20h 30: Tr Gi.—24d 23h 58: Ci SF Ta MB.—*25d 17h 53:* twelve.—*25d 22h 03:* twelve.—*26d 20h 46:* five.—27d 01h 46: CF MB.—*28d 02h 10:* fifteen.—28d 17h 11: Ka Qu Wa.—28d 20h 26: Gi Ta.—*29d 00h 57:* eight.—29d 17h 51: Cm Gi Ta.—30d 20h 50: Gi Ta Bi.—*31d 00h 35:* nine.—31d 11h 44: Ap Am.

Sudden impulses found in the magnetograms (s.i.)

1956 January 05d 00h 34m: Tn El.—05d 07h 32: Wn Ci.—05d 16h 23: Ta MB.—06d 11h 44: MB Tn.—09d 13h 25: Le Qu Ta.—*09d 16h 23:* six (p.s.c.?).—10d 15h 24: Wn Wi Gi Ta.—11d 00h 45: Ta MB Bi El.—11d 08d 52: Ta Bi.—11d 09h 44: Wn Ta.—11d 10h 20: Wn Ta MB.—13d 12h 20: Tr MB Hr.—*14d 09h 22:* nine.—18d 05h 45: Ta Bi.—18d 08h 45: Ta El (p.s.c.?).—18d 11h 34: Ta MB El Hr.—18d 11h 43: Bi Tn.—18d 17h 47: MB Bi Tn.—19d 08h 32: Ta MB Tn.—20d 22h 27: Tr So (p.s.c.?).—22d 00h 01: Ta MB.—22d 00h 20: Ta MB Bi Tn.—*22d 19h 40:* sixteen.—27d 09h 35: Ta MB.—*27d 16h 28:* seven.—28d 15h 00: Ta MB.—31d 20h 58: Wn Gi Ta MB.

1956 February 11d 19h 30m: Ta Tn.—11d 21h 03: Ta MB Hr.—11d 22h 25: Ta Tn.—12d 09h 02: Ta Bi (p.s.c.?).—12d 11h 08: Ta Bi (p.s.c.?).—16d 07h 47: Tn Hr.—17d 03h 32: Ta MB (p.s.c.?).—*19d 14h 43:* thirteen.—*22d 11h 07:* eight.—24d 16h 49: IK Gi Bi.—*26d 09h 29:* thirteen.—29d 08h 01: Wn Wi Ab.

1956 March 03d 18h 16m: Wn CF.—*06d 12h 58:* nine.—*10d 10h 58:* twelve (s.s.c.?).—10d 18h 12: MB AM (s.s.c.?).—12d 12h 36: Fu MB Bi.—13d 14h 52: MB Va.—*19d 00h 53:* twenty-five.—21d 21h 37: Tr Gi (p.s.c.?).—22d 00h 28: Gi Ta MB Bi.—*22d 01h 01:* five.—22d 01h 50: Gi MB.—22d 21h 13: Wn Hr (p.s.c.?).

Preliminary Report on Solar-Flare Effects

Effects confirmed by ionospheric or solar observations are in italics.

1956 January 09d 16h 23m-16h 57m: Ch.—11d 08h 52-09h 08: El.—14d 09h 22?-10h 00: Wi Gi Hr.—14d 09h 57?- . . . : Wi.—*15d 12h 34-12h 40:* Wi CF. - *15d 15h 25-* . . . : Hu.—*19d 00h 10-* . . . : Ka.—*19d 03h 30-* . . . : Ka.—21d 16h 43-17h 32: Va.—26d 10h 02-10h 20: Bi.—28d 15h 03-15h 18: SJ. 31d 09h 28-09h 42: IK Bi.—31d 12h 19- . . . : IK.

1956 February *04d 09h 28m-09h 40m:* CF.—04d 12h 45-12h 50: SM.—05d 15h 20- . . . : Hu.—07d 20h 35- . . . : Hu.—*10d 20h 48-* . . . : Hu.—*10d 21h*

12- . . . : Hu Am.—*13d 14h 41-15h 07:* Es Eb Hu Va Hr.—*14d 05h 39-06h 44:* Ka Al Hr.—*17d 04h 47-05h 15:* Ka.—17d 17h 25- . . . : Hu.—*18d 15h 42-* . . . : Hu.—*19d 14h 42-15h 00:* Le Es CF Eb Ch Hu.—19d 15h 06 -. . . : Ch.—19d 18h 03- . . . : Hu.—20d 09h 30- . . . : Es.—*20d 18h 24-* . . . : Hu.—21d 20h 01-20h 27: Si Va.—22d 00h 15-00h 41: Si.—*23d 03h 34-04h 42:* Ka.—23d 16h 48-16h 57: SJ.—24d 16h 39- . . . : Hu.—24d 16h 48-17h 44: Va.—27d 09h 48-09h 55: SM.

1956 March 06d 13h 12m-13h 45m: El.—06d 14h 37- . . . : Hu.—06d 16h 23- . . . : Hu.—*06d 17h 25-* . . . : Hu.—06d 18h 00- . . . : Hu.—*10d 04h 35-05h 55:* Ka.—10d 18h 10- . . . : Hu.—*13d 14h 51-15h 08:* Wi SM Hu Hr.—15d 16h 22-16h 56: CF Eb Ch SJ Hu Va Hr.—*17d 02h 19-02h 30:* Ka.—*17d 03h 11-03h 35:* Ka.—17d 13h 50-14h 02: Le Es Wi CF Eb Hu Hr.—19d 00h 53- . . . : Si.—20d 11h 46- . . . : Gi.—*28d 09h 40-09h 50:* CF.—29d 16h 03- . . . : Hu.—*31d 13h 51-14h 02:* Eb.

Ionospheric or solar disturbances without clear geomagnetic effect

1956 January 14d 19h 25m: Hu.—16d 13h 45: Hu.—16d 16h 46: Hu.—17d 18h 41: Hu.—17d 20h 16: Hu.—18d 17h 58: Hu.—19d 15h 52: Hu.—19d 19h 12: Hu.—19d 21h 27: Hu.—23d 16h 20: Hu.

1956 February: None.

1956 March: None.

Minor disturbances reported by one station only are listed in the De Bilt quarterly circular, but omitted here.

Table 2—*Monthly mean values of Ci, Cp, and Ap*

Index	Jan. 1956	Feb. 1956	Mar. 1956
Mean *Ci*	0.94	0.68	0.89
Mean *Cp*	0.83	0.63	0.82
Mean *Ap*	15	15	20

Committee on Rapid Variations and Earth Currents

A. Romañá, *Chairman*, Observatorio del Ebro, Tortosa, Spain

Committee on Characterization of Magnetic Disturbances

J. Bartels, *Chairman*
University
Göttingen, Germany

J. Veldkamp
Kon. Nederlandsch Meteorologisch Instituut
De Bilt, Holland

PROVISONAL SUNSPOT-NUMBERS FOR APRIL TO JUNE, 1956

(Dependent on observations at Zurich Observatory and its stations at Locarno and Arosa)

Day	April	May	June
1	60	78	98
2	69	93	107
3	66	138	117
4	66	169	106
5	50	158	117
6	45	162	118
7	63	162	111
8	86	186	90
9	103	180	85
10	145	178	89
11	144	175	87
12	160	163	94
13	178	142	98
14	164	133	108
15	150	110	114
16	120	122	132
17	130	132	120
18	140	144	130
19	130	136	171
20	140	127	166
21	140	144	162
22	120	119	150
23	115	82	139
24	96	102	125
25	104	103	106
26	88	120	70
27	94	115	71
28	67	137	122
29	32	136	135
30	70	146	162
31		123	
Means.....	104.5	136.0	116.7
No. days.....	30	31	30

Mean for quarter: 119.3 (91 days)

M. Waldmeier

Swiss Federal Observatory
Zurich, Switzerland

CHELTENHAM THREE-HOUR-RANGE INDICES *K* FOR APRIL TO JUNE, 1956

[$K9 = 500\gamma$; scale-values of variometers in γ/mm: $D = 5.4$; $H = 1.7$; $Z = 4.3$]

Gr. day	April 1956 Values *K*	Sum	May 1956 Values *K*	Sum	June 1956 Values *K*	Sum
1	3440 1102	15	4544 3222	26	4444 2233	26
2	2122 3223	17	1221 1012	10	2332 3332	21
3	3532 3212	21	3312 2133	18	3211 2223	16
4	3434 2231	22	2112 2233	16	2213 2222	16
5	3332 2334	23	3233 2342	22	1232 2332	18
6	2222 4234	21	1333 2223	19	2233 4323	22
7	5233 3232	23	3323 2132	19	2221 2332	17
8	2243 2222	19	1122 2121	12	3334 2334	25
9	1232 3122	16	2211 1111	10	3243 3333	24
10	1234 3413	21	1110 1111	7	3232 2444	24
11	2312 3233	19	2000 0014	7	4454 3333	29
12	3232 3321	19	4544 5455	36	3331 1122	16
13	2222 1112	13	3456 3223	28	4322 3234	23
14	0221 1222	12	3233 3233	22	3333 2344	25
15	2211 0222	12	3454 4443	31	5533 3234	28
16	2321 0233	16	6786 7666	52	2332 3233	21
17	5533 3233	27	6644 4123	30	2211 2234	17
18	2342 1133	19	2333 2223	20	3221 1212	14
19	2342 2122	18	2223 1132	16	2122 2224	17
20	3221 0123	14	2236 5454	31	3212 2133	17
21	3334 4366	32	4532 2232	23	3222 1122	15
22	6775 3334	38	2344 3133	23	3211 2222	15
23	4322 2122	18	3123 3345	24	2212 2246	21
24	2301 1012	10	6655 5567	45	5422 3355	29
25	4103 1223	16	7665 3124	34	6652 3332	30
26	2434 4247	30	4221 0123	15	2243 3334	24
27	9996 5665	55	3122 0223	15	2543 2332	24
28	7632 1356	33	3411 2121	15	2442 2233	22
29	7553 3322	30	2121 2355	21	2355 3343	28
30	5553 4443	33	3332 2323	21	2544 3334	28
			2311 0213	13		

Ralph R. Bodle
Observer-in-Charge

Cheltenham Magnetic Observatory
Cheltenham, Maryland, U.S.A.

PRINCIPAL MAGNETIC STORMS

(Advance knowledge of the character of the records at some observatories as regards disturbances)

Observatory (Observer-in-Charge)	Greenwich date	Storm-time		Sudden commencement				C-figure, degree of activity[4]	Maximal activity on K-scale 0 to 9			Ranges		
		GMT of begin.	GMT of ending[1]	Type[2]	Amplitudes[3]				Gr. day	Gr. 3-hr. period	K-index	D	H	Z
					D	H	Z							
(1)	(2)	(3)	(4)	(5)	(6)	(7)	(8)	(9)	(10)	(11)	(12)	(13)	(14)	(15)
	1956	*h m*	*d h*		′	γ	γ					′	γ	γ
College	Apr. 21	18 00	23 04	.....	.....	.....	.....	ms	22	4	7	365	1710	153
(C. J. Beers)	Apr. 26	21 11	1 19	s.c.*	33	60	−28	s	27	4, 6	8	490	2850	194
	May 11	23 40	13 19	.....	.....	.....	.....	ms	12	5	7	220	1390	76
	May 14	08 00	17 18	.....	.....	.....	.....	s	16	3	8	330	2520	139
									17	3	8			
	May 20	06 39	22 22	s.c.*	3	−39	7	ms	20	4	7	230	1440	76
	May 23	07 00	26 10	.....	.....	.....	.....	s	25	3	8	310	2180	134
	May 31	22 00	2 01	.....	.....	.....	.....	ms	1	3, 4	6	180	1210	100
	June 23	18 05	27 23	.....	.....	.....	.....	ms	24	6	7	420	1720	188
									25	2	7			
Sitka	Apr. 21	08 ..	23 04	.....	.....	.....	.....	s	22	4	9	239	1733	94
(J. L. Bottum)	Apr. 26	21 11	28 13	s.c.*	+27	−11	−32	s	27	2, 4	9	345	2234	115
	Apr. 28	17 27	29 21	s.c.	−3	+21	+6	s	29	1	8	90	791	44
	Apr. 30	01 38	1 15	s.c.*	−7	+159	+25	ms	30	2, 4	7	83	912	56
	May 11	23 42	13 17	s.c.	−2	+17	+5	s	13	4	8	95	1010	64
	May 15	00 ..	17 17	.....	.....	.....	.....	s	16	3, 5	9	320	1559	119
	May 20	06 38	21 09	s.c.*	−7	+63	+15	s	20	4	9	147	1120	62
	May 23	09 ..	26 09	.....	.....	.....	.....	s	25	3	9	305	1748	124
	June 23	18 ..	25 19	.....	.....	.....	.....	s	25	2	9	344	1742	87
Witteveen	Apr. 21	11 00	22 24	s.c.*	−5	+55	0	ms	21	6, 7	6	45	280	18
(D.van Sabben)									22	1, 2, 3	6			
	Apr. 26	21 11	28 08	s.c.*	−6	+141	−5	s	27	1, 2	9	60	805	47
	Apr. 28	17 27	29 17	s.c.	−3	+40	0	ms	28	8	6	40	295	6
									29	1, 2	6			
	Apr. 30	01 38	30 24	s.c.*	−6	+54	−2	ms	30	1, 2	6	25	210	10
	May 11	23 41	13 12	s.c.	−1	+16	0	ms	13	3	6	30	250	9
		23 54		s.c.	−1	+45	0							
	May 15	10 00	17 15	.....	.....	.....	.....	ms	15	6	7	55	450	30
									16	2, 5, 8	7			
	May 20	06 37	21 07	s.c.	+8	−28	+1	m	20	4, 5, 7, 8	5	25	180	6
									21	1	5			
	May 23	11 00	25 15	.....	.....	.....	.....	ms	24	5	7	50	280	18
									25	2	7			
	June 23	18 06	25 19	s.c.	−2	+34	0	ms	24	5, 6	6	35	240	16
									25	1	6			
Cheltenham	Apr. 21	18 ..	22 12	.....	.....	.....	.....	ms	22	2, 3	7	66	289	43
(R. R. Bodle)	Apr. 26	21 12	30 23	s.c.	+1	+131	−3	s	27	1, 2, 3	9	158	949	80
	May 11	23 55	13 15	s.c.	−1	+17	....	ms	13	4	6	36	120	1
	May 16	04 ..	17 15	.....	.....	.....	.....	s	16	3	8	66	480	6
	May 20	06 38	21 06	s.c.*	+5	+36	+2	ms	20	4	6	34	113	1
	May 23	19 ..	25 14	.....	.....	.....	.....	ms	24	8	7	45	395	3
									25	1	7			
	June 23	18 ..	24 06	.....	.....	.....	.....	ms	23	8	6	25	174	1
	June 24	13 ..	25 09	.....	.....	.....	.....	ms	24	8	6	44	190	1
									25	1	6			
	June 29	05 ..	30 16	.....	.....	.....	.....	m	29	3, 4	5	21	83	

[1]Approximate time of ending of storm construed as the time of cessation of reasonably marked disturbance movements in t traces; more specifically, when the *K*-index measure diminished to 2 or less for a reasonable period.

[2]s.c. = sudden commencement; s.c.* = small initial impulse followed by main impulse (the amplitude in this case is that of t *main impulse only*, neglecting the initial brief pulse; . . . = gradual commencement.

[3]Signs of amplitudes of *D* and *Z* taken algebraically; *D* reckoned positive if towards the east and *Z* reckoned positive if ver cally downwards.

[4]Storm described by three degrees of activity: *m* for moderate (when *K*-index as great as 5); *ms* for moderately severe (wh *K* = 6 or 7); *s* for severe (when *K* = 8 or 9).

PRINCIPAL MAGNETIC STORMS—Continued

Observatory (Observer-in-Charge)	Greenwich date	Storm-time GMT of begin.	Storm-time GMT of ending[1]	Sudden commencement Type[2]	Amplitudes[3] D	H	Z	C-figure, degree of activity[4]	Maximal activity on K-scale 0 to 9 Gr. day	Gr. 3-hr. period	K-index	Ranges D	H	Z
(1)	(2)	(3)	(4)	(5)	(6)	(7)	(8)	(9)	(10)	(11)	(12)	(13)	(14)	(15)
	1956	*h m*	*d h*		′	γ	γ					′	γ	γ
Tucson	Apr. 21	08 00	23 13	.....	.....	.....	.....	ms	22	2, 3, 4	6	25	202	97
(R. F. White)	Apr. 26	21 12	28 12	s.c.	−5	66	−3	ms	27	1, 2, 3	7	35	322	103
	Apr. 28	17 27	29 17	.....	.....	.....	.....	ms	28	8	6	26	142	47
									29	1, 2	6			
	Apr. 30	01 38	1 15	s.c.*	−1	30	−4	ms	30	2	6	14	138	45
	May 11	23 42	13 13	s.c.	−1	28	5	m	12	3, 5, 6	5	17	105	42
									13	2, 3, 4	5			
	May 15	04 15	17 15	.....	.....	.....	.....	ms	16	2, 3, 5	6	18	177	90
	May 20	06 36	21 09	s.c.	2	45	4	m	20	4, 7	5	18	109	43
	May 23	09 33	25 13	.....	.....	.....	.....	ms	25	3	7	29	190	76
	June 23	18 07	25 19	.....	.....	.....	.....	ms	25	1	6	23	151	70
San Juan	Apr. 21	11 01	22 12	s.c.	−4	+6	−2	ms	21	7	7	21	230	58
(P. G. Ledig)	Apr. 26	21 11	28 08	s.c.*	+1	+41	−9	ms	26	8	7	17	246	54
									27	1	7			
	Apr. 28	17 26	29 17	s.c.	0	+12	−2	ms	28	8	6	13	102	36
	Apr. 30	01 38	1 07	s.c.	+1	+24	−5	m	30	1, 2, 3	5	12	80	10
	May 11	23 41	13 11	s.c.	0	+8	−2	m	13	4	5	7	68	35
	May 16	04 18	17 12	s.c.	0	+28	−6	ms	16	3, 4	6	17	166	14
	May 20	06 37	21 05	s.c.	−1	+17	−4	m	20	4	5	10	69	19
									21	1	5			
	May 23	19 ..	25 10	.....	.....	.....	.....	ms	23	8	6	13	139	43
									24	1	6			
	June 23	18 06	25 12	s.c.	0	+12	−3	ms	25	1	6	11	105	29
Honolulu	Apr. 21	11 00	23 13	.....	.....	.....	.....	ms	21	7	6	5	230	30
(M. L. Cleven)									22	2	6			
	Apr. 26	21 13	29 18	s.c.	−1	+48	+26	s	27	1	8	9	410	45
	Apr. 30	01 38	1 17	s.c.	0	+15	+11	ms	30	2	6	5	95	40
	May 16	01 00	17 15	.....	.....	.....	.....	ms	16	2	7	8	150	45
	May 23	19 00	25 15	.....	.....	.....	.....	ms	25	3	6	7	220	50
	June	None												
Alibag	Jan. 10	04 00	12 00	.....	.....	.....	.....	ms	11	7	6	6	165	56
(A. S. Chaubal)	Jan. 12	04 10	13 00	.....	.....	.....	.....	m	12	7	5	3	161	30
	Jan. 17	23 00	20 00	.....	.....	.....	.....	m	18	1 to 7	5	5	179	38
									19	5, 7	5			
	Jan. 21	16 43	23 00	s.c.	0	+19	−4	m	22	1	5	6	95	37
	Jan. 27	08 59	29 00	s.c.	0	+26	−5	ms	27	5	6	4	149	44
	Feb. 11	00 56	12 14	s.c.	−1	+17	−8	m	12	4	5	4	156	46
	Feb. 19	02 20	20 00	s.c.	0	+26	−1	m	19	1, 4, 5	5	2	128	23
	Feb. 21	20 02	22 21	s.c.	0	+20	−3	m	22	4, 5	5	2	88	30
		(*Note:* Another sudden impulse on Feb. 22 at $00^h\ 16^m$ (D = 1.′2; H = +36γ, and Z = −12γ)												
	Feb. 25	03 06	25 22	s.c.	−1	+39	−14	s	25	3	8	6	356	49
	Feb. 26	09 28	27 06	s.c.	−1	+30	−12	m	26	4	5	2	57	19
	Feb. 29	08 02	1 00	s.c.	0	+15	−11	m	29	6	5	2	63	42
	Mar. 2	23 42	4 16	s.c.	−1	+13	−10	ms	3	4	7	6	294	65
	Mar. 20	11 45	23 17	s.c.	0	+8	−5	m	21	2, 3	5	7	165	69
									22	7, 8	5			
Instituto	Apr. 21	11 01	22 17	s.c.*	+3	+33	+3	ms	21	5, 7	6	9	504	62
Geofísico de	Apr. 26	21 11	29 06	s.c.*	+1	+103	+17	ms	26	8	7	13	345	45
Huancayo	Apr. 30	01 38	30 21	s.c.	+1	+41	+8	m	30	2, 5	5	6	286	62
(A. A. Giesecke,	May 11	23 54	12 21	s.c.	0	+12	0	ms	12	6	6	5	188	21
Jr.)	May 16	04 18	17 04	s.c.	0	+41	+13	ms	16	5, 6	7	14	265	43
	May 23	22 00	25 11	.....	.....	.....	.....	ms	24	6	6	11	250	54
	June 23	18 07	27 07	s.c.	0	+38	−5	ms	24	6	6	5	284	35
Cassouras	Jan. 27	08 59	28 09	s.c.	0	28	+8	m	27	6	5	17	258	51
Celio I.	Feb. 25	03 07	25 22	s.c.	+3	52	+14	ms	25	4	6	19	248	96
(Cama)	Mar. 2	23 41	4 07	s.c.	+1	24	+6	ms	3	4	6	13	175	59
	Mar. 21	16 15	23 08	s.c.*	+2	21	+6	m	22	1	5	12	193	39

PRINCIPAL MAGNETIC STORMS—Continued

Observatory (Observer-in-Charge)	Greenwich date	Storm-time: GMT of begin.	Storm-time: GMT of ending[1]	Sudden commencement: Type[2]	Sudden commencement: Amplitudes[3] D	H	Z	C-figure, degree of activity[4]	Maximal activity on K-scale 0 to 9: Gr. day	Gr. 3-hr. period	K-index	Ranges: D	H	Z
(1)	(2)	(3)	(4)	(5)	(6)	(7)	(8)	(9)	(10)	(11)	(12)	(13)	(14)	(15)
	1956	*h m*	*d h*		′	γ	γ					′	γ	γ
Elizabethville	Jan. 27	09 00	28 00	s.c.	−1	+32	−3	ms	27	5, 6	.....	11	212	30
(A. Alexandre)	Feb. 25	03 09	26 00	s.c.	−1	+45	+2	ms	25	3, 4	.....	22	344	41
	Mar. 3	.....	.....	.....	.....	.....	.....	ms	.....	.....	.....	.....	.....	.....
		(*Note:* L'enrégistrement manque du 2 mars a 2100z au 3 mars a 0600z)												
Apia	Mar. 9	21 20	12 01	.....	.....	.....	.....	m	10	8	5	8	179	48
(A.A. Thomson)	Mar. 20	11 47	23 09	.....	.....	.....	.....	ms	22	1	6	6	214	38
	Mar. 26	07 40	27 03	.....	.....	.....	.....	m	26	4	5	4	110	15
	Mar. 28	09 45	29 23	.....	.....	.....	.....	m	28	8	5	5	101	37
									29	4	5			
	Apr. 21	11 02	24 04	s.c.	0	+14	−6	ms	21	7	7	7	245	46
	Apr. 25	11 32	26 21	.....	.....	.....	.....	m	26	3, 4	5	6	111	24
	Apr. 26	21 12	30 01	s.c.	−1	+45	−13	ms	27	1, 4	7	8	405	77
	Apr. 30	01 37	1 18	s.c.	0	+16	−7	m	30	1, 2	5	6	80	26
	May 11	23 41	13 15	.....	.....	.....	.....	ms	13	3	6	6	173	26
	May 13	22 20	18 12	.....	.....	.....	.....	ms	16	2	7	8	223	43
	May 20	06 37	21 10	s.c.	0	+23	−10	m	20	4	5	4	96	27
	May 23	09 20	26 10	.....	.....	.....	.....	ms	23	8	6	5	247	36
									25	1, 3	6			
	June 14	19 40	16 14	.....	.....	.....	.....	m	15	8	5	2	70	18
	June 23	18 06	25 19	s.c.	0	+3	−1	m	23	8	5	5	168	32
									24	7	5			
									25	1, 2	5			
Binza	Jan. 21	16 45	23 17	s.c.*	−1	18	−1	m	22	1	.....	6	100	42
(Ch. Staes)	Jan. 27	09 10	28 24	s.c.	−1	37	....	ms	27	6, 7	.....	8	248	146
	Feb. 19	02 20	20 15	s.c.*	−1	42	−2	m	19	4	.....	7	106	50
	Feb. 25	03 10	27 03	s.c.	−1	54	−2	s	25	4, 5	.....	15	304	40
	Mar. 2	23 45	4 15	s.c.*	−1	23	1	s	3	3, 4	.....	10	276	40
	Mar. 22	0 30	23 24	s.c.	−1	33	3	ms	22	1	.....	8	143	31
Watheroo	Apr. 21	11 01	23 00	s.c.*	0	+17	0	ms	21	4, 7, 8	6	21	228	120+
(A. F. Tillott)	Apr. 26	21 11	28 08	s.c.*	+7	+21	+40	ms	27	1, 6, 7	7	27	324	190+
	Apr. 28	17 ..	29 17	.....	.....	.....	.....	ms	29	1	6	27	149	124
	Apr. 30	01 38	30 20	s.c.*	0	−15	+4	m	30	1, 2	5	16	62	93
	May 11	23 41	13 16	s.c.	+1	+3	+3	m	12	5	5	20	160	117
									13	3	5			
	May 15	05 50	17 15	.....	.....	.....	.....	ms	16	4	7	32	165	170+
	May 20	06 38	21 03	s.c.*	+2	+37	+8	ms	20	4	6	19	114	130+
	May 23	10 10	25 15	.....	.....	.....	.....	ms	24	4, 5, 7	6	30	183	162
	June	None												
Toolangi	Jan. 17	23 51	20 00	s.c.	−2	+4	0	ms	18	2	6	31	183	45
(I. B.	Jan. 21	16 44	25 09	s.c.	+2	+27	+6	m	22	1, 2, 3	5	24	150	56
Everingham)									24	2, 4, 7	5			
	Jan. 27	08 59	30 00	s.c.	0	+36	+6	m	27	4, 5, 6, 7	5	25	194	6
									28	2, 3	5			
									29	5	5			
	Feb. 25	03 07	26 15	s.c.	−2	+5	+15	s	25	4	8	64	318	30
	Mar. 2	23 42	4 16	s.c.	−4	−18	+5	ms	3	4, 5, 7	6	28	220	17
	Mar. 20	11 45	23 08	.....	.....	.....	.....	m	21	3, 7, 8	5	23	175	7
									22	1,8	5			
	Apr. 21	11 02	23 13	s.c.	−2	32	6	ms	21	7	6	34	214	10
									22	4	6			
	Apr. 26	21 11	28 09	s.c.	4	−28	0	s	27	4	8	63	330	21
	Apr. 28	18 57	29 21	s.c.	3	19	0	ms	29	1	6	23	134	4
	Apr. 30	01 37	1 13	s.c.	−5	−33	0	m	30	1, 2, 3	5	24	143	3
	May 11	23 41	13 15	.....	.....	.....	.....	ms	13	3	6	22	200	7
	May 16	04 21	17 15	s.c.	1	−25	0	ms	16	6	7	50	227	16
	May 20	06 37	21 09	s.c.	−2	−59	1	ms	20	4	6	30	156	3
	May 23	09 03	25 16	.....	.....	.....	.....	ms	24	4	6	40	175	7
	June	None												

PRINCIPAL MAGNETIC STORMS—Concluded

Observatory (Observer-in-Charge)	Greenwich date	Storm-time GMT of begin.	Storm-time GMT of ending[1]	Sudden commencement Type[2]	Sudden commencement Amplitudes[3] D	H	Z	C-figure, degree of activity[4]	Maximal activity on K-scale 0 to 9 Gr. day	Gr. 3-hr. period	K-index	Ranges D	H	Z
(1)	(2)	(3)	(4)	(5)	(6)	(7)	(8)	(9)	(10)	(11)	(12)	(13)	(14)	(15)
	1956	*h m*	*d h*		′	γ	γ					′	γ	γ
Amberley	Mar. 24	10 ..	30 10	.....	.....	.....	.....	m	26	4	5	21	153	63
(A. L. Cullington)									29	3	5			
	Apr. 21	08 ..	23 14	.....	.....	.....	.....	ms	21	7	6	37	239	182
									22	3, 4	6			
	Apr. 26	21 11	29 17	s.c.*	−10	−76	+41	s	27	4	8	67	356	288
	Apr. 30	01 37	2 12	s.c.	+4	+39	−14	m	30	1, 2	5	21	124	59
	May 11	23 42	13 18	s.c.*	+1	+13	−2	m	12	2	5	24	176	89
									13	3, 4	5			
	May 13	22 22	17 18	s.c.*	−1	−2	+3	ms	16	3	7	34	276	208
	May 20	06 37	21 15	s.c.	+2	+49	−7	m	20	4	5	16	121	66
	May 23	19 ..	26 12	.....	.....	.....	.....	ms	25	3	7	48	269	141
	June	None												

LETTERS TO EDITOR

AURORAL RADIATION IN THE 2 TO 3 MICRON RANGE

A radiometer was constructed to measure radiation in the 2 to 3 micron range. The instrument consisted of a cooled lead-sulfide cell connected in a direct-current bridge with an unexposed cell to reduce zero drift associated with temperature changes. The field of view was defined by a 4-inch Cassegrain telescope. A combination of the protective glass cover and an interference filter produced a pass band whose limits were approximately 2 and 3 microns. A Brush DC amplifier and recorder were used to amplify and record the signal. A reference source, whose temperature could be varied, was used as a control and as an approximate calibrator.

The auroral measurements were made at Ballaines Lake, which is 3 km north-northeast of College, Alaska. The location was selected on the basis of relative freedom from interference of artificial lights. The observations were made in periods when there were no clouds. The air temperature was in the $-37°$C to $-40°$C range.

The radiation from the night sky and from the auroral rays and arcs with visual intensity 3 to 4 on the International Intensity Scale was less than that detectable by the radiometer described above. Based on the calibration with the reference sources, this minimum detectable energy is approximately 10^{-10} effective watt at the PbS cell. Effective watts are obtained from the integral $A\int_0^\infty Jf(\mathrm{PbS})t\,d\lambda$ for the appropriate field of view, where J gives the spectral energy distribution of the source of radiation, $f(\mathrm{PbS})$ is the relative spectral sensitivity of the PbS cell normalized to 1 at 2.1 microns, t is the transmission of the filter, and A is the area of the telescope mirror.

The authors wish to acknowledge the assistance and cooperation given to them by the personnel at the Geophysical Institute, University of Alaska, and the assistance and encouragement given to them by L. W. Nichols, E. Regelson, C. P. Pentoney, and Z. W. Hohanshelt.

Edward V. Ashburn
J. G. Moore
Pierre St. Amand

Michelson Laboratory,
U. S. Naval Ordnance Test Station,
China Lake, California, May 7, 1956
(Received May 14, 1956)

COSMIC-RAY INTENSITY AT HIGH ALTITUDES ON FEBRUARY 23, 1956*

A balloon flight of a single Geiger tube was made[1,2] from Iowa City ($\lambda = 52°N$) during the period $19^h\ 33^m$ to $21^h\ 12^m$ GMT on February 23, 1956. The apparatus consisted of a single Victoreen 1B85 Geiger tube of calibrated effective length and a radio transmitter, all housed in a pressure-tight aluminum shell of wall thickness 0.032″. Identical apparatus has been flown by this laboratory on previous occasions by means of balloons and rockets. The axis of the tube was nearly vertical. The geomagnetic latitude of equipment while at the highest altitude was estimated to be 53°N.

The raw counting rate of the Geiger tube during the ascent of the balloon is shown as a function of time in Figure 1. The measured effective length of the tube

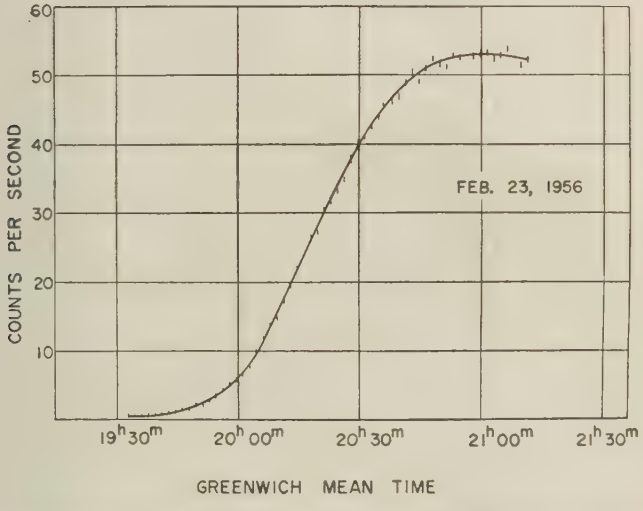

FIG. 1—Raw counting rate of single Geiger tube during ascent of balloon on February 23, 1956

was 6.8 ± 0.2 cm, and the diameter was 1.90 ± 0.02 cm. The maximum observed value of the counting rate was 53.0 ± 0.3 counts/second during the period $20^h\ 55^m$ to $21^h\ 08^m$ GMT. Correcting for dead time and intrinsic efficiency ($\epsilon = 0.98$) and dividing by the appropriate geometric factor of the counter,[3] we find

$$\bar{J} = 0.76 \pm 0.03 \text{ (cm}^2 \text{ sec sterad)}^{-1} \quad \ldots\ldots\ldots\ldots\ldots\ldots (1)$$

*Assisted by National Science Foundation and by joint program of Office of Naval Research and Atomic Energy Commission.

[1]The authors are indebted to Dr. J. A. Simpson for informing us of the fact that a great cosmic-ray storm was in progress. The onset of the storm occurred at $03^h\ 48^m$ GMT, February 23.

[2]S. E. Forbush, J. Geophys. Res., **61**, 155 (1956).

[3]E. C. Ray, M.S. thesis, State University of Iowa (June 1953).

for the angular average value, over the upper hemisphere, of the unidirectional intensity of all charged particles, the average being taken in the usual manner.[4] An equivalent statement of the result is

$$J_0 = 4.8 \pm 0.2 \text{ (cm}^2 \text{ sec)}^{-1} \quad \ldots\ldots\ldots\ldots\ldots\ldots (2)$$

where J_0 is the flux through a sphere of unit cross-section.

During the period 1950-1956, this laboratory has made a large number of balloon and rocket flights of single Geiger tubes and Geiger tube telescopes at geomagnetic latitudes ranging from 41°N to 89°N. A summary of pertinent results[3,4,5] is given in Table 1.

TABLE 1—*Normal cosmic-ray intensities of charged particles at Pfotzer-Regener maximum at* $\lambda = 52°$ *to* $53°$ *north*

$\bar{J} = 0.54 \pm 0.02$ (cm² sec sterad)$^{-1}$ $J_0 = 3.37 \pm 0.12$ (cm² sec)$^{-1}$	E. C. Ray (1953)
$\bar{J} = 0.54 \pm 0.01$ (cm² sec sterad)$^{-1}$	R. G. Tuckfield (1954)

By means of Table 1, it is seen that the intensity values (1) and (2) given above were 1.4 times as great as the normal values at the Pfotzer-Regener maximum at this latitude.

No suitable barometer was at hand for the February 23 flight. Thus, there were no observed atmospheric pressure data. The validity of the conclusion of the preceding paragraph is unaffected by this lack of information. But it is of further interest to replot the observed data on an atmospheric pressure basis

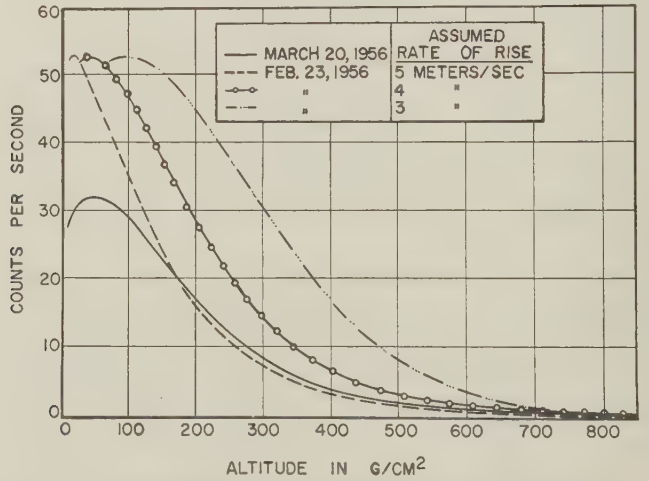

FIG. 2—Replot of corrected Geiger tube data of Figure 1 for three assumed constant rates of rise and comparison with similar data of flight of identical equipment on March 20, 1956. The latter flight was equipped with a barograph.

[4]L. H. Meredith, J. A. Van Allen, and M. B. Gottlieb, Phys. Rev., **99**, 198 (1955).
[5]R. G. Tuckfield, M.S. thesis, State Unversity of Iowa (February 1954).

assuming various constant rates of ascent in m/sec, an assumption concerning balloon performance which is well-grounded in our experience with flights of clusters of rubber balloons of the type used. The results of this process are shown by the upper three curves of Figure 2. Also shown in Figure 2 (by the solid curve) are the counting rate data obtained on March 20, 1956, in a flight from Iowa City of apparatus identical with that of the February 23 flight. The March 20 flight carried a barograph. On the latter date, the maximum counting rate of 32 ± 1.5 counts/sec (at 47 g/cm^2) was less than that observed at about 21^h on February 23 by the factor 1.65.

From Figure 2, it appears likely that the actual rate of rise of the February 23 flight was about 4 m/sec and that the previously quoted intensities (1) and (2) refer to the vicinity of the Pfotzer-Regener maximum. It should be noted that the February 23 flight reached its full altitude at about 17 hours after onset of the storm. The results herein therefore refer to the dying phase of the storm.[2]

We are particularly indebted to Drs. F. B. McDonald and K. A. Anderson and to Messrs. G. Ludwig and W. R. Webber for assistance.

J. A. Van Allen
C. E. McIlwain

Department of Physics,
State University of Iowa,
Iowa City, Iowa, July 3, 1956
(Received July 5, 1956)

THE SUN'S DISK IN LYMAN-ALPHA RADIATION*

An ultraviolet monochromatic camera was flown in an intermediate Aerobee rocket on May 8, 1956, at 7:55 a.m., MST. The instrument was designed to photograph the disk of the sun in Lyman-alpha radiation (1215.7A). The optical components of the camera were made of lithium fluoride and consisted of two 15° prisms and one lens. The resolving power was of the order of 1/20 the solar diameter, and the band-pass about 40A.

Four photographs of the sun were obtained with Eastman 103UV sensitized film at exposure times of two seconds each and at a height of about 145 km. The images (diameter 2.8 mm) were comparable to the scattered white-light background in density.

The camera was directed at the sun by an electronic pointing control.[1] Oscillations in pointing direction during the two-second exposures may have been as large as two minutes of arc. A reproduction (negative) of the sun's image in Lyman-alpha radiation is shown in Figure 1(*a*). In (*c*) and (*b*) are shown, respectively, photographs (positives) of the sun on May 8 in calcium II light (3934A) and in hydrogen H_α light (6563A). The latter two photographs were taken at the McMath-Hulbert Observatory. There is a strong correlation between the positions of regions of enhanced Lyman-alpha intensity and those of the active sunspot and plage areas.

*The research reported in this paper has been sponsored by the Geophysics Research Directorate of the Air Force Cambridge Research Center, Air Research and Development Command.

[1]R. A. Nidey and D. S. Stacey, Rev. Sci. Instr., **27**, 216 (1956).

The orientation of the sun's image on the rocket photograph was determined independently by a study of rocket aspect data. It was found to agree with the orientation suggested by comparison of the image with (*b*) and (*c*) in Figure 1.

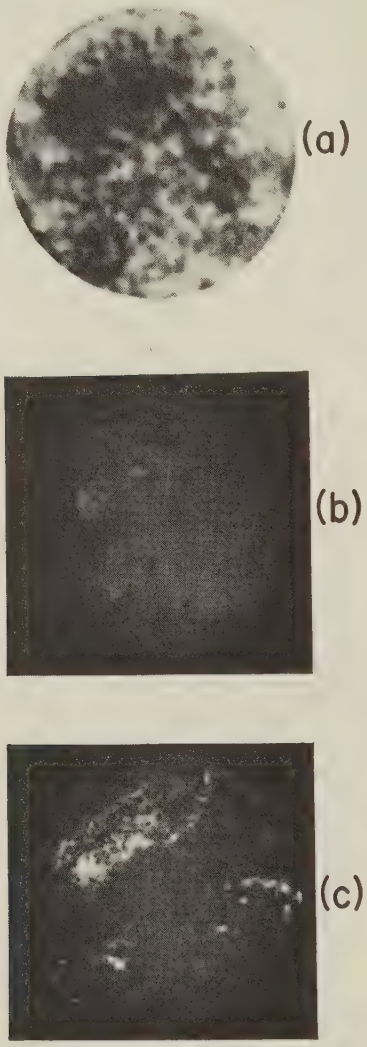

Fig. 1—A photograph (negative) of the sun in Lyman-alpha radiation (1215.7A) taken on May 8, 1956, from an intermediate Aerobee rocket at an altitude of about 145 km is shown in (*a*). The camera optics consisted of two 15° prisms and a lens, all made of lithium fluoride. Four such photographs were obtained with exposure times of two seconds. Resolving power was about 1/20 the solar diameter. Scattered white light and film granularity contributed to poor image quality. For comparison are shown two photographs (positives) of the sun taken on the same day; (*b*) with H_α light (6563A) and (*c*) in CaII light (3934A). The latter photographs were obtained through the kindness of Drs. McMath and Dodson of the McMath-Hulbert Observatory. North is up and east is to the right.

Although a quantitative analysis of the photograph is not complete, it appears that there is marked enhancement of Lyman-alpha radiation in the plage areas. Therefore, an appreciable variation in intensity of Lyman-alpha radiation following the sunspot cycle in general, and individual solar disturbances in particular, is to be expected.

R. Mercure
S. C. Miller, Jr.
W. A. Rense
F. Stuart

University of Colorado,
Boulder, Colorado, July 11, 1956
(Received July 14, 1956)

ABSORPTION OF COSMIC RADIO NOISE AT 22.2 MC/SEC FOLLOWING SOLAR FLARE OF FEBRUARY 23, 1956

Reports of widespread ionospheric disturbances on the dark hemisphere of the earth, accompanying the great solar flare of February 23, 1956, have been noted by a number of groups. A. Shapley has reported an increase in ionospheric absorption at vertical sounding stations in high latitudes,[1] commencing a few minutes after the flare and lasting many hours, while Ellison and Reid,[2] and Gold and Palmer,[3] have reported a sudden decrease in 27-kc/sec atmospherics at the time of the flare, coming too early and much too suddenly to be due to sunrise effect. In the auroral zone, effects were noted by the Geophysical Institute at College, Alaska,[4] whose records of galactic radio noise at 30 Mc/sec showed an increase in absorption shortly after the flare, increasing gradually to a maximum of 1.8 db over the period $04^h\ 20^m$ to $09^h\ 00^m$ UT.

Absorption effects of a different nature have been found on radio-source records taken at the Seneca Radio Observatory of the Carnegie Institution, near Washington, D. C. The equipment consisted of a phase-switching interferometer[5] tuned to 22.2 Mc/sec, utilizing a pair of small antennas which were normally used for observations of the planet Jupiter, but which observe a number of other radio sources as well. Comparison of the record obtained near the time of the flare with a record taken the previous night showed a noticeable difference for a short period when Virgo A (IAU 12N1A) was being observed. The apparent intensity of the source on February 23 compared to the intensity of the previous night is shown in Figure 1. The horizontal lines give the relative intensity, averaged over the period indicated by the length of the line. Since the observation was made with a phase-switching interferometer which gives zero output when the source is near quadrature in the interference pattern, the averages were taken over the peaks, when the source is near a maximum or minimum in the interference pattern. From $04^h\ 02^m$ to $04^h\ 18^m$, the equipment was being calibrated,

[1] A. Shapley, private communication.
[2] M. A. Ellison and J. H. Reid, J. Atmos. Terr. Phys., 8, 291 (1956).
[3] T. Gold and D. R. Palmer, *ibid.*, p. 287.
[4] Geophysical Institute, University of Alaska: Abstr. of terrestrial phenomena observed following solar flare 23 Feb. 1956, 0334.
[5] M. Ryle, Proc. R. Soc., A, 211, 351 (1952).

and hence no data are available over this period. The experimental uncertainty is determined by the background noise fluctuations, and since the source is not a strong one we estimate that the relative intensity may be subject to a probable error of the order of magnitude ± 0.1.

For purposes of comparison, the cosmic-ray increase observed[6] by the large shielded Carnegie ion-chamber, also near Washington, is plotted in Figure 1, the

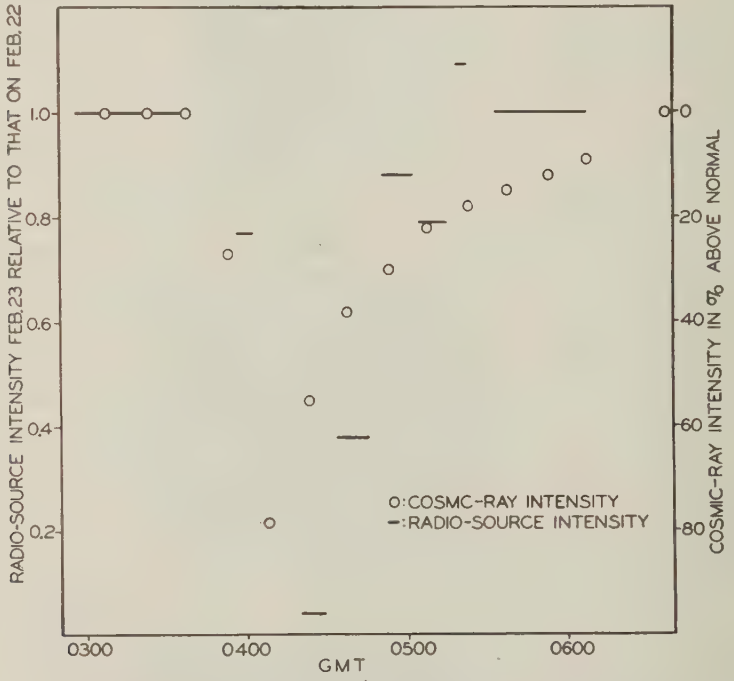

FIG. 1-ABSORPTION ON 22 MC SEC^{-1} FROM RADIO SOURCE VIRGO A AND INCREASE IN COSMIC-RAY INTENSITY NEAR WASHINGTON, D.C., FOLLOWING SOLAR FLARE OF FEBRUARY 23, 1956

similarity of the two curves showing clearly. The initial increase in absorption, at $04^h\ 00^m$, may not be real, however, since the uncertainty is large; the later points are unquestionably indicative of strong absorption, reaching a maximum of at least 6 db and probably greater. The commencement time is not well defined, but is certainly no later than $04^h\ 20^m$.

Ionospheric vertical-sounding records from the National Bureau of Standards station at Fort Belvoir, Virginia, showed no unusual increase in absorption at the time,[1] which would imply that the material responsible for the 22.2-Mc/sec absorption was not located below the $F2$ layer. Furthermore, the obscuration of a point source was observed, and it is not possible to say whether a localized absorbing cloud or a general absorbing blanket over the entire sky was responsible. Ellison and Reid[3] reported no observable absorption of the galactic background

[6]H. E. Tatel, private communication.

noise at 18 Mc/sec, an observation which might favor the hypothesis of a localized absorbing cloud, but since their observation was made at a different location on the earth, no definite conclusion can be reached.

S. E. Forbush
B. F. Burke

Department of Terrestrial Magnetism,
Carnegie Institution of Washington,
Washington 15, *D. C., July 16, 1956*
(Received July 17, 1956)

DAYTIME MEASUREMENT OF POSITIVE AND NEGATIVE ION COMPOSITION TO 131 KM BY ROCKET-BORNE SPECTROMETER

The ambient positive and negative ion composition in the mass range 5 to 60 atomic mass units was measured between 93 and 131 km by two Bennett radio-frequency mass spectrometers.[1] The spectrometers were flown in Aerobee rocket NRL No. 24 at White Sands Proving Ground, New Mexico, at 10:16 MST, November 29, 1955. Except for the time of day and year, this experiment was identical to the night-time experiment previously reported.[2] Again, the experimental equipment performed well, the mass spectra were apparently not influenced by the rocket or its gases, and interpretation of the telemetered data was simple and unambiguous.

The results of this daytime flight differ completely from those of the night-time flight in which only the mass 28 positive ion was detected. No positive ions were detected on this daytime flight. Instead, negative ions of atomic mass numbers 46, 32, 29, 22, and 16 were detected. Mass 46 was predominant, the relative abundances being approximately 96.5, 1.6, 0.2, 1.0, and 0.7 in the order of decreasing mass number. The most probable chemical identification of masses 46, 32, and 16 is thought to be NO_2^-, O_2^-, and O^-. In terms of the normal constituents of air, a chemical identification of masses 29 and 22 is not apparent.

The absence of positive ions in this flight is particularly striking. Telemetered spectrometer functions indicate that the positive ion spectrometer performed normally throughout flight. As the spectrometers were dimensionally identical and had symmetrical field configurations, it is reasonable to assume that the collection properties of the two spectrometers were equal. Under this condition, positive ions would have been detected if their concentration had been as much as that of the less abundant negative ions such as masses 16 and 29.

A complete paper on the day and night-time flights will appear in a subsequent issue.

Charles Y. Johnson
James P. Heppner

Naval Research Laboratory,
Washington 25, *D.C., July 17, 1956*
(Received July 18, 1956)

[1]The ion composition spectrometers used in this experiment differ from the neutral gas spectrometer used by Meadows and Townsend (see Letter to Editor this issue of the Journal) in the following manner. In the ion spectrometers, ambient ions are drawn directly from the ionosphere into the analyzing section of the spectrometer; the neutral gas composition spectrometer takes in neutral gas and ionizes it by electron bombardment before analysis.

[2]C. Y. Johnson and J. P. Heppner, J. Geophys. Res., 60, 533 (1955).

NEUTRAL GAS COMPOSITION OF THE UPPER ATMOSPHERE BY A ROCKET-BORNE MASS SPECTROMETER

This is a preliminary report on the night-time flight of a mass spectrometer designed to investigate the composition of the upper atmosphere. From 113 km altitude to 141.6 km, the peak of flight, on the ascent of the rocket, and from 141.6 km to 74 km on the descent, the spectrometer detected the usual constituents of air. In the vicinity of 85 km on the descent, components with mass number 46 and 23 were detected and are tentatively identified as nitrogen dioxide and sodium, respectively.

The Bennett-type radio-frequency mass spectrometer was flown in Aerobee NRL-28 at 2200 MST, December 12, 1955, from White Sands Proving Ground, New Mexico. Mass spectra between 56 and 6 atomic mass units of the ambient atmospheric gas were obtained. The experiment was similar to that in Aerobee

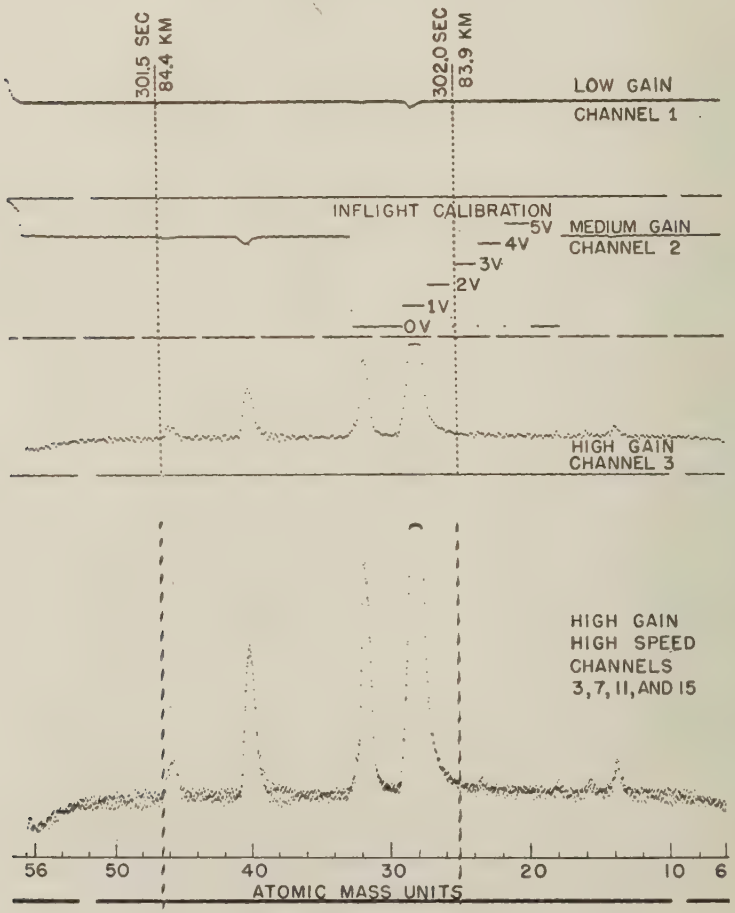

Fig. 1—Aerobee NRL-28, portion of telemetering record

NRL-13 previously reported,[1] except that increased resolution was obtained by use of a four-stage spectrometer tube and that the nose-tip of the rocket was thrown off, exposing the evacuated spectrometer tube directly to the atmosphere. Due to an instrumental difficulty, the electron emission in the ion source was less than 10 per cent of normal and peak amplitudes were generally small.

The sample of mass spectra shown on the telemetering record in Figure 1 was obtained as the rocket descended at an angle of 11° with respect to vertical,[2] tail first, and with a velocity of 1.06 km per second. This near-vertical attitude and high velocity decreased the pressure within the spectrometer by about an order of magnitude below ambient. The spectrum shows peaks corresponding to the usual constituents of air: carbon dioxide (and nitrous oxide, N_2O) at mass number 44, argon at 40, oxygen at 32 and 16, nitrogen at 28 and 14, and water vapor at 18. Other peaks are at mass numbers 46 and 23.

The relative amplitudes of the peaks depend, not only on the relative composition of the corresponding gases in the atmosphere, but also on their relative ionization efficiency in the ion source. When the pressure in the spectrometer is high (above 10^{-4} mm Hg), the relative amplitudes also depend on the cross-section of the ions with respect to the neutral molecules. Discrimination by mass number may also take place in the gas flow when the ambient atmospheric pressure is above 10^{-3} mm Hg and considerably higher than the pressure within the spectrometer tube.

The atomic ions, O and N, at mass numbers 16 and 14 are formed within the ion source and do not necessarily indicate the presence of atomic oxygen and nitrogen in the ambient atmosphere. In contrast to the Aerobee NRL-13 flight, peaks attributable to gases originating from the rocket are notably absent. In particular, a peak of mass 30, which is the major peak in the spectra of the red fuming nitric acid used as a rocket propellant, is absent. Hence, it is believed that the peak at mass 46 is from the ambient atmosphere and may be due to NO_2 . The probability that the peak at mass 23 is a doubly ionized particle of mass 46 is low, because the 45-volt electrons used in the ion source have a low efficiency for production of doubly charged ions. Hence, it is believed that the peak of mass number 23 is due to sodium in the ambient atmosphere.

The peaks of mass numbers 23 and 46 were detected between 88 and 80 km, and between 90 and 75 km, respectively; both reached maximum amplitude at about 85 km. The photometer experiment flown by Koomen, Scolnik, and Tousey[3] in this rocket found sodium *D* radiation to be most intense at about 85 km, with the top and bottom of the luminous layer at 100 and 80 km, respectively.

Edith B. Meadows
John W. Townsend, Jr.

Naval Research Laboratory,
Washington 25, *D.C., July 17, 1956*
(Received July 18, 1956)

[1] J. W. Townsend, Jr., E. B. Meadows, and E. C. Pressly, Rocket exploration of the upper atmosphere, edited by R. L. F. Boyd and M. Seaton, Interscience Publishers, Inc., New York (1954); pp. 169-188.

[2] Aspect was determined from the photometer night airglow experiment in the same rocket; Martin J. Koomen, private communication.

[3] M. Koomen, R. Scolnik, and R. Tousey, Distribution of night airglow (OI) 5577A and Na *D* layers measured from a rocket, J. Geophys. Res., **61**, 304-306 (1956).

NOTES

(21) *Fall meeting of URSI*—A fall meeting, sponsored by the USA National Committee of the International Scientific Radio Union (URSI), is scheduled to be held at the University of California, Berkeley, California, on October 11 and 12, 1956. A combined technical session of interest to all participants is scheduled for the morning of October 11, to be followed by one or more sessions in each of the following fields: Commission 2—Radio and Troposphere; Commission 3—Ionosperic Radio; and Commission 4—Radio Noise of Terrestrial Origin.

(22) *New officers of the American Geophysical Union*—Dr. Maurice Ewing, Director of Columbia University's Lamont Geological Laboratory, at Palisades, New York, was elected President of the American Geophysical Union at its thirty-seventh annual meeting held in Washington, D. C., April 20 to May 3, 1956. Dr. Lloyd V. Berkner, President, Associated Universities, Inc., New York City, was elected Vice-President, and Dr. A. Nelson Sayre, of the United States Geological Survey, was chosen General Secretary.

(23) *First annual report of the Boulder Laboratories*—The first annual report of the National Bureau of Standards' Boulder Laboratories, covering the period July 1, 1954, to June 30, 1955, has been issued. This attractive and welcome NBS Report No. 3566 contains 125 pages plus five appendices listing Bureau publications. Over half of the volume is devoted to the varied objectives of the work of the Central Radio Propagation Laboratory, which is responsible for the collection, analysis, and interpretation of basic data pertaining to the propagation of radio waves over long distances through the earth's outer atmosphere and for the centralization and coordination of information in this field on a national and international basis. Because the ionosphere plays a determining role in the long distance propagation of radio waves, a major portion of the program is directed at a study of this medium.

(24) *New director for Mount Stromlo*—An outstanding American astronomer has been named Director of the Commonwealth Observatory in Australia. Dr. Bart J. Bok, of Harvard Observatory, will assume this post on February 1, 1957, succeeding Prof. R. v. d. R. Woolley, who has become eleventh Astronomer Royal of England, in charge of the Greenwich Observatory. The Commonwealth Observatory, on Mount Stromlo near the Australian capital city of Canberra, is one of the best equipped in the world. There the new director will have excellent facilities for continuing and expanding the studies of the southern Milky Way on which he has been engaged for many years at Harvard. Dr. Bok is an active leader in the relatively new field of radio astronomy. At Harvard, he and his coworkers completed the installation of a new 60-foot parabolic antenna, at present the largest such instrument in the United States. At Mount Stromlo, he will concentrate primarily on optical studies of galactic structure, working in close collaboration with the radiophysics laboratory at Sydney.

(25) *Radio telescope on Palomar Mountain*—On April 10, a 32-foot microwave antenna began operation on Palomar Mountain in southern California, where the 200-inch reflector is located. The operation of this radio telescope marks the beginning of a long-term radio astronomy program by the California Institute of Technology, with support in excess of $400,000 from the Office of Naval Research. The new equipment will serve mainly as a pilot model and as a training instrument for astronomers and electronics personnel. Within another year, Caltech expects to mount three additional parabolic reflectors. One of these will also be 32 feet and the others 90 feet in diameter. The latter will be located on a California desert site, probably in the Owens Valley to the east of the Sierra Nevada range. This region offers extremely good protection against man-made radio interference and is reasonably near both Mount Wilson and Palomar Observatories.

(26) *Proposed U. S. National Radio Observatory*—Proposal has been made for a "National Radio Observatory," in the belief that there is no substitute for a large radius in building an antenna to achieve resolution, speed, and sensitivity. Plans are now under way to build a first national radio-telescope with a 140-foot paraboloidal antenna at Green Bank, in the mountains of southeastern West Virginia, where the noise level is very low, and there are hopes that a 600-foot instrument may be constructed later and that a national park may be established there. The site selected is about 35 miles south of Elkins, West Virginia.

(27) *Geomagnetic activities of the U. S. Coast and Geodetic Survey*—Fredericksburg Magnetic Observatory was dedicated in a formal ceremony on May 23, 1956. About 150 persons, including many eminent geophysicists, attended to inspect the new installation and to hear addresses by the Honorable Sinclair Weeks, Secretary of Commerce, Rear Admiral H. Arnold Karo, Director of the Coast and Geodetic Survey, Captain Elliott B. Roberts, Chief of the Geophysics Division, and Mr. Robert L. Gebhardt, Observer-in-Charge. It is expected to continue operation of the old observatory at Cheltenham for several months to provide an adequate overlap and insure proper correlation of standards.

Sr. Augusto Llano, of the Chilean Meteorological Office, and Mr. Radomir Turajlic, of the University of Belgrade, have been studying the methods and procedures of the Coast and Geodetic Survey in office and field work in geomagnetism.

(28) *Personalia*—The eighteenth annual William Bowie Medal for 1956 was awarded by the American Geophysical Union to a Finnish geophysicist, Dr. *W. A. Heiskanen*. Dr. Heiskanen is Director of the Institute of Geodesy at Ohio State University and also Director of the Finnish Geodetic Institute.

Dr. *Gerhard Oertel*, prominent European geologist, has been appointed an associate professor of geology at Pomona College, Claremont, California, for the academic year beginning in September, 1956. A native of Leipzig, Germany, Dr. Oertel studied at the Universities of Graz in Austria and Bonn in Germany. He taught in the geology department at the University of Bonn from 1946 to 1948 and the following year served as a temporary member of the geology faculty at the University of Edinburgh. In recent years, he has served as exploration geologist in connection with the search for oil and ore deposits in Portugal and Portuguese India.

On July 1, 1956, Dr. *E. H. Vestine*, chairman of the Section of Analytical Geophysics, Department of Terrestrial Magnetism, Carnegie Institution of Washington, assumed duties, on leave of absence, as head of the Data Coordination Center for the International Geophysical Year, 1957-58, with offices in the National Academy of Sciences, 2101 Constitution Avenue, N.W., Washington 25, D.C.

Dr. *Walter S. Adams*, Director of Mount Wilson Observatory from 1923 until 1946, died on May 11, 1956, in Pasadena, California, at the age of seventy-nine. He received many honors for his outstanding contributions to astronomy.

It was with feeling of profound sorrow and great loss, as this issue is being printed, that the death of Dr. *John A. Fleming*, former Editor of this Journal and Director of the Department of Terrestrial Magnetism, Carnegie Institution of Washington, occurred on July 29, 1956, at the age of seventy-nine. The news of his sudden death will come as a great shock to his friends and colleagues in all parts of the world. It is planned to give in the next issue a sketch of Dr. Fleming's many accomplishments, especially in the field of geophysics.

LIST OF RECENT PUBLICATIONS

By W. E. SCOTT

Department of Terrestrial Magnetism,
Carnegie Institution of Washington,
Washington 15, D. C.

(Received July 3, 1956)

A—*Terrestrial Magnetism*

ANDRESCIANI, V. Metodi di misura del campo magnetico. Ricerca Sci., **26**, No. 1, 25-63 (1956). [English, French, and German abstracts.]

BORGNE, E. LE. Susceptibilité magnétique anormale du sol superficiel. Ann. Géophys., **11**, No. 4, 399-419 (1955).

CHARGOY, A. Movimiento del campo magnético terrestre dado por los términos de sugundo orden de la ecuación del potencial. Ann. Inst. Geophys., Univ. Nac. Autonoma Mexico, **1**, 24-37 (1955).

COPENHAGEN, Det Danske Meteorologiske Institut. Magnetisk årbog. 1ste del: Danmark (undtagen Grönland)—Annuaire magnétique, 1ère partie: Le Danemark (excepté le Groenland), 1954. Köbenhavn, 27 pp. (1955). 32 cm.

DOELL, R. R. Remanent magnetization of the upper-Miocene 'blue' sandstones of California. Trans. Amer. Geophys. Union, **37**, No. 2, 156-167 (1956).

DRIGO, A. Lo studio del ferromagnetismo nell'Istituto di fisica dell'Università di Ferrara. Ricerca Sci., **26**, No. 1, 138-143 (1956). [English, French, and German abstracts.]

EGEDAL, J., AND N. AMBOLT. The effect on geomagnetism of the solar eclipse of 30 June 1954 (supplementary communication). J. Atmos. Terr. Phys., 8, Nos. 1/2, 105-107 (1956).

EPSTEIN, P. S. Theory of wave propagation in a gyromagnetic medium. Rev. Modern Phys., 28, No. 1, 3-17 (1956).

FANSELAU, G., UND E. THIELE. Geomagnetische Kennziffern 1890 bis 1907 (nebst einigen Ergänzungen). [Potsdamer.] Berlin, Akad.-Verlag., Abh. No. 17, 48 pp. (1955). 30 cm. [Published under the auspices of the Meteorologischer Dienst der Deutschen Demokratischen Republik.]

HOPE, E. R. Spiral patterning of solar corpuscular precipitation. Nature, **177**, 571-572 (March 24, 1956).

LI, Y.-Y. Domain walls in antiferromagnets and the weak ferromagnetism of α-Fe_2O_3. Phys. Rev., **101**, No. 5, 1450-1454 (1956).

LYNCH, A. C., AND J. WATKINS. Some recent developments in magnetism. Nature, **177**, 517-518 (March 17, 1956). [Résumé of an informal symposium by the Institute of Physics, London, Sept. 23-24, 1955.]

MAEDA, H. Daily variations of the electrical conductivity of the upper atmosphere as deduced from the daily variations of geomagnetism. Part I—Equatorial zone. Rep. Ionosphere Res. Japan, **9**, No. 3, 148-165 (1955).

MCCLAY, J., AND B. SHUMAN. Magnetic compensation of aircraft. Air Force Cambridge Research Center, Geophys. Res. Dir., Instrumentation for Geophysical Research, No. 4, 48 pp., mim. (August 1955). 28 cm.

MCDONALD, K. L. Penetration of the secular field through a mantle with variable conductivity. Salt Lake City, University of Utah, Tech. Rep. No. 19, 26 pp. + 22 figs., mim. (April 1, 1956)

MILLER, E. T., AND M. EWING. Geomagnetic measurements in the Gulf of Mexico and in the vicinity of Caryn Peak. Geophysics, **21**, No. 2, 406-432 (1956).

NAGATA, T., AND H. MUZUNO. S_q-field in the polar region on absolutely quiet days. Kyoto, J. Geomag. Geoelectr., **7**, No. 3, 69-74 (1955).

NORWAY. A magnetic survey of Norway II. Magnetisk Byrå (Bergen) and Norges Sjøkartverk (Oslo), Jordmagnetiske Pub. No. **2**, 36 pp. + 6 magnetic maps (1955). 31 cm.

Olczak, T. Über die Säkularänderungen des Erdmagnetismus in Polen im Zeitraum von 1901.0 bis 1935.0. Acta Geophys. Polonica, **3**, No. 4, 145-154 (1955).

Peru. Carta geomagnetica del Perú a 1955.0. Ministerio de Fomento, Instituto Geofísico de Huancayo, Pub. Esp. No. 1, 11 pp. + geomagnetic map (1955). 33 cm.

Procopiu, St. Momentul magnetic al globului pămîntesc a început să crească. Bull. Stiintific, **7**, No. 4, 1063-1093 (1955). [French and Russian abstracts.]

Rikitake, T. Growth of the magnetic field of the self-exciting dynamo in the earth's core. Bull. Earthquake Res. Inst., Tokyo, **33**, Pt. 4, 571-582 (1955).

Rikitake, T. Magneto-hydrodynamic oscillations of finite amplitude of a conducting fluid sphere. Bull. Earthquake Res. Inst., Tokyo, **33**, Pt. 4, 583-592 (1955).

Roberts, E. B., and D. G. Knapp. Geomagnetism in the International Geophysical Year. J. Coast Geod. Surv., No. 6, 4-10 (Aug. 1955).

Roquet, J. Étude des propriétés magnétiques de roches volcaniques à aimantation naturelle inversée. Ann. Géophys., **11**, No. 4, 461-474 (1955).

Runcorn, S. K. Paleomagnetic survey in Arizona and Utah: Preliminary results. Bull. Geol. Soc. Amer., **67**, No. 3, 301-316 (1956).

Schwerdtfeger, W., y C. J. Vasino. La variación secular de la continentalidad en la Republica Argentina. Meteoros, **5**, No. 3, 177-184 (1955).

Sekido, Y. Two types of geomagnetic disturbance. Rep. Ionosphere Res. Japan, **9**, No. 3, 182 (1955). [Short note.]

Selzer, É. Propriétés caractéristiques des galvanomètres suramortis montés en flux mètres partiels. Paris, C.-R. Acad. sci., **242**, No. 11, 1422-1425 (1956).

Slaucitajs, L. Sobre el uso de los magnetómetros QHM y BMZ en la campaña y en el observatorio magnético. Meteoros, **5**, No. 3, 155-162 (1955).

Urquhart, H. M. A., and J. E. Goldman. Magnetostrictive effects in an antiferromagnetic hematite crystal. Phys. Rev., **101**, No. 5, 1443-1450 (1956).

Wingst Observatorium. Ergebnisse der erdmagnetischen Beobachtungen im Observatorium Wingst in den Jahren 1951 und 1952. D. Hydrogr. Inst., Hamburg, Jahrb. No. 8, 150 pp. (1955). 25 cm.

Wingst Observatorium. Magnetogramme Wingst, 1954. D. Hydrogr. Inst., Hamburg, Pub. No. 2503, 98 pp. (1955). 25 cm.

Wood, F. W., and I. B. Everingham. A provisional isogonic map of Australia and New Quinea showing predicted values for the epoch 1955.5. Commonwealth of Australia, Bureau of Mineral Resources, Geology and Geophysics, Rep. No. 14, 6 pp. + map (1953).

B—*Terrestrial Electricity*

Arlick, A. B. Spontaneous generation of negative charge beneath a column of water. Science and Culture, **21**, No. 8, 444-447 (1956). [Letter to Editor.]

Chalmers, J. A. The electrical charge on the earth. J. Atmos. Terr. Phys., 8, Nos. 1/2, 124-125 (1956). [Research note.]

Holzer, R. E., and O. E. Deal. Low audio-frequency electromagnetic signals of natural origin. Nature, **177**, 536-537 (March 17, 1956). [Letter to Editor.]

Malan, D. J. La distribution verticale de la charge négative orageuse. Ann. Géophys., **11**, No. 4, 420-426 (1955).

Malan, D. J. Les décharges lumineuses dans les nuages orageux. Ann. Géophys., **11**, No. 4, 427-434 (1955).

Simpson, G. The charging of rain by splashing. Q. J. R. Met. Soc., 82, No. 351, 103 (1956). [Correspondence.]

Venkiteshwaran, S. P., and B. B. Huddar. Variation of electrical potential gradient with height at Poona from 31 October to 2 November 1953. Indian J. Met. Geophys., 7, No. 1, 61-64 (1956).

C—*Cosmic Rays*

Assies, M. A., and H. F. Jongen. Cosmic-ray intensity during solar flare of February 23, 1956. Physica, **22**, No. 4, 355 (1956). [Letter to Editor.]

Bartol Research Foundation. Fifth annual report of the work of the Bartol Research Foundation of the Franklin Institute. Swarthmore, The Franklin Institute, 126 pp., mim. (Sept. 30, 1955). [Contains chapter on cosmic rays.]

Crawshaw, J. K., and H. Elliot. Search for a sidereal variation of the cosmis ray intensity at high energies. Proc. Phys. Soc., A, **69**, No. 434, 102-109 (1956).

Dauvillier, A. Puissant flux solaire nocturne de rayons cosmiques pénétrants. Paris, C.-R. Acad. sci., **242**, No. 11, 1399-1401 (1956).

Delibrias, G., et M.-T. Perquis. Augmentation anormale d'intensité observée à Saclay le 23 février 1956. Paris, C.-R. Acad. sci., **242**, No. 13, 1722-1724 (1955).

De Vries, H. Cosmic radiation during the solar flare of February 23d and its effect on ^{14}C age measurements. Physica, **22**, No. 4, 357 (1956). [Letter to Editor.]

Ehmert, A., und G. Pfotzer. Ein neuer Ausbruch solarer Ultrastrahlung am 23. Februar 1956. Mitt. Max Planck-Institüt für Physik der Stratosphäre, Weissenau bei Ravensburg, No. 5, 7 pp., mim. (1956). 29 cm.

Jory, F. S. Influence of geomagnetic quadrupole fields upon cosmic-ray intensity. Phys. Rev., **102**, No. 4, 1167-1173 (1956).

Kessler, D., et R. Maze. Une expérience avec compteurs sur les gerbes pénétrantes produites par les mésons μ. Physica, **22**, No. 2, 69-85 (1956).

McDonald, F. B. Direct determination of primary cosmic ray alpha particle energy spectrum by a new method. Iowa Ciry, State University of Iowa, Dept. of Phys., Pub. SUI-56-4, 35 pp. + 16 figs., mim. (March 1956). 28 cm.

Messerschmidt, W. Ultrastrahlung von der Sonne. Naturwiss., **43**, Heft 8, 174 (1956).

Morrison, P. Solar origin of cosmic-ray time variations. Phys. Rev., **101**, No. 4, 1397-1404 (1956).

Norman, R. J. Influence of the earth's magnetic field on air showers. Phys. Rev., **101**, No. 4, 1405-1406 (1956).

Sekido, Y. Cosmic rays and corpuscles from the sun. Rep. Ionosphere Res. Japan, **9**, No. 3, 181-182 (1955). [Short note.]

Sekido, Y., M. Wada, I. Kondoh, and K. Kawabata. Correlation among magnetic storms, solar phenomena and cosmic-ray storms. Rep. Ionosphere Res. Japan, **9**, No. 3, 174-180 (1955).

Standil, S., and R. W. Pringle. Scintillation spectrometer study of cosmic radiation at great depths. Phys. Rev., **101**, No. 4, 1395-1396 (1956).

Steinmaurer, R. Ein ungewöhnlicher, plötzlicher Intensitätsansteig der kosmischen Strahlung. Naturwiss., **43**, Heft 8, 174 (1956).

Vallarta, M. S. Sobre la relation entre la radiacion electromagnética y la radiación cósmica emitidas por el sol. Ann. Inst. Geophys., Univ. Nac Autonoma Mexico, **1**, 134-139 (1955).

Vallarta, M. S. Sobre el problema del campo magnético general del sol y el efecto de albedo. Ann. Inst. Geophys., Univ. Nac. Autonoma Mexico, **1**, 140-147 (1955).

Van Allen, J. A., and C. E. McIlwain. Cosmic ray intensity at high altitudes on February 23, 1956. Iowa City, State University of Iowa, Dept. of Phys., Pub. SUI-56-5, 6 pp. + 2 figs., mim. (March 12, 1956). 28 cm.

Webber, W. R. A new determination of the intensities of primary cosmic-ray alpha particles and Li, Be, B nuclei at $\lambda = 41.5°$ using a Čerenkov detector. Iowa City, State University of Iowa, Dept. of Phys., Pub. SUI-56-6, 39 pp. + 9 figs., mim. (rec'd April 19, 1956). 28 cm.

Webber, W. R., and F. B. McDonald. Determination of the intensities of low-Z components of the primary cosmic radiation at $\lambda = 41°$ using a Čerenkov detector. Phys. Rev., **100**, No. 5, 1460-1467 (1955).

Yagoda, H. Observations on stars and heavy primaries recorded in emulsions flown in Viking rocket No. 9. Can. J. Phys., **34**, No. 1, 122-146 (1956).

D—*Upper Air Research*

Beynon, W. J. G., and G. M. Brown. Region E and the S_q current system. Nature, **177**, 583-584 (March 24, 1956). [Letter to Editor.]

Boulder Laboratories. First annual report of the Boulder Laboratories, July 1, 1954 to June

30, 1955. Boulder, Colorado, Nation. Bur. Stan., Rep. No. 3566, 125 pp. + 5 app., mim. (rec'd April 19, 1956). [Contains report of Central Radio Propagation Laboratory.]

Bowhill, S. A. Pulse synchronization equipment and wide-band 75 Kc T.R.F. receiver. Pennsylvania State University, Ionosphere Res. Lab., Sci. Rep. No. 82, 24 pp., mim. (Feb. 1, 1956).

Bramley, E. N. Tilts in the ionosphere during the solar eclipse of 30 June 1954. J. Atmos. Terr. Phys., 8, Nos. 1/2, 98-104 (1956).

Bray, W. J., J. A. Saxton, R. W. White, and G. W. Luscombe. V.H.F. propagation by ionospheric scattering and its application to long-distance communication. Proc. Inst. Elec. Eng., B, 103, No. 8, 236-257 (1956).

Burkard, O. Die tages- und jahreszeitlichen Variationen der F_1-Ionisation Ein Deutungsversuch. J. Atmos. Terr. Phys., 8, Nos. 1/2, 83-90 (1956).

Chvojková, E. Methoda ionosférických prognos. Rozpravy, Czechosl. Acad. Sci., Pub. No. 26, 54 pp. (1955). 24 cm.

Chvojková, E. Ionospheric layers during photoionization. I. Theory of bifurcation. Bull. Astron. Inst. Czechosl., 7, No. 2, 33-38 (1956).

Dave, J. V., and K. R. Ramanathan. On the intensity and polarisation of the light from the sky during twilight. Proc. Indian Acad. Sci., 43, No. 2, A, 67-78 (1956).

deBettencourt, J. T., and W. A. Whitcraft, Jr. Long range meteoric echoes via F-layer reflections. Trans. Inst. Radio Eng. Prof. Group on Antennas and Propagation, AP-4, No. 1, 72-76 (1956).

Dufay, J., et T. Mao-Lin. Sur l'altitude des couches atmosphériques émettant les raies [OI] 5577Å, [OI] 6300Å et NoI 892Å. Ann. Géophys., 11, No. 4, 387-398 (1955).

Dungey, J. W. The influence of the geomagnetic field on turbulence in the ionosphere. J. Atmos. Terr. Phys., 8, Nos. 1/2, 39-42 (1956).

Ellis, G. R. The Z propagation hole in the ionosphere. J. Atmos. Terr. Phys., 8, Nos. 1/2, 43-54 (1956).

Ghosh, M. Determination of the F-region collisional frequency (over Calcutta). J. Atmos. Terr. Phys., 8, Nos. 1/2, 116-118 (1956). [Research note.]

Groves, G. V. Introductory theory for upper atmosphere wind and sonic velocity determination by sound propagation. J. Atmos. Terr. Phys., 8, Nos. 1/2, 24-38 (1956).

Hibberd, F. H. On the observation of ionospheric self-interaction. J. Atmos. Terr. Phys., 8, Nos. 1/2, 120-122 (1956). [Research note.]

Huruhata, M., H. Tanabe, and T. Nakamura. Photoelectric studies of the night sky light. Rep. Ionosphere Res. Japan, 9, No. 3, 136-147 (1955).

Huxley, L. G. H. The interpretation of measurements of radio-wave interaction. J. Atmos. Terr. Phys., 8, Nos. 1/2, 118-120 (1956). [Research note.]

International Scientific Radio Union, Commission II on Radio and Troposphere. Proceedings of the XIth General Assembly held in The Hague from August 23rd to September 2nd, 1954. Secretary General of U.R.S.I., Brussels, Vol. X, Pt. 2, 91 pp. (1954). 24 cm. [This publication is available from the General Secretariat of the U.R.S.I., 42 Rue des Minimes, Brussels, Belgium, at the following price: 100 Belgian francs, or £0.14.6, or $2.00 U.S. (postage included).

International Scientific Radio Union, Commission VII on Radioelectronics. Proceedings of the XIth General Assembly held in The Hague from August 23rd to September 2nd, 1954. Secretary General of U.R.S.I., Brussels, Vol. X, Pt. 7, 140 pp. (1954). 24 cm. [This publication is available from the General Secretariat of the U.R.S.I., 42 Rue des Minimes, Brussels, Belgium, at the following price: 150 Belgian francs, or £1.1.6, or $3.00 U.S. (postage included).

Jones, F. E., and H. S. W. Massey. Rocket exploration of the upper atmosphere. Nature, 177, 643-645 (April 7, 1956).

Maeda, H. On the disturbance daily variations and the lunar daily variations in the $F2$ region of the ionosphere on the magnetic equator. Kyoto, J. Geomag. Geoelectr., 7, No. 3, 75-85 (1955).

Matsushita, S. Sequential E_s and lunar effects on the equatorial E_s . Kyoto, J. Geomag. Geoelectr., 7, No. 3, 91-95 (1955). [Letter to Editor.]

Mitra, A. P. A method of determining the relative amounts of *D*- and *E*-region absorptions of medium and short radio waves. Indian J. Phys., **38**, No. 11, and Proc. Indian Assoc. Cultivation Science, **38**, No. 11, 518-521 (1955).

Pettit, H. B., and E. Manring. Intensity variations of [OI] 5577 and sodium D in the nightglow. Ann. Géophys., **11**, No. 4, 377-386 (1955).

Rao, B. R., M. S. Rao, and D. S. Murthy. Investigation of winds in the ionosphere by spaced receiver method. J. Sci. Industr. Res., New Delhi, A, **15**, No. 2, 75-81 (1956).

Ratcliffe, J. A. Movements in the ionosphere. Nature, **177**, 307-308 (Feb. 18, 1956). [Meeting of the Royal Astronomical Society, Nov. 25, 1955, on the subject of irregularities in the ionosphere and their horizontal movements.]

Ratcliffe, J. A., E. R. Schmerling, C.S.G.K. Setty, and J. O. Thomas. The rates of production and loss of electrons in the *F* region of the ionosphere. Phil. Trans. R. Soc., A, **248**, No. 956, 621-642 (1956).

Rogers, G. L. A new method of analysing ionospheric movement records. Nature, **177**, 613-614 (March 31, 1956).

St. Amand, P. Instrumentation for nightglow research. Ann. Géophys., **11**, No. 4, 435-449 (1955).

St. Amand, P. Some possible relations between the nightglow and the ionosphere. Ann. Géophys., **11**, No. 4, 450-460 (1955).

Sato, T. On the scattering of the sun's ray in the high atmosphere (I). J. Met. Soc. Japan, **33**, No. 5, 194-204 (1955).

Schmerling, E. R., and J. O. Thomas. The distribution of electrons in the undisturbed F_2 layer of the ionosphere. Phil. Trans. R. Soc., A, **248**, No. 956, 609-620 (1956).

Seaton, M. J. On the extinction correction used in the determination of airglow emission heights by the van Rhijn method. J. Atmos. Terr. Phys., **8**, Nos. 1/2, 115-116 (1956). [Research note.]

Seaton, M. J. A possible explanation of the drop in *F*-region critical densities accompanying major ionospheric storms. J. Atmos. Terr. Phys., **8**, Nos. 1/2, 122-124 (1956). [Research note.]

Shearman, E. D. R. A study of ionospheric propagation by means of ground back-scatter. Proc. Inst. Elec. Eng., B, **103**, No. 8, 203-209 (1956).

Shearman, E. D. R. The technique of ionospheric investigation using ground back-scatter. Proc. Inst. Elec. Eng., B, **103**, No. 8, 210-223 (1956).

Sheriff, R. M. A study of the total electron content of the *F*-region of the ionosphere over Ahmedabad (23°N, 72° 38′E), India. J. Atmos. Terr. Phys., **8**, Nos. 1/2, 91-97 (1956).

Singer, S. F. The artificial earth satellite. Discovery, **17**, No. 4, 140-145 (1956).

Sinno, K. Studies on the disturbances in *F*2 layer associated with geomagnetic disturbances. Rep. Ionosphere Res. Japan, **9**, No. 3, 166-173 (1955).

Szendrei, M. E., and M. W. McElhinny. Preliminary results of the ionospheric solar eclipse of 25 December 1954. J. Atmos. Terr. Phys., **8**, Nos. 1/2, 108-114 (1956).

Verma, J. K. D., and R. Roy. Polarization of the echoes from the ionosphere. Indian J. Phys., **30**, No. 1, and Proc. Indian Assoc. Cultivation Science, **39**, No. 1, 36-46 (1956).

Wild, J. P., and J. A. Roberts. The spectrum of radio-star scintillations and the nature of irregularities in the ionosphere. J. Atmos. Terr. Phys., **8**, Nos. 1/2, 55-75 (1956).

Yonezawa, T. On the influence of electron-ion diffusion on the electron density and height of the nocturnal *F*2 layer (supplement). J. Radio Res. Lab. Japan, **2**, No. 9, 281-291 (1955).

E—*Radio Astronomy*

Boischot, A., E. J. Blum, M. Ginat, et E. Le Roux. Observation d'une éclipse de la Nébuleuse du Crabe. Paris, C.-R. Acad. sci., **242**, No. 15, 1849-1852 (1956).

Carter, A. W. L. The angular size of the variable radio source Hydra-A. Aust. J. Phys., **8**, No. 4, 564-567 (1955).

Czyzewski, O., J. de Mezer, and A. Strzalkowski. Observations of solar radio radiation during the eclipse of June 30, 1954. I. Acta Geophys. Polonica, **3**, No. 4, 155-160 (1955).

Eriksen, G., Ø. Hauge, and E. Tandberg-Hanssen. Radio-frequency observations of the solar eclipse of June 30, 1954. Astroph. Norvegica, **5**, No. 4, 131-152 (1955).

Firor, J. Brightness distribution of the sun at 1.45 meters. Astroph. J., 123, No. 2, 320-324 (1956).
Goodman, B. Radio astronomy. QST, 40, No. 5, 17-19 (1956).
Link, F. Occultations des radiosources par la lune et phénonènes connexes. Bull. Astron. Inst. Czechosl., 7, No. 1, 1-5 (1956).
Lovell, A. C. B. Radio astronomy and the fringe of the atmosphere. Q. J. R. Met. Soc., 82, No. 351, 1-14 (1956).
McClain, E. F. A note on the potentialities of large radio telescopes. Astroph. J., 123, No. 2, 367-368 (1956).
McKinley, D. W. R. Radar-echo duration and height of a Perseid meteor. J. Atmos. Terr. Phys., 8, Nos. 1/2, 76-82 (1956).
Roman, N. G., and F. T. Haddock. A model for non-thermal radio source spectra. Washington, D. C., Naval Research Laboratory, NRL Rep. No. 4712, 6 pp. + 2 figs. (March 1, 1956). 26 cm.
Shakeshaft, J. R., M. Ryle, J. E. Baldwin, B. Elsmore, and J. H. Thomson. A survey of radio sources between declinations −38° and +83°. Mem. R. Astr. Soc., 67, Pt. 3, 106-154 (1955).

F—*Earth's Crust and Interior*

Aubrey, K. V. Frequency-distributions of elements in igneous rocks. Geochim. et Cosmochim., 9, Nos. 1/2, 83-89 (1956).
Bartels, J. (Ed.) Handbuch der Physik (Encyclopedia of Physics), Volume 47—Geophysics I: The earth's body. Springer-Verlag, Berlin, 659 pp. + 289 figs. (1956); available in U.S. from Walter J. Johnson, Inc., 125 East 23rd Street, New York 10, N.Y. [Published under direction of S. Flügge, Marburg, Germany.]
California, State of, Department of Resources. Earthquakes in Kern County, California, during 1952. San Francisco, Division of Mines, Bull. No. 171, Pt. II—Seismology, pp. 129-210 (1955). 28 cm. [Chapters by B. Gutenberg, H. Benioff, V. L. Vander Hoof, C. F. Richter, F. Neumann, and W. K. Cloud.]
Flathe, H. A practical method of calculating geoelectrical model graphs for horizontally stratified media. Geophysical Prospecting, 3, No. 3, 268-294 (1955).
Gutenberg, B. Geophysical data implied in isostatic calculations. Helsinki, Veröff. Finn. Geod. Inst., No. 46, 43-50 (1955). [From publication dedicated to Weikko A. Heiskanen on the occasion of his 60th anniversary.]
Hahn, O. Radioactive methods for geologic and biologic age determinations. Sci. Mon., 82, No. 5, 258-265 (1956).
Hurley, P. M., E. S. Larsen, Jr., and D. Gottfried. Comparison of radiogenic helium and lead in zircon. Geochim. et Cosmochim., 9, Nos. 1/2, 98-102 (1956).
Katz, S., and M. Ewing. Seismic-refraction measurements in the Atlantic Ocean. Part VII: Atlantic Ocean Basin, west of Bermuda. Bull. Geol. Soc. Amer., 67, No. 4, 475-509 (1956).
Krauskopf, K. B. Factors controlling the concentrations of thirteen rare metals in sea-water. Geochim. et Cosmochim., 9, Nos. 1/2, 1-32 (1956).
Mead, J. Investigation of possible vertical reflections from deep crustal discontinuities (final report). Indiana University, Dept. of Geology, 7 pp., mim. (April, 1956).
Mühlen, W. von zur. Ergebnisse der "Steinbruch-Seismik" in Siegerland, Kraichgau und in Hessen/Unterfranken. Geol. Jahrb., 71, 569-594 (Feb. 1956).
Munk, W. H. Polar wandering: a marathon of errors. Nature, 177, 551-554 (March 24, 1956).
Nanda, J. N. Fragmentation and continents. Indian J. Met. Geophys., 7, No. 1, 92 (1956). [Letter to Editor.]
Nockolds, S. R., and R. Allen. The geochemistry of some igneous rock series—III. Geochim. et Cosmochim., 9, Nos. 1/2, 34-77 (1956).
Rubin, M., and H. E. Suess. U. S. Geological Survey radiocarbon dates III. Science, 123, 442-448 (March 18, 1956).
Russell, R. D., and D. W. Allan. The age of the earth from lead isotope abundances. Mon. Not. R. Astr. Soc., Geophys. Sup., 7, No. 2, 80-101 (1955).

Shimazu, Y. Chemical structure and physical property of the earth's mantle inferred from chemical equilibrium condition. J. Earth Sci., **3**, No. 2, 85-90 (1955).

Suess, H. E. Absolute chronology of the last glaciation. Science, **123**, 355-357 (March 2, 1956).

Suess, H. E., and H. C. Urey. Abundances of the elements. Rev. Modern Phys., **28**, No. 1, 53-74 (1956).

G—*Miscellaneous*

Athay, R. G., and R. N. Thomas. Some characteristics of a chromospheric model. Astroph. J., **123**, No. 2, 309-319 (1956).

Bureau, R., et M. Bertrand. Perturbation exceptionnelle du rayonnement solaire le 23 février 1956 vers o 345 T.U. Paris, C.-R. Acad. sci., **242**, No. 16, 2025-2027 (1956).

Chapman, S., and K. C. Westfold. A comparison of the annual mean solar and lunar atmospheric tides in barometric pressure, as regards their worldwide distribution of amplitude and phase. J. Atmos. Terr. Phys., **8**, Nos. 1/2, 1-23 (1956).

Ellison, M. A. The sun and its influence. London, Routledge and Kegan Paul, Ltd., xii + 235, with tables, diagrams, and 9 pls. (1955).

Jensen, E., J. Nordø, and T. S. Ringnes. Variations in the structure of sunspots in relation to the sunspot cycle. Astroph. Norvegica, **5**, No. 6, 167-205 (1955).

Kopecký, M. The outline of the theory of distribution and occurrence of sunspots on the solar disc. Praha, Astron. Inst., Czechosl. Acad. Sci., Pub. No. 28, 60 pp. (1956). 21 cm.

Kuiper, G. P. The formation of the planets, Part I. J. R. Astr. Soc. Can., **50**, No. 2, 57-68 (1956). [Lecture, joint meeting of the Royal Canadian Institute and the Royal Astronomical Society of Canada, Nov. 12, 1955.]

Pecker, C., and J.-C. Pecker. Le nombre d'atomes d'hydrogène sur les niveaux $n = 1$ et $n = 2$ dans la chromosphère solaire. Paris, C.-R. Acad. sci., **242**, No. 9, 1130-1132 (1956).

NOTICE

When available, single unbound volumes can be supplied at $6 each and single numbers at $2 each, postpaid.

Charges for reprints and covers

Reprints can be supplied, but prices have increased considerably and costs depend on the number of articles per issue for which reprints are requested. It is no longer possible to publish a schedule of reprint charges, but if reprints are requested approximate estimates will be given when galley proofs are sent to authors. Reprints without covers are least expensive; standard covers (with title and author) can be supplied at an additional charge. Special printing on covers can also be supplied at further additional charge.

Fifty reprints, without covers, will be given to institutions paying the publication charge of $8 per page.

Alterations

Major alterations made by authors in proof will be charged at cost. Authors are requested, therefore, to make final revisions on their typewritten manuscripts.

Orders for back issues and reprints should be sent to Editorial Office, 5241 Broad Branch Road, N.W., Washington 15, D.C., U.S.A.

Subscriptions are handled by The Editorial Office, 5241 Broad Branch Road, N.W., Washington 15, D.C., U.S.A.

CONTENTS—Concluded

JOURNAL OF GEOPHYSICAL RESEARCH